

WIND TURBINE IMPACTS ON ENVIRONMENT CANADA WEATHER RADAR DATA

CAROLYN JEAN RENNIE

A THESIS SUBMITTED TO

THE FACULTY OF GRADUATE STUDIES

IN PARTIAL FUFILLMENT OF THE REQUIREMENTS

FOR THE DEGREE OF

MASTER OF SCIENCE

GRADUATE PROGRAM IN EARTH & SPACE SCIENCE

YORK UNIVERSITY

TORONTO, ONTARIO

MAY 2015

© CAROLYN JEAN RENNIE, 2015

Abstract

This thesis investigates the occurrence of wind turbine clutter (WTC) on Canadian weather radar data and provides a detailed comparison to expectations from developed radar line of sight (RLOS) tools for three wind farms under standard atmospheric conditions. Tools were developed to study factors which impact WTC such as wind turbine orientation, and atmospheric propagation of the radar beam using atmospheric profile data. The results indicate that standard methods of RLOS calculations may need to take into account other factors as WTC was observed even when RLOS tools indicated the wind turbines would not intercept the main radar beam. Additionally, Canadian Turbine Interference Products (C-TRIP) were created in order to assist Environment Canada's meteorologists in the identification of WTC given existing wind farm locations.

Acknowledgements

This work would not be possible without the support of my friends, family and co-workers who helped keep me motivated through all the hills and valleys I have gone through over the past years.

Specifically, I would like to thank the following people from Environment Canada who offered support through data, programs and personal encouragement: Jim Young, Marie MacPhee, Norman Donaldson, Robert Crawford, Janti Reid, Stephen Holden, Ron Ruff, David Hudak, and George Isaac. I would also like to thank Joel Baker, the President and CEO of my current employer CatIQ, for providing me resources, time and support to work on my thesis.

Additionally, I would like to thank my friends and family who have helped support me emotionally through the hectic months of thesis writing: Catherine Rennie, Scott Rennie, Elizabeth Rennie, Barbara Durnford, David Durnford, Joanne Kennell, and especially Jonathan Poelstra.

Lastly, my greatest encouragement has come from my Master's Supervisors Peter Taylor and Dave Sills who believe in me even when I may not have believed in myself. I have a very ambitious outlook when it comes to research and they have been instrumental in shaping realistic expectations of me and my research.

Table of Contents

Abstract.....	ii
Acknowledgements.....	iii
Table of Contents.....	iv
List of Figures	vii
List of Tables	xiv
1. Introduction	1
1.1 Thesis Background.....	1
1.1.1 Thesis Motivation	1
1.1.2 Thesis Objectives	1
1.2 Weather Radars	2
1.2.1 Radar Meteorology Background.....	2
1.2.2 Radar Beam Propagation.....	4
1.2.3 Canadian Radar Network	7
1.3 Wind Turbines	9
1.3.1 Wind Energy in Canada.....	10
1.4 Wind Turbine Impacts to Weather Radar Data	11
1.4.1 Effects	12
1.4.2 Factors Affecting Detection of Wind Turbine Clutter (WTC)	17
1.4.3 Identification and Mitigation of Wind Turbine Clutter (WTC)	19
1.4.4 Wind Farms in Proximity to Environment Canada Weather Radar.....	20
2. Analysis Methodology.....	22
2.1 Wind Farm Selection	22
2.2 Radar Line of Sight (RLOS).....	22
2.2.1 Wind Farm Analysis	23
2.2.2 IDL Beamwidth.....	26
2.2.3 GIS Viewsheds.....	28

2.3	C-TRIP	31
2.3.1	Wind Farm Box Geometry	33
2.4	Productx Utility	36
2.5	Wind Turbine Orientation Model	37
2.6	Data Requirements	38
2.6.1	IRIS Files & CARDS Products	38
2.6.2	MOLTS Data	38
2.6.3	Digital Elevation Model Data	40
2.6.4	Wind Turbine Operational Data	41
3.	Results: Wind Farm Case Studies	42
3.1	Melancthon Wind Farm	42
3.1.1	Wind Farm & Weather Radar Specifications.....	42
3.1.2	Wind Turbine Orientation Model	44
3.1.3	RLOS Analyses.....	45
3.1.4	WTC Examples	48
3.2	Greenwich Wind Farm.....	51
3.2.1	Wind Farm & Weather Radar Specifications.....	51
3.2.2	Wind Turbine Orientation Model	53
3.2.3	RLOS Analyses.....	54
3.2.4	WTC Examples	57
3.3	Nuttby Mountain Wind Farm	60
3.3.1	Wind Farm & Weather Radar Specifications.....	60
3.3.2	Wind Turbine Orientation Model	62
3.3.3	RLOS Analyses.....	63
3.3.4	WTC Examples	66
4.	Case Study: Modeling Radar Beam Propagation from the Gore Weather Radar to the Nuttby Mountain Wind Farm	70

4.1	Case Study Methodology	70
4.2	Results	73
5.	Case Studies.....	82
5.1	Melancthon Wind Farm / King City Weather Radar	82
5.2	Greenwich Wind Farm / Lasseter Lake Weather Radar	88
5.3	Nuttby Mountain Wind Farm / Gore Weather Radar	93
5.4	Case Study Summary.....	100
6.	Conclusions and Recommendations	101
6.1	Conclusions.....	101
6.2	Future Research and Recommendations	102
	References	103
	Appendix A: IDL Program: calc_beamheight.pro	106
	Appendix B: C-TRIP Code	109
	Appendix C: Melancthon Turbine Coordinates (UTM Zone 17T)	113
	Appendix D: Productx Output WTC Examples of the Melancthon Wind Farm / King City Weather Radar Pair.....	115
	Appendix E: C-TRIP Output WTC Examples of the Melancthon Wind Farm / King City Weather Radar Pair.....	119
	Appendix F: Greenwich Turbine Coordinates (UTM Zone 16 U)	123
	Appendix G: Productx Output WTC Examples of the Melancthon Wind Farm / King City Weather Radar Pair.....	124
	Appendix H: C-TRIP Output WTC Examples of the Greenwich Wind Farm / Lasseter Lake Weather Radar Pair	128
	Appendix I: Nuttby Mountain Coordinates (Decimal Degrees Latitude and Longitude)	132
	Appendix J: Productx Output WTC Examples of the Nuttby Mountain Wind Farm / Gore Weather Radar Pair	133
	Appendix K: C-TRIP Output WTC Examples of the Nuttby Mountain Wind Farm / Gore Weather Radar Pair.....	137

List of Figures

Figure 1: Height of radar beams at given elevation angles (in °) above the Earth (in km) given standard atmospheric conditions (Fogarty, 2013).....	5
Figure 2: Radar site locations in Canada including EC sites, DND sites and the McGill radar site along with their Doppler and Conventional coverage	7
Figure 3: Simple flowchart of Environment Canada's radar signal, how it is processed and the output data.....	8
Figure 4: Components of a wind turbine (European Commission Energy, 2013).....	10
Figure 5: Installed capacity of wind energy in Canada as at December 2014 (CanWEA, 2014)	11
Figure 6: One day radar accumulation image at Montreal River weather radar with two radial lines to the southeast and one to the southwest of lower precipitation due to blockage from communication towers 31.56, 45.37 and 265 meters from the transmitting radar	12
Figure 7: Multi-path scattering example at Environment Canada's Val d'Irene weather radar where the white circles represent the locations of Lac Alfred wind turbines and the pixel colours represent Doppler corrected reflectivity (in DBZ)	13
Figure 8: Radar reflectivity (top) and relative velocity (bottom) of two wind farms (circled in yellow) located approximately 60 and 80 km northeast of the Gore weather radar in comparison to weather in the west	15
Figure 9: 168 hour (7-day) radar accumulation product from the Gore weather radar near Halifax, Nova Scotia. Two wind farms are circled which show overestimations of precipitation and partial blockage is seen to the east-southeast from a nearby (74.32 m away) communication tower.	16
Figure 10: Wind turbine contamination (green box) approximately 100 km from the weather radar (center) in Manitoba on a clear air day with no significant weather in the area	17
Figure 11: Location of existing wind turbines (green diamonds) in Canada (as at July 31, 2013) with respect to Canadian weather radars (red).....	21
Figure 12: Wind Farm Analysis output GIF file: The top image shows the ground elevation in green, the radar as a red star, and the turbine as a red line. The second image presents a depiction of the radar beam and its elevation angle. Blue lines indicate any existing terrain blockage.	24

Figure 13: Example of a Wind Farm Summary output text file provided by Environment Canada's internal Wind Farm Analysis software	25
Figure 14: Wind Farm Analysis KML output example where the radar is indicated in red and the turbines are indicated with colours which define their turbine tip visibility (as seen in Table 2) displayed in Google Earth.	26
Figure 15: IDL Beamwidth output example of the appearance of a specified turbine located at 24.53 km from XNI (Lasseter Lake weather radar) with DOPVOL1A elevation angles 0.2° (winter) and 0.5° (summer).	28
Figure 16: Illustration of how OFFSET's are determined (ArcGIS, 2012).....	29
Figure 17: Direction values of azimuth in degrees (°) (ArcGIS, 2012).....	30
Figure 18: Illustration of the angles for VERT1 & VERT2 (ArcGIS, 2012).....	30
Figure 19: Illustration of the distances RADIUS1 and RADIUS2 as well as AZIMUTH1 and AZIMUTH2 (ArcGIS, 2012)	30
Figure 20: Sample viewshed display where the blue dot is the observation point, green areas are visible and pink areas are locations which are not visible to the observation point (created using ArcGIS 10.2.1).....	31
Figure 21: Representation of a wind farm box location (green star) with respect to the radar (red star) at the origin (240,240) where R is the path distance, θ is the bearing in °, θ' is measured from the X axis and X' and Y' are calculated values	35
Figure 22: Example of output produced using data provided by Productx utility where maximum azimuthal reflectivity values of DBT and DBZ are compared at distances from the weather radar.	37
Figure 23: Location of requested (purple) and provided (yellow) MOLTS points to model the radar beam path from the King City weather radar to the Melancthon Wind Farm.....	40
Figure 24: Example of downloaded CDED data for the 011E tile (GeoGratis, 2014)	41
Figure 25: Wind farm summary output file for Melancthon wind farm / King City weather radar pair.....	43
Figure 26: Location of Melancthon wind turbines (green and yellow as described by Table 2) and King City weather radar (red)	43

Figure 27: Visual representation of the Melancthon Wind Farm / King City weather radar wind turbine orientation model.....	44
Figure 28: Wind Farm Analysis Tool - RLOS analysis performed on Melancthon turbines 74 (left) and 75 (right) as seen from the King City weather radar. Figure explanation found in Section 2.2.1 and Figure 12 caption.....	45
Figure 29: IDL Beamwidth Tool - RLOS analysis performed on Melancthon turbines 74 (top) and 75 (bottom) as seen from the King City weather radar. Figure explanation found in Section 2.2.2 and Figure 15 caption. *Note that analysis was completed given -0.1° as the winter DOPVOL1A angle however the operational elevation angle has since changed to 0°	46
Figure 30: King City weather radar (radar dish) summer viewshed where Melancthon turbine locations are indicated in black. Locations which turbines would be visible in the center of the main beam (0.5°) are red and locations which turbines would be visible in the bottom of the main beam (0.175°) are indicated in orange. (Created using ArcGIS 10.2.1)	47
Figure 31: King City weather radar (radar dish) winter viewshed where Melancthon turbine locations are indicated in black. Locations which turbines would be visible in the center of the main beam (0°) are red and locations which turbines would be visible in the bottom of the main beam (-0.325°) are indicated in orange. (Created using ArcGIS 10.2.1).....	48
Figure 32: Example King City Productx output for 2013-08-16-0800Z where the maximum DBT and DBZ values for the azimuth range of 276° - 291° are displayed.....	49
Figure 33: Example King City C-TRIP CLOGZPPI product on 2013-08-16 at 0800Z created using the DOPVOL1A WKR weather radar IRIS file where the Melancthon wind farm is outlined with the largest green box to the left of the radar (at the center in the image)	50
Figure 34: Wind farm summary output file for Greenwich wind farm / Lasseter Lake weather radar pair	52
Figure 35: Location of Greenwich wind turbines (pink and yellow as described in Table 2) and Lasseter Lake weather radar (red)	52
Figure 36: Visual representation of the Greenwich Wind Farm / Lasseter Lake weather radar wind turbine orientation model	53
Figure 37: Wind Farm Analysis Tool - RLOS analysis performed on Greenwich turbines 3 (left) and 7 (right) as seen from the Lasseter Lake weather radar. Figure explanation found in Section 2.2.1 and Figure 12 caption.....	54

Figure 38: IDL Beamwidth Tool - RLOS analysis performed on Greenwich turbines 3 (top) and 7 (bottom) as seen from the Lasseter Lake weather radar. Figure explanation found in Section 2.2.2 and Figure 15 caption.....	55
Figure 39: Lasseter Lake weather radar (radar dish) summer viewshed where Greenwich turbine locations are indicated in black. Locations which turbines would be visible in the center of the main beam (0.5°) are red and locations which turbines would be visible in the bottom of the main beam (-0.05°) are indicated in orange. (Created using ArcGIS 10.2.1)	56
Figure 40: Lasseter Lake weather radar (radar dish) winter viewshed where Greenwich turbine locations are indicated in black. Locations which turbines would be visible in the center of the main beam (0.2°) are red and locations which turbines would be visible in the bottom of the main beam (-0.35°) are indicated in orange. (Created using ArcGIS 10.2.1)	57
Figure 41: Example Lasseter Lake Productx output for 2013-08-16-0800Z where the maximum DBT and DBZ values for the azimuth range of 103° - 123° are displayed	58
Figure 42: Example Lasseter Lake C-TRIP CLOGZPPI product on 2013-08-16 at 0800Z created using the DOPVOL1A XNI weather radar IRIS file where the Greenwich wind farm is outlined with the green box.....	59
Figure 43: Wind farm summary output file for Nuttby Mountain wind farm / Gore weather radar pair.....	61
Figure 44: Location of Nuttby Mountain wind turbines (yellow as described in Table 2) and Gore weather radar (red)	61
Figure 45: Visual representation of the Nuttby Mountain Wind Farm / Gore weather radar wind turbine orientation model.....	62
Figure 46: Wind Farm Analysis Tool - RLOS analysis performed on Nuttby Mountain turbines 4 (left) and 9 (right) as seen from the Gore weather radar. Figure explanation found in Section 2.2.1 and Figure 12 caption.....	63
Figure 47: IDL Beamwidth Tool - RLOS analysis performed on Nuttby Mountain turbines 4 (top) and 9 (bottom) as seen from the Gore weather radar. Figure explanation found in Section 2.2.2 and Figure 15 caption.	64
Figure 48: Gore weather radar (radar dish) summer viewshed where Nuttby Mountain turbine locations are indicated in black. Locations which turbines would be visible in the center of the	

main beam (0.5°) are red and locations which turbines would be visible in the bottom of the main beam (0.175°) are indicated in orange. (Created using ArcGIS 10.2.1)	65
Figure 49: Gore weather radar (radar dish) winter viewshed where Nuttby Mountain turbine locations are indicated in black. Locations which turbines would be visible in the center of the main beam (0°) are red and locations which turbines would be visible in the bottom of the main beam (-0.325°) are indicated in orange. (Created using ArcGIS 10.2.1).....	66
Figure 50: Example Gore Productx output for 2013-08-16-0710Z where the maximum DBT and DBZ values for the azimuth range of 34° - 38° are displayed	67
Figure 51: Example Gore C-TRIP CLOGZPPI product on 2013-08-16 at 0710Z created using the DOPVOL1A XGO weather radar IRIS file where the Nuttby Mountain wind farm is outlined with the smallest green box closest to the center of the radar	68
Figure 52: Location of requested (purple) and provided (yellow) MOLTS center points to model the radar beam path from the Gore weather radar to the Nuttby Mountain Wind Farm.....	70
Figure 53: C-TRIP CLOGZPPI, VRPPI and PRECIP products of the Nuttby Mountain wind farm box on 2014-07-07 from 0700 Z – 0750 Z created using the DOPVOL1A and DOPVOL2 XGO IRIS files	75
Figure 54: C-TRIP CLOGZPPI, VRPPI and PRECIP products of the Nuttby Mountain wind farm box on 2014-07-07 from 0800 Z – 0850 Z created using the DOPVOL1A and DOPVOL2 XGO IRIS files	78
Figure 55: C-TRIP CLOGZPPI, VRPPI and PRECIP products of the Nuttby Mountain wind farm box on 2014-07-07 from 0800 Z – 0850 Z created using the DOPVOL1A and DOPVOL2 XGO IRIS files	81
Figure 56: C-TRIP CLOGZPPI product of the WKR radar which depicts lower reflectivity of possible biological clutter near the Melancthon wind farm (large green box) on 2013-08-16 at 2000Z	83
Figure 57: Sample King City Productx output for 2014-08-16-0800Z where the maximum DBT and DBZ values for the azimuth range of 276° - 291° are displayed. Additional Productx images for WKR are found in Appendix D.	84
Figure 58: Sample C-TRIP CLOGZPPI, VRPPI and PRECIP products of the Melancthon wind farm box on 2013-08-16 from 0800 Z – 0850 Z created using the DOPVOL1A and DOPVOL2	

WKR IRIS files. The white quarter circle lines in the first two images are the 60 km range rings. Additional C-TRIP images for WKR are found in Appendix E.	85
Figure 59: Sample King City Productx output for 2014-08-16-2010Z where the maximum DBT and DBZ values for the azimuth range of 276° - 291° are displayed. Additional Productx images for WKR are found in Appendix D.	86
Figure 60: C-TRIP CLOGZPPI product of the XNI radar which depicts lower reflectivity radar echoes near the Greenwich wind farm (large green box) on 2013-08-16 at 2000Z	89
Figure 61: Sample Lasseter Lake Productx output for 2013-08-16-0800Z where the maximum dBT and dBZ values for the azimuth range of 103° - 123° are displayed. Additional Productx images for WKR are found in Appendix G.	90
Figure 62: Sample Lasseter Lake Productx output for 2013-08-16-2010Z where the maximum dBT and dBZ values for the azimuth range of 103° - 123° are displayed. Additional Productx images for WKR are found in Appendix G.	91
Figure 63: Sample C-TRIP CLOGZPPI, VRPPI and PRECIP products of the Greenwich wind farm box on 2013-08-16 from 2000 Z – 2050 Z created using the DOPVOL1A and DOPVOL2 XNI IRIS files. Additional C-TRIP images for WKR are found in Appendix H.	92
Figure 64: Sample Gore Productx output for 2013-08-16-1930Z where the maximum dBT and dBZ values for the azimuth range of 34° - 38° are displayed. Additional Productx images for XGO are found in Appendix J.	95
Figure 65: Representation of operational wind turbine data (Table 18) where all Nuttby wind turbines are operating and moderate impacts are expected on 2013-11-15 morning hour based on Table 16 and Figure 45 of the wind turbine orientation model	96
Figure 66: Sample C-TRIP CLOGZPPI, VRPPI and PRECIP products of the Nuttby Mountain wind farm box on 2013-11-15 from 2000 Z – 2050 Z created using the DOPVOL1A and DOPVOL2 XGO IRIS files. Additional C-TRIP images for XGO are found in Appendix K.	97
Figure 67: Representation of operational wind turbine data (Table 19) where all Nuttby wind turbines are operating and green represent marginal expected impact and yellow moderate impact expected on 2013-11-15 afternoon hour based on Table 16 and Figure 45 of the wind turbine orientation model.	98

Figure 68: Representation of operational wind turbine data for 2014-07-07 from 0700 Z – 0950 Z where Nuttby wind turbines which are operating are in yellow representing moderate expected impacts on Table 16 and Figure 112 and turbines not in operation are shown in red99

List of Tables

Table 1: Wind farm / radar pairs selected for case studies including wind farm name, number of turbines, radar name and ID as well as minimum distance from the radar to the wind farm	22
Table 2: Wind Farm Analysis output KML Google Earth pin colors with respect to tip visibility ..	26
Table 3: Snapshot of input attribute table of observation points used to create ArcGIS viewsheds	29
Table 4: Defined coordinate locations of wind farm boxes with respect to image size (240 – VRPPI & CLOGZPPI) (480 – PRECIP) with beginning X and Y coordinates widths and heights in pixels.....	34
Table 5: Requested MOLTS data points and actual MOLTS points available for wind farms, radar and points in between.....	39
Table 6: Information about the King City weather radar.....	42
Table 7: King City weather radar Doppler scan elevation angles (°)	43
Table 8: Wind turbine orientation model calculations for the Melancthon wind farm where wind direction ranges and predicated WTC impact are shown based on impacted azimuth angles ...	44
Table 9: Case study day weather information provided for Toronto Buttonville Airport	49
Table 10: Information about the Lasseter Lake weather radar.....	51
Table 11: Lasseter Lake weather radar Doppler scan elevation angles (°)	51
Table 12: Wind turbine orientation model calculations for the Greenwich wind farm where wind direction ranges and predicated WTC impact are shown based on the impacted azimuth angles	53
Table 13: Case study day weather information provided for Thunder Bay Airport	58
Table 14: Information about the Gore weather radar	60
Table 15: Gore weather radar Doppler scan elevation angles (°)	60
Table 16: Wind turbine orientation model calculations for the Nuttby Mountain wind farm where wind direction ranges and predicated WTC impact are shown based on impacted azimuth angles	62
Table 17: Case study day weather information provided for Halifax International Airport	67

Table 18: Nacelle orientation in ° for each turbine in the Nuttby Mountain wind farm for the 04:00 hour on 2013-11-15 as provided by Nova Scotia Power.....	69
Table 19: Nacelle position in ° for each turbine in the Nuttby Mountain wind farm for the 16:00 hour on 2013-11-15	69
Table 20: Height above sea level for each point along the path from the Gore weather radar to the Nuttby Mountain wind farm along with the distance from one point to the next.....	71
Table 21: Radar beam modeling results on 2014-07-07 from 0700 Z – 0750 Z using MOLTS points described in Table 5 and Table 20.....	73
Table 22: Radar beam modeling results on 2014-07-07 from 0800 Z – 0850 Z using MOLTS points described in Table 5 and Table 20.....	76
Table 23: Radar beam modeling results on 2014-07-07 from 0900 Z – 0950 Z using MOLTS points described in Table 5 and Table 20.....	79

1. Introduction

1.1 Thesis Background

This thesis investigates the occurrence of wind turbine clutter (WTC) on Canadian weather radar data and provides a detailed comparison to expectations from radar line of sight (RLOS) for three wind farms during standard atmospheric conditions. Tools are developed in order to assist Environment Canada's meteorologists to identify WTC in the Canadian weather radar network. Additionally, atmospheric profile data for one particular wind farm / radar pair is used to determine the effectiveness of modeling radar beam propagation to predict WTC impacts.

1.1.1 Thesis Motivation

The presence of wind turbines in proximity to weather radar stations can greatly impact the quality of radar data as well as cause misleading signatures on radar products used by forecasters, modelers and the general public. The interaction between wind turbines and weather radars is an emerging science. Before beginning the research for this thesis (prior to 2012) there had been very little work done in Canada to not only analyze and mitigate the impacts but to inform the general public about the issue. In Spain and the United States, promising research has been able to provide insight into the identification of WTC in raw Level I radar data (Gallardo-Hernando, 2008) (Isom, 2007). However, these data are not readily available in the Canadian weather radar network. In Canada, efforts have been made (Donaldson et al., 2008) (Rennie et al., 2012) in order to provide methods which would assist in the siting of wind turbines in proximity to weather radar. This thesis describes the analysis of available Level II moment data and Level III post-processed radar data with the aim of assisting with the identification of WTC for Environment Canada's meteorologists and the general public.

1.1.2 Thesis Objectives

This thesis looks into three cases of wind turbine interference and provides a comparison of the expected impacts given standard atmospheric conditions. The variable nature of WTC is explored in each case. For one specific case, the radar beam's propagation through the atmosphere based on meteorological model data is also taken into account.

There are three main objectives of this thesis:

1. Use tools to identify, analyze and compare WTC which take into account:
 - a. RLOS
 - b. Wind turbine orientation
 - c. Atmospheric propagation of the radar beam
2. Analyze expected WTC based on RLOS in standard atmospheric conditions for three wind farms and make comparisons to observed WTC
3. Determine the added value of modeling the path of the radar beam with calculated atmospheric refractivity for one particular wind farm case

1.2 Weather Radars

Radar (RADio Detection And Ranging) provides a way to determine the location and relative intensity of specific targets. The radar emits pulses of energy at a specified wavelength sent out from the radar antenna. The energy is an electromagnetic pulse that travels at the speed of light (Butler & Johnson, 2003). The energy travels out at specified angles and beam width and is absorbed and scattered off of objects. The time period it takes for the radar antenna to receive a portion of the initial pulse back, can be used to determine the range of the target relative to the radar.

Doppler radars also have the ability to detect the relative velocity of targets by comparing the outgoing frequency of the pulse to the incoming frequency of the pulse. The speed of the target is measured relative to the radar; as in a target travelling at such speed toward or away from the radar (commonly measured in ms^{-1}). If the target is moving towards the radar there will be a positive phase shift, and if the target is moving away from the radar there will be a negative phase shift. The size of the shift can be related to the targets velocity.

1.2.1 Radar Meteorology Background

In the case of weather radar, the radar aims to detect meteorological targets (hydrometeors) such as rain, snow and hail. Hydrometeors are very good at reflecting microwave energy (wavelengths ranging from between 1 mm – 1 m in length). There are three main types of weather radars being used around the world which have been defined as X-band ($\lambda \sim 2.5\text{-}4\text{ cm}$), C-band ($\lambda \sim 4\text{-}8\text{ cm}$) and S-band ($\lambda \sim 8\text{-}15\text{ cm}$) (Rinehart, 1991). Since the majority of hydrometeors have diameters smaller than these wavelengths the properties of Rayleigh scattering apply; where a portion of the energy is scattered back towards the radar. Radar

pulses move out from the antenna in a conical shape with defined elevation angles and beam widths. Weather radars are normally singularly polarized, meaning the energy signal is traveling in a single orientation (commonly horizontal). Dual-polarization radars can send signals out in both the horizontal and vertical orientations. The comparison between the returns from horizontal and vertical can allow one to determine the shapes, orientations and types of meteorological targets within a scanned volume.

As previously mentioned, the pulses of microwave energy have specific beam widths. The radar beam is not a pencil beam but a cone. This thesis investigates Environment Canada (EC) radars with beam widths of 0.65° and 1.1° in both elevation and azimuth (Donaldson et al., 2003). Generally, when one speaks of the radar beam to determine RLOS they are referring to the center of the beam and may not be taking into account the full radar beam (Best, 2009).

The power returned to the radar can be calculated using the standard radar equation shown in Equation 1. The radar reflectivity factor (z) in mm^6/m^3 can be determined by rearranging the equation and can also be expressed with respect to the various diameters of particles within a unit volume in the beam (Equation 2).

Equation 1: Standard radar equation (Muller, 2015)

$$P_r = \frac{P_t G^2 \theta^2 h \pi^3 K^2 l z}{1024 (\ln 2) \lambda^2 r^2}$$

$$z = \frac{P_r 1024 \ln(2) \lambda^2 r^2}{\pi^3 P_t G^2 \theta^2 K^2 l}$$

Where P_r = (power returned to radar from target in watts), P_t = (power transmitted from radar in watts), G = (antenna gain), θ = (radar beam width in radians), h = (pulse length in meters), π = ($\pi \sim 3.14$), K = (constant related to target), l = (signal loss factor associated with attenuation), z = (radar reflectivity factor in mm^6/m^3), λ = (transmitted wavelength in meters), and r = (range to target).

Equation 2: Radar reflectivity factor (z) in mm^6/m^3 represented with respect to drop diameters (D) in mm (Rinehart, 1991)

$$z = \sum_{\text{volume}} D^6$$

Furthermore, the radar reflectivity factor (z) can be used to determine the rate of precipitation through Z-R relationships. The Z-R relationship relates the fact that the radar reflectivity factor (z) is dependent on the size of the drops and the rate of precipitation (R) is dependent on the drop size distribution (Fournier, 1999). The relationship can be expressed as $z = AR^B$ where z is

in mm^6/m^3 and R is in mm/h (Rinehart, 1991). The constants A & B are determined empirically depending on the local environments, known raindrop sizes, precipitation types and fall velocities. In the case of weather radars, the target diameters range from very small (in the case of small rain droplets) to very large (in the case of hail). Because of this, the radar reflectivity factor is normally expressed in decibels (dB) of reflectivity (Z) in units DBZ as shown in Equation 3.

Equation 3: Conversion to reflectivity Z (in DBZ) from the radar reflectivity factor z (in mm^6/m^3)

$$Z = 10 \log_{10} \left(\frac{z}{1 \text{mm}^6/\text{m}^3} \right)$$

The frequency of microwave energy is sensitive to meteorological targets, however there are other objects that can reflect this energy and produce false echoes. Microwave energy can reflect off birds or insects causing what are called biological clutter. Additionally, objects such as buildings, towers, trees and terrain can contaminate weather radar by either scattering or blocking the pulses of energy (Best, 2009). When microwave energy is scattered from objects other than meteorological or biological targets it is called ground clutter. Luckily, most ground clutter can be removed through the use of Doppler radar filtering algorithms performed in the signal processor. Since Doppler radar measures the relative velocity of the targets and ground clutter is stationary with a zero velocity, this information can be filtered out in both reflectivity and velocity measurements within Doppler range.

1.2.2 Radar Beam Propagation

Radar beam propagation refers to the nature of the radar beam as it travels through the atmosphere over the Earth. The curvature of the Earth dictates that although the radar beam is emitted at a specific elevation angle, with respect to the Earth, the beam will appear to be curved upward (Figure 1). Figure 1 is produced using Equation 4 which defines the height a radar beam will be above the Earth at a given distance from the radar.

Equation 4: Height of the radar beam above the Earth at a specific range (in kilometers (km)) and elevation angle (in radians)

$$H = \left(\sqrt{r^2 + (Ka)^2 + 2rKasin\theta} \right) - Ka + h$$

Where K is a property of atmospheric refractivity, a is the Earth's radius (6371 km), r is the distance from the radar to the target (km), θ is the elevation angle above the radar horizon (in radians) and h is the height of the radar feed horn (where the energy is emitted from).

Equation 4 references K which is referred to as the effective Earth radius factor (Barué, 2008). This factor modifies the actual Earth's radius with respect to the change in refractivity index (n) with respect to height and is defined by Equation 5.

Equation 5: Effective Earth radius factor (K) (Barué, 2008)

$$K = \frac{1}{1 + a \left(\frac{dn}{dh} \right)}$$

The refractive index of the atmosphere (n) is normally slightly larger than 1 and is commonly expressed in N-units defined with $N = (n-1) \times 10^6$ where N is refractivity. Under standard atmospheric conditions the refractivity is around 315 N-units providing a value of K near 4/3. In weather radars, this value is used as the effective Earth radius factor with standard atmospheric conditions being assumed.

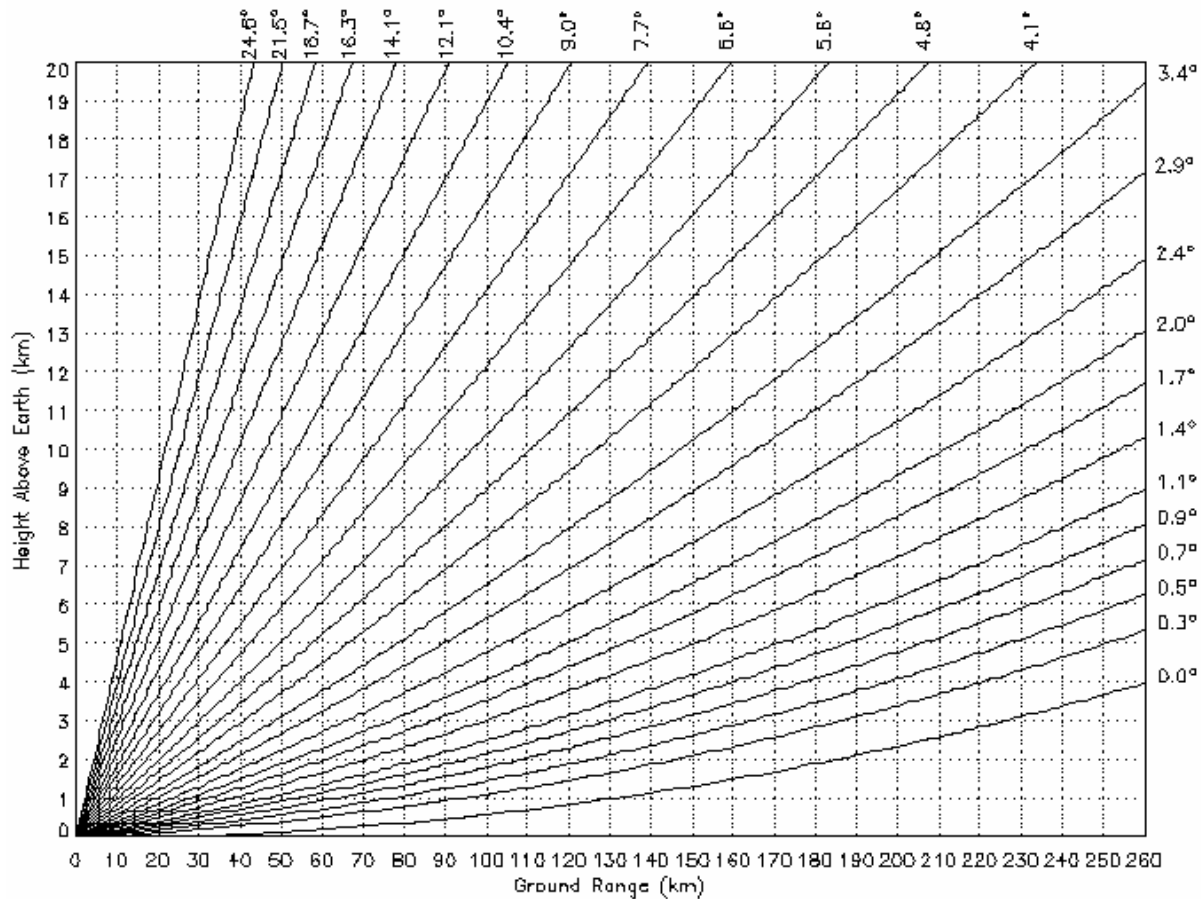


Figure 1: Height of radar beams at given elevation angles (in °) above the Earth (in km) given standard atmospheric conditions (Fogarty, 2013)

However, the atmosphere is rarely “perfect” and as such different atmospheric conditions will produce different values of refractivity which will change the way the radar beam propagates through the atmosphere. The radar beam will bend just like light as it passes through mediums with different refractivity. The radar beam’s propagation is governed by Snell’s Law (Equation 6). Deviations from the expected beam path are referred to as subrefraction and superrefraction. Subrefraction occurs when the atmosphere causes the beam to refract less than normal and the beam is actually higher than calculated. Subrefraction normally occurs when moisture increases with height (Hirt et al., 2010). Superrefraction occurs when the atmosphere causes the beam to refract more than expected and the beam is actually closer to the ground. Superrefraction commonly occurs due to a temperature inversion.

Equation 6: Snell's law of refraction from one medium to another

$$\frac{n_1}{n_2} = \frac{\sin \theta_2}{\sin \theta_1}$$

Refractivity is influenced by atmospheric pressure, temperature and the concentration of water leading to the relation defined in Equation 7.

Equation 7: Refractivity expressed with respect to pressure, temperature and water vapor pressure (Barué, 2008)

$$N = 77.6 \frac{P}{T} + (3.732 \times 10^5) \frac{e}{T^2}$$

Where T is temperature in Kelvin (K), P is atmospheric pressure in hPa and e is water vapor pressure in hPa.

The change in refractivity with height can be used to determine the refractive state of the atmosphere where (Willis, 2007):

- For a standard atmosphere: dN/dh is approximately -40 N-units per km
- dN/dh greater than -40 N-units per km is subrefractive
- dN/dh less than -40 N-units per km is superrefractive

While looking into how temperature inversions can impact the propagation of the radar beam, another factor was discovered called the local refraction coefficient introduced by Bahnert in 1987 as seen in Equation 8. The local refraction coefficient is used to produce GIS viewsheds (described more in Section 2.2.3).

Equation 8: Local refraction coefficient (χ) as a function of the vertical temperature gradient (Bahnert, 1987)

$$\chi = 503 \frac{P}{T^2} \left(0.0343 + \frac{\partial T}{\partial z} \right)$$

Where T is temperature in Kelvin, P is atmospheric pressure in hPa and $\frac{\partial T}{\partial z}$ is in K/m.

1.2.3 Canadian Radar Network

In Canada, the weather radar network consists of 28 C-band (5 cm wavelength) radar which are owned by EC, 2 C-band radars owned by the Department of National Defence and 1 S-band (10 cm wavelength) radar owned by McGill University (Fortin, 2014) (Figure 2). Presently, of the EC radars, 27 are singularly polarized Doppler radars and one is a dual-polarized Doppler radar, the King City weather radar. EC's weather radars emit energy at frequencies between 5600 – 5650 MHz (Environment Canada, 2011).

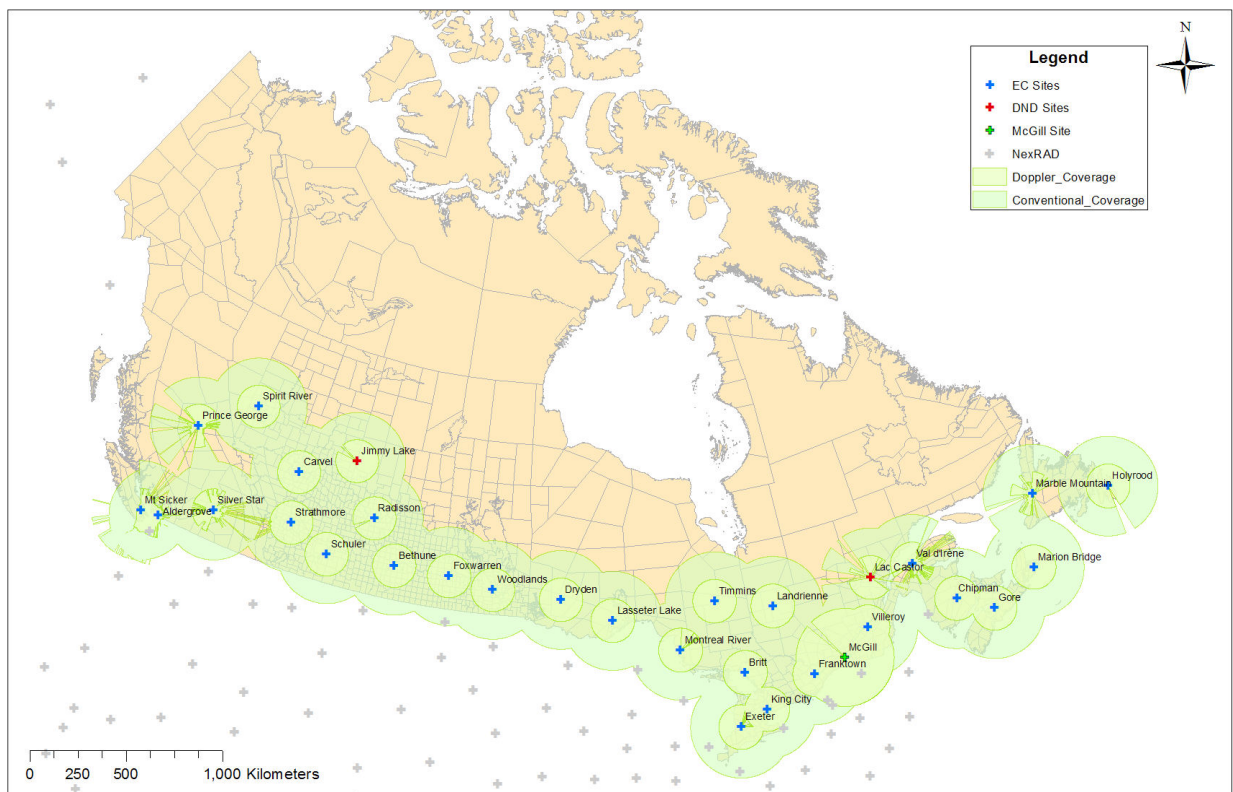


Figure 2: Radar site locations in Canada including EC sites, DND sites and the McGill radar site along with their Doppler and Conventional coverage

Weather radar data from EC go through many steps before being displayed to the general public or used for forecasting severe weather (Figure 3). EC's radar scan strategies define

which elevation angles to use in each scan. The elevation angles are defined as angles above and below the radar horizon where 0° represents energy emitted from the feed horn parallel to the ground. Common elevation angles used are between -0.6° and 24° . During a full ten minute radar scan, five different scan strategies are used. The first scan collects non-Doppler (conventional) data for 24 elevation angles and 360° . The other scans collect Doppler data for one specific elevation angle and 360° . During each scan, multiple signals are sent out based on the specified pulse repetition frequency (PRF). The PRF indicates how many pulses are sent out each second. For a single pulse, the returned energy comes back to the radar in the form of a signal called IQ (In-phase and Quadrature-phase) data. EC's weather radars then process the Level I IQ data using Vaisala's signal processor. The signal processor outputs Level II moment data such as mean radial velocity (V), spectrum width (W), corrected reflectivity (DBZ) and uncorrected total reflectivity (DBT) in the form of IRIS (Interactive Radar Information Systems) files. Ground clutter suppression is performed within the signal processor which can use the IQ data and transform them into a velocity spectrum. The velocity spectrums can then be edited to remove ground clutter.

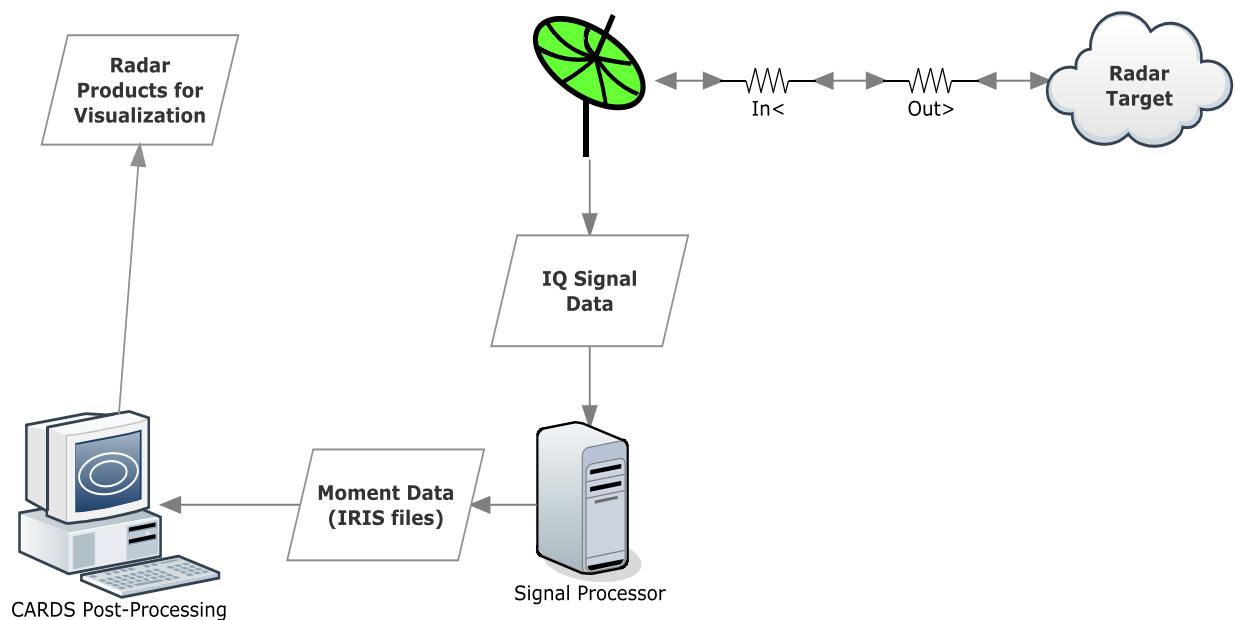


Figure 3: Simple flowchart of Environment Canada's radar signal, how it is processed and the output data

IRIS files are named by scan types such as CONVOL, DOPVOL1A, DOPVOL1B, DOPVOL1_C, and DOPVOL2. CONVOL is a conventional volume scan which scans 360° at 24 elevation

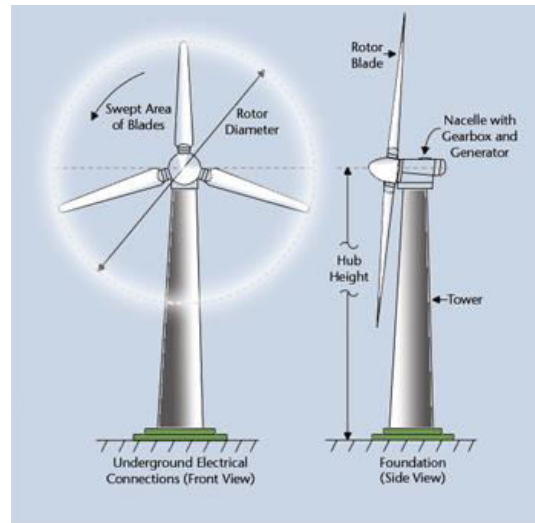
angles at radar specific beam widths with a resolution of 1° in azimuth by 1 km in range. The 24 conventional scans primarily measure reflectivity and have ranges out from the radar of up to about 250 km. DOPVOL (Doppler volume) scans collect both reflectivity and relative velocity data. Each DOPVOL1 scan type collects data at only one elevation angle for 360° with a resolution of 0.5° by 0.5 km out to about 128 km. The DOPVOL2 scan collects data at one elevation angle for 360° with a resolution of 1° by 1 km out to about 250 km.

EC utilizes an in-house radar product generator which processes Level II IRIS files to be displayed through CARDS (Canadian Radar Decision Support system). It is known within EC as URP (Unified Radar Processor) (Joe & Lapczak, 2002). CARDS was created to ingest Level II radar data, analyze it and produce imagery. CARDS is considered post-processing where additional clutter filters can be implemented producing Level III radar data. For visualization of the data, CARDS also has configuration files of background geography, or geodefs for each radar. Two different radar displays are commonly used, PPI (plan position indicator) and CAPPI (constant altitude plan position indicator) displays. PPI displays show a visualization of radar data at a specific elevation angle. CAPPI displays show a visualization of radar data at a constant altitude using blocks of CONVOL data to portray a horizontal cross-section of radar data. CARDS can produce outputs of many different radar products which are used internally by EC's meteorologists and some which are made public (described further in Section 2.3).

1.3 Wind Turbines

Wind energy is a renewable energy source. Wind turbines are tall structures composed of a fixed tower and rotating blades from a centralized rotor and control system (hub or nacelle). Recent wind turbine installations have tower heights around 100 meters and blade lengths of 50 meters, producing large structures approximately 150 meters high (Figure 4).

In order for the wind turbine blades to capture energy from wind, the system controller rotates the hub so that the plane of rotation of the blade is oriented approximately perpendicular to the direction of the incoming wind. The siting of wind towers in Canada involves wind resource assessments which are made using in-situ measurements from meteorological towers. Months and years of data from these meteorological towers are used with the turbine manufacturers' power curve to determine how much power can be extracted from wind turbines and wind farm as a whole.



Drawing of the rotor and blades of a wind turbine, courtesy of ESN

Figure 4: Components of a wind turbine (European Commission Energy, 2013)

1.3.1 Wind Energy in Canada

Wind energy is a growing sector in the energy industry in Canada, currently meeting 3% of Canada's electricity needs (CanWEA, 2014). There are numerous wind farms in Canada which are presently operating, in construction or in development. The current installed capacity in Canada (as at December 2014) is 9,219 MW spread out between 10 provinces and 2 territories (Figure 5). The Canadian Wind Energy Association (CanWEA) outlined a plan for wind energy development in Canada called "WindVision 2025" in the hopes for wind energy to meet 20% of Canada's electricity demand by 2025 (CanWEA, 2008). WindVision 2025 has brought on multiple federal, provincial and municipal initiatives which will increase the number of wind farms in Canada. The growing demand for wind power emphasizes the need to find a way for wind farms and Canadian weather radar to co-exist. The siting of wind turbines and connections to the energy grid are controlled on the provincial level.



Figure 5: Installed capacity of wind energy in Canada as at December 2014 (CanWEA, 2014)

1.4 Wind Turbine Impacts to Weather Radar Data

There are many interactions that can occur between weather radars and wind turbines. WTC occurs if the wind turbines are within RLOS. EC's tallest radar tower emits energy at 30 meters off the ground, while wind turbines have heights around 150 meters. Assuming flat terrain and standard atmospheric conditions, this means that a turbine within approximately 50 km of a weather radar has the potential to be visible to the radar beam (Equation 4 & Figure 1). Turbines are visible in the lowest angle radar scans which cause impacts to the radar scans used for the detection of shallow snow squalls and low level rotation of severe thunderstorms.

There are many factors which affect how wind turbines are seen on radar data, discussed in Section 1.4.2. Each wind farm interacts differently with each weather radar. Weather radar data contamination that occurs due to wind turbines is caused by three main impacts which are explored more in Section 1.4.1:

1. Radar beam blockage
2. Multi-path scattering
3. False reflectivity and velocity echoes

Some of these impacts can be mitigated and there is ongoing research into many fields which is discussed further in Section 1.4.3. Additionally, Section 1.4.4 provides a brief description of existing wind farms near Canadian weather radar sites.

1.4.1 Effects

Radar beam blockage was mentioned briefly in the description of ground clutter where objects within the radar beam can block all or a portion of the energy being emitted from the radar. An example of partial radar beam blockage can be seen in Figure 6 where three communication towers are located very close to the Montreal River weather radar. Although partial blockage is not as severe, any targets behind the blocking object, in that radial or radar beam ray, will be attenuated (have reduced reflectivity values).

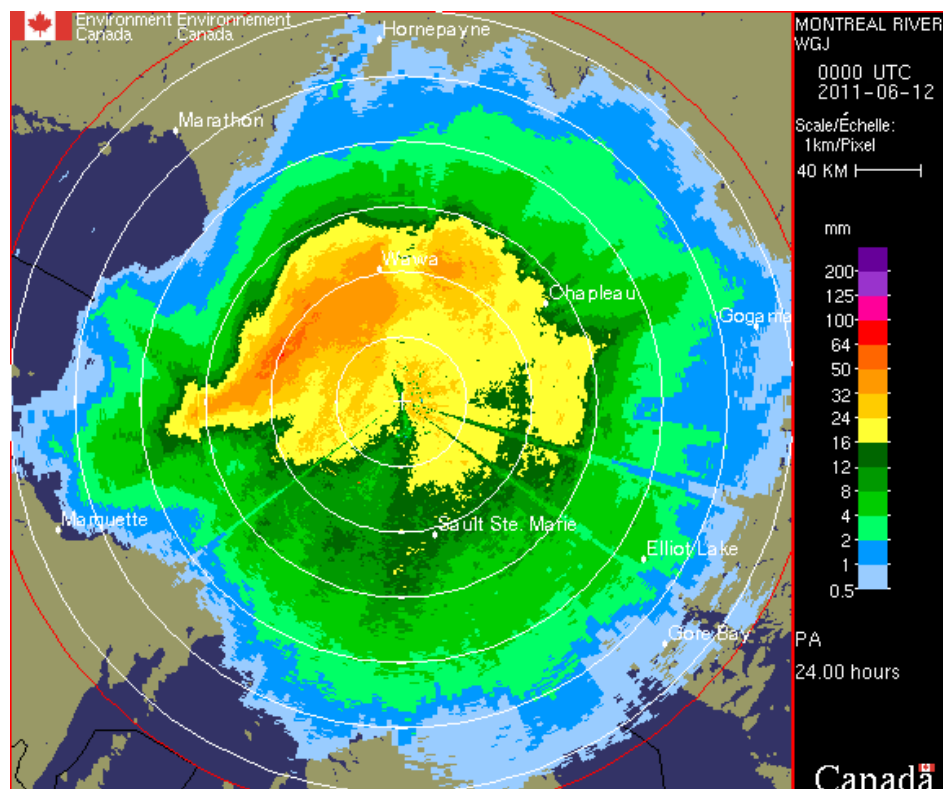


Figure 6: One day radar accumulation image at Montreal River weather radar with two radial lines to the southeast and one to the southwest of lower precipitation due to blockage from communication towers 31.56, 45.37 and 265 meters from the transmitting radar

In Figure 6, the radials where the towers are located have lower precipitation accumulation measurements than the surrounding areas because some of the energy in the radar beam is being blocked. Blockage becomes less of an issue if an object is further from the weather radar, as the beam is able to reform behind the object (RABC, 2013). In Canada, blockage from communication towers is evident up to about one kilometer from the radar. Similar blockage effects would thus be expected for wind turbine towers within one kilometer of a weather radar.

However, turbine towers are solid structures and may block more energy than communication towers which are thinner, lattice-type structures.

Another impact that can be caused by multiple turbines near a weather radar is multi-path scattering. Multi-path scattering occurs when the radar beam bounces between multiple targets before returning to the radar, and the radar processor subsequently depicts a ‘ghost echo’ – a long “spike” of low reflectivity behind the actual objects. The long spike occurs because the processor is unable to determine the location of the target as the pulse return time is longer when the energy scatters off multiple targets. Multi-path scattering can occur between wind turbines, wind turbines and the ground, or wind turbines and surrounding meteorological targets.

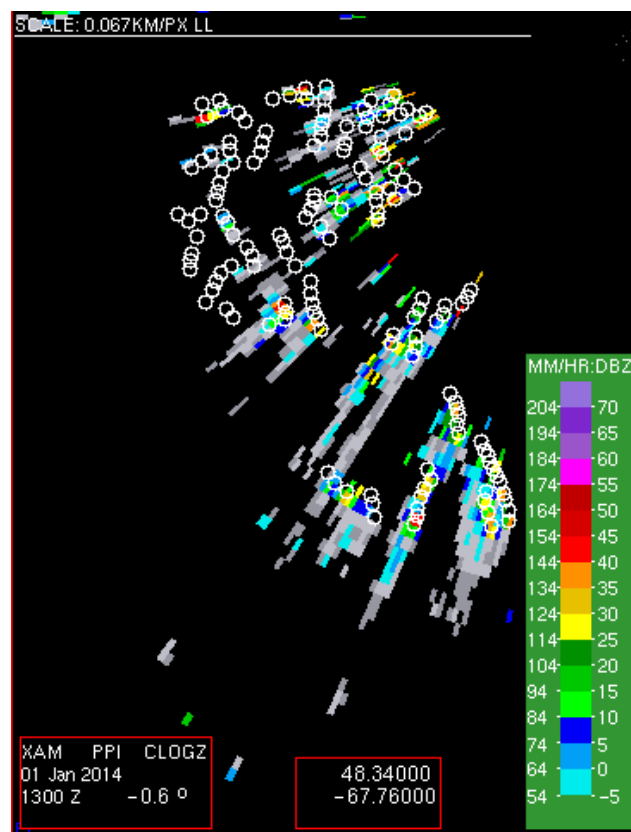


Figure 7: Multi-path scattering example at Environment Canada’s Val d’Irene weather radar where the white circles represent the locations of Lac Alfred wind turbines and the pixel colours represent Doppler corrected reflectivity (in DBZ)

Figure 7 displays a zoomed-in example of multi-path scattering in Canada at the Val d’Irene weather radar (XAM). The Lac Alfred wind farm consists of 75 wind turbines located approximately 9 km away from the radar. The locations of the individual turbines are shown by the white circles and the radar image shows Doppler corrected reflectivity in DBZ. Figure 7

illustrates these radial lines or spikes of reflectivity evident past the turbines themselves (with the XAM radar being located to the northeast of the wind farm).

Wind turbine blades and towers are extremely reflective to the microwave energy emitted and received by the weather radar. If blockage and multi-path scattering are not an issue with a particular wind farm, due to distance or elevation difference (to be discussed further in Section 1.4.2), there is still a possibility of reflectivity and velocity contamination. The ability to scatter microwave energy means that when the radar beam comes into contact with the wind turbines, a significant amount of energy is reflected back to the radar and registers with high reflectivity values in DBZ (decibels relative to equivalent reflectivity Z) (Equation 1 and 3). Some reflections caused by the stationary turbine towers can be filtered out as the towers have zero radial velocities. However, since the turbine blades are rotating, reflectivity measurements remain significant as seen in Figure 8. Since the Doppler velocity measurements are made relative to the position of the radar (i.e. towards or away), this means that in the position where the blade swept area is perpendicular to the radar beam (Figure 4 – left side) the blades will appear stationary to the radar. However, when the blades are oriented at any direction but perpendicular, the rotating blades can measure high tip speeds towards and away from the radar (seen as red and blue pixels in the bottom image of Figure 8). Such high velocity and reflectivity measurements can accompany severe weather, and thus wind farms with multiple turbines can look reminiscent of thunderstorm cells with wind shear.

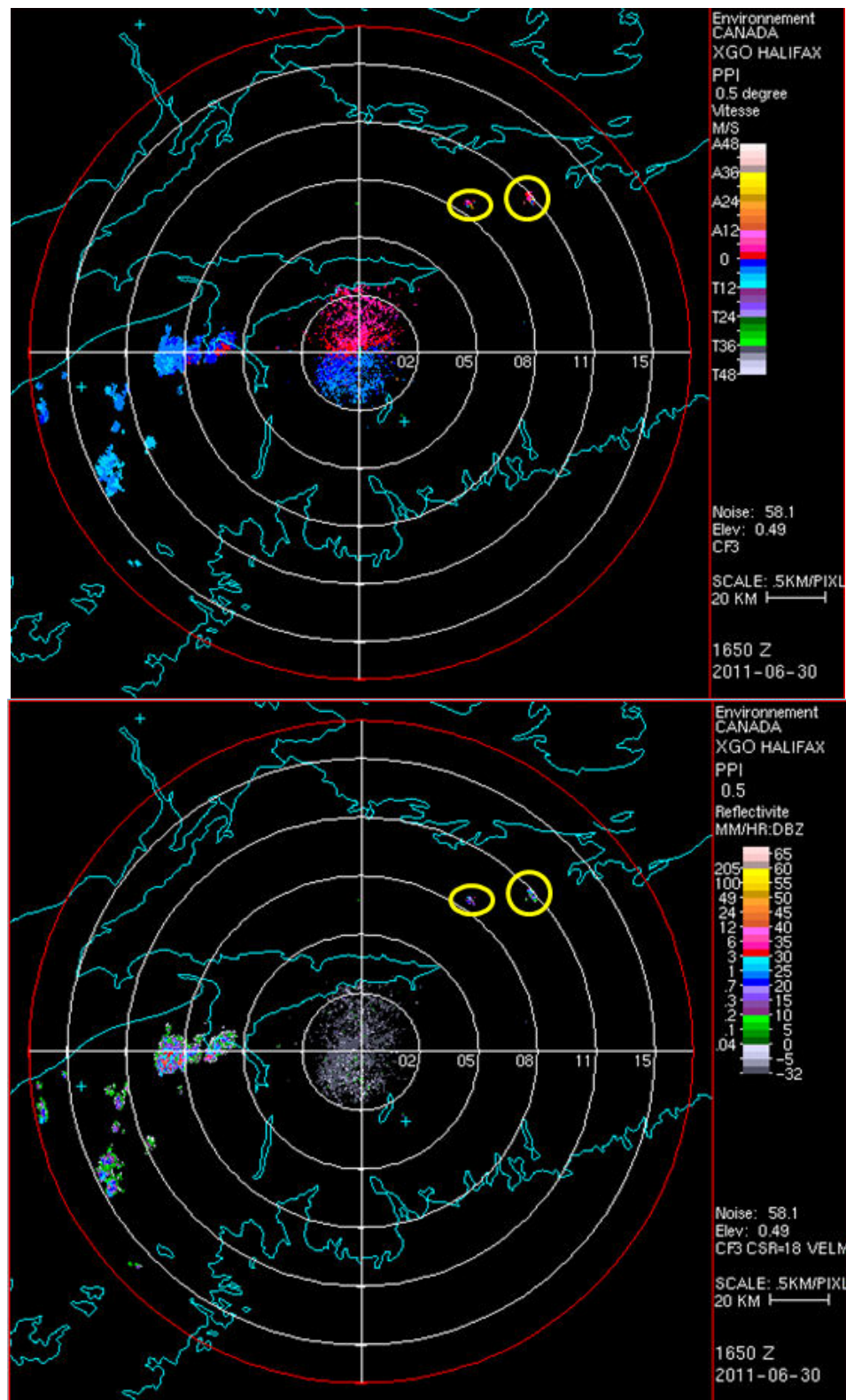


Figure 8: Radar reflectivity (top) and relative velocity (bottom) of two wind farms (circled in yellow) located approximately 60 and 80 km northeast of the Gore weather radar in comparison to weather in the west

Additionally, due to these high reflectivity returns, overestimations of precipitation can occur in what are referred to as QPE's (Quantitative Precipitation Estimates). QPE's are created by summing up the radar reflectivity values over different time periods (such as hours, days or months). Since radar reflectivity can be used as an estimate of the precipitation amounts in an area (i.e. mm/hr or cm/hr) using Z-R relationships, adding up consecutive reflectivity data can produce estimations of how much precipitation accumulated during that time period. Areas where wind farms are in RLOS will have QPE's which greatly overestimate the actual precipitation accumulated in that area. For example, in Figure 9 pixels within the two wind farms have accumulation values up to 250 mm during the 7-day period whereas the surrounding pixels are more on the order to 20-40 mm. Additionally, blockage is seen from a communication tower to the south west with the radial experiencing attenuation with reduced accumulation values

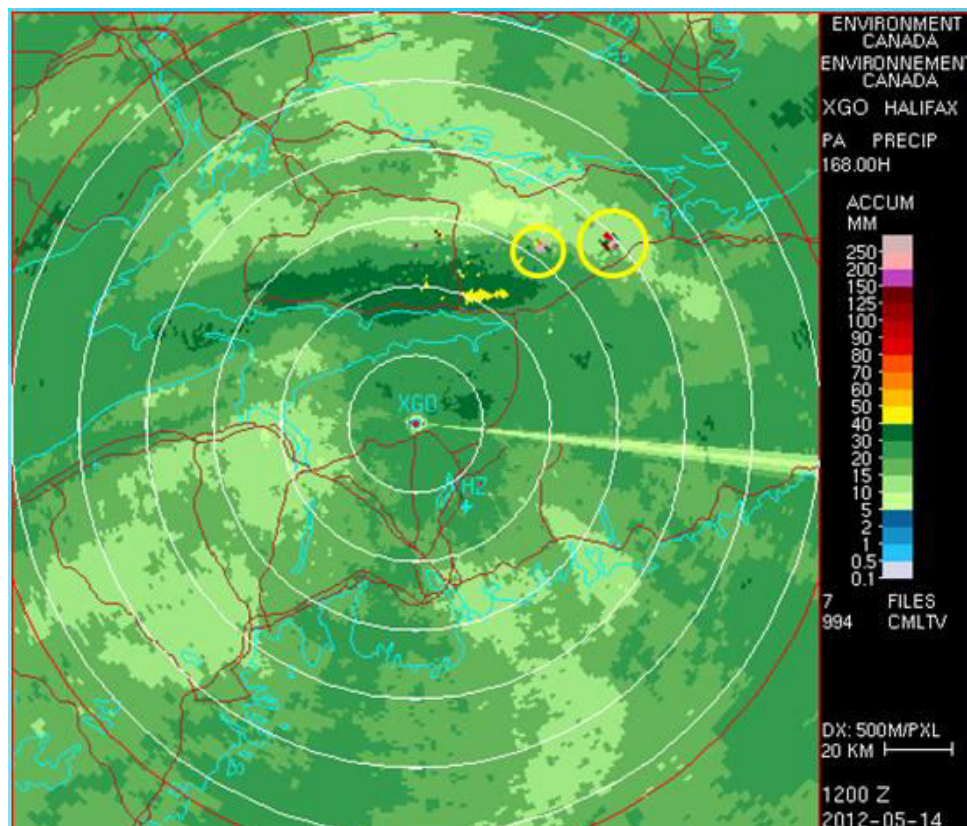


Figure 9: 168 hour (7-day) radar accumulation product from the Gore weather radar near Halifax, Nova Scotia. Two wind farms are circled which show overestimations of precipitation and partial blockage is seen to the east-southeast from a nearby (74.32 m away) communication tower.

1.4.2 Factors Affecting Detection of Wind Turbine Clutter (WTC)

The radar returns from wind turbines are highly variable and are dependent on a number of factors including local topography, curvature of the Earth, atmospheric conditions and the orientation of the wind turbines. As previously mentioned, although the radar beam may be travelling straight, the radar beam will seem to bend upwards with distance as seen in Figure 1 and explained in Equation 4. This means that, normally, less contamination is expected if wind turbines are further from the radar; however, local topography (or terrain elevation) needs to be accounted for. Ideally, weather radars would be most effective when placed on elevations higher than the local terrain. However, radar siting is not always ideal and higher topography may still exist. Figure 10 shows a wind farm that is visible on weather radar although it is located about 100 km away. The wind farm appears due to its location on a high ridge. Additionally, if terrain exists that is already blocking a sector of the radar, such as a mountain range, wind turbines placed behind this terrain would not make a difference to the impact of data in that sector as they would no longer be within RLOS.

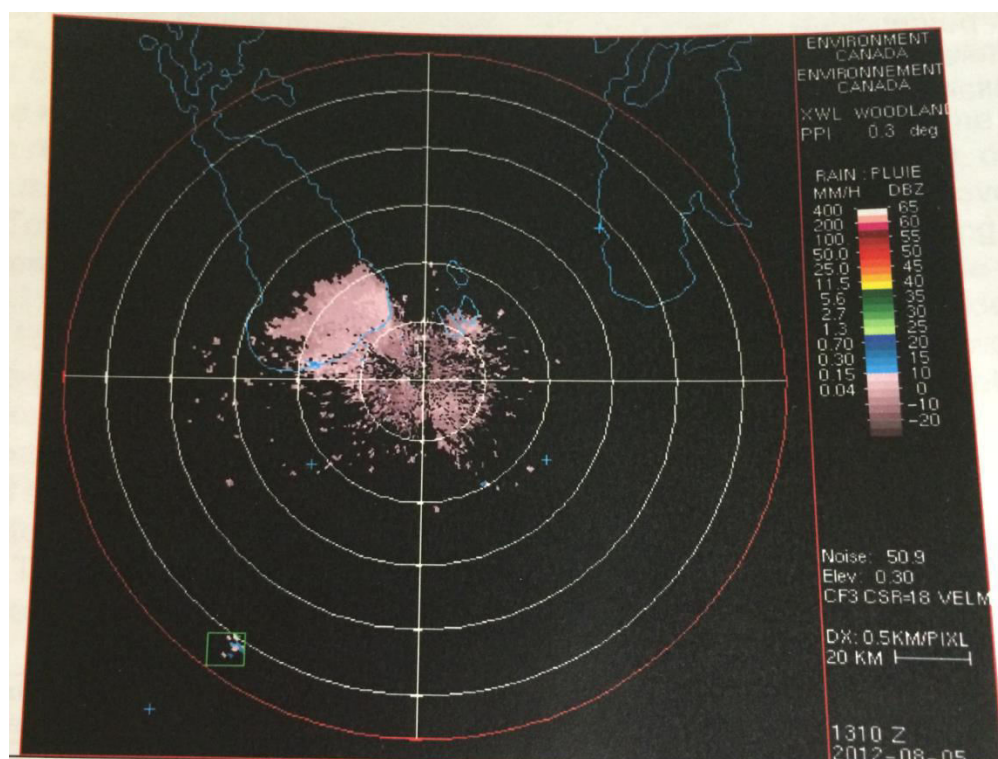


Figure 10: Wind turbine contamination (green box) approximately 100 km from the weather radar (center) in Manitoba on a clear air day with no significant weather in the area

Even when taking into account RLOS, there are cases where wind farms contaminate weather radar data unexpectedly. Standard RLOS calculations are performed on the main beam, however there are side lobes which are additional energy sent and picked up outside of the main cone shaped beam. Although a turbine may appear to be out of RLOS, the radar beam can be refracted towards the ground due to its particular propagation through the atmosphere (Hood et al., 2010). As described in Section 1.2.2, atmospheric superrefraction can occur where the radar beam is bent down towards the Earth due to changes in relative humidity or when there are temperature inversions in the atmospheric profile (Hirt et al., 2010). These atmospheric changes may occur suddenly due to changing weather patterns or incoming fronts, may be standard for a particular climate, or may change due to diurnal variations. Atmospheric ducting may occur with strong temperature inversions and is prominent in the morning hours. The modeling and impact of atmospheric propagation is explored further in the following chapters.

A further influence on the impact of WTC is the number of turbines in the wind farm. Multi-path scattering contamination is proportional to the number of turbines, as there are more targets for the beam to bounce off of. However, the impact can change based on the layout of the wind farm. The most preferable, and least detrimental, layout would be when the turbines are lined up in a radial with respect to the radar (i.e. one behind the other) (Vogt et al., 2009). The line of turbines would then only cause impacts to that radial, limiting the amount of blockage, if applicable, and limiting the span of contamination due to attenuation.

The variation and occurrence of WTC is also affected by the orientation of the wind turbines. For commercial turbines, turbine orientation is controlled by sensors that attempt to maximize energy production by orienting the blades perpendicular to the direction of the wind (ProQuest, 2008). Since Doppler algorithms can filter out targets which are not moving with respect to the weather radar, this means that if turbine blades are “perfectly” perpendicular to the weather radar they could be filtered out. This also means that the worst-case scenario for velocity interference would then be when the wind turbine blades are parallel to the weather radar (Nai et al., 2011). The reflectivity however, would be at a minimum when the blades are parallel to the weather radar and a maximum when the blades are perpendicular to the radar due to a greater radar cross section (Kong et al., 2013). Although WTC in both velocity and reflectivity is variable, with a given wind direction an estimation of the severity of contamination could be made.

1.4.3 Identification and Mitigation of Wind Turbine Clutter (WTC)

In order for wind turbines and weather radars to co-exist, mitigation measures need to be explored and implemented. The ultimate solution for the suppression of WTC would be an upgrade to the radar's signal processor. Ideally, the WTC signature would be separated from the radar data and filtered out without removing any important weather information. Since WTC is so variable, research has been conducted in order to identify WTC within weather radar data. At this time, identification has only been made possible using Level I radar time series data (IQ data). Studies performed in Spain (Gallardo-Hernando et al., 2008) and in the United States (Isom, 2007) have been able to identify WTC as discrete flashes across Doppler spectrum data. The methods for identification have not been made in real-time operational modes as of yet. Additionally, at this time, IQ time series data are not operationally collected in Canada's weather radar system so any identification would have to be done in the Level II moment data (IRIS files) or after processing in CARDS (Level III radar data).

Over the years, many strategies have been suggested and some employed in order to mitigate WTC. With respect to Level I IQ radar data, promising research has been produced in this field in the United States in association with the National Oceanic and Atmospheric Administration (NOAA) and the University of Oklahoma. Studies began in 2006 to gather IQ time series data of WTC from two weather radar sites (Isom, 2007). Mitigation was explored using multiquadratic interpolation schemes but it was determined to not be useful for operational purposes as it reduced the resolution of the radar data (Nai et al., 2011). Interpolation schemes were also explored in Spain (Gallardo-Hernando et al., 2010). Further research led to the creation of an automatic detection algorithm in 2009. The algorithm used temporal and spectral features along with fuzzy logic to identify WTC (Hood et al., 2010). Next, mitigation methods were explored using range-Doppler domain signal processing. However, the technique produced a model which did not work well for weak contamination (Nia et al., 2011). Studies are continuing in the field including looking into WTC in dual-polarized radar data (Kong et al., 2013) as well as characterizing the small scale micro-Doppler radar signature of WTC (Kong et al., 2014).

Provided a signal processing strategy is proven successful, an operational solution (available to EC's meteorologists and the general Canadian public) would still not be available for a number of years. In the short-term there are four main types of mitigation options available including: siting considerations of both the radar and turbines; adjustments to the material and operation of

the wind turbines; adjustments to the operation of weather radars; and the implementation of supplementary instruments.

Since WTC occurs when a wind turbine is within RLOS, one strategy would be to move the turbines or the weather radar tower. By adjusting the relative locations and using proper siting considerations, WTC could be reduced (Kong et al., 2013). Considerations in terms of adjusting the material of the wind turbines themselves have been explored by the wind turbine company Vestas Wind Systems. The company has been working on the development and implementation of stealth blades covered with frequency-specific paint to absorb specific wavelengths of energy. In France, EDF Energies Nouvelles is working to install Vestas-built turbines using stealth blade technology (Douet, 2014). The paint would prevent the energy from returning back from the radar and, in theory, eliminate WTC.

Another potential strategy is wind turbine curtailment. Curtailment involves an agreement made between weather forecasters and wind farm operators in which the forecasters would notify the operators to stop the turbine blades during severe weather situations so the radar data would become free of contamination. In the United States, three agreements are presently in place (Ciardi, 2013). Additionally, changes could be made to the operation of the weather radars. Depending on which elevation angles are used to scan for meteorological targets, using higher operational elevation angles could mean wind turbines would no longer be in RLOS. However, this method is not preferred by meteorologists as the low levels of radar data are critical for the detection of severe weather. A final mitigation strategy would be employing supplementary meteorological instruments. This could be as simple as weather stations sensors and as advanced as in-fill / gap-fill weather radars (Brenner et al., 2008).

Since weather radar data in Canada are post-processed using CARDS, there is currently potential to implement adjustments to the display of processed radar data. This could be done by simply identifying the location of the wind farms using C-TRIP wind farm boxes (Section 2.3.1). The display could assist meteorologists in the identification of wind farms in Canada. Recent initiatives made by the Radar Operations Centre in the United States include the overlay of GIS polygons similar to those developed in this thesis (Ciardi, 2013).

1.4.4 Wind Farms in Proximity to Environment Canada Weather Radar

Given the impacts of wind turbines to weather radar data, in 2007, Environment Canada's National Radar Program (NRP) began analyzing and consulting with wind energy proponents

wishing to construct wind farms in close proximity to a weather radar. Siting considerations provided by the Radio Advisory Board of Canada (RABC) originally stated consultation should be made with wind farms proposed within 80 km of a weather radar site. However, given the influx of consultation submissions this was adjusted to 50 km (RABC, 2013). In 2011, increased interest in NRP's wind farm file resulted in the hire of the thesis author to catalogue existing and proposed wind farms in Canada. An Existing Canadian Wind Farms database was developed and individual turbine locations were plotted with the use of ArcGIS, Google Earth maps, and available industry information (Figure 11). A recent update of the database (as of July 31, 2013) identified at least 73 wind farms within Doppler range (128 km) of a Canadian weather radar and at least 15 wind farms within 50 km of a weather radar. Internal NRP studies and consultations resulted in the selection of the three wind farms used in this thesis (Section 2.1).

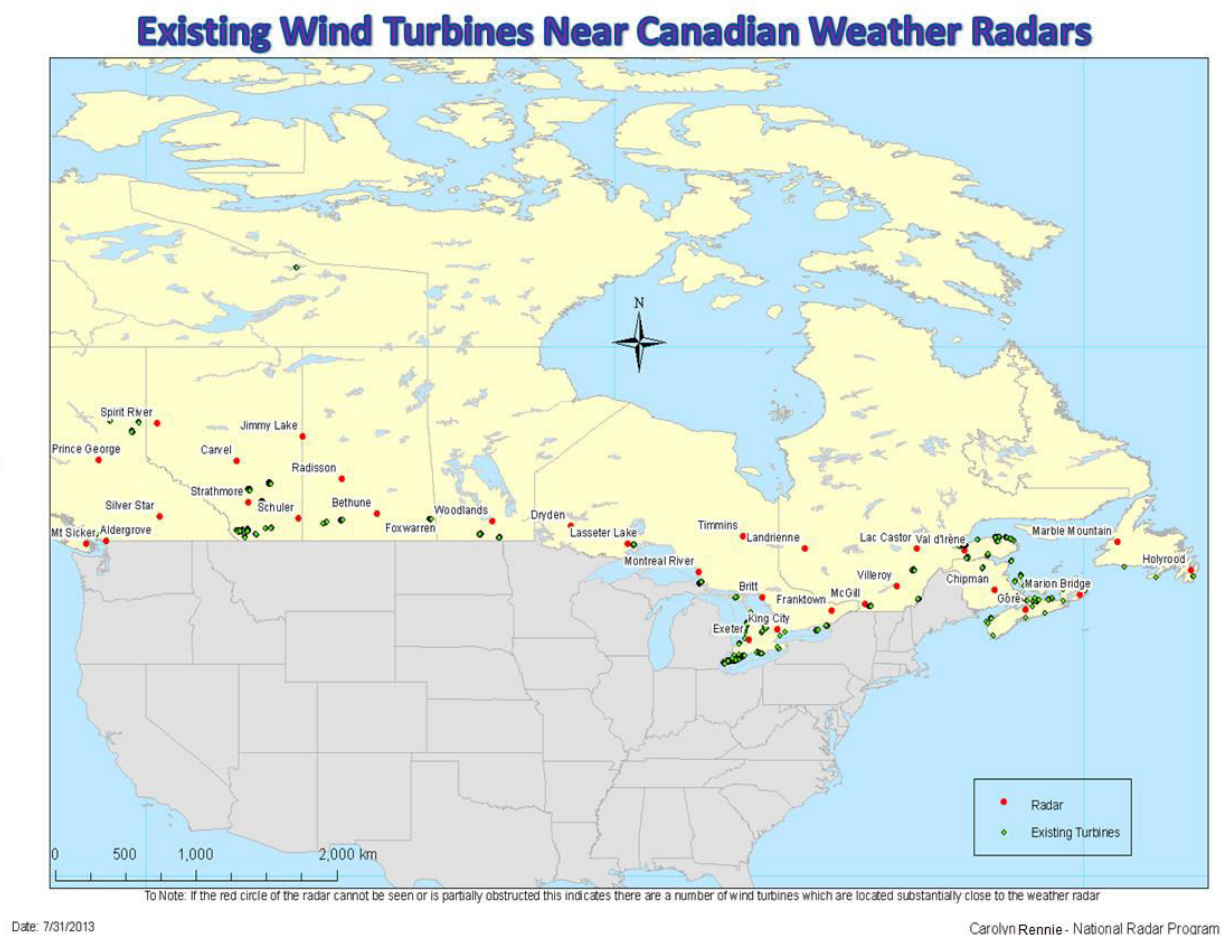


Figure 11: Location of existing wind turbines (green diamonds) in Canada (as at July 31, 2013) with respect to Canadian weather radars (red).

2. Analysis Methodology

The following chapter details the wind farms selected and tools developed in order to meet the thesis objectives including: three tools used to determine RLOS, two tools used to visually display radar data, and two models created to assist in radar beam propagation calculations and wind turbine orientation. Additionally, this chapter outlines the data required to complete the respective analyses.

2.1 Wind Farm Selection

As previously stated, there are over 73 existing wind farms in Doppler range of Canadian weather radars. Each wind farm / radar pair is different based on many different factors including: the local terrain, distance from the radar, number of turbines, size of the turbines, layout of the turbines, and the radars' scan strategy. Informal analysis has been completed on all existing Canadian wind farm / radar pairs by the thesis author.

Two main factors were considered when selecting which wind farm / radar pairs to study in this thesis:

1. The divergence from expected outcomes vs. the observed WTC
2. Variability or consistency of WTC

Through consultation with EC's research scientists, engineers, and meteorologists the Nuttby Mountain, Melancthon (phases I & II), and Greenwich Lake wind farms were selected. Table 1 provides some brief information about the wind farm / radar pairs but each are described in more detail in Chapter 3.

Table 1: Wind farm / radar pairs selected for case studies including wind farm name, number of turbines, radar name and ID as well as minimum distance from the radar to the wind farm

Wind Farm Name	# of Turbines	Radar Name	Radar SiteID	Distance (km)
Greenwich Lake	43	Lasseter Lake	XNI	22
Melancthon (I&II)	133	King City	WKR	55
Nuttby Mountain	22	Gore	XGO	62.5

2.2 Radar Line of Sight (RLOS)

Wind turbines cause impacts to weather radar data when they are within line of sight of the weather radar. Calculations of RLOS can provide an early warning as to the impacts which may

occur and aid in proper wind turbine siting. For the purposes of providing a full analysis of RLOS for each selected wind farm / radar pair, the following tools have been developed and used.

2.2.1 Wind Farm Analysis

The first tool used to analyze RLOS is the “Wind Farm Analysis” software which was created by Dr. Norman Donaldson of EC. The tool was originally developed in 2007 to provide the NRP a quick summary as to whether or not proposed turbine locations would be visible to any Canadian weather radar site.

In order to complete the Wind Farm Analysis, there are mandatory and optional inputs required which are outlined on EC’s website (EC, 2013):

1. Height of turbine tower(s)
2. Turbine blade sweep diameter (or length of turbine blades)
 - a. With the assumption that diameter = 2 x blade length
3. Turbine base diameter (optional)
4. Coordinate locations of turbine(s) either in:
 - a. Latitude and Longitude in decimal degrees format
 - b. UTM (Universal Transverse Mercator) coordinates with zone reference
 - c. If coordinate locations are not known a central wind farm coordinate location would suffice

The software was created in the C programming language preset with a SRTM03 (Shuttle Radar Topography Mission - 2003) digital elevation map (DEM). Additionally, the program includes information on the location of existing weather radar including their geographic position, ground height above sea level, and the height above the ground the radar antenna transmits at (feed horn height). Once the turbine information is submitted a formatted CSV file of the turbine locations and heights is created. To run the software, there are two configurable files used: “dataInjestConfig” and “siteCheckConfig”. When run, the dataInjestConfig converts the provided inputs into a “standard” CSV file which is used in the siteCheckConfig. Once the inputs are provided, the software estimates RLOS based on standard atmosphere propagation (with $K = 4/3$ based on Equation 4), DEM, and the closest weather radars. The outputs of the software include analysis for each wind turbine / radar pair. Each wind turbine / radar pair is then modeled to determine a cross-section of the ground elevation and the height of the radar beam

as it travels from the radar towards the turbine. Once completed, this is visualized in a GIF file (Figure 12).

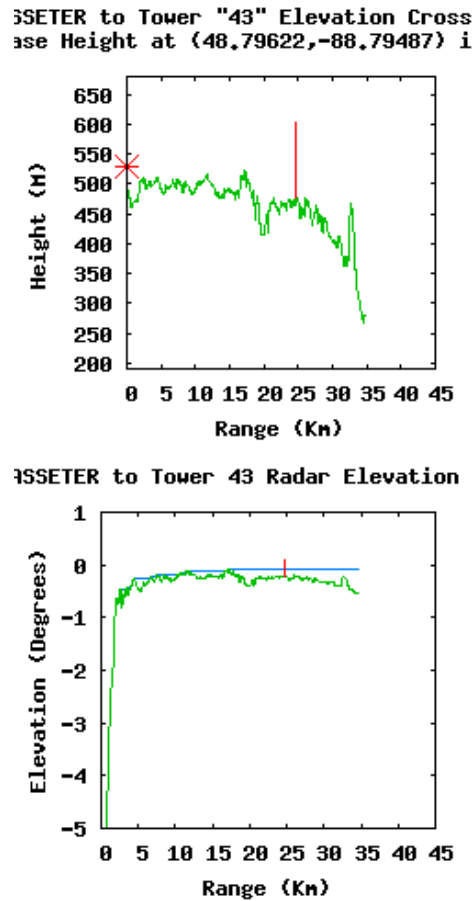
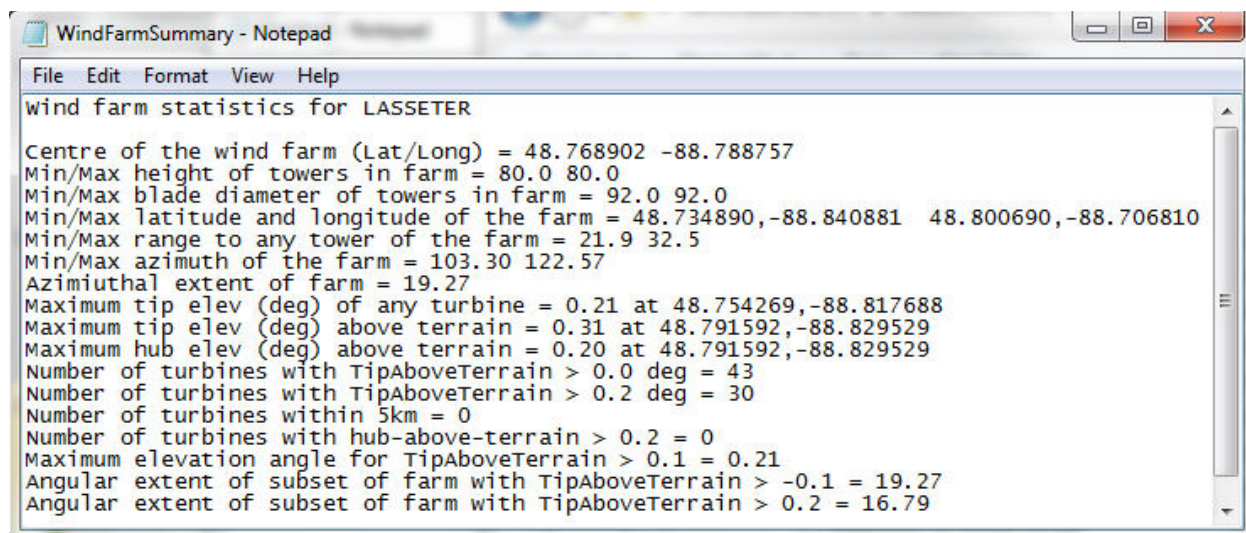


Figure 12: Wind Farm Analysis output GIF file: The top image shows the ground elevation in green, the radar as a red star, and the turbine as a red line. The second image presents a depiction of the radar beam and its elevation angle. Blue lines indicate any existing terrain blockage.

The software also produces a "Wind Farm Summary" text file containing statistics specific to the interaction between the input wind turbine(s) and the nearest weather radar. The Wind Farm Summary file also contains key information used to determine the impact of the wind farm including: the location of the center of the wind farm, the range of the wind farm to the radar in km, the azimuthal extent of the wind farm relative to the radar, and tip/hub elevation information. An example of the output can be found in Figure 13.



```
WindFarmSummary - Notepad
File Edit Format View Help
wind farm statistics for LASSETER

Centre of the wind farm (Lat/Long) = 48.768902 -88.788757
Min/Max height of towers in farm = 80.0 80.0
Min/Max blade diameter of towers in farm = 92.0 92.0
Min/Max latitude and longitude of the farm = 48.734890,-88.840881 48.800690,-88.706810
Min/Max range to any tower of the farm = 21.9 32.5
Min/Max azimuth of the farm = 103.30 122.57
Azimuthal extent of farm = 19.27
Maximum tip elev (deg) of any turbine = 0.21 at 48.754269,-88.817688
Maximum tip elev (deg) above terrain = 0.31 at 48.791592,-88.829529
Maximum hub elev (deg) above terrain = 0.20 at 48.791592,-88.829529
Number of turbines with TipAboveTerrain > 0.0 deg = 43
Number of turbines with TipAboveTerrain > 0.2 deg = 30
Number of turbines within 5km = 0
Number of turbines with hub-above-terrain > 0.2 = 0
Maximum elevation angle for TipAboveTerrain > 0.1 = 0.21
Angular extent of subset of farm with TipAboveTerrain > -0.1 = 19.27
Angular extent of subset of farm with TipAboveTerrain > 0.2 = 16.79
```

Figure 13: Example of a Wind Farm Summary output text file provided by Environment Canada's internal Wind Farm Analysis software

Another useful output of the software is the visEstimates.dat file. This file contains a summary of the visibility estimates for each wind turbine including the range from the radar, the turbine's bearing (or angle) from the radar, the turbine's coordinates in latitude, longitude or UTM, the relative radar elevation angle to have the top of the tower (hub) visible, and the relative radar elevation angle to have the tip of the blades visible. Some of these data are used in the IDL Beamwidth program described in Section 2.2.2.

One of the most crucial data points obtained from the Wind Farm Analysis software is the tip and hub elevation information. The software considers the elevation angle of the center of the main radar beam as it travels through the atmosphere. For each wind turbine, the tip and hub elevations above terrain, or visibilities, are calculated which represent the maximum elevation angle the radar would need to be pointed to "see" the turbine blades (tip) or towers (hub). For example: a tip visibility of 0.31° with a hub visibility of 0.20° means the turbine tips will be visible for all radar elevations less than or equal to 0.31° and the towers will be visible for all radar elevations less than 0.20°. Knowing the specific radar scan strategy and the tip or hub visibilities, one can determine which scans will be impacted by the wind turbine(s).

The final output is a KML (Keyhole Mark-up Language) file which can be viewed in Google Earth illustrating the locations of the turbines (pin colours defined in Table 2) relative to the radar (red pushpin) (Figure 14).

Table 2: Wind Farm Analysis output KML Google Earth pin colors with respect to tip visibility

Pin Colour	Description
Red	Radar
Green	Tip vis < 0.0°
Yellow	0.0° < Tip vis < 0.19°
Pink	0.2° < Tip vis < 0.49°
Purple	Tip vis > 0.5°

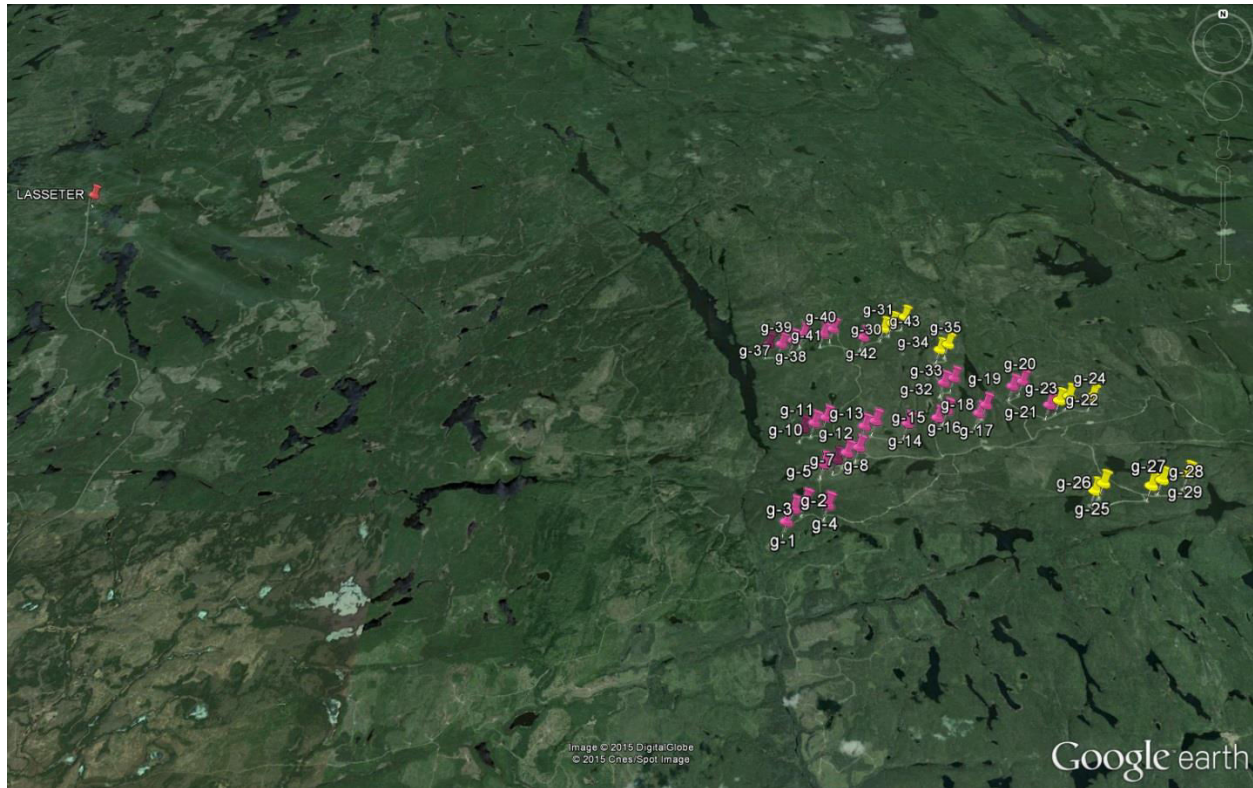


Figure 14: Wind Farm Analysis KML output example where the radar is indicated in red and the turbines are indicated with colours which define their turbine tip visibility (as seen in Table 2) displayed in Google Earth.

2.2.2 IDL Beamwidth

The next tool, “IDL Beamwidth” was developed originally by Sudesh Boodoo of EC and was later modified by York University Earth & Space Science Master’s candidate and former NRP employee Joanne Kennell and the thesis author. The tool was developed using IDL (Interactive Data Language) and a program file called “calc_beamheight.pro” (Appendix A). The program provides a visualization of the radar beam with respect to terrain as seen from one specific Canadian weather radar at one specific azimuthal angle. Originally only the center of the main beam was modeled; however, modifications were made to allow the program to display the

whole main beam (including top and bottom of the main beam calculated using the radar specific beam width). The tool uses input wind turbine and radar information as well as radar specific digital elevation model (DEM) metafiles (XXXTopo_edit.met) to calculate RLOS. The IDL program then produces a horizontal cross-section depicting the main radar beam and location of the turbine (Figure 15). The program has many configurable options which are outlined below (in order of their appearance in the code found in Appendix A):

- `bw = #`
 - This variable represents the radar beam width which is either 1.1 or 0.65 depending on which radar is being used
- `xrng = [0,#]`
 - This defines the range of the x-axis and can be adjusted depending on the distance from the distance of the turbine and the view the user wishes to have in the output image
- `yrange = [0,#]`
 - This defines the range of the y-axis and can be adjusted depending on the height of the terrain and radar for each case
- `'XXXTopo_edit.met'`
 - This opens up the DEM meta file created for each radar based on the 3 character radar siteID (XXX)
- `az = #`
 - This variable represents the azimuth direction of the turbine
- `oplot,[X,X],[Y,Y], linestyle = #`
 - This creates a line to be used for the turbine tower or blade based on a defined X location (range from radar) and two defined Y locations (start and stop of line) along with a line style of solid (0) or dashed (3)
- `elev_arr0 = [#,#,#,#...]`
 - This is used to define which elevation angle(s) will be used to display the radar beam
- `tle = '...'`
 - This is the title used on the image
- `pngout = '...'`
 - This is the name of the output image
- `h0 = #`

- This is used to define where the main beam will start at as the radar height above sea level and height of the radar feed horn

Figure 15 is an example of the output image where height above sea level is on the left of the chart (y-axis) and range from the radar on the bottom (x-axis). The green line indicates the height of the terrain, the black solid line indicates the turbine tower, the black dotted line indicates the turbine blade, the red lines indicate the center of the main radar beam elevation angles 0.2° and 0.5° , and the blue lines indicate the sides of each main radar beam as defined by the radar beam width. The output can be used to determine if the turbine will be visible to the radar and at which elevation angles. The visualization can also provide insight into possible terrain blockage and what percentage of the radar beam (in the vertical) will be affected by the wind turbine.

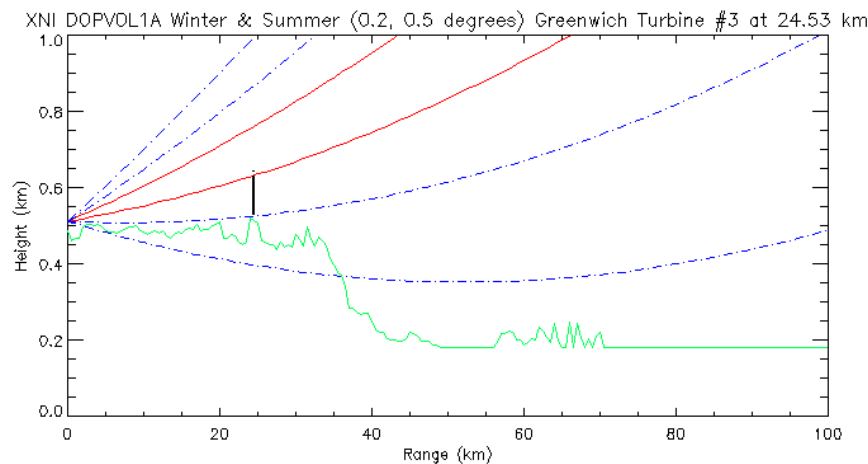


Figure 15: IDL Beamwidth output example of the appearance of a specified turbine located at 24.53 km from XNI (Lasseter Lake weather radar) with DOPVOL1A elevation angles 0.2° (winter) and 0.5° (summer).

2.2.3 GIS Viewsheds

The next tools used to illustrate and visualize RLOS are GIS viewsheds. ArcGIS is a geographic information system (GIS) software created by ESRI. The ArcGIS viewshed tool produces an output of a raster surface which can identify which locations will be visible from a specific observation point. A raster surface is a representation of a real-world object utilizing pixels (or cells) rather than lines (vector format). The viewshed raster surface is binary with an output of 1 or 0 (1 being visible and 0 being not visible). The main input for the viewshed tool is a surface elevation raster such as a digital elevation model (DEM) with pixel values representing ground

height. The second input required is an observation point location. For this thesis, the observation point is considered to be the location of the weather radar. Additionally, certain variables need to be pre-set into the attribute table (Table 3) of the observation point and these variables are described below:

Table 3: Snapshot of input attribute table of observation points used to create ArcGIS viewsheds

Site Name	SiteID	Lat	Lon	OFFSETA	OFFSETB	VERT2	RADIUS2
Aldergrove	WUJ	49.01661	-122.48706	20.4	100	0.3	250000
Bethune	XBE	50.57117	-105.18267	15.1	100	0	250000
Britt	WBI	45.79313	-80.53378	27.5	100	0	250000
Carvel	WHK	53.56052	-114.14481	14.1	100	0	250000
Chipman	XNC	46.22211	-65.69917	23.1	100	0.1	250000
Dryden	XDR	49.85809	-92.79675	29	100	0.1	250000
Exeter	WSO	43.37199	-81.38056	23.5	100	-0.1	250000

- OFFSETA is the height of the observation point (Figure 16) above the ground in meters
 - Defined as the height the radar beam is being emitted from (or the feed horn height)
- OFFSETB is the height of the object being viewed above the ground in meters
 - Defined as the height of the turbine tower or the total height of the turbine from the ground to the blade tips
 - An example turbine of tower height 100 meters is used in Table 3



Figure 16: Illustration of how OFFSET's are determined (ArcGIS, 2012)

- AZIMUTH1 & AZIMUTH2 are values indicating direction in degrees based on Figure 17
 - The default values in ArcGIS' viewshed tool are 0° & 360° respectively so as to cover an entire circle around the radar (Figure 19)
 - Since the default values are the values required, this information does not need to be included in Table 3

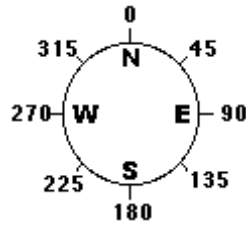


Figure 17: Direction values of azimuth in degrees (°) (ArcGIS, 2012)

- VERT1 & VERT2 are values indicating vertical elevation angles in degrees above or below the radar horizon (0°) (Figure 18)
 - The default values in ArcGIS' viewshed tool are 90° and -90° respectively to cover all vertical angles
 - Since radars scan at specified elevation angles, the lowest angle (VERT2) is defined as each radar's lowest scanning angle
 - VERT1 does not need to be defined in this case because if the turbine is visible at VERT2 it will be visible at VERT1 as well

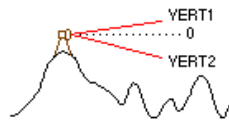


Figure 18: Illustration of the angles for VERT1 & VERT2 (ArcGIS, 2012)

- RADIUS1 & RADIUS2 are values indicating the distance the viewshed should search out to in meters (Figure 19)
 - RADIUS1 indicates where the viewshed should start (default 0 m – or at the radar location)
 - RADIUS2 indicates where the viewshed should end
 - RADIUS2 is defined as 250 km in Table 3 (conventional range of Canadian weather radars)

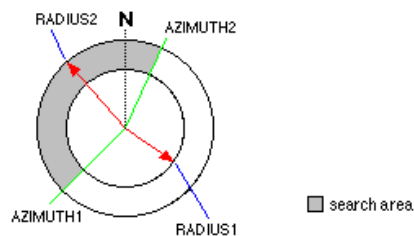


Figure 19: Illustration of the distances RADIUS1 and RADIUS2 as well as AZIMUTH1 and AZIMUTH2 (ArcGIS, 2012)

The final variable to be defined is the local refractivity coefficient which is used as an Earth curvature correction and varies depending on atmospheric conditions (Equation 8). The default value of 0.13 represents the average value of refractivity in standard atmospheric conditions calculated by Carl Friedrich Gauss (Hirt et al., 2010). The ArcGIS viewshed tool creates an output where locations are identified within the range defined which would be visible to the observation point. Figure 20 illustrates an example viewshed output where green areas are visible to the observation point and pink areas are not visible to the observation point. Chapter 3 provides viewsheds specific to each wind farm / radar pair.

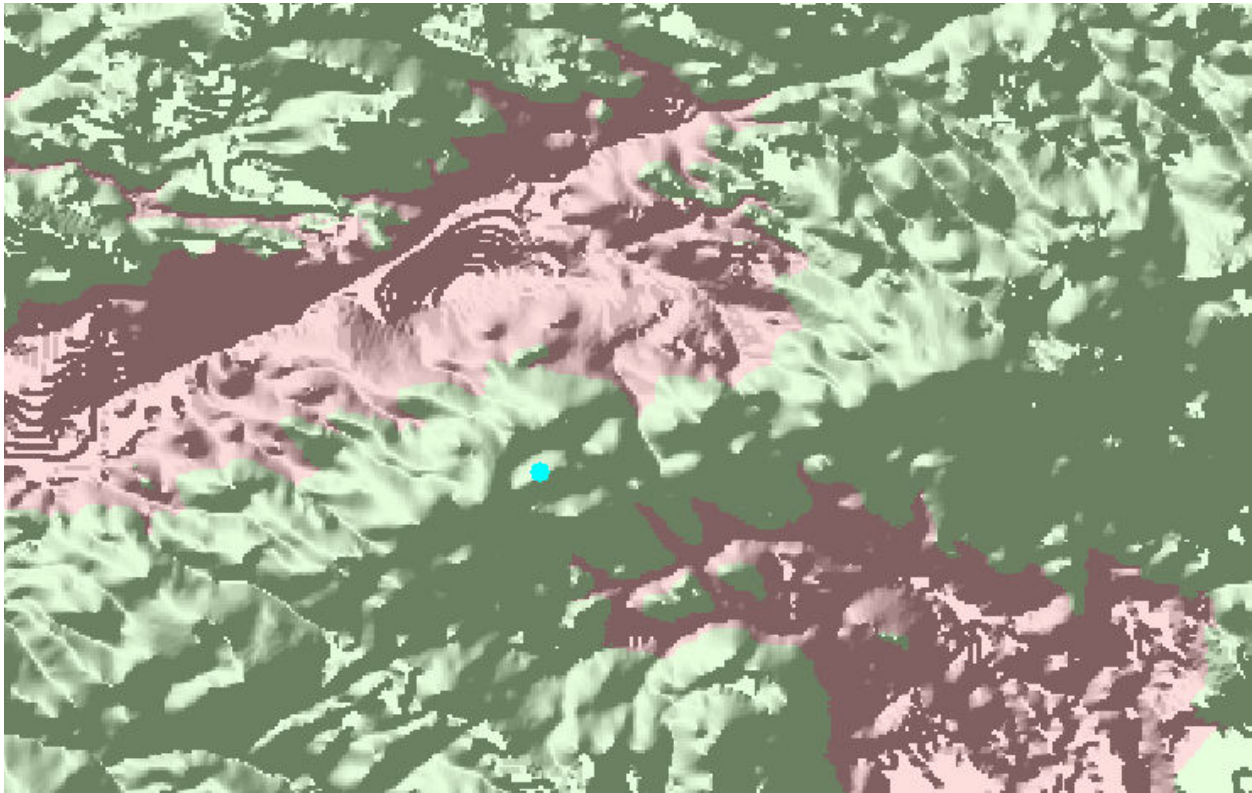


Figure 20: Sample viewshed display where the blue dot is the observation point, green areas are visible and pink areas are locations which are not visible to the observation point (created using ArcGIS 10.2.1)

2.3 C-TRIP

Canadian Turbine Radar Interference Products (C-TRIP) are user-friendly configurable scripts which were created using PERL scripting language. C-TRIP was created to allow for the visualization of Level II IRIS data utilizing existing CARDS products and identifying the locations of existing wind farms using green wind farm boxes (Section 2.3.1). Examples of C-TRIP outputs are seen throughout the thesis in Chapters 3 & 4. For the purposes of analyzing WTC,

three CARDS products are used: CLOGZPPI, VRPPI and PRECIP. Both CLOGZPPI and VRPPI are products most commonly used by EC's meteorologists where a two dimensional PPI (plan position indicator) display of the radar data is shown. CLOGZ stands for the corrected reflectivity or (DBZ) moment data display of DOPVOL radar scans. DOPVOL1A is commonly the lowest to the ground Doppler scan of the radar with the finest resolution of 0.5° in azimuth by 0.5 km in range for each pixel. DOPVOL1A was selected to be used because WTC is only seen at lower elevation scans of the radar. DOPVOL1A is also used in the product VRPPI, which shows a PPI display of radial velocity data or (V) moment data in ms⁻¹. PRECIP stands for precipitation and has also been used to analyze WTC as it is the product used to display radar data to the public through EC's website. PRECIP combines DOPVOL2 (PPI) data close to the radar and CONVOL data (similar to a CAPPI (constant altitude PPI) display) past Doppler data ranges.

In order to create CARDS products, product keys are used in the format of: **Major Product Type : Time : Minor Product Type [, Parameter List] [~Minor Product Type [, Parameter List]] : Geographic Definition : Image/Numerical Definition : Format**. The C-TRIP code (Appendix B) was produced with help from EC colleagues Jim Young, Sudesh Boodoo, Norman Donaldson and Janti Reid. The code can be configured to specify which product to create and display using specific imagedef backgrounds as explained in Section 2.3.1. The C-TRIP code, displayed in Appendix B, defines many different variables in the format (\$name) which are explained in more detail below by order of appearance:

The first section is a user input section:

- \$site = <XXX>
 - This variable is a variable input by the user to define which radar site to produce the radar images for (ex: XGO = Gore weather radar or WKR = King City weather radar)
- \$y = <YYYY>
 - This variable is a variable input by the user to define which year to produce the radar images for (ex: 2012, 2013...)
- \$m = <MM>
 - This variable is a variable input by the user to define which month to produce the radar images for (ex: 01, 02 ...)

- \$d = <DD>
 - This variable is a variable input by the user to define which day to produce the radar images for (ex: 01, 02 ...)

The next section defines variables configurable within the code to create products:

- \$scan = "DOPVOL1_A"
 - This variable is configurable within the code and selects which radar scan is required for the creation of the CARDS product (CONVOL, DOPVOL1_A, DOPVOL1_B etc.)
- \$scan2 = "CONVOL"
 - This variable is configurable within the code and selects the second radar scan required for the creation of the PRECIP product
- \$product = "CLOGZPPI"
 - This variable is configurable within the code and selects the CARDS product to produce (CLOGZPPI, VRPPI or PRECIP)
- \$geodef = \$site."_240KM"
 - This variable is configurable within the code and selects the geographic definition file for the radar. In the case of the PRECIP product 240KM is changed to 480KM
- \$imagedef = \$site."_".\$product."_WF"
 - This variable is configurable within the code and selects the edited imagedef files created in Section 2.3.1 which display a green box around each existing wind farm near the select radar \$site
- \$provar = "18,MPRATE"
 - This variable is configurable within the code and defines the product variables as recommended in CARDS user manual documentation
- \$type = "URPClogzPPI"
 - This variable is configurable within the code and defines the URP creation file for the CARDS product

2.3.1 Wind Farm Box Geometry

In order to properly identify which pixels on the radar image are produced by the wind farm, the location of each wind farm needed to be clearly identified. The idea to create green boxes around the wind farm was chosen as the best way to identify WTC within a CARDS product. Images created through CARDS were created as an X,Y pixel representation of the recorded

weather radar data with the center of the radar at 240,240. The location of the radar at a central point was used with standard geometry rules and methods to determine the X and Y coordinates of each wind farm. Once the wind farm box coordinates were calculated using geometry methods, they were edited into existing background images to be called upon in the C-TRIP code called “imagedef” files. Additionally, in C-TRIP, two geodef files (or image sizes) are used: \$site_240KM and \$site_480KM. 240KM geodef files are used where each side of a pixel within the grid image represents a 0.5 km distance for Doppler radar data such as VRPPI and CLOGZPPI. 480KM geodef files have pixels within the grid image represented as 1 km distances for conventional radar data such as PRECIP. An example of a wind farm box can be seen in Figure 11. The following is the methodology used to determine the coordinates of the wind farm boxes defined in table 4:

Table 4: Defined coordinate locations of wind farm boxes with respect to image size (240 – VRPPI & CLOGZPPI) (480 – PRECIP) with beginning X and Y coordinates widths and heights in pixels.

Wind Farm Box Geometry						
Radar	Wind Farm	Image size (pix)	X	Y	Width	Height
WKR	Melancthon	240	110	242	22	44
WKR	Melancthon	480	175	241	11	22
XNI	Greenwich	240	280	214	20	16
XNI	Greenwich	480	260	227	10	8
XGO	Nuttby	240	310	339	10	8
XGO	Nuttby	480	275	290	5	4

Steps used to create wind farm boxes:

- First, the outputs from the WindFarmAnalysis were used to plot the locations of the radars and the wind turbines for those each wind farm / radar pair
- Then, a box was carefully drawn around each wind farm making sure to create straight paths in Google Earth with the map properly oriented with North being up and all wind turbines to be included within each box
- It was then important to take into account the lowest X and Y location of the wind farm box as it would appear on the CARDS image output grid – this would be different for each wind farm depending on the quadrant it fell in with respect to the location of the weather radar (Figure 21)

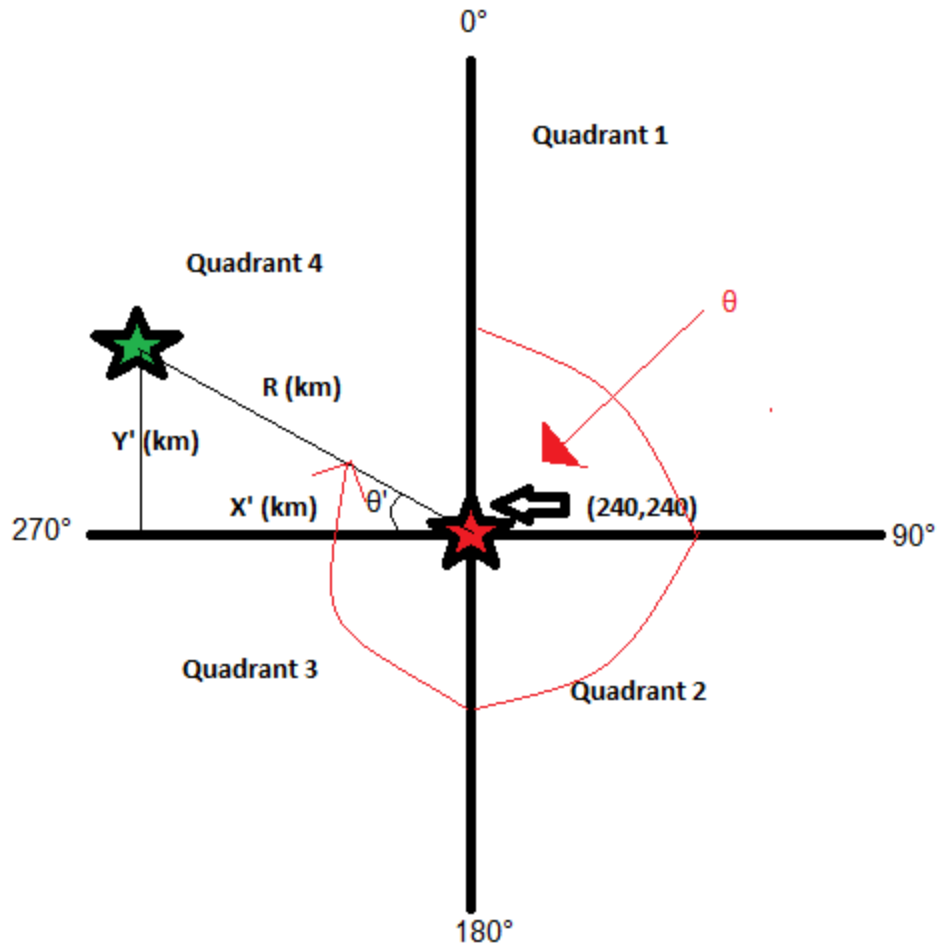


Figure 21: Representation of a wind farm box location (green star) with respect to the radar (red star) at the origin (240,240) where R is the path distance, θ is the bearing in $^\circ$, θ' is measured from the X axis and X' and Y' are calculated values

- A measured line was then created from the radar to the lowest X and Y location of the wind farm box and the distance in km (R) and bearing (θ) in $^\circ$ was recorded
- Simple geometry using sine and cosine rules were then performed where θ' was measured up or down from the x-axis (Figure 21) (Equation 9):

Equation 9: X' and Y' calculations based on θ' measured from the x axis

$$X' = R \cos \theta'$$

$$Y' = R \sin \theta'$$

- Then, the actual grid X and Y values were calculated for 240 images and 480 images using Equations 10 and 11 with the \pm dependent upon the location relative to the origin (240, 240):

Equation 10: X and Y calculations for the 240 background imagedef based on X' and Y' where \pm is dependent upon the location of the wind farm relative to the origin

$$X(240) = 240 \pm 2X'$$

$$Y(240) = 240 \pm 2Y'$$

Equation 11: X and Y calculations for the 480 background imagedef based on X' and Y' where \pm is dependent upon the location of the wind farm relative to the origin

$$X(480) = 240 \pm X'$$

$$Y(480) = 240 \pm Y'$$

- The final determination of width and height are the calculated values of the length and width of the boxes created in Google Earth in (km)
 - For the 240 background imagedef the width and height values are multiplied by 2 as each pixel represents half a kilometer

2.4 Productx Utility

Product examiner (Productx) is a utility created by Vaisala in order to display the information contained within an IRIS file (Vaisala, 2014). IRIS files contain a multitude of information but are in binary code and the information normally needs to be displayed in an image format through a system like CARDS or images produced via C-TRIP code. Access to the tool was provided by the NRP using a very simple command line code: `product -width=10000 filename.iri`. The width designation is used to ensure all data are displayed on the terminal and no data are skipped over. Once the IRIS file is open using Productx, header data about the specific scan are displayed. For the purposes of this thesis, Productx was only run on DOPVOL1A IRIS files. The product contains options for which calculated moment data to display such as V, DBT, DBZ or W (as explained in Section 1.2.3). The data are then displayed for each ray (with given azimuth range) and each 0.5 km value at ranges away from the radar in the specified azimuth direction.

Productx data for DBT (total reflectivity – before Doppler correction), DBZ (corrected reflectivity – after Doppler processing) and V (velocity data) was extracted for each wind farm / radar pair and copied into Excel spreadsheets. The output data, originally in comma separated format, were then separated into cells. Since each wind farm spans multiple radar beams (rays), a simple maximum calculation was performed on the data points for each specified radar range. The data were then plotted on a graph to best represent the reflectivity vs. the Doppler range from the radar (110 km). As seen in Figure 22, overlaying DBZ on DBT can provide an indication of which signals have been filtered out using Doppler correction. Between the 25 and 45 km range there are lone DBT signals (green) which indicate ground clutter and ranges

without signals indicate no radar returns. Additionally, a wind farm located between 54 and 63 km from the radar is clearly shown in blue (DBZ) along with the magnitude of maximum reflectivity within the specific azimuth range.

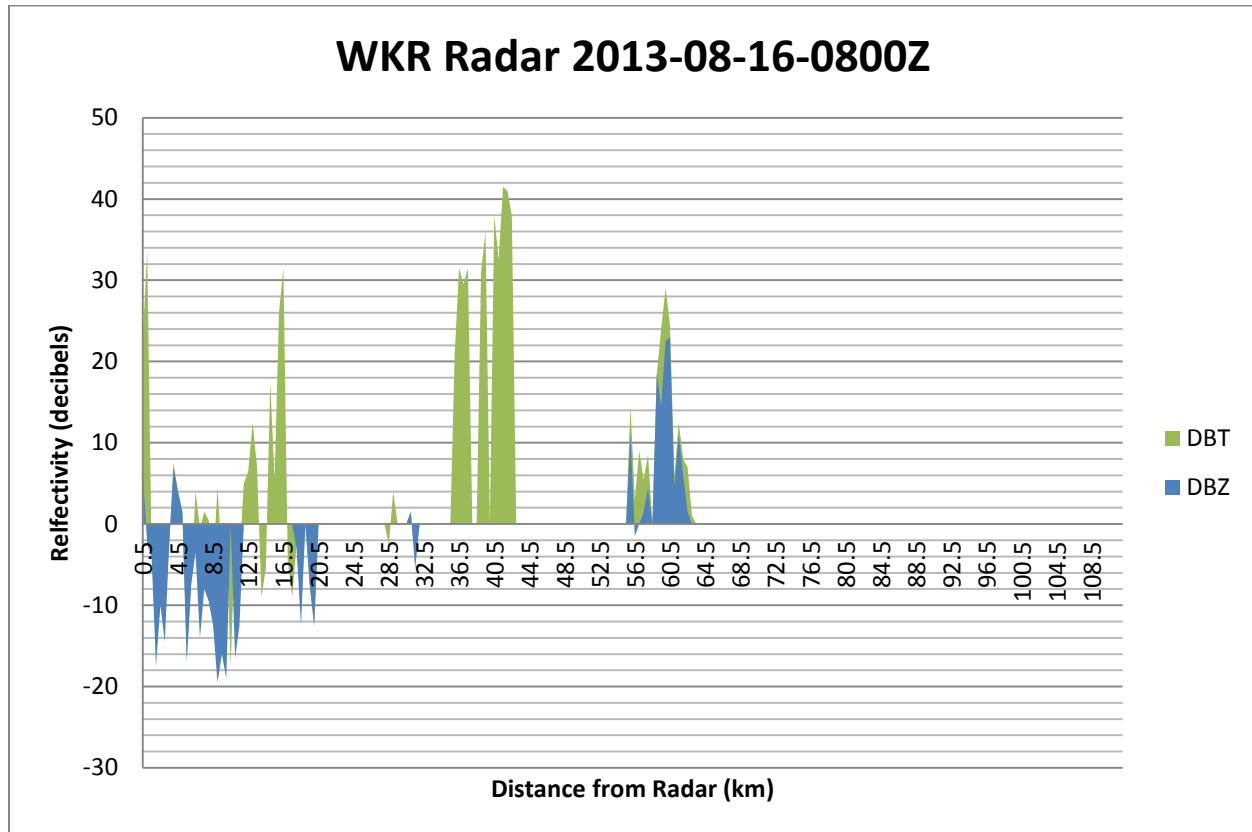


Figure 22: Example of output produced using data provided by Productx utility where maximum azimuthal reflectivity values of DBT and DBZ are compared at distances from the weather radar.

2.5 Wind Turbine Orientation Model

In order to determine the impact of a wind turbines' orientation with respect to a weather radar, the Wind Turbine Orientation Model was created. Wind turbine blade orientation depends on the meteorological wind direction. As previously stated, the maximum energy output from a turbine occurs when the turbine blades are perpendicular to the wind. The radial velocity recorded by a radar is at a minimum when the turbine blades are oriented exactly perpendicular to the weather radar. The best case scenario, in terms of minimal WTC, would occur if the radial velocity was at a minimum and thus would be when the wind direction is parallel to the radar azimuth. There would only be one ideal situation for each turbine, as the radar azimuth differs between turbines. However, the Wind Turbine Orientation Model takes into account the whole wind farm and thus a range between the two azimuths (minimum and maximum) is used.

The Wind Turbine Orientation Model for a particular wind farm / radar pair includes an estimation of the severity of WTC based on the meteorological wind direction where impacts are:

- Marginal
 - When the wind direction is equal to the azimuth range (for each wind farm)
 - Wind direction min = Azimuth min or Wind direction = Azimuth min + 180°
 - Wind direction max = Azimuth max or Wind direction = Azimuth max + 180°
- Severe
 - When the wind direction is perpendicular to the azimuth range
 - Wind direction min = Azimuth min \pm 90°
 - Wind direction max = Azimuth max \pm 90°
- Moderate
 - All other wind directions

2.6 Data Requirements

The following sections provide details on the acquisition and availability of data to be used in the tools outlined in sections 2.2 – 2.5.

2.6.1 IRIS Files & CARDS Products

IRIS files produced by Vaisala's signal processor are created for each weather radar and each radar scan approximately every ten minutes. Obtaining these files from EC's weather radars, specifically Gore, Lasseter Lake and King City were crucial to visualizing WTC on EC radar data. Additionally access was required to EC's post-processing system, CARDS. Required IRIS files and access to CARDS were made available through close correspondence with EC's NRP and the King City weather radar research group.

2.6.2 MOLTS Data

In order to model radar beam propagation, vertical profiles of the atmosphere are required. Model Location Time Series (MOLTS) data are available at 2.5 km grid locations from the High Resolution Deterministic Prediction System (HRDPS) of the Global Environmental Multistage (GEM) atmospheric model. MOLTS data were requested through EC's Cloud Physics and Severe Weather Section. Table 5 shows a list of locations which were requested for each of the

selected wind farm / radar pairs. The locations were selected to provide multiple views of the atmosphere from the radar to the wind farm at $\frac{1}{4}$, $\frac{1}{2}$ and $\frac{3}{4}$ distance (Figure 23). The center coordinates of the HRDPS grid appropriate for each requested location are also displayed in Table 5 along with their distance from the requested location. The points have been labeled as 9## where ## refers to the MOLTS data file and a 9 was used to not confuse the points with points which already exist in the database. The MOLTS data files extracted contain vertical profiles of relative humidity, temperature, wind speed, wind direction as well as surface variables predicted at 5 minute intervals for 24 hours. Section 4.1 provides further detail on the variables used to calculate the atmospheric refractivity at each MOLTS point for one specific wind farm / radar pair.

Table 5: Requested MOLTS data points and actual MOLTS points available for wind farms, radar and points in between.

Requested Points				MOLTS Point				
Name	ID	Latitude	Longitude	Domain	PT #	Latitude	Longitude	Distance (km)
King City	WKR	43.964	-79.574	East	927	43.973	-79.573	1.00
Melanchthon	MEL	44.090	-80.308	East	931	44.094	-80.297	0.98
1/4_Mel	MLL	44.059	-80.126	East	920	44.053	-80.139	1.23
1/2_Mel	MML	44.028	-79.943	East	917	44.034	-79.950	0.87
1/4_Mell	MEE	43.996	-79.756	East	921	43.992	-79.761	0.60
Lasseter Lake	XNI	48.853	-89.122	East	929	48.850	-89.108	1.08
Greenwich	GRN	48.769	-88.789	East	926	48.766	-88.782	0.61
1/4_Green	GNN	48.790	-88.871	East	918	48.782	-88.854	1.53
1/2_Green	GGN	48.811	-88.954	East	916	48.817	-88.964	0.99
1/4_Greenw	GRR	48.833	-89.039	East	919	48.833	-89.036	0.22
Gore	XGO	45.099	-63.704	Maritimes	943	45.093	-63.700	0.74
Nuttby	NUT	45.561	-63.224	Maritimes	947	45.565	-63.233	0.83
1/4_Nut	NTT	45.446	-63.344	Maritimes	939	45.457	-63.339	1.28
1/2_Nut	NNT	45.329	-63.466	Maritimes	936	45.319	-63.461	1.18
1/4_Nutt	NUU	45.216	-63.584	Maritimes	940	45.211	-63.566	1.52

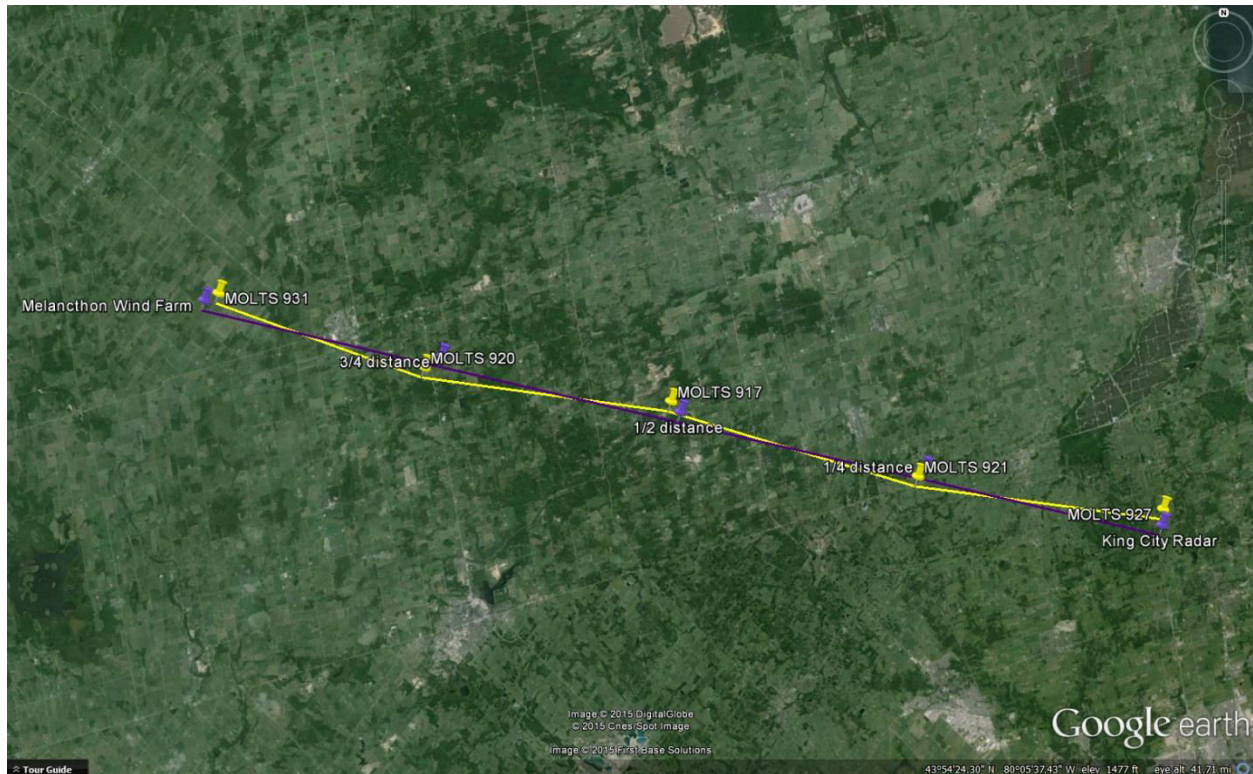


Figure 23: Location of requested (purple) and provided (yellow) MOLTS points to model the radar beam path from the King City weather radar to the Melancthon Wind Farm

2.6.3 Digital Elevation Model Data

A digital elevation model (DEM) was required to produce GIS viewsheds. The most readily available dataset of digital elevation data in Canada is the Canadian Digital Elevation Data (CDED) provided by GeoGratis Client Services run by Natural Resources Canada. The data were made available from their online GeoGratis website from the most recent update on 2014-09-01. Different grids of data were extracted around each wind farm / radar pair in order to produce the viewsheds and were offered at grid resolutions between 8 m and 23 m for the 1:50,000 tiles provided (NRC, 2014). The ground elevations in the CDED are recorded relative to mean sea level in meters with the horizontal reference datum NAD83 (North American Datum 1983). Figure 24 shows an example of one of the tiles downloaded through GeoGratis.



Figure 24: Example of downloaded CDED data for the 011E tile (GeoGratis, 2014)

2.6.4 Wind Turbine Operational Data

Operational wind turbine data were requested in order to determine the number of turbines in operation, the ground wind speed, and the orientation of the wind turbines within the wind farm. Unfortunately, only one wind farm, Nuttby Mountain Wind Farm, was able to supply such data (Chapter 4). The data graciously supplied by Nova Scotia power was provided in an Excel Spreadsheet format with ten minute data for each wind turbine within the wind farm for the specified case study day including the following recorded variables; minimum, average and maximum wind speed (ms^{-1}), rotation speed (rpm), and power (kW); and the nacelle position of each turbine in degrees for each ten minute period.

3. Results: Wind Farm Case Studies

The following chapter provides detailed information on the selected wind farm / radar pairs. The tools developed and described in Chapter 2 were used to create models and analyze the RLOS for each wind farm / radar pair under standard atmospheric conditions. Additionally, this chapter presents WTC observed from each wind farm / radar pair using Productx and C-TRIP tools. Two case studies days were selected to observe WTC in the morning (04:00 local time) and in the afternoon (16:00 local time). The first case study was selected to show summer elevation angles (2013-08-16) and the second to show winter elevation angles (2013-11-15). The weather conditions during each time period are displayed for each wind farm / radar pair. Chapter 5 provides a comparison of the expected results from the RLOS analyses to the observed WTC results.

3.1 Melancthon Wind Farm

The first wind farm / radar pair studied is the Melancthon wind farm located west of the King City weather radar near Shelburne, Ontario. This wind farm / radar pair was selected because observed WTC from the wind farm is very variable and the size of the wind farm has the potential to cause misleading radar signatures which can resemble severe weather. The wind farm was constructed in two phases consisting of a total of 133 turbines. The Phase I turbines have been in commercial operation since March 4, 2006 and consists of 45 turbines producing 67.5 MW of power. Phase II has been in commercial operation since November 24, 2008 and consists of 88 turbines producing 132 MW of power.

3.1.1 Wind Farm & Weather Radar Specifications

The Melancthon wind farm is located approximately 55 km from the King City weather radar (WKR). Each of the turbines in the wind farm are General Electric (GE) 1.5 MW models with tower heights of 80 meters and a swept area of 82 meters for a total height around 121 meters off the ground. The coordinates of the Melancthon turbines in northing and easting for zone 17T can be found in Appendix C and are seen in Figure 26.

Table 6: Information about the King City weather radar

King City Radar Information	Site ID	Lat	Lon	Height (mASL)	Feed horn (m)	Beamwidth (°)
	WKR	43.964	-79.574	360	30.5	0.65

Table 7: King City weather radar Doppler scan elevation angles (°)

WKR Doppler Scans	DOPVOL1A	DOPVOL1B	DOPVOL1C	DOPVOL2
Summer	0.5	1.5	3.5	0.3
Winter	0	1.5	3.5	0

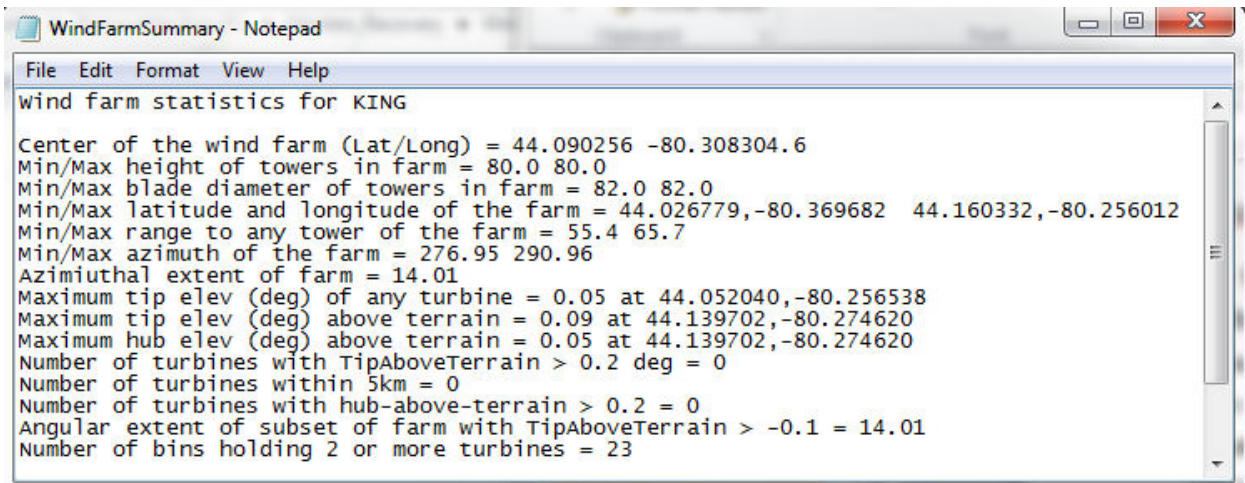


Figure 25: Wind farm summary output file for Melancthon wind farm / King City weather radar pair

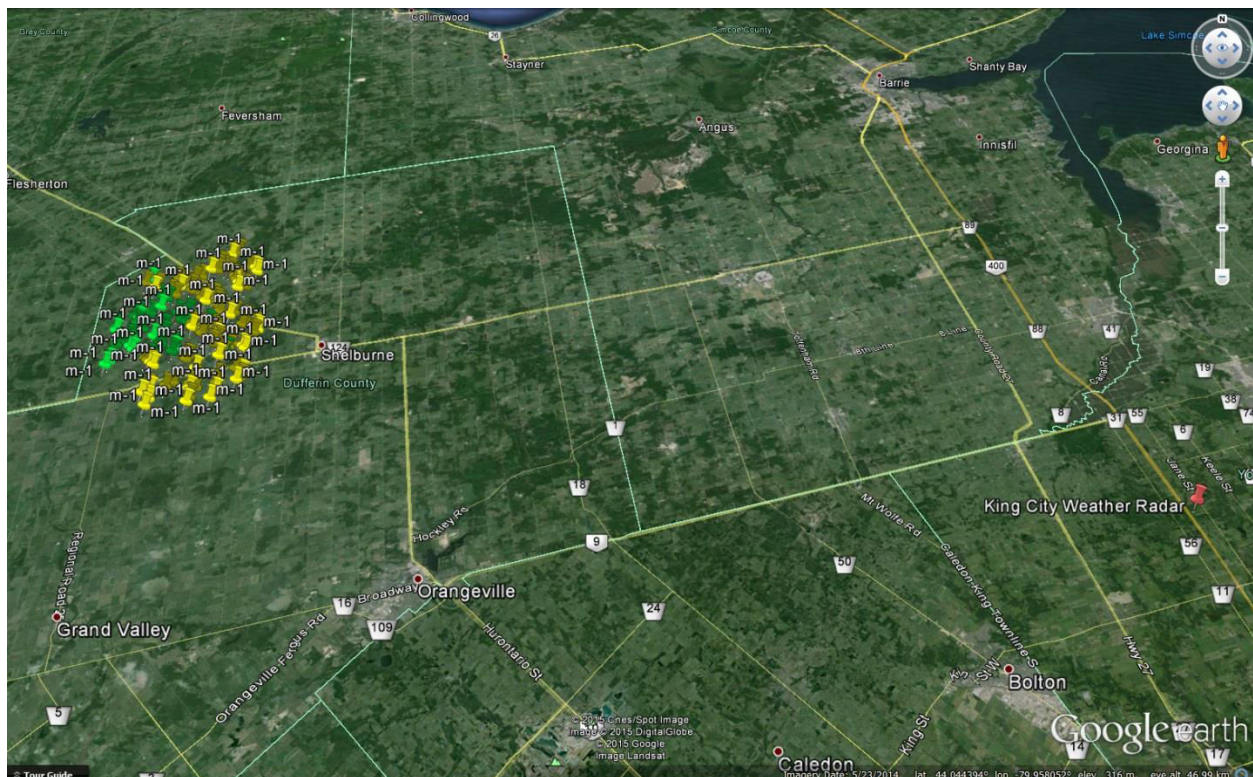


Figure 26: Location of Melancthon wind turbines (green and yellow as described by Table 2) and King City weather radar (red)

3.1.2 Wind Turbine Orientation Model

Based on the azimuth range of the Melancthon wind farm as shown in Figure 25, a wind turbine orientation model has been created. The model, Table 8 & Figure 27, provides an estimation of the severity of WTC as determined by the direction of the wind and described in Section 2.5.

Table 8: Wind turbine orientation model calculations for the Melancthon wind farm where wind direction ranges and predicated WTC impact are shown based on impacted azimuth angles

Melancthon Wind Turbine Orientation Model		
Wind Dir. Min	Wind Dir. Max	WTC Impact
0	5	Moderate
6	21	Severe
22	95	Moderate
96	111	Marginal
112	185	Moderate
186	201	Severe
202	275	Moderate
276	291	Marginal
292	359	Moderate

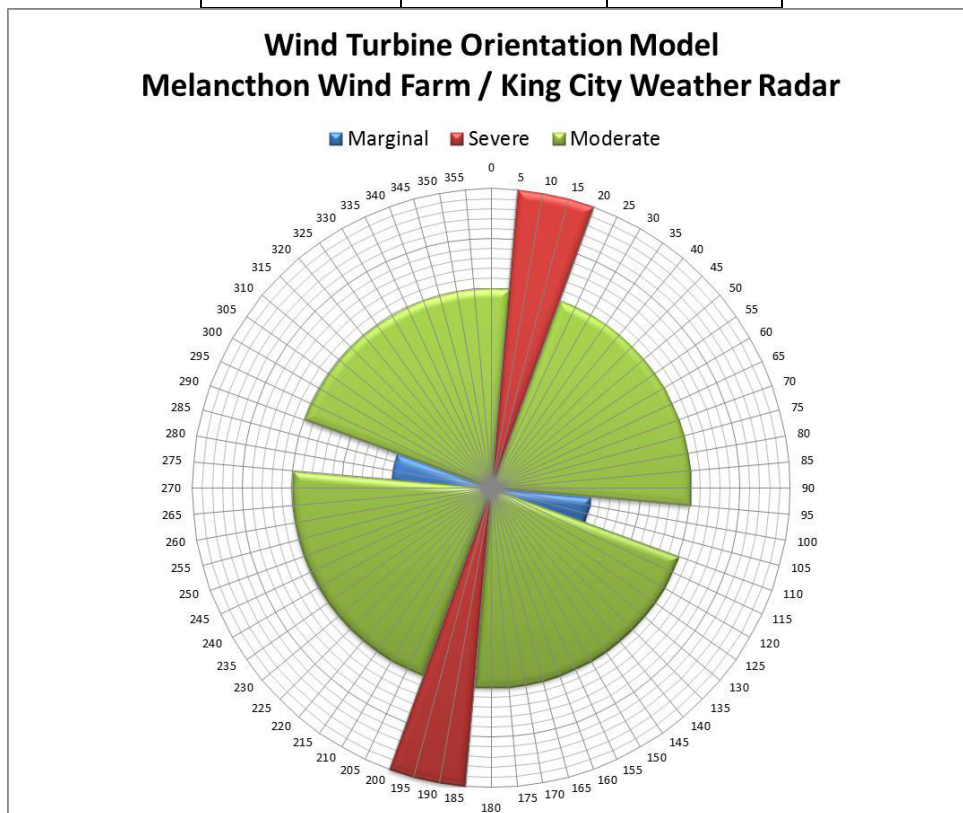


Figure 27: Visual representation of the Melancthon Wind Farm / King City weather radar wind turbine orientation model

3.1.3 RLOS Analyses

The following RLOS analyses are completed for the two wind turbines (74 & 75) which are closest to the King City weather radar using the Wind Farm Analysis (Section 2.2.1) and IDL Beamwidth (Section 2.2.2) tools.

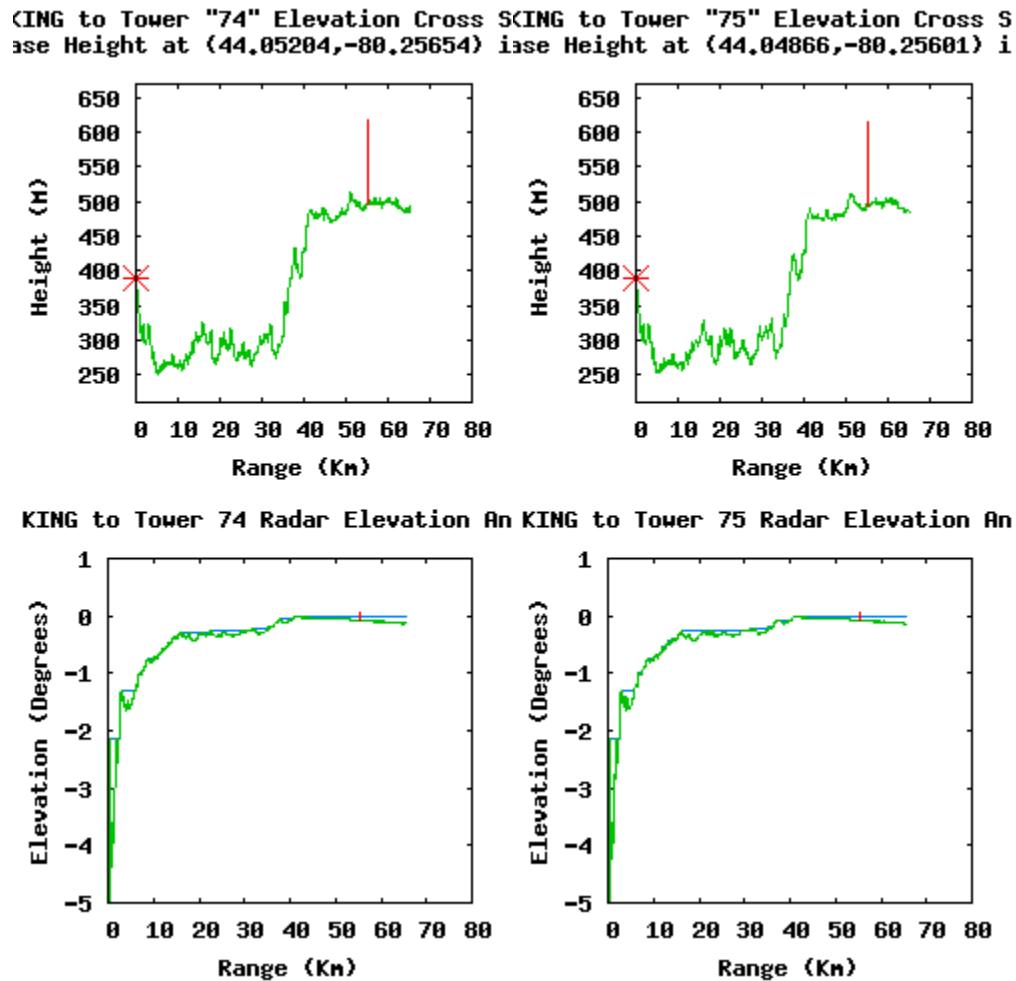
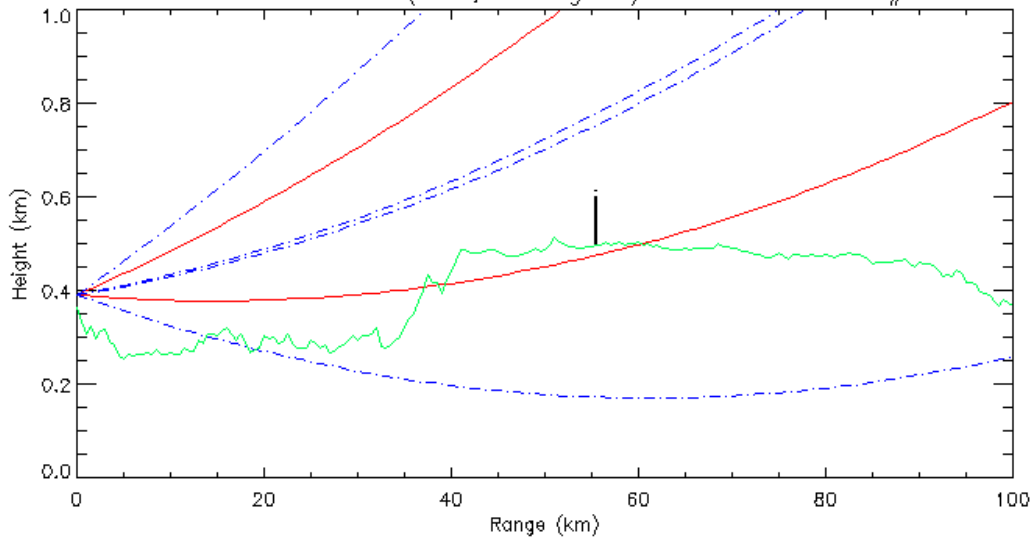


Figure 28: Wind Farm Analysis Tool - RLOS analysis performed on Melancthon turbines 74 (left) and 75 (right) as seen from the King City weather radar. Figure explanation found in Section 2.2.1 and Figure 12 caption.

WKR DOPVOL1A Winter & Summer ($-0.1, 0.5$ degrees) Melancthon Turbine #74 at 55.47 km



WKR DOPVOL1A Winter & Summer ($-0.1, 0.5$ degrees) Melancthon Turbine #75 at 55.36 km

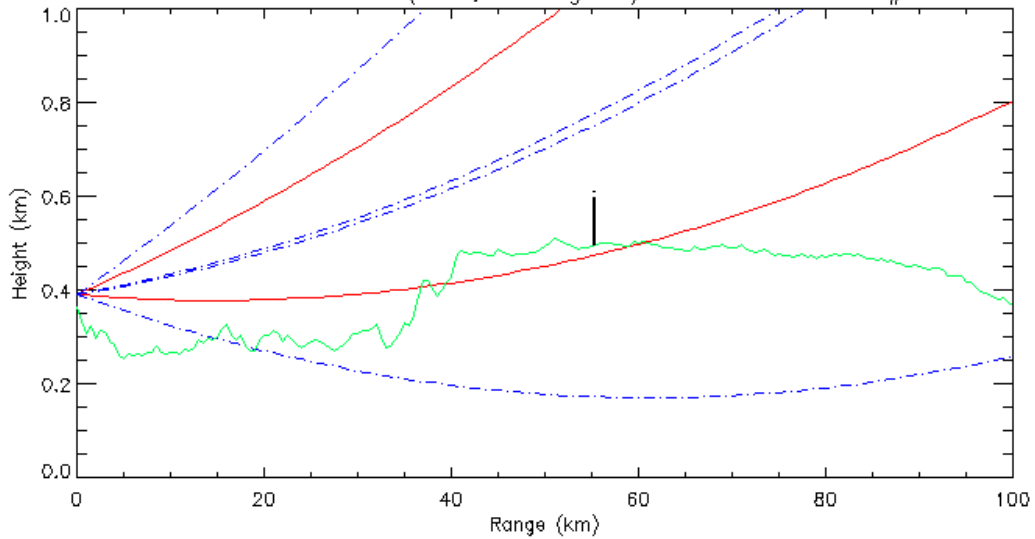


Figure 29: IDL Beamwidth Tool - RLOS analysis performed on Melancthon turbines 74 (top) and 75 (bottom) as seen from the King City weather radar. Figure explanation found in Section 2.2.2 and Figure 15 caption. *Note that analysis was completed given -0.1° as the winter DOPVOL1A angle however the operational elevation angle has since changed to 0° *

The following GIS viewsheds were completed to display the location of the turbines relative to the radar with specified radar elevation angles. Each image displays the DOPVOL1A scan elevation angles in either winter or summer for the radar where red areas show where turbines would be visible to the center of the main beam and orange areas show where turbines would be visible to the bottom of the main beam.

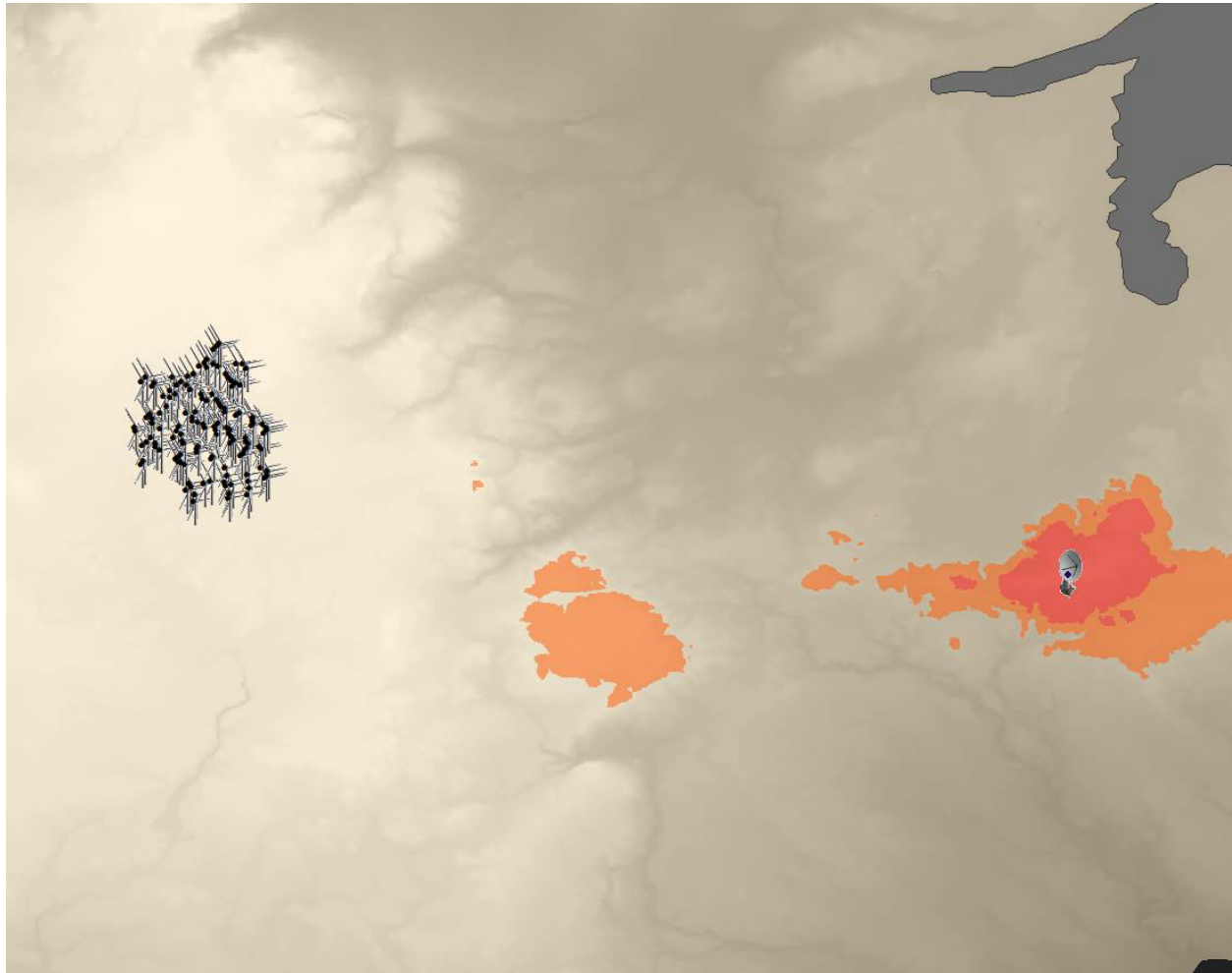


Figure 30: King City weather radar (radar dish) summer viewshed where Melancthon turbine locations are indicated in black. Locations which turbines would be visible in the center of the main beam (0.5°) are red and locations which turbines would be visible in the bottom of the main beam (0.175°) are indicated in orange. (Created using ArcGIS 10.2.1)

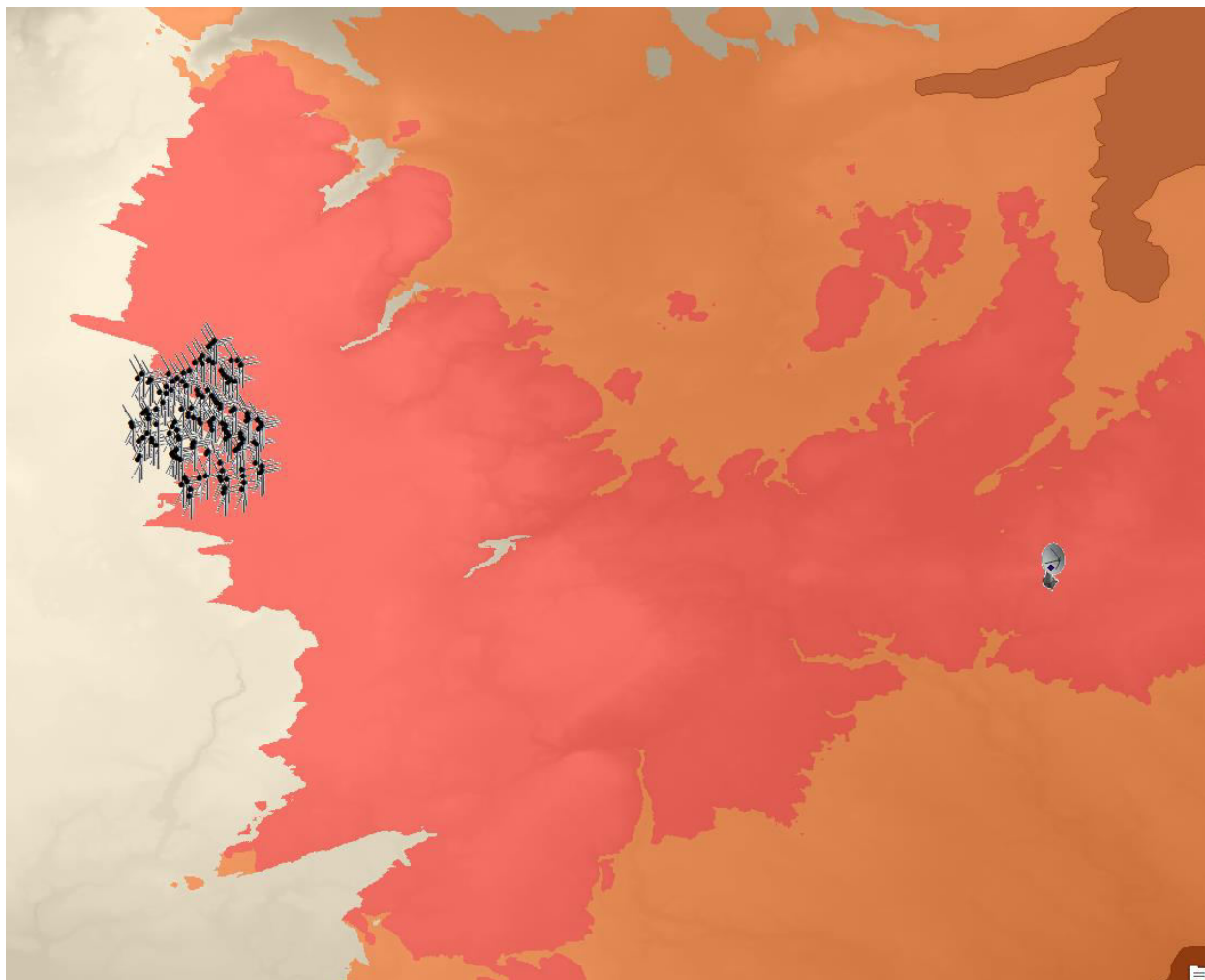


Figure 31: King City weather radar (radar dish) winter viewshed where Melancthon turbine locations are indicated in black. Locations which turbines would be visible in the center of the main beam (0°) are red and locations which turbines would be visible in the bottom of the main beam (-0.325°) are indicated in orange. (Created using ArcGIS 10.2.1)

3.1.4 WTC Examples

The following section describes WTC examples of the Melancthon wind farm as seen from the King City weather radar created using the Productx and C-TRIP tools from the two case study days which are described in Table 9. Weather data were collected from Environment Canada's climate data archive at Toronto Buttonville Airport, which was found to be the closest hourly reporting weather site near the wind farm / radar pair. Productx images were created using maximum DBT and DBZ values for the WKR radar rays within the azimuth range 276° - 291° out to the Doppler range of 110 km (Figure 32). Additional Productx image for the case study days can be found in Appendix D. The C-TRIP images, like Figure 33, are zoomed in to display

the Melancthon wind farm box only. WTC as seen from CLOGZPPI, VRPPI and PRECIP products for the selected case study days can found in Appendix E.

Table 9: Case study day weather information provided for Toronto Buttonville Airport

Date	2013-08-16			
Time	04:00 EDT	05:00 EDT	16:00 EDT	17:00 EDT
Weather Conditions	Temperature (°C), Relative Humidity (%), Weather			
Toronto Buttonville Airport	10.8, 94, Clear	10.3, 96, Clear	24, 50, Mainly Clear	23.9, 48, Mainly Clear
Date	2013-11-15			
Time	04:00 EST	05:00 EST	16:00 EST	17:00 EST
Weather Conditions	Temperature (°C), Relative Humidity (%), Weather			
Toronto Buttonville Airport	5.3, 47, Mainly Clear	4.8, 48, Mainly Clear	9.6, 57, Mostly Cloudy	8.6, 60, Mostly Cloudy

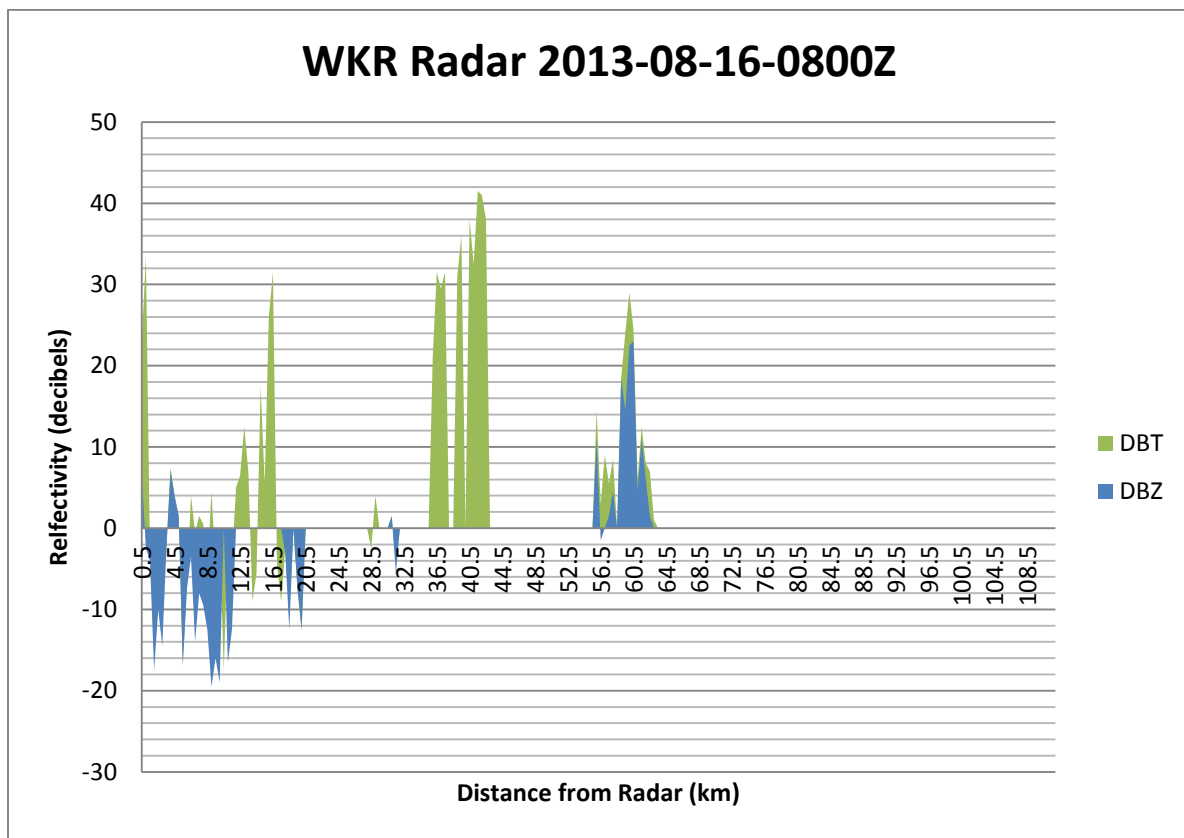


Figure 32: Example King City Productx output for 2013-08-16-0800Z where the maximum DBT and DBZ values for the azimuth range of 276° - 291° are displayed

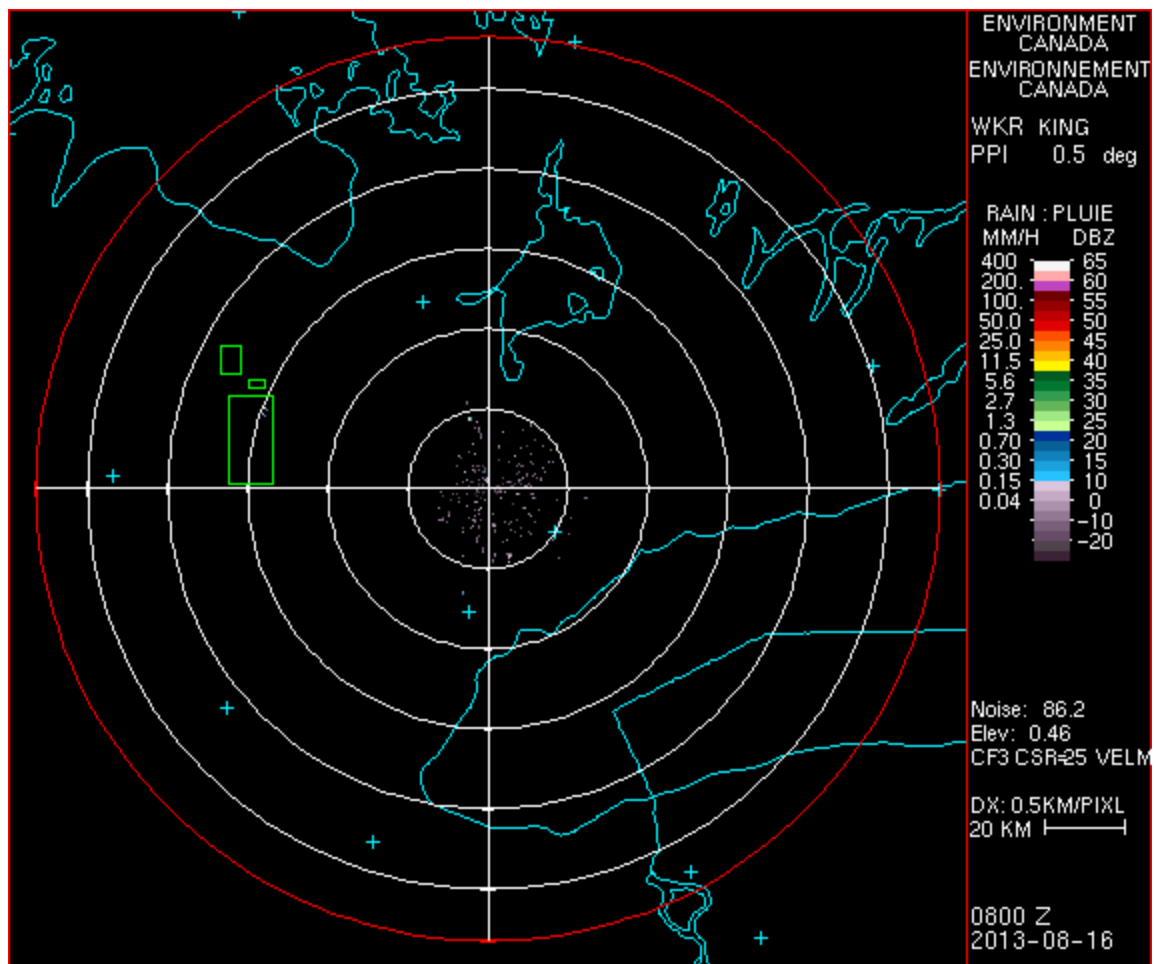


Figure 33: Example King City C-TRIP CLOGZPPI product on 2013-08-16 at 0800Z created using the DOPVOL1A WKR weather radar IRIS file where the Melancthon wind farm is outlined with the largest green box to the left of the radar (at the center in the image)

3.2 Greenwich Wind Farm

The second wind farm / radar pair studied is the Greenwich wind farm located northeast of Thunder Bay, Ontario and the Lasseter Lake weather radar. This pair was selected because observed WTC from the wind farm is minimal even though at one point it was the second closest wind farm to a Canadian weather radar. Due to the close proximity there has been informal discussion that there should be more impacts from the wind turbines to the weather radar data. The wind farm has been in commercial operation since October 14, 2011 and consists of 43 turbines producing 98.9 MW of power.

3.2.1 Wind Farm & Weather Radar Specifications

The Greenwich wind farm is located approximately 22 km from the Lasseter Lake weather radar (XNI). Each of the turbines in the wind farm are Siemens 2.3MW models with tower heights of 80 meters and a swept area of 92 meters for a total height around 126 meters off the ground. The coordinates of the Greenwich turbines in northing and easting for zone 16U can be found in Appendix F and are seen in Figure 35.

Table 10: Information about the Lasseter Lake weather radar

Lasster Lake Radar Information	Site ID	Lat	Lon	Height (mASL)	Feed horn (m)	Beamwidth (°)
	XNI	48.853	-89.122	488	23.1	1.1

Table 11: Lasseter Lake weather radar Doppler scan elevation angles (°)

XNI Doppler Scans	DOPVOL1A	DOPVOL1B	DOPVOL1C	DOPVOL2
Summer	0.5	1.5	3.5	0.3
Winter	0.2	1.5	3.5	0.2

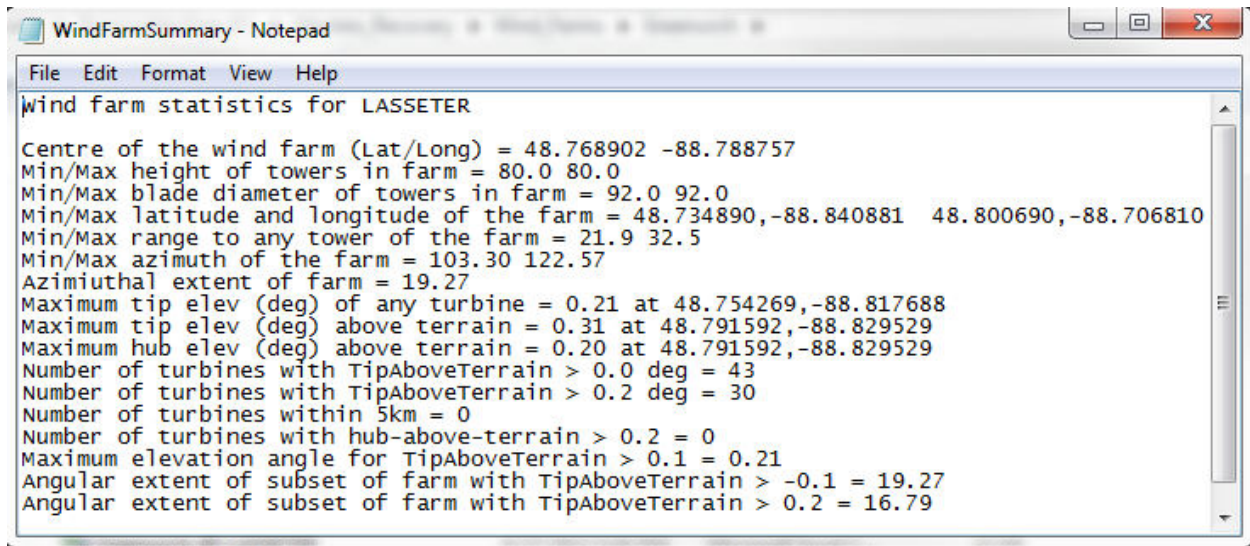


Figure 34: Wind farm summary output file for Greenwich wind farm / Lasseter Lake weather radar pair

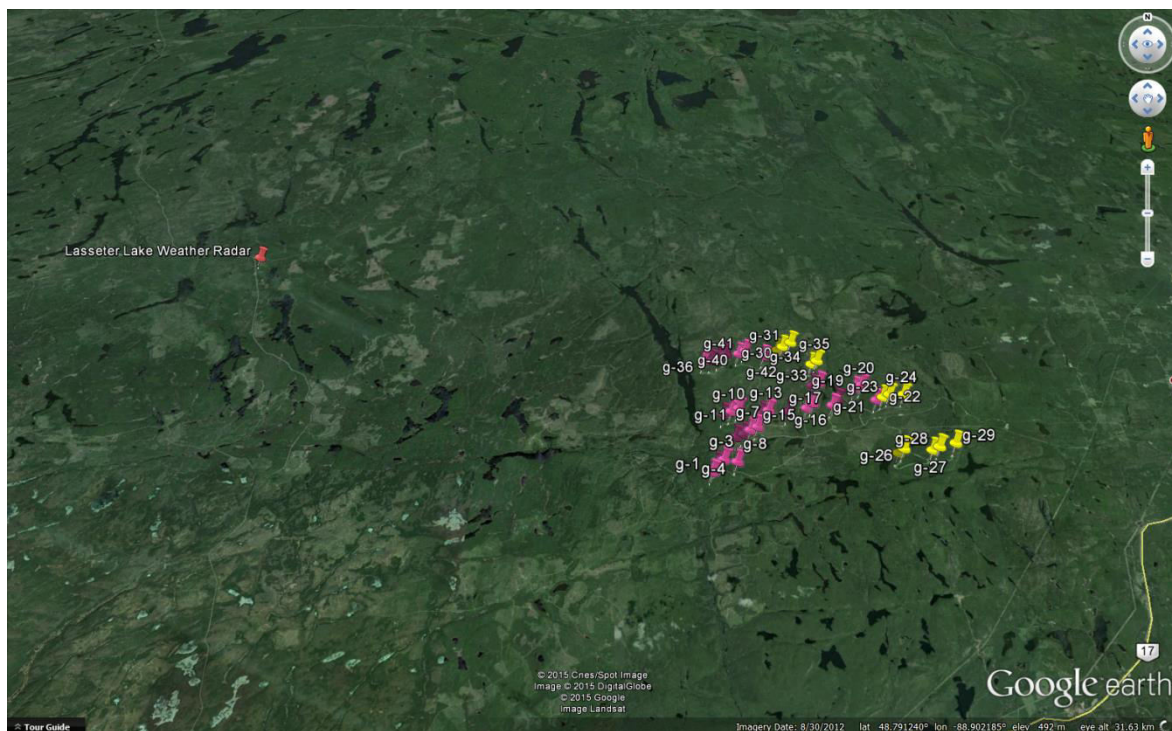


Figure 35: Location of Greenwich wind turbines (pink and yellow as described in Table 2) and Lasseter Lake weather radar (red)

3.2.2 Wind Turbine Orientation Model

Based on the azimuth range of the Greenwich wind farm as shown in Figure 34, a wind turbine orientation model has been created. The model, Table 12 & Figure 36, provides an estimation of the severity of WTC as determined by the direction of the wind and described in Section 2.5.

Table 12: Wind turbine orientation model calculations for the Greenwich wind farm where wind direction ranges and predicated WTC impact are shown based on the impacted azimuth angles

Greenwich Wind Turbine Orientation Model		
Wind Dir. Min	Wind Dir. Max	WTC Impact
0	12	Moderate
13	33	Severe
34	102	Moderate
103	123	Marginal
124	192	Moderate
193	213	Severe
214	282	Moderate
283	303	Marginal
304	359	Moderate

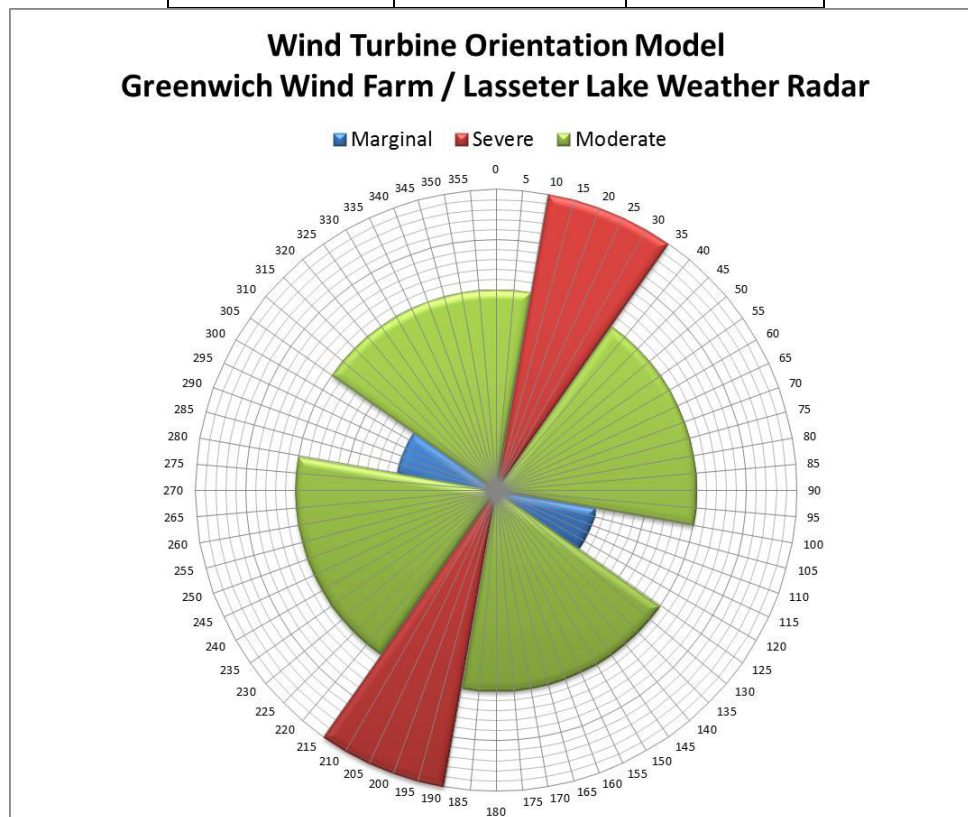


Figure 36: Visual representation of the Greenwich Wind Farm / Lasseter Lake weather radar wind turbine orientation model

3.2.3 RLOS Analyses

The following RLOS analyses are completed for the two wind turbines (3 & 7) which are closest to the Lasseter Lake weather radar using the Wind Farm Analysis (Section 2.2.1) and IDL Beamwidth (Section 2.2.2) tools.

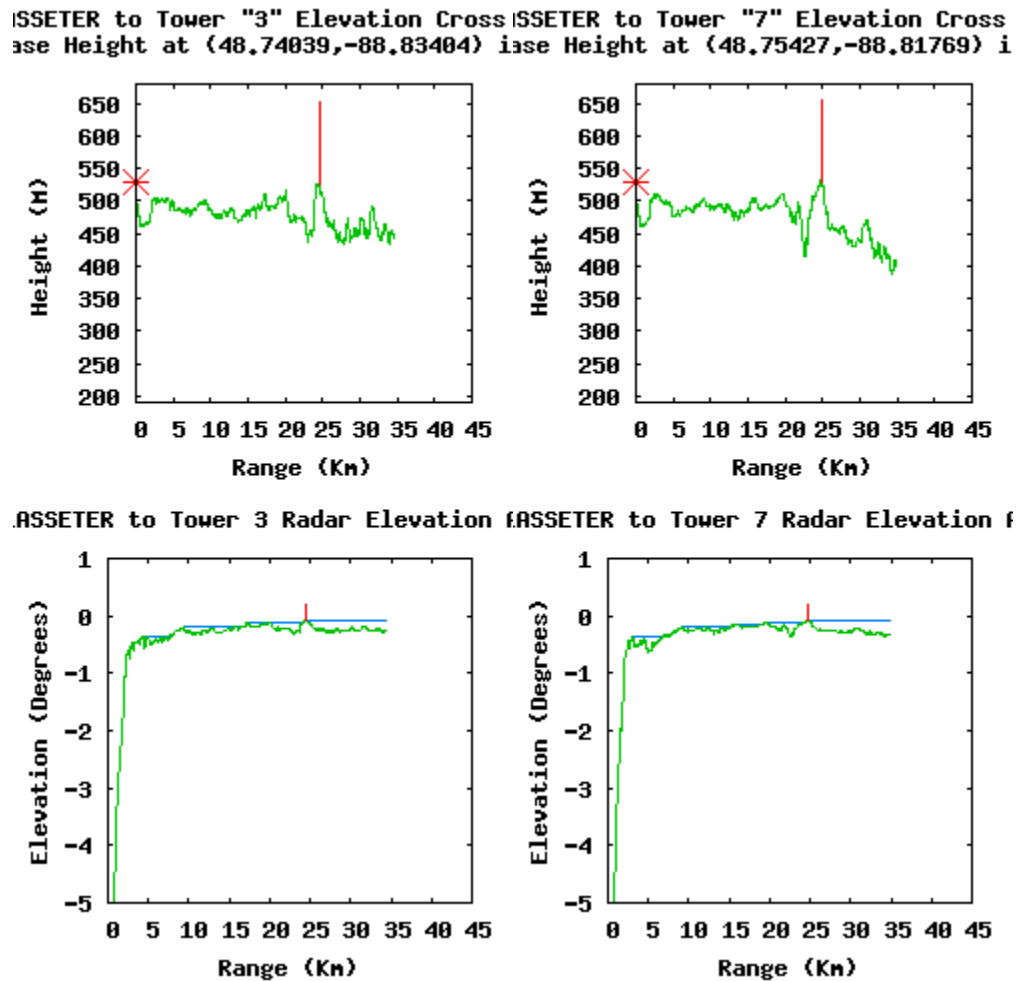


Figure 37: Wind Farm Analysis Tool - RLOS analysis performed on Greenwich turbines 3 (left) and 7 (right) as seen from the Lasseter Lake weather radar. Figure explanation found in Section 2.2.1 and Figure 12 caption.

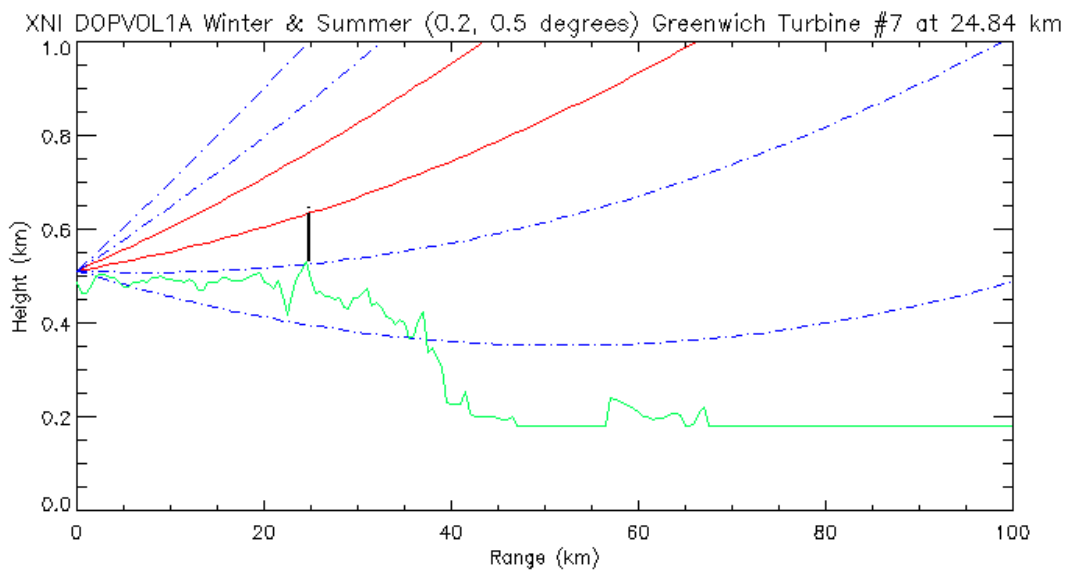
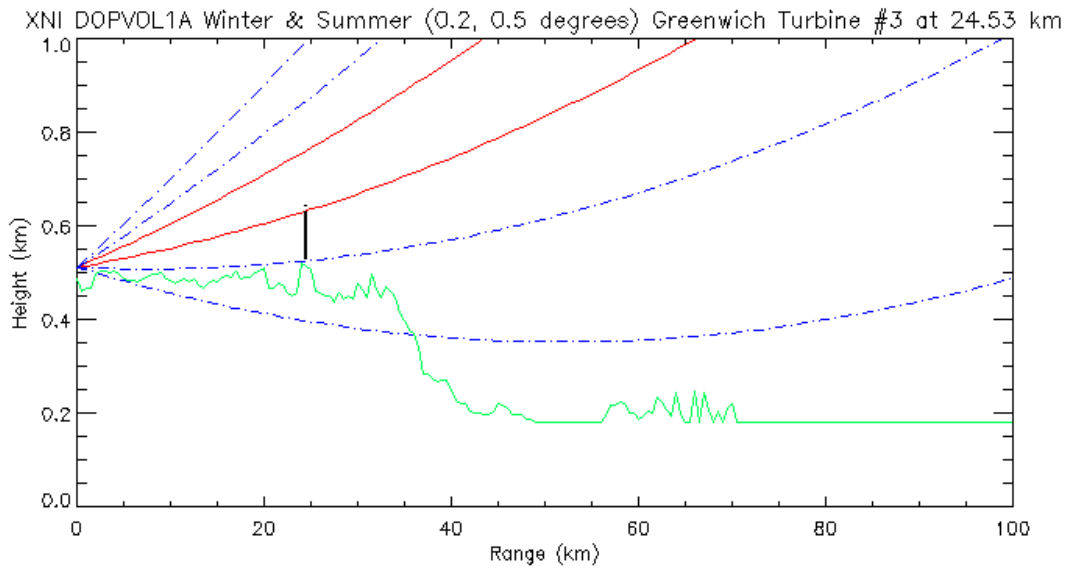


Figure 38: IDL Beamwidth Tool - RLOS analysis performed on Greenwich turbines 3 (top) and 7 (bottom) as seen from the Lasseter Lake weather radar. Figure explanation found in Section 2.2.2 and Figure 15 caption.

The following GIS viewsheds were completed to display the location of the turbines relative to the radar with specified radar elevation angles. Each image displays the DOPVOL1A scan elevation angles in either winter or summer for the radar where red areas show where turbines would be visible to the center of the main beam and orange areas show where turbines would be visible to the bottom of the main beam.

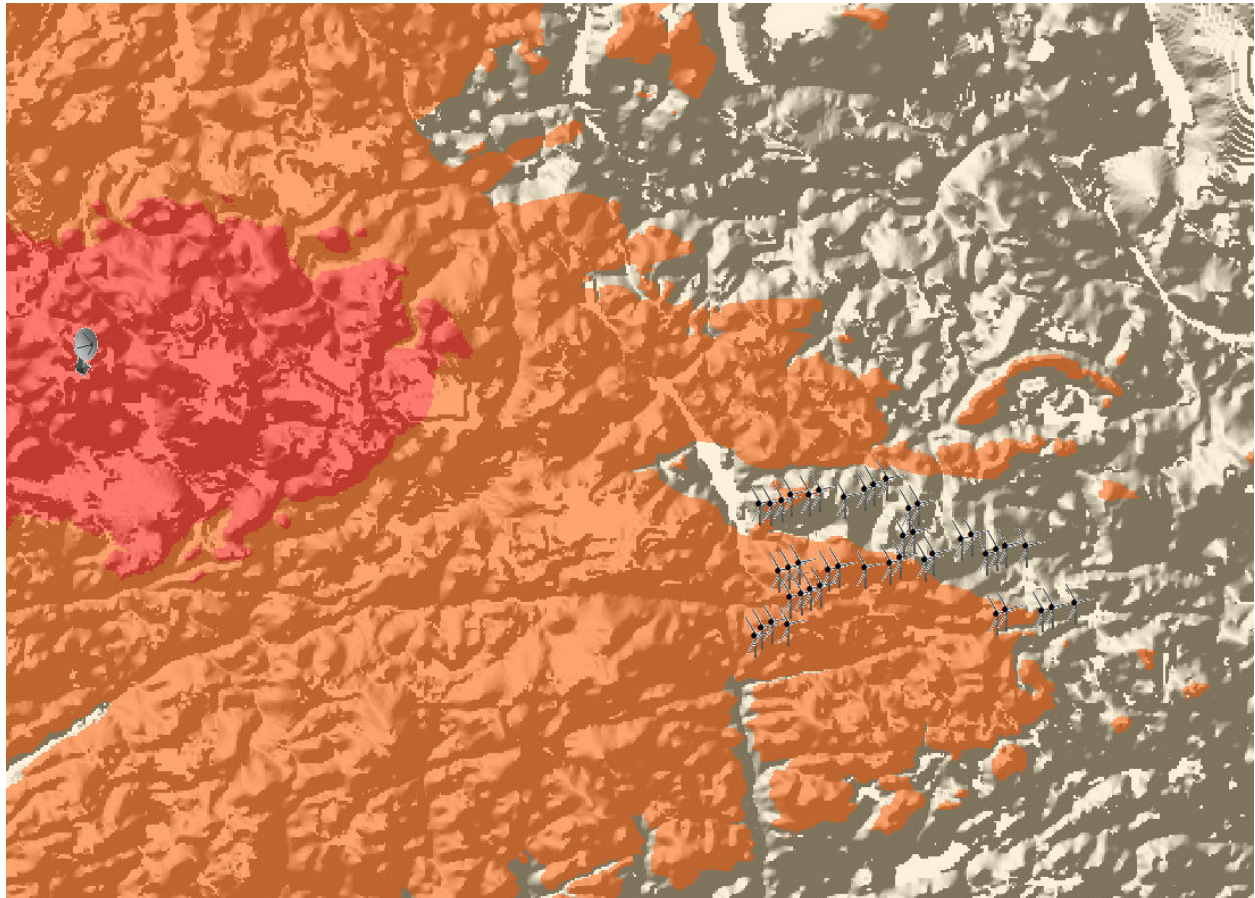


Figure 39: Lasseter Lake weather radar (radar dish) summer viewshed where Greenwich turbine locations are indicated in black. Locations which turbines would be visible in the center of the main beam (0.5°) are red and locations which turbines would be visible in the bottom of the main beam (-0.05°) are indicated in orange. (Created using ArcGIS 10.2.1)

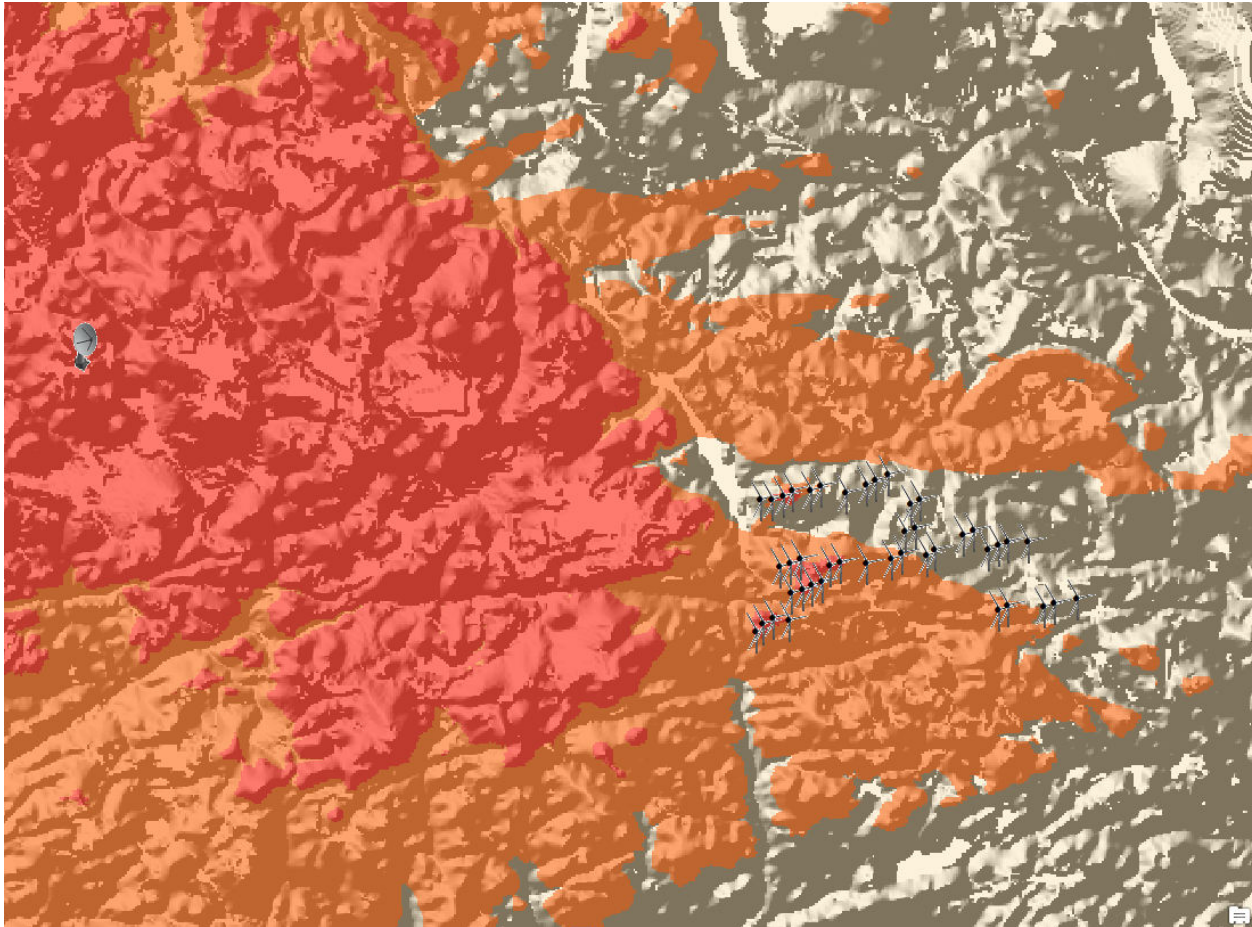


Figure 40: Lasseter Lake weather radar (radar dish) winter viewshed where Greenwich turbine locations are indicated in black. Locations which turbines would be visible in the center of the main beam (0.2°) are red and locations which turbines would be visible in the bottom of the main beam (-0.35°) are indicated in orange. (Created using ArcGIS 10.2.1)

3.2.4 WTC Examples

The following section displays WTC examples of the Greenwich wind farm as seen from the Lasseter Lake weather radar using the Productx and C-TRIP tools from the two case study days which are described in Table 13. Weather data were collected from Environment Canada's climate data archive at Thunder Bay Airport, which was found to be the closest hourly reporting weather site near the wind farm / radar pair. Productx images were created using maximum DBT and DBZ values for the XNI radar rays within the azimuth range 103° - 123° out to the Doppler range of 110 km (Figure 41). Additional Productx image for the case study days can be found in Appendix G. The C-TRIP images, like Figure 42, are zoomed in to display the Greenwich wind farm box only. WTC as seen from CLOGZPPI, VRPPI and PRECIP products for the selected case study days can found in Appendix H.

Table 13: Case study day weather information provided for Thunder Bay Airport

Date	2013-08-16			
Time	04:00 EDT	05:00 EDT	16:00 EDT	17:00 EDT
Weather Conditions	Temperature (°C), Relative Humidity (%), Weather			
Thunder Bay Airport	11.5, 94, Clear	11.5, 95, Clear	25.9, 38, Mainly Clear	25.4, 42, Mainly Clear
Date	2013-11-15			
Time	04:00 EST	05:00 EST	16:00 EST	17:00 EST
Weather Conditions	Temperature (°C), Relative Humidity (%), Weather			
Thunder Bay Airport	-1.6, 96, Cloudy	-0.9, 94, Snow	7.8, 48, Clear	6.1, 56, Clear

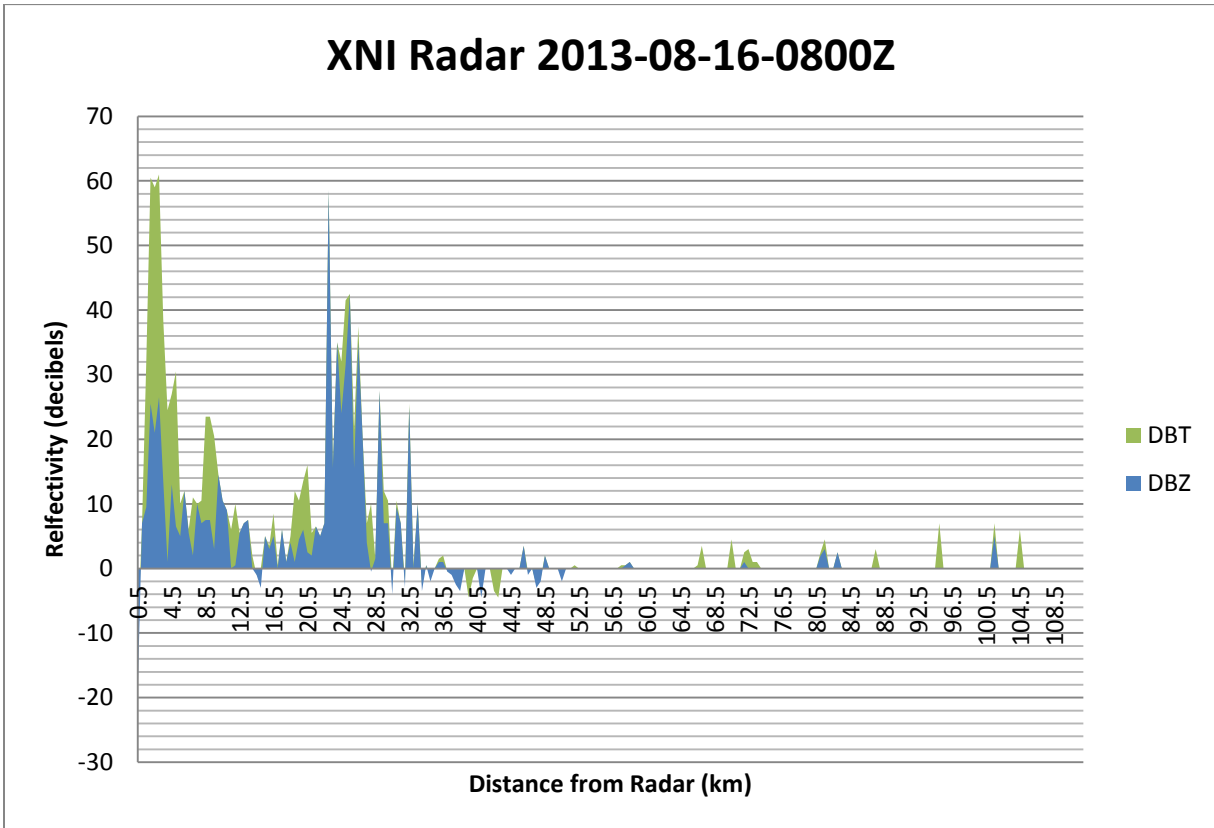


Figure 41: Example Lasseter Lake Productx output for 2013-08-16-0800Z where the maximum DBT and DBZ values for the azimuth range of 103° - 123° are displayed

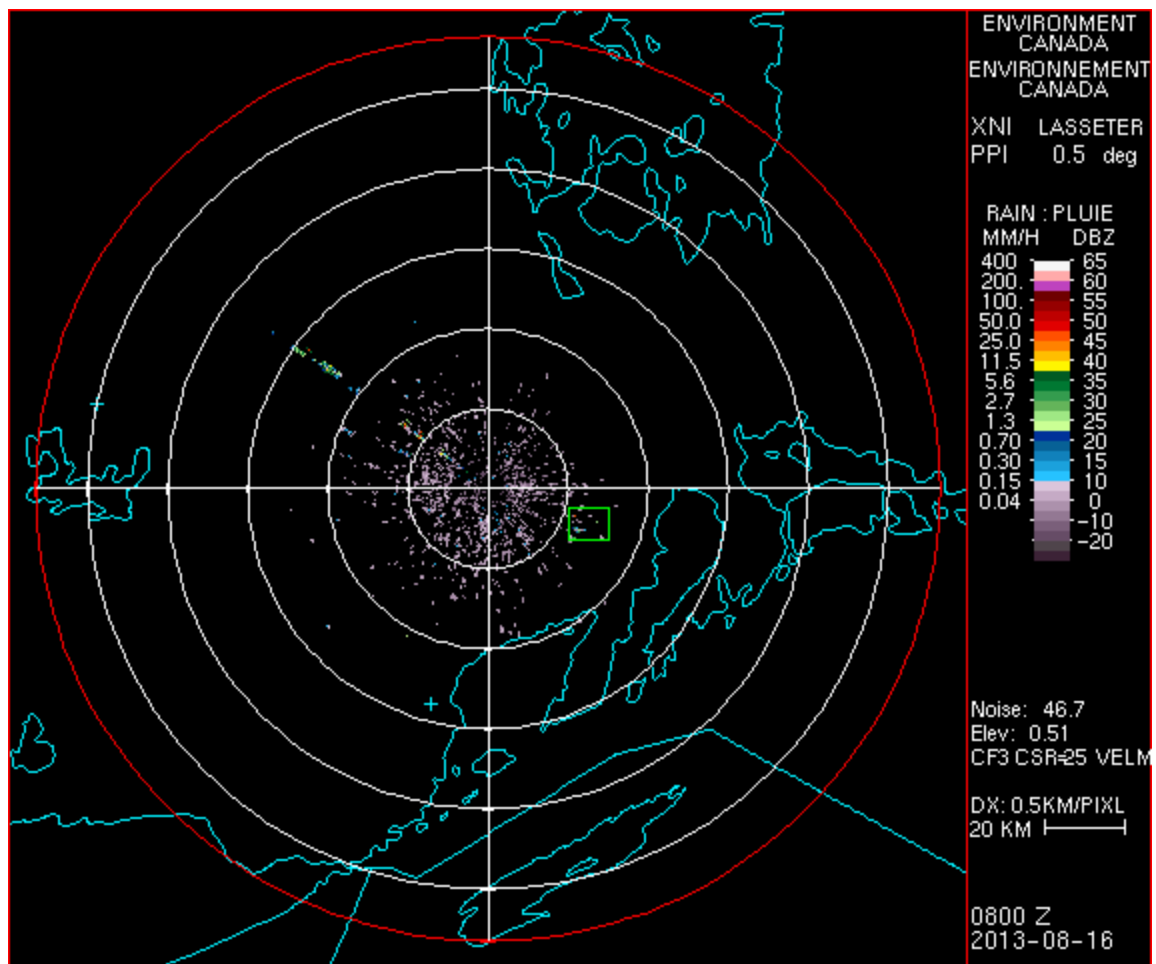


Figure 42: Example Lasseter Lake C-TRIP CLOGZPPI product on 2013-08-16 at 0800Z created using the DOPVOL1A XNI weather radar IRIS file where the Greenwich wind farm is outlined with the green box

3.3 Nuttby Mountain Wind Farm

The final wind farm / radar pair studied is the Nuttby Mountain wind farm located north of Truro, Nova Scotia and the Gore weather radar. This wind farm / radar pair was selected because observed WTC from the wind farm is substantial and consistent although RLOS calculations show that it should not be visible. The wind farm has been in commercial operation since 2010 and consists of 22 turbines producing 50.6 MW of power.

3.3.1 Wind Farm & Weather Radar Specifications

The Nuttby Mountain wind farm is located approximately 62.5 km from the Gore weather radar (XGO). Each of the turbines in the wind farm are 2.3MW models with tower heights of 80 meters and a swept area of 90 meters for a total height around 125 meters off the ground. The coordinates of the Nuttby Mountain turbines in decimal degrees latitude and longitude can be found in Appendix I and Figure 44.

Table 14: Information about the Gore weather radar

Gore Radar Information	Site ID	Lat	Lon	Height (mASL)	Feed horn (m)	Beamwidth (°)
	XGO	45.099	-63.704	219	21.5	0.65

Table 15: Gore weather radar Doppler scan elevation angles (°)

XGO Doppler Scans	DOPVOL1A	DOPVOL1B	DOPVOL1C	DOPVOL2
Summer	0.5	1.5	3.5	0.3
Winter	0	1.5	3.5	0.1

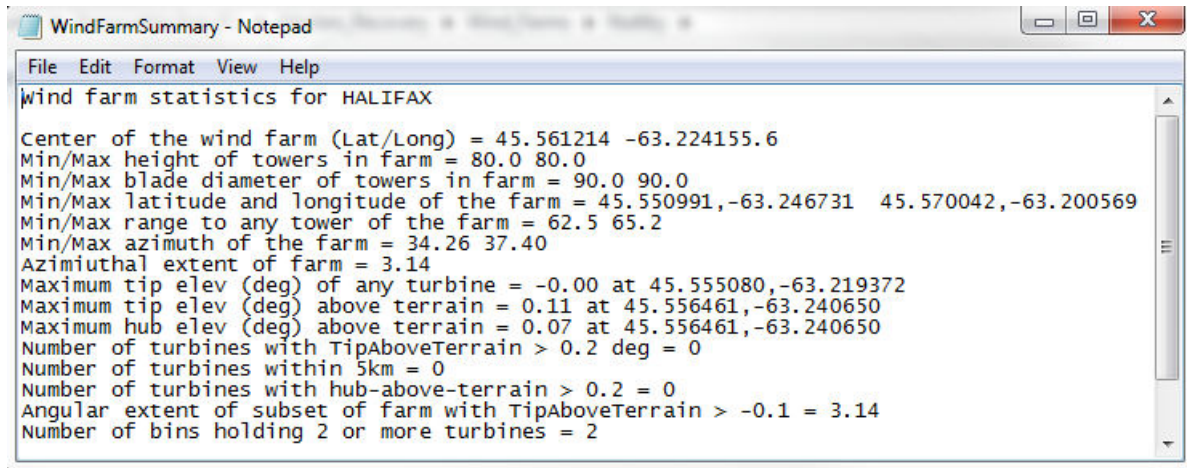


Figure 43: Wind farm summary output file for Nuttby Mountain wind farm / Gore weather radar pair



Figure 44: Location of Nuttby Mountain wind turbines (yellow as described in Table 2) and Gore weather radar (red)

Based on the azimuth range of the Nuttby Mountain wind farm as shown in Figure 43, a wind turbine orientation model has been created. The model, Table 16 and Figure 45, provides an estimation of the severity of WTC as determined by the direction of the wind and described in Section 2.5. This is discussed in comparison to operational wind turbine data found in Section 3.3.4 further in Chapter 5.

Nuttby Mountain Wind Turbine Orientation Model		
Wind Dir. Min	Wind Dir. Max	WTC Impact
0	33	Moderate
34	38	Marginal
39	123	Moderate
124	128	Severe
129	213	Moderate
214	218	Marginal
219	303	Moderate
304	308	Severe
309	359	Moderate



3.3.3 RLOS Analyses

The following RLOS analyses are completed for the two wind turbines (4 & 9) which are closest to the Gore weather radar using the Wind Farm Analysis (Section 2.2.1) and IDL Beamwidth (Section 2.2.2) tools.

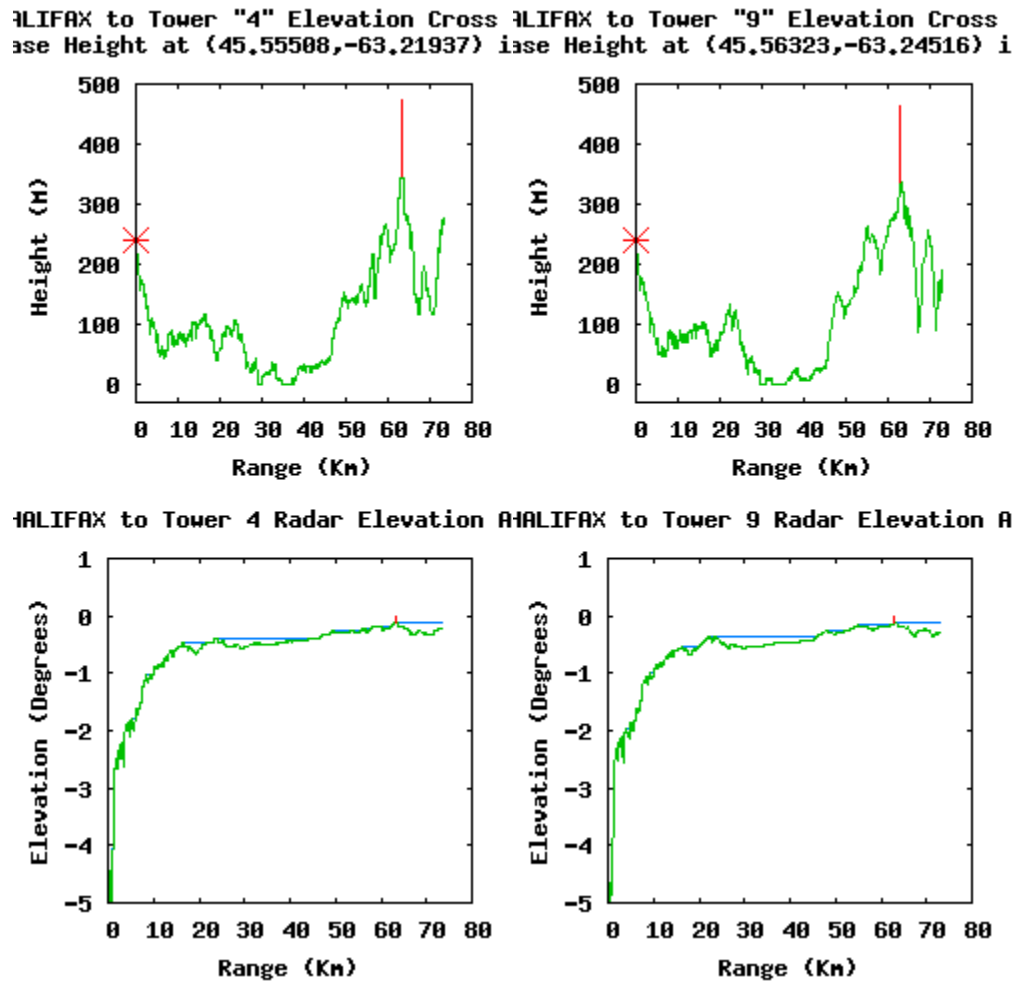


Figure 46: Wind Farm Analysis Tool - RLOS analysis performed on Nuttby Mountain turbines 4 (left) and 9 (right) as seen from the Gore weather radar. Figure explanation found in Section 2.2.1 and Figure 12 caption.

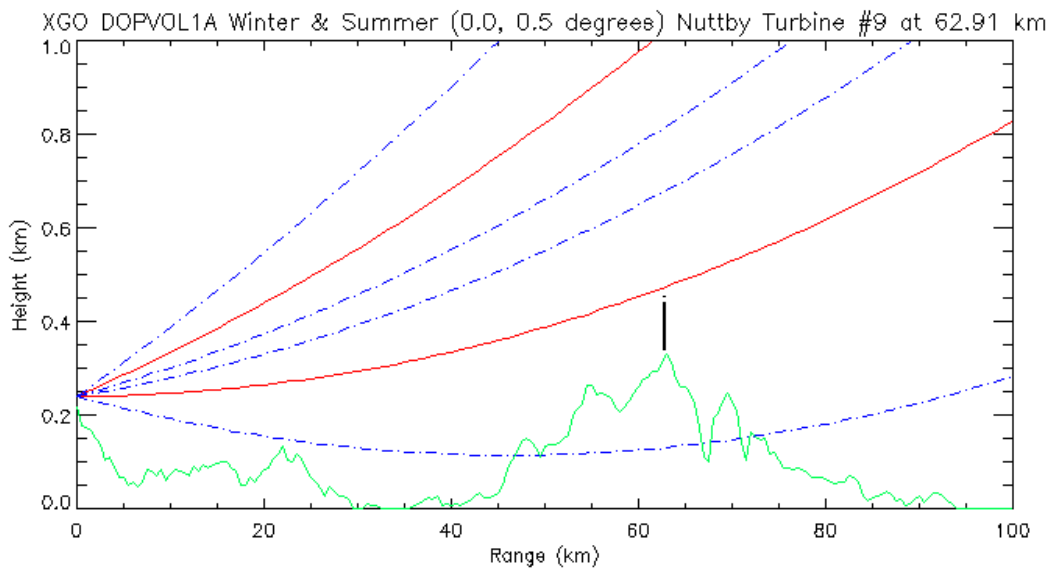
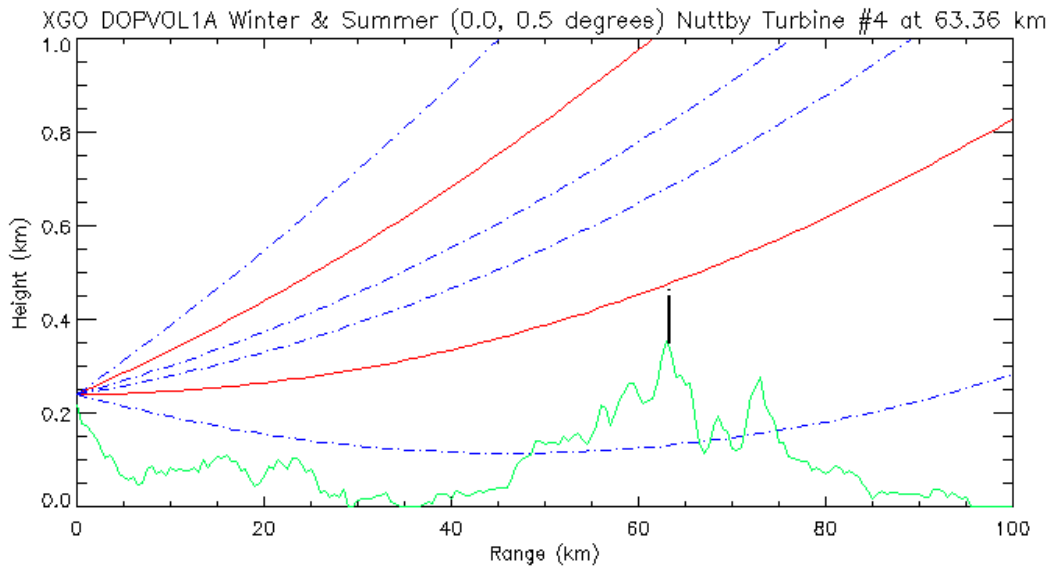


Figure 47: IDL Beamwidth Tool - RLOS analysis performed on Nuttby Mountain turbines 4 (top) and 9 (bottom) as seen from the Gore weather radar. Figure explanation found in Section 2.2.2 and Figure 15 caption.

The following GIS viewsheds were completed to display the location of the turbines relative to the radar with specified radar elevation angles. Each image displays the DOPVOL1A scan elevation angles in either winter or summer for the radar where red areas show where turbines would be visible to the center of the main beam and orange areas show where turbines would be visible to the bottom of the main beam.

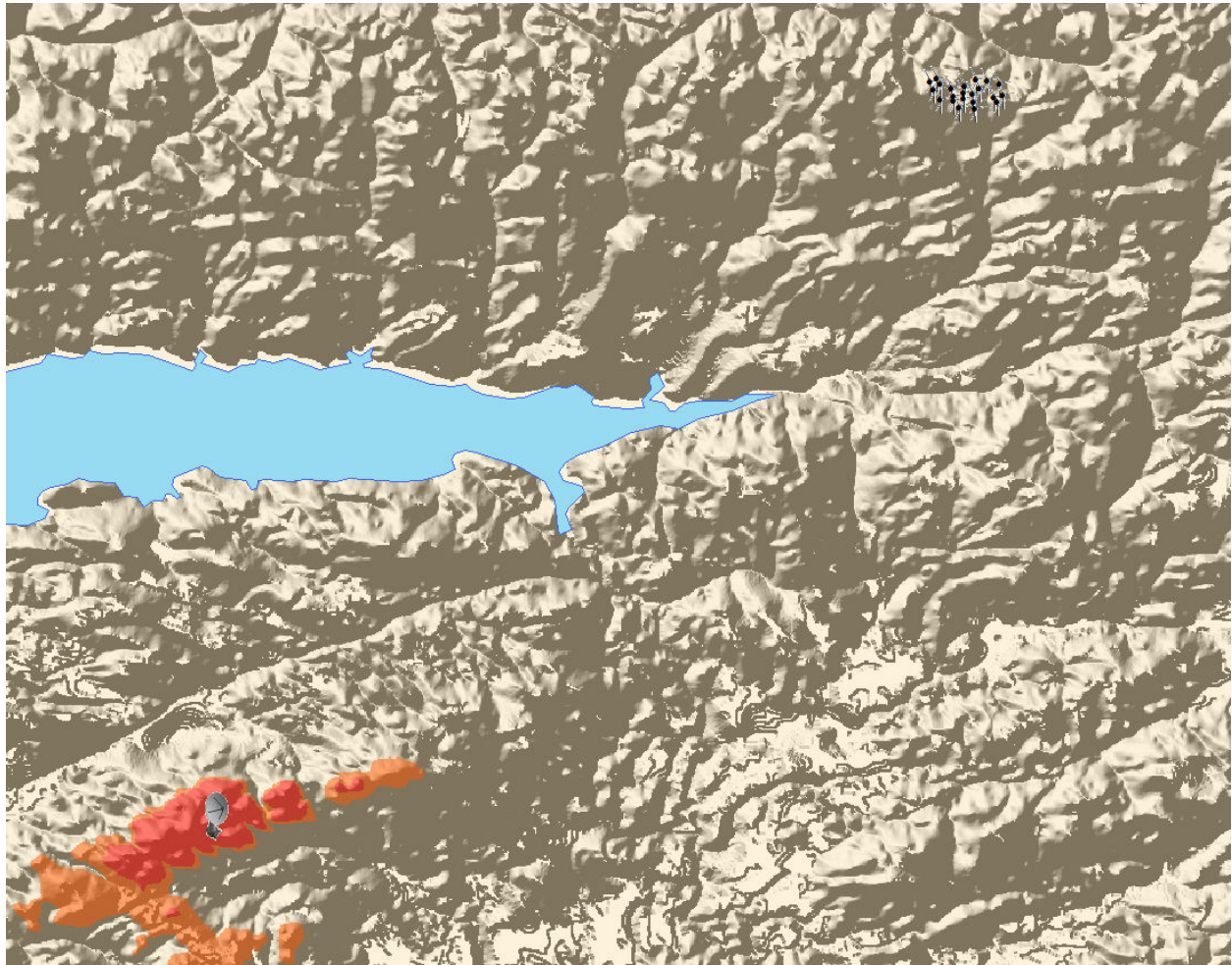


Figure 48: Gore weather radar (radar dish) summer viewshed where Nuttby Mountain turbine locations are indicated in black. Locations which turbines would be visible in the center of the main beam (0.5°) are red and locations which turbines would be visible in the bottom of the main beam (0.175°) are indicated in orange. (Created using ArcGIS 10.2.1)

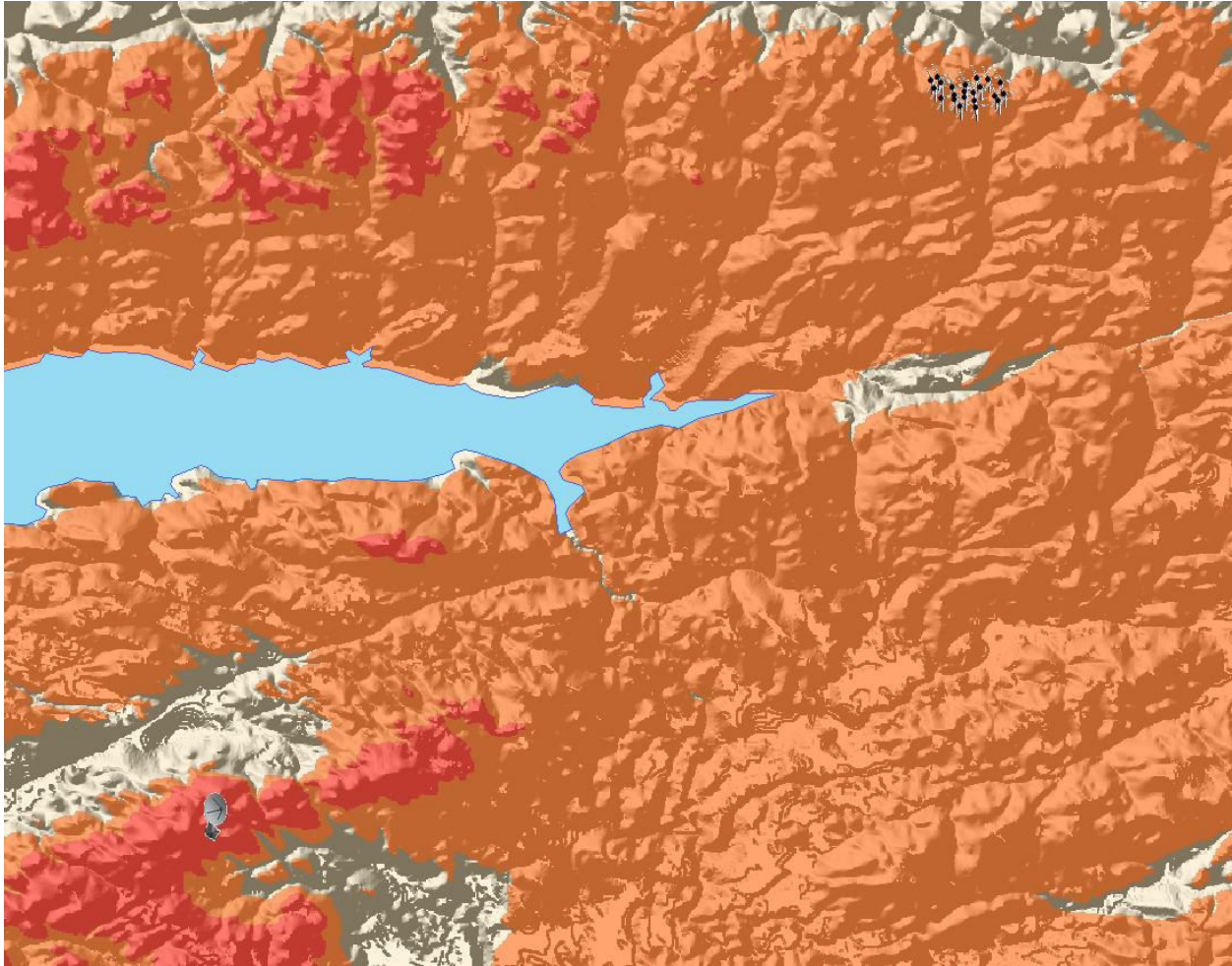


Figure 49: Gore weather radar (radar dish) winter viewshed where Nuttby Mountain turbine locations are indicated in black. Locations which turbines would be visible in the center of the main beam (0°) are red and locations which turbines would be visible in the bottom of the main beam (-0.325°) are indicated in orange. (Created using ArcGIS 10.2.1)

3.3.4 WTC Examples

The following section displays WTC examples of the Nuttby Mountain wind farm as seen from the Gore weather radar using the Productx and C-TRIP tools from the two case study days which are described in Table 17. Weather data were collected from Environment Canada's climate data archive at Halifax International Airport, which was found to be the closest hourly reporting weather site near the wind farm / radar pair. Productx images were created using maximum DBT and DBZ values for the XGO radar rays within the azimuth range 34° - 38° out to the Doppler range of 110 km (Figure 50). Additional Productx image for the case study days can be found in Appendix J. The C-TRIP images, like Figure 51, are zoomed in to display the Nuttby Mountain wind farm box only. WTC as seen from CLOGZPPI, VRPPI and PRECIP products for

the selected case study days can found in Appendix K. Due to data availability of operational wind turbine data, further analysis was completed to aid in the verification of the wind turbine orientation model displayed in 3.3.2 and the data in Tables 18 and 19.

Table 17: Case study day weather information provided for Halifax International Airport

Date	2013-08-16			
Time	04:00 ADT	05:00 ADT	16:00 ADT	17:00 ADT
Weather Conditions	Temperature (°C), Relative Humidity (%), Weather			
Halifax International Airport	13.7, 73, Mainly Clear	13.5, 74, Mainly Clear	21.8, 48, Mostly Cloudy	20.4, 58, Mainly Clear
Date	2013-11-15			
Time	04:00 AST	05:00 AST	16:00 AST	17:00 AST
Weather Conditions	Temperature (°C), Relative Humidity (%), Weather			
Halifax International Airport	3.1, 79, Cloudy	3.4, 77, Cloudy	8.8, 72, Mostly Cloudy	6.7, 80, Mainly Clear

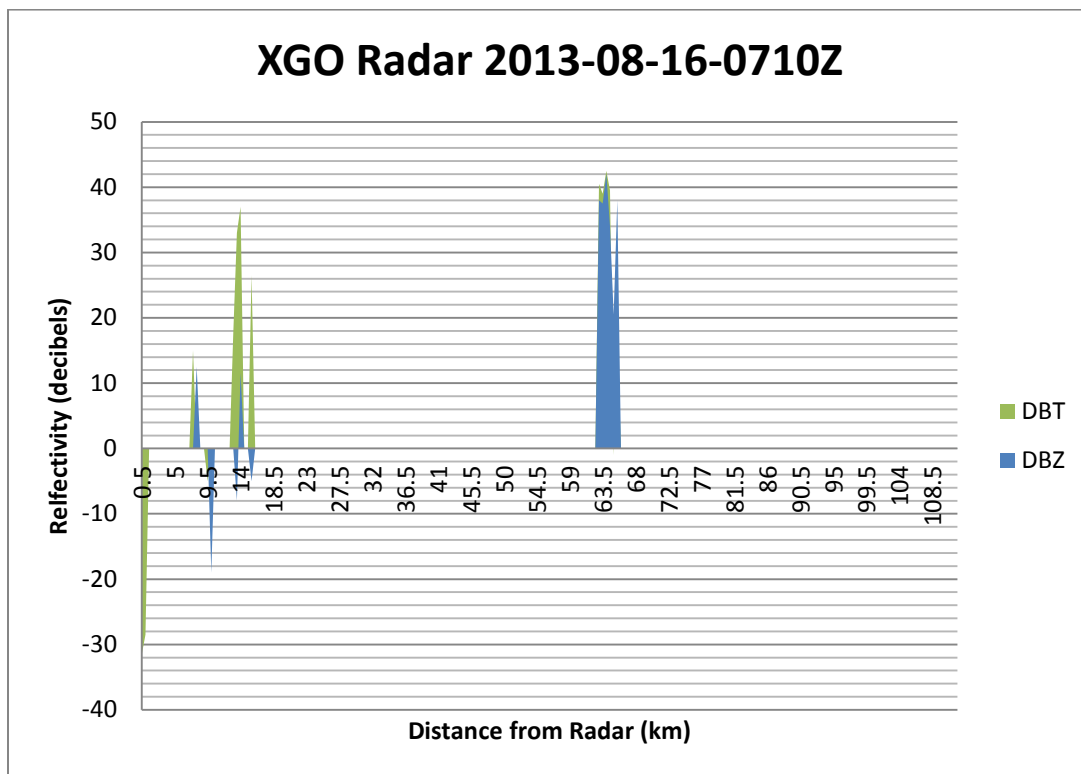


Figure 50: Example Gore Productx output for 2013-08-16-0710Z where the maximum DBT and DBZ values for the azimuth range of 34° - 38° are displayed

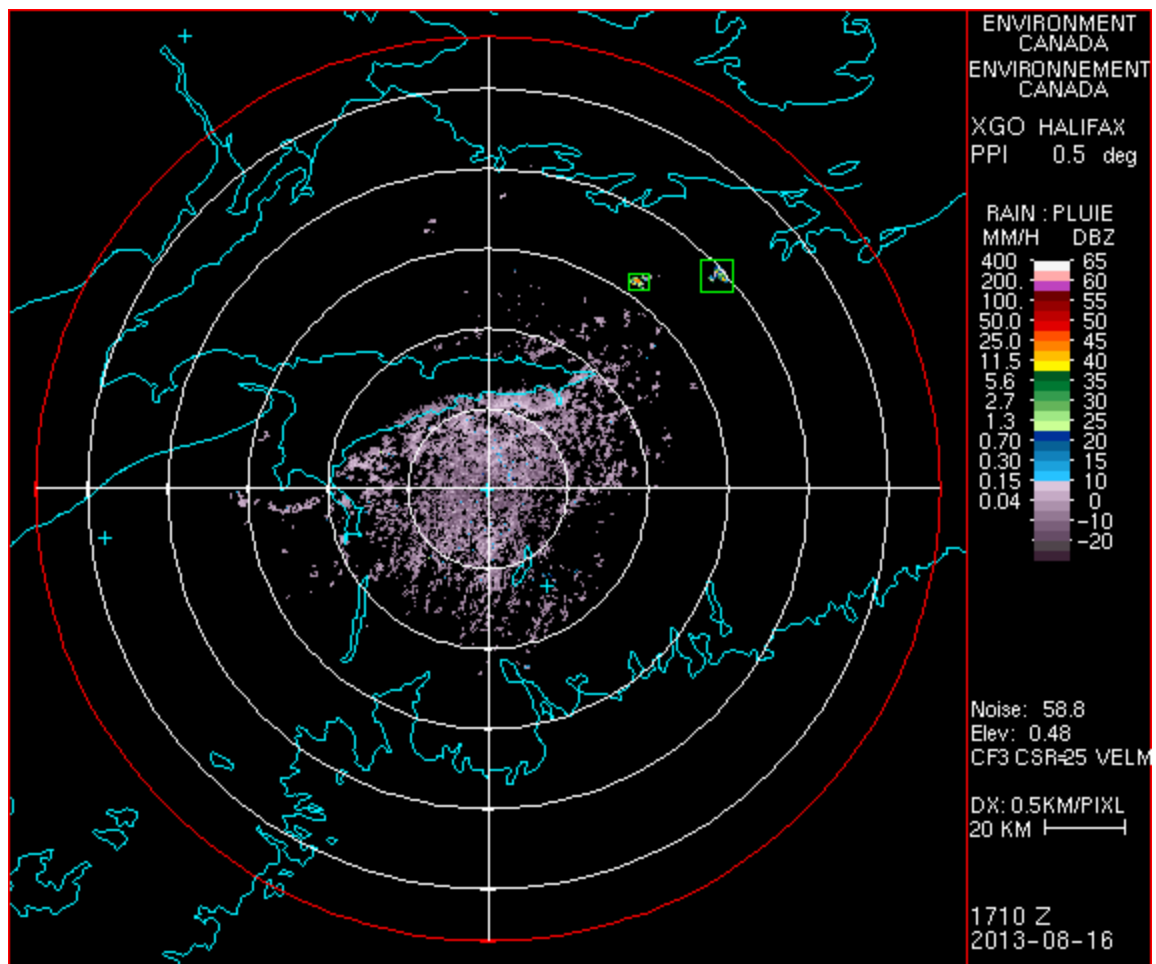


Figure 51: Example Gore C-TRIP CLOGZPPI product on 2013-08-16 at 0710Z created using the DOPVOL1A XGO weather radar IRIS file where the Nuttby Mountain wind farm is outlined with the smallest green box closest to the center of the radar

Table 18: Nacelle orientation in ° for each turbine in the Nuttby Mountain wind farm for the 04:00 hour on 2013-11-15 as provided by Nova Scotia Power

Turbine	4:00 AM (°)	4:10 AM (°)	4:20 AM (°)	4:30 AM (°)	4:40 AM (°)	4:50 AM (°)
1	278	245	241	244	250	256
2	282	272	256	257	265	265
3	263	268	243	242	255	251
4	287	285	267	267	276	278
5	282	287	264	262	274	273
6	262	266	255	241	252	249
7	276	276	264	257	264	261
8	275	275	275	271	267	267
9	294	294	293	283	282	283
10	282	283	283	273	269	274
11	286	284	277	256	264	270
12	277	278	275	259	259	267
13	241	253	238	226	230	234
14	272	283	260	257	255	258
15	275	273	261	253	257	257
16	266	279	266	244	257	262
17	268	271	255	251	252	254
18	260	258	243	238	242	246
19	272	281	265	253	268	269
20	264	259	235	240	253	253
21	271	277	254	252	258	263
22	279	279	280	272	269	273

Table 19: Nacelle position in ° for each turbine in the Nuttby Mountain wind farm for the 16:00 hour on 2013-11-15

Turbine	4:00 PM (°)	4:10 PM (°)	4:20 PM (°)	4:30 PM (°)	4:40 PM (°)	4:50 PM (°)
1	243	236	235	235	235	235
2	241	237	235	235	235	235
3	220	220	221	220	221	221
4	245	245	245	245	245	245
5	241	241	238	238	238	238
6	221	218	216	216	216	216
7	228	226	223	223	223	223
8	223	223	219	219	219	219
9	243	242	238	238	238	238
10	232	232	228	226	226	226
11	238	238	236	236	237	236
12	233	232	228	228	230	231
13	203	200	198	198	199	199
14	229	231	231	228	230	228
15	218	218	218	218	218	218
16	225	223	219	219	220	219
17	226	227	227	227	227	227
18	216	216	216	216	216	216
19	233	233	230	228	228	228
20	225	225	224	223	222	222
21	227	226	224	224	224	224
22	229	229	225	225	225	225

4. Case Study: Modeling Radar Beam Propagation from the Gore Weather Radar to the Nuttby Mountain Wind Farm

This chapter provides a methodology for studying the effects of radar beam propagation on WTC as described in Section 1.2.2. Collected MOLTS points are used to model the Gore weather radar beam for a particular day and case study times as it travels toward the Nuttby Mountain wind farm. The results are discussed in further detail in Section 5.3.

4.1 Case Study Methodology

Although MOLTS points were selected for all wind farm / radar pairs (as described in Section 2.6.2), due to limited wind farm operational data availability, only the Nuttby Mountain wind farm / Gore weather radar pair was selected for the study. The date selected was 2014-07-07. In order to model how the radar beam propagates through the atmosphere five data points were selected: one at near the radar, one near the wind farm, one in between the wind farm and the radar and two points in between at approximately $\frac{1}{4}$ and $\frac{3}{4}$ distances. MOLTS data are approximated for each requested point in a 2.5 km grid (as seen in Table 5) and shown in Figure 52.

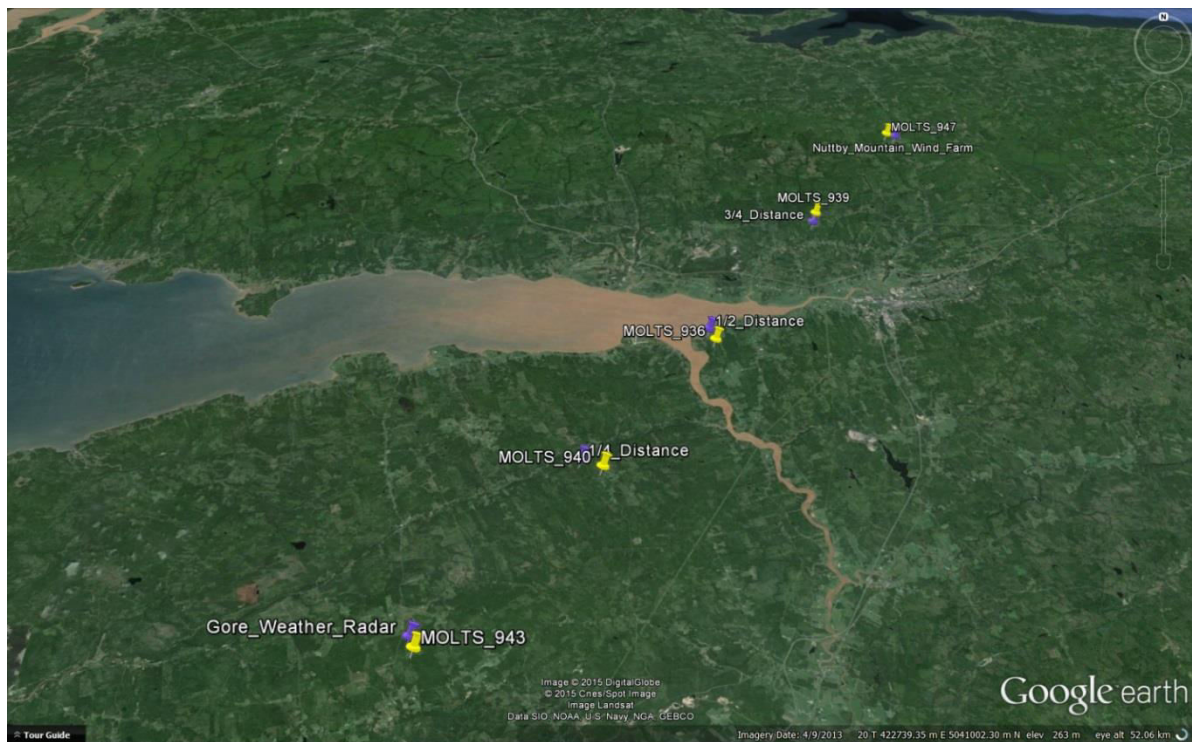


Figure 52: Location of requested (purple) and provided (yellow) MOLTS center points to model the radar beam path from the Gore weather radar to the Nuttby Mountain Wind Farm

The height of the radar beam was modeled using Equation 4 where the K (effective Earth radius factor) value is updated based on the calculated N (refractivity) value from provided MOLTS meteorological data using Equation 7. Since multiple MOLTS points are used (as seen in Table 20), an average of two K values (for example K12) is used to approximate the height of the radar beam at each point. The height of the radar beam at the Nuttby Mountain wind farm is then an addition of these heights subtracting the difference in elevation from the first point to the last. A comparison of the usefulness of this calculation is then made when comparing to standard atmospheric conditions (where $K = \frac{3}{4}$) and observed WTC show using C-TRIP during the tested time periods. During standard atmospheric conditions the center of the radar beam would be approximately 678 meters above the wind farm and the bottom of the main beam would be 316 meters above the wind farm.

Table 20: Height above sea level for each point along the path from the Gore weather radar to the Nuttby Mountain wind farm along with the distance from one point to the next

Location	Height ASL (km)	K #	Distance from Previous (km)
Gore Weather Radar	0.215	K1	
1/4 Distance	0.101	K2	16.07
1/2 Distance	0.013	K3	15.60
3/4 Distance	0.084	K4	16.14
Nuttby Mountain Wind Farm	0.310	K5	15.85
Total Distance - K12345 (km)			63.66

In order to calculate K for each time period for each point location, the change in refractivity (N) by height is required. Since some MOLTS variables are collected at 58 vertical levels in the atmosphere, it was decided to find the value of dN/dH for approximately the first kilometer (H_1). In order to calculate the refractivity (N) at the surface (H_0) and at H_1 the following variables are required:

- Pressure (P) in hectopascals – hPa
 - Only surface pressure is available, therefore pressure at H_1 needs to be calculated
- Temperature (T) in Kelvin – K
 - Temperature is available for H_0 and H_1 in degrees Celsius and can be converted to Kelvin by adding 273.15 to the value

- Water vapour pressure (e) in hPa
 - Water vapour pressure is not available, but can be computed knowing the temperature, and relative humidity at the surface and H₁

The following calculations and variables were performed and collected to obtain the required meteorological variables to calculate N at H₀ and at the closest vertical level to one kilometer (H₁) where H is in meters above ground level:

1. The change in temperature (dT) was calculated by subtracting the temperature at H₁ by the surface temperature
2. The pressure in at H₁ was calculated using Equation 12:

Equation 12: Pressure at H₁ calculated from rearranging hypsometric equation

$$P_1 = \frac{P_0}{e^{\frac{g}{R\bar{T}}(h_1-h_0)}}$$

Where *g* is the acceleration due to gravity (9.81 ms⁻²), *Rd* is the gas constant for dry air (287.15 JK⁻¹kg⁻¹), *h* is the height difference in m, *P* is the pressure in hPa and \bar{T} is the average temperature in K

3. The saturation vapour pressure (e_s) was calculated for H₀ and H₁ using Equation 13:

Equation 13: Calculation for saturation vapour pressure given temperature

$$e_s = 6.1121e^{\left(\frac{17.502T}{240.97+T}\right)}$$

Where *T* is in °C

4. The water vapour pressure was then calculated for H₀ and H₁ using Equation 14:

$$e = e_s \left(\frac{RH}{100} \right)$$

Where *RH* is the relative humidity in %

5. The values of N at H₁ and H₀ were then calculated using Equation 7

Once the refractivity values were known at H₁ and H₀, dN/dH (in N-units per kilometer) is easily calculated and converted to dn/dh by multiplying by 10⁻⁶. Using Equation 5, the value of K can then be calculated and using in Equation 4 to determine the height of the radar beam. The height of the radar beam for each point is then normalized based on the point location height above sea level.

4.2 Results

This section displays WTC examples of the Nuttby Mountain wind farm as seen from the Gore weather radar using the C-TRIP tool from 2014-07-07 for 3 hours. The C-TRIP images are zoomed in to display the CLOGZPPI, VRPPI and PRECIP products defined by the Nuttby Mountain wind farm box. Additionally, this section provides the results of modeling the height of the Gore weather radar beam over the Nuttby Mountain wind farm using MOLTS points described in Section 4.1 for 2014-07-07 from 0700 Z – 0950Z. Section 5.3 will discuss these results and draw conclusions on the comparison between modeled RLOS and observed WTC.

Table 21: Radar beam modeling results on 2014-07-07 from 0700 Z – 0750 Z using MOLTS points described in Table 5 and Table 20

2014-07-07 0700Z	Values	Averages	Height above K1 horizon (km)	
K1	1.2693		Center of Beam	Bottom of Beam
K2	1.2529	1.2611	0.1348	0.0437
K3	1.2829	1.2679	0.1531	0.0634
K4	1.2494	1.2662	0.1552	0.0648
K5	1.2572	1.2533	0.1531	0.0638
Height above Nuttby Mountain Wind Farm (km)			0.5012	0.1407
2014-07-07 0710Z	Values	Averages	Height above K1 horizon (km)	
K1	1.2698		Center of Beam	Bottom of Beam
K2	1.2662	1.2680	0.1347	0.0436
K3	1.2870	1.2766	0.1530	0.0633
K4	1.2497	1.2683	0.1552	0.0648
K5	1.2561	1.2529	0.1531	0.0638
Height above Nuttby Mountain Wind Farm (km)			0.5011	0.1405
2014-07-07 0720Z	Values	Averages	Height above K1 horizon (km)	
K1	1.2734		Center of Beam	Bottom of Beam
K2	1.2730	1.2732	0.1347	0.0432
K3	1.2930	1.2830	0.1529	0.0632
K4	1.2553	1.2741	0.1551	0.0647
K5	1.2561	1.2557	0.1531	0.0638
Height above Nuttby Mountain Wind Farm (km)			0.5008	0.1399
2014-07-07 0730Z	Values	Averages	Height above K1 horizon (km)	
K1	1.2804		Center of Beam	Bottom of Beam

K2	1.2823	1.2814	0.1345	0.0433
K3	1.3002	1.2913	0.1528	0.0631
K4	1.2607	1.2805	0.1551	0.0647
K5	1.2535	1.2571	0.1531	0.0678
Height above Nuttby Mountain Wind Farm (km)			0.5005	0.1439
2014-07-07 0740Z	Values	Averages	Height above K1 horizon (km)	
K1	1.2892		Center of Beam	Bottom of Beam
K2	1.2889	1.2891	0.1345	0.0433
K3	1.3053	1.2971	0.1528	0.0630
K4	1.2640	1.2847	0.1550	0.0646
K5	1.2495	1.2568	0.1531	0.0638
Height above Nuttby Mountain Wind Farm (km)			0.5004	0.1397
2014-07-07 0750Z	Values	Averages	Height above K1 horizon (km)	
K1	1.2974		Center of Beam	Bottom of Beam
K2	1.2958	1.2966	0.1344	0.0432
K3	1.3131	1.3045	0.1527	0.0630
K4	1.2697	1.2914	0.1549	0.0645
K5	1.2475	1.2586	0.1531	0.0638
Height above Nuttby Mountain Wind Farm (km)			0.5001	0.1395

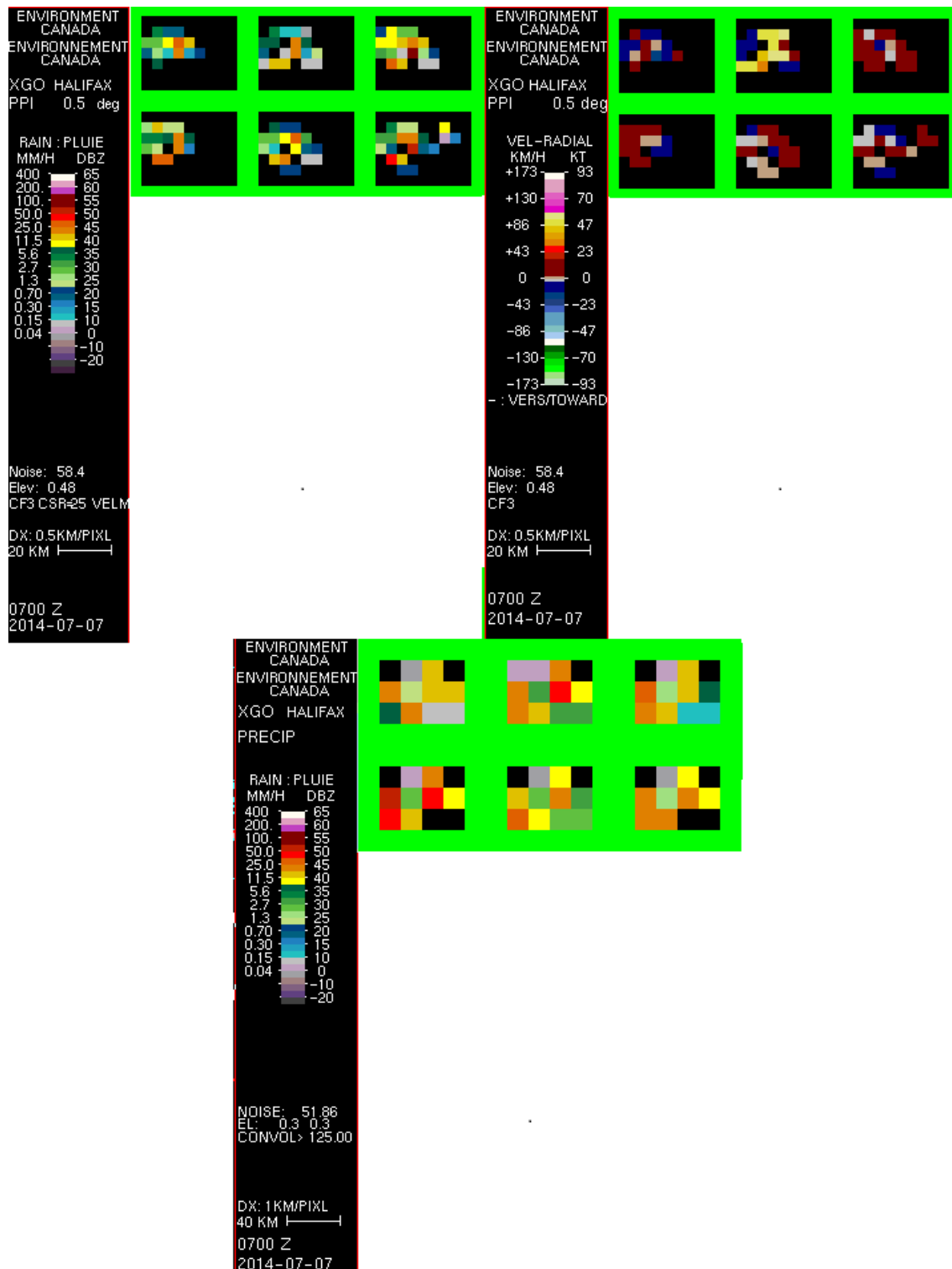


Figure 53: C-TRIP CLOGZPPI, VRPPI and PRECIP products of the Nuttby Mountain wind farm box on 2014-07-07 from 0700 Z – 0750 Z created using the DOPVOL1A and DOPVOL2 XGO IRIS files

Table 22: Radar beam modeling results on 2014-07-07 from 0800 Z – 0850 Z using MOLTS points described in Table 5 and Table 20

2014-07-07 0800Z	Values	Averages	Height above K1 horizon (km)	
K1	1.3028		Center of Beam	Bottom of Beam
K2	1.3015	1.3022	0.1343	0.0431
K3	1.3234	1.3125	0.1526	0.0627
K4	1.2784	1.3009	0.1548	0.0644
K5	1.2474	1.2629	0.1531	0.0638
Height above Nuttby Mountain Wind Farm (km)			0.4998	0.139
2014-07-07 0810Z	Values	Averages	Height above K1 horizon (km)	
K1	1.3051		Center of Beam	Bottom of Beam
K2	1.3037	1.3044	0.1343	0.0431
K3	1.3288	1.3162	0.1525	0.0628
K4	1.2827	1.3058	0.1548	0.0643
K5	1.2486	1.2657	0.1531	0.0638
Height above Nuttby Mountain Wind Farm (km)			0.4997	0.1390
2014-07-07 0820Z	Values	Averages	Height above K1 horizon (km)	
K1	1.3073		Center of Beam	Bottom of Beam
K2	1.3058	1.3065	0.1343	0.0431
K3	1.3334	1.3196	0.1525	0.0628
K4	1.2869	1.3101	0.1547	0.0643
K5	1.2498	1.2684	0.1531	0.0638
Height above Nuttby Mountain Wind Farm (km)			0.4996	0.1390
2014-07-07 0830Z	Values	Averages	Height above K1 horizon (km)	
K1	1.3093		Center of Beam	Bottom of Beam
K2	1.3083	1.3088	0.1342	0.0431
K3	1.3376	1.3230	0.1525	0.0627
K4	1.2910	1.3143	0.1547	0.0642
K5	1.2514	1.2712	0.1531	0.0638
Height above Nuttby Mountain Wind Farm (km)			0.4995	0.1388

2014-07-07 0840Z	Values	Averages	Height above K1 horizon (km)	
K1	1.3109		Center of Beam	Bottom of Beam
K2	1.3108	1.3108	0.1342	0.0430
K3	1.3406	1.3257	0.1524	0.0627
K4	1.2946	1.3176	0.1546	0.0642
K5	1.2522	1.2734	0.1531	0.0638
Height above Nuttby Mountain Wind Farm (km)			0.4993	0.1387
2014-07-07 0850Z	Values	Averages	Height above K1 horizon (km)	
K1	1.3125		Center of Beam	Bottom of Beam
K2	1.3139	1.3132	0.1342	0.0430
K3	1.3440	1.3290	0.1524	0.0627
K4	1.2985	1.3213	0.1546	0.0642
K5	1.2534	1.2760	0.1531	0.0638
Height above Nuttby Mountain Wind Farm (km)			0.4993	0.1387

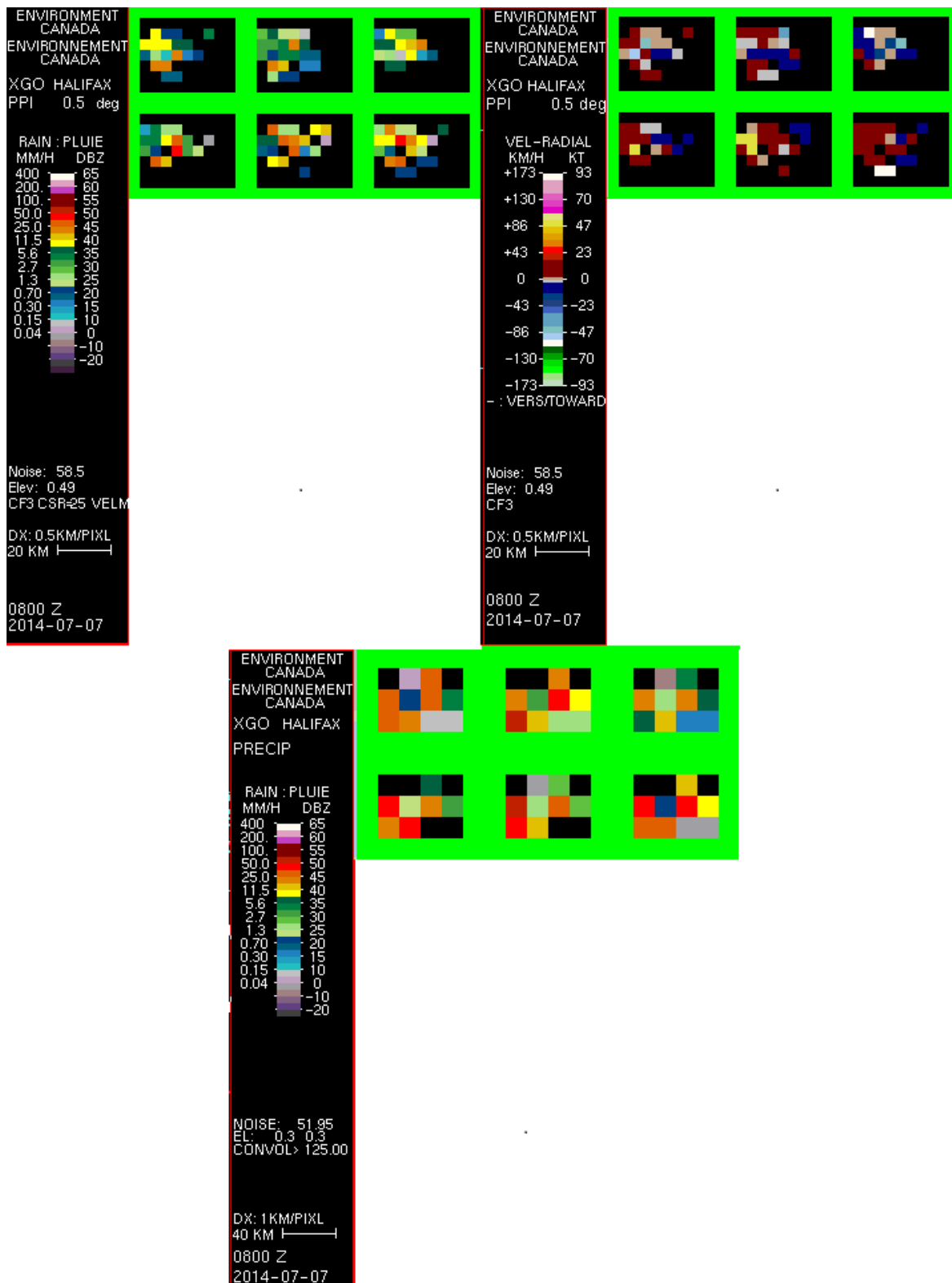


Figure 54: C-TRIP CLOGZPPI, VRPPI and PRECIP products of the Nuttby Mountain wind farm box on 2014-07-07 from 0800 Z – 0850 Z created using the DOPVOL1A and DOPVOL2 XGO IRIS files

Table 23: Radar beam modeling results on 2014-07-07 from 0900 Z – 0950 Z using MOLTS points described in Table 5 and Table 20

2014-07-07 0900Z	Values	Averages	Height above K1 horizon (km)	
K1	1.314501071		Center of Beam	Bottom of Beam
K2	1.317445517	1.3160	0.1341	0.0430
K3	1.347589299	1.3325	0.1524	0.0626
K4	1.302602885	1.3251	0.1545	0.0641
K5	1.255016492	1.2788	0.1531	0.0638
Height above Nuttby Mountain Wind Farm (km)			0.4991	0.1385
2014-07-07 0910Z	Values	Averages	Height above K1 horizon (km)	
K1	1.3160		Center of Beam	Bottom of Beam
K2	1.3212	1.3186	0.1341	0.0430
K3	1.3522	1.3367	0.1523	0.0626
K4	1.3066	1.3294	0.1545	0.0641
K5	1.2580	1.2823	0.1531	0.0638
Height above Nuttby Mountain Wind Farm (km)			0.4990	0.1385
2014-07-07 0920Z	Values	Averages	Height above K1 horizon (km)	
K1	1.317806721		Center of Beam	Bottom of Beam
K2	1.325409464	1.3216	0.1341	0.0429
K3	1.357164287	1.3413	0.1523	0.0626
K4	1.31071516	1.3339	0.1544	0.0640
K5	1.261119828	1.2859	0.1531	0.0638
Height above Nuttby Mountain Wind Farm (km)			0.4989	0.1383
2014-07-07 0930Z	Values	Averages	Height above K1 horizon (km)	
K1	1.3206		Center of Beam	Bottom of Beam
K2	1.3302	1.3254	0.1340	0.0429
K3	1.3625	1.3463	0.1522	0.0625
K4	1.3146	1.3386	0.1544	0.0640
K5	1.2644	1.2895	0.1531	0.0638
Height above Nuttby Mountain Wind Farm (km)			0.4987	0.1382

2014-07-07 0940Z	Values	Averages	Height above K1 horizon (km)	
K1	1.3231		Center of Beam	Bottom of Beam
K2	1.3348	1.3289	0.1340	0.0428
K3	1.3678	1.3513	0.1522	0.0624
K4	1.3181	1.3429	0.1543	0.0639
K5	1.2675	1.2928	0.1531	0.0638
Height above Nuttby Mountain Wind Farm (km)			0.4986	0.1379
2014-07-07 0950Z	Values	Averages	Height above K1 horizon (km)	
K1	1.3261		Center of Beam	Bottom of Beam
K2	1.3387	1.3324	0.1339	0.0428
K3	1.3728	1.3558	0.1521	0.0624
K4	1.3213	1.3471	0.1543	0.0639
K5	1.2703	1.2958	0.1531	0.0638
Height above Nuttby Mountain Wind Farm (km)			0.4984	0.1378

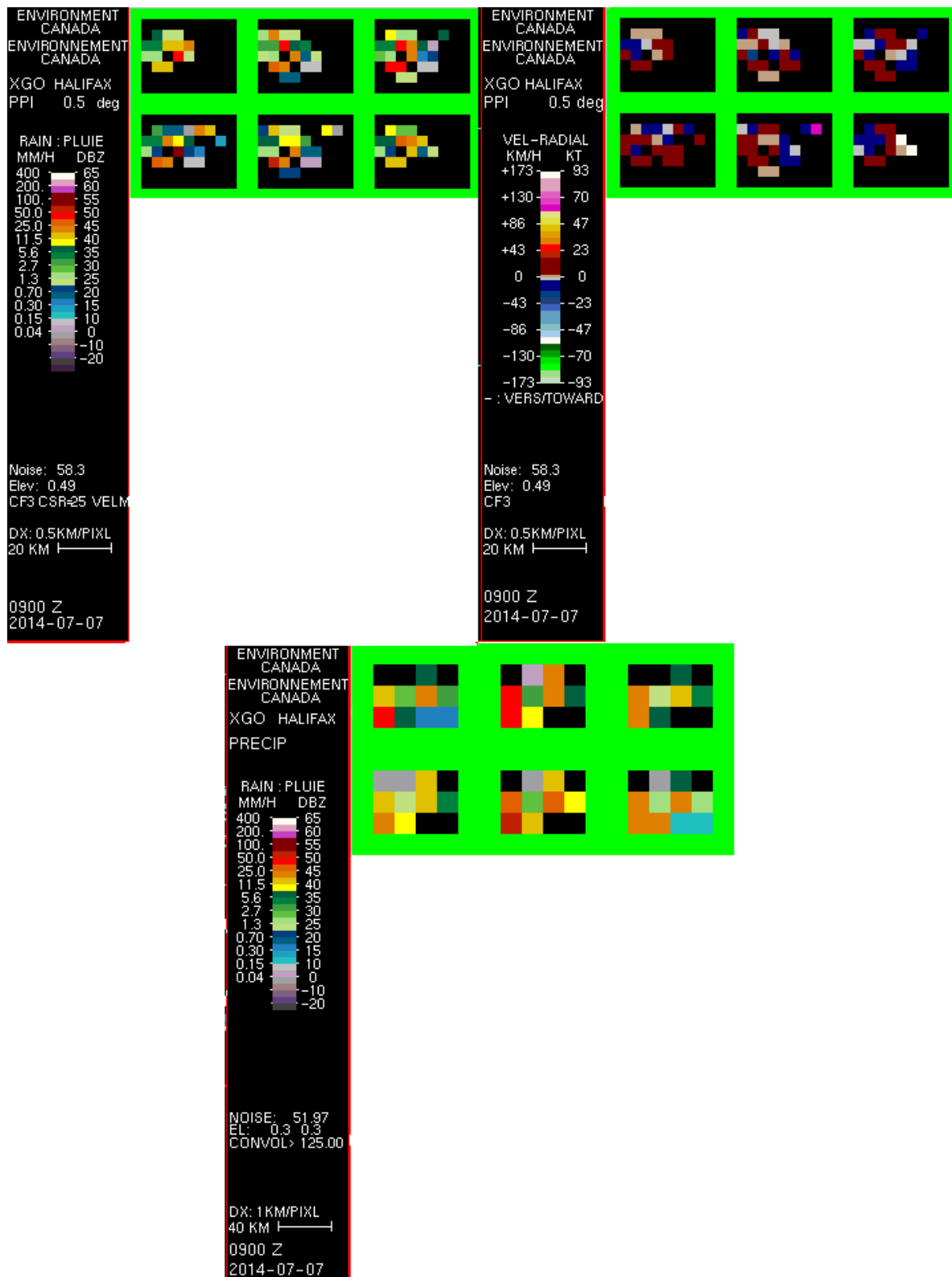


Figure 55: C-TRIP CLOGZPPI, VRPPI and PRECIP products of the Nuttby Mountain wind farm box on 2014-07-07 from 0800 Z – 0850 Z created using the DOPVOL1A and DOPVOL2 XGO IRIS files

5. Case Studies

The following chapter provides a discussion of the comparison of RLOS and observed WTC for the three selected wind farm / radar pairs. The discussion includes comparisons of RLOS under standard atmospheric conditions using Wind Farm Analysis, IDL Beamwidth and GIS Viewshed tools as described in Section 2.2. The expected WTC based on RLOS is then compared to observed WTC using Productx and C-TRIP tools for the two selected summer and winter case study days during a morning hour (04:00 local time) and afternoon hour (16:00 local time).

Although wind turbine orientation models were created for each wind farm / radar pair, operational wind turbine data were only made available for the Nuttby Mountain wind farm and as such, only the Nuttby Mountain wind turbine orientation model found in Section 3.3.2 is compared to operational wind turbine data on the winter case study day. Additionally, Section 5.3 includes a discussion of the results from Chapter 4 where propagation of the Gore radar beam was modeled using collected MOLTS data. Finally Section 5.4 provides a summary of findings from the case studies.

5.1 Melancthon Wind Farm / King City Weather Radar

As previously stated in Section 3.1, the Melancthon wind farm was selected as a case study due to the fact that WTC seen in King City weather radar data is variable. The Melancthon wind turbines are located within 55 and 66 km from the King City weather radar with total heights of 121 meters.

All RLOS studies were completed using standard atmospheric conditions where $K = 4/3$. The output of the Wind Farm Summary, Figure 25, indicates that the tips of the turbine should not be visible at elevation angles greater than 0.09° . King City weather radar scan elevation angles for DOPVOL1A, Table 7, are approximately 0.5° for the center of the main beam in the summer and 0° for the center of the main beam in the winter. Taking into account these operational radar scan angles, one would assume that the Melancthon wind turbines would only be visible in the winter. This is further shown in Figure 29 where the two closest wind turbines, turbines 74 and 75, are not seen in the summer main beam but are seen in the winter main beam. Also shown in Figure 28 is that the wind farm is located on much higher elevations due to its location on the Niagara Escarpment. Also seen is that there may be partial blockage of the radar beam by terrain before the beam “sees” the turbines at winter scanning elevation angles as they are 0° rather than 0.5° in the summer. Further verification is found in Figures 30 and 31 where the

turbines are not visible according to GIS Viewsheds in the summertime but some turbines are visible according to GIS Viewsheds in the winter time – with turbines in the west section of the wind farm not being visible.

Two case studies days were selected to study, a summer one (2013-08-16) and a winter one (2013-11-15) for the hours of 04:00 and 16:00 local time. Table 9 displays that for both days and both hours the weather conditions at the nearest hourly weather station, Toronto Buttonville Airport, were mainly clear. For the purposes of this thesis it was decided to only focus on clear-air radar images where weather would not be confused for WTC and vice-versa. However, when viewing radar images from the summer case study day (2013-08-16) it was discovered that although the weather reported was clear and mainly clear there did appear to be some lower reflectivity signatures recorded near the radar at the second study hour (2000 Z) and thus this case needs to take into account the possible data contamination (Figure 56). The lower reflectivity appears to be biological clutter related to insects lofted by lake-breeze fronts, a common phenomenon in the Great Lakes area.

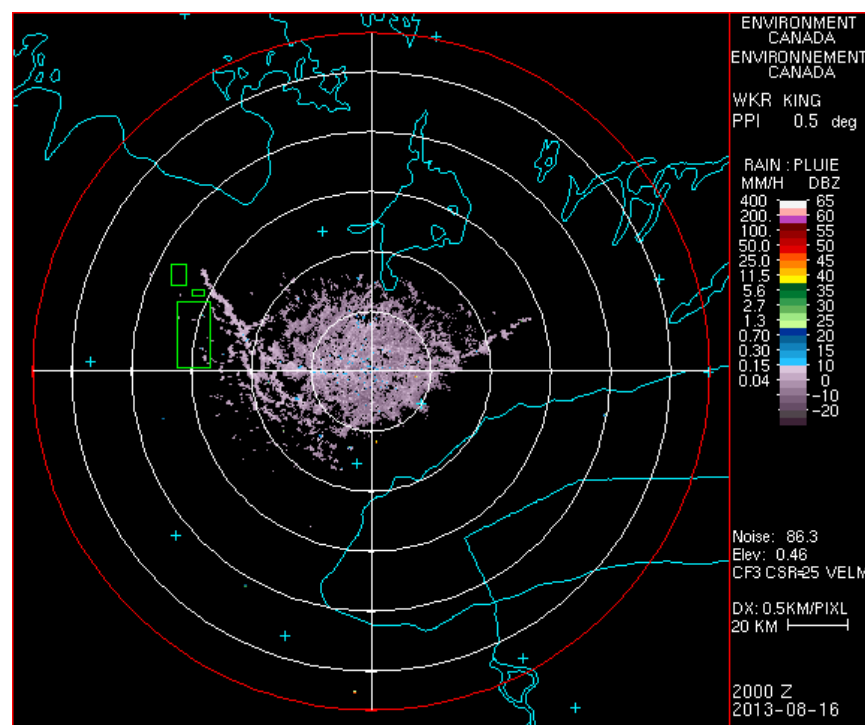


Figure 56: C-TRIP CLOGZPPI product of the WKR radar which depicts lower reflectivity of possible biological clutter near the Melancthon wind farm (large green box) on 2013-08-16 at 2000Z

Appendix D, section i: displays outputs of the DOPVOL1A IRIS files for 0800Z – 0850Z for the King City weather radar (WKR) created using Productx and then plotted in Excel. The maximum

values in the impacted azimuth WKR radar rays of corrected reflectivity (labeled DBZ) and the total reflectivity (DBT) are shown as blue and green respectively. In all images there are three major spikes of reflectivity seen (sample seen in Figure 57).

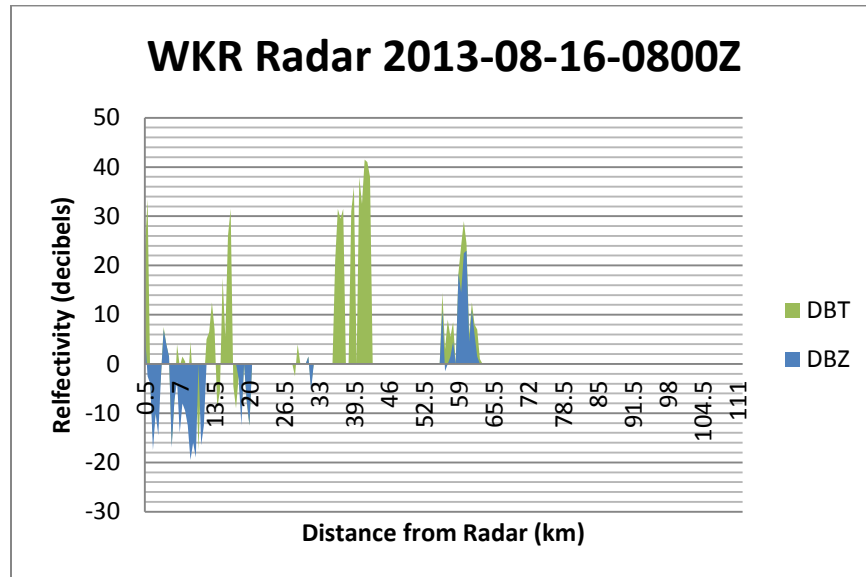


Figure 57: Sample King City Productx output for 2014-08-16-0800Z where the maximum DBT and DBZ values for the azimuth range of 276° - 291° are displayed. Additional Productx images for WKR are found in Appendix D.

The first is a green spike close to the weather radar, a second green spike between 35 and 45 km from the weather radar and a final blue and green spike between 55 and 65 km. Since the first two spikes are only green, representing DBT, this means that the radar processor has filtered them out meaning that the reflectivity values do not have associated velocity values and are thus due to ground clutter. This makes sense knowing the local terrain in the area where the beginning of the Niagara Escarpment is located approximately 35 km from the King City weather radar. The first spike of ground clutter seen at approximately 12 km away is also due to a raise in terrain elevation that intercepts the bottom of the radar beam. The final spike in reflectivity which is evident in both DBT and DBZ is due to the wind farm and is the first indication of WTC. The maximum reflectivity seen from the WTC between 0800 and 0820 Z is about 25 DBZ but rises to around 34 DBZ at 0830 and 0840 Z and almost up to 40 DBZ by 0850 Z. From the Productx outputs one would expect the WTC to thus be more severe in the latter 10 minute radar images.

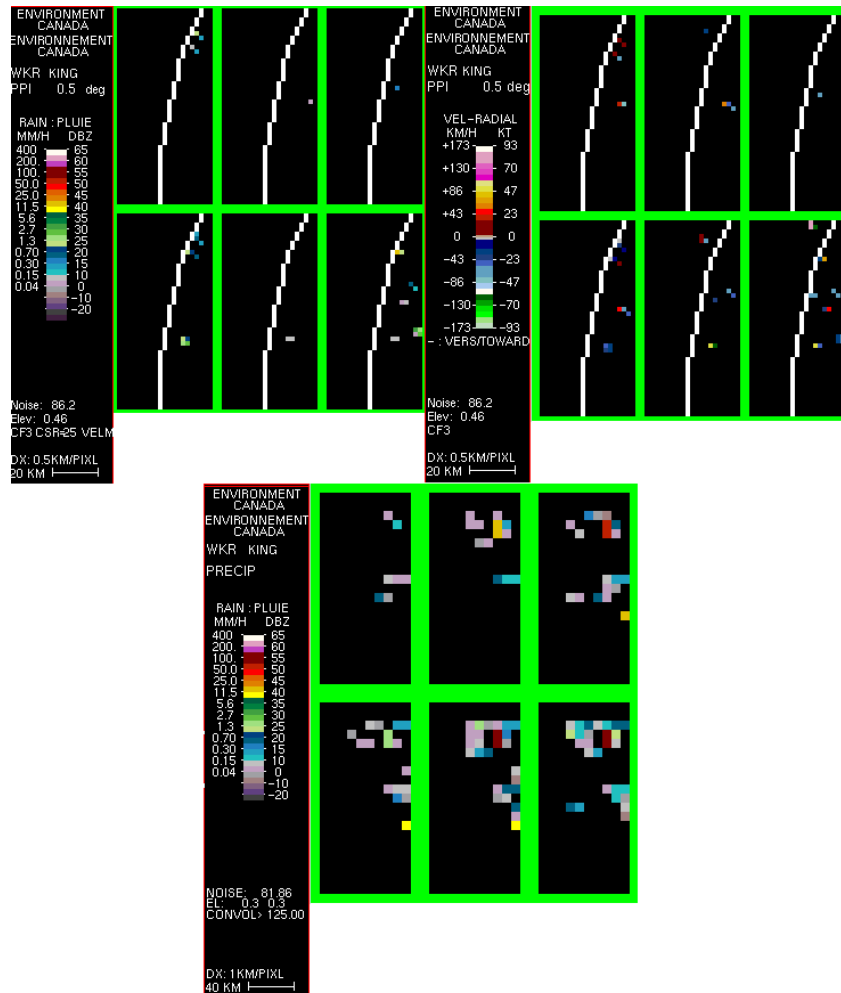


Figure 58: Sample C-TRIP CLOGZPPI, VRPPI and PRECIP products of the Melancthon wind farm box on 2013-08-16 from 0800 Z – 0850 Z created using the DOPVOL1A and DOPVOL2 WKR IRIS files. The white quarter circle lines in the first two images are the 60 km range rings. Additional C-TRIP images for WKR are found in Appendix E.

C-TRIP images displaying WTC for the Melancthon wind farm are found in Appendix E. Figure 58 at the top left displays a CLOGZPPI product zoomed into the Melancthon wind farm box as created using C-TRIP at an actual elevation angle of 0.46°. In terms of impacted pixels, WTC is mainly appearing on the eastern side of the wind farm, while according to standard RLOS, no turbines were expected to be visible in the summer. Although the Productx images in Appendix D suggested maximum reflectivities within the first 30 minutes to be around 25 DBZ, it seems that they are actually much lower and only a few pixels are impacted. In the final 30 minute time period, there are more pixels and higher reflectivities are recorded but are closer to 35 DBZ with one pixel in the 0850Z time period recording with a reflectivity of approximately 40 DBZ. The lower reflectivities suggest that there is further clutter suppression being performed in the post-

processing of IRIS files through CARDS. Next taking a look at the top right of Figure 58, the VRPPI product shows the relative velocities being impacted by the wind turbines. This could also be due to CARDS post-processing where some pixels are being rejected as clutter when viewed using the CLOGZPPI product. The velocities recorded by the wind turbines vary with some toward the radar (green/blue) and others away from the radar (red/yellow/pink). At 0850 Z velocities up to about 70 knots or 130 km/h away from the radar are recorded. The bottom image in Figure 58, displays the PRECIP product which was created by DOPVOL2 at an elevation of approximately 0.3°. DOPVOL2 IRIS files have lower resolution and the pixels are displayed as 1 km per pixel as opposed to the DOPVOL1A 0.5 km per pixel representation. The PRECIP product shows many more impacted pixels recording reflectivity than CLOGZPPI product with reflectivity values over 55 DBZ in some cases. This suggests that there may be less clutter filters performed in PRECIP product or that the lower resolution may cause multiple turbines to be located within the same pixels causing greater reflectivity returns.

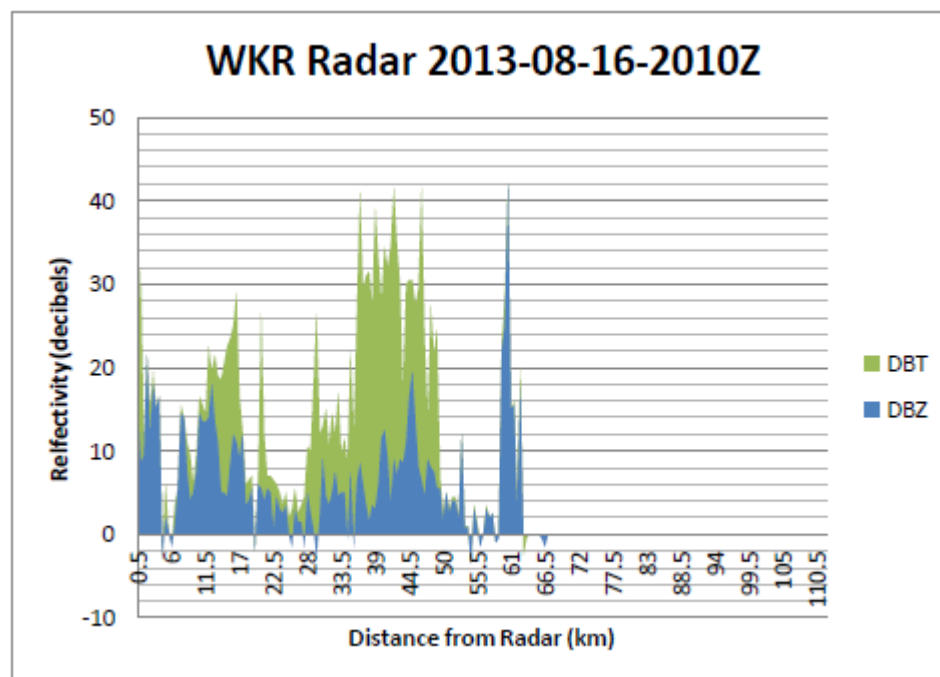


Figure 59: Sample King City Productx output for 2014-08-16-2010Z where the maximum DBT and DBZ values for the azimuth range of 276° - 291° are displayed. Additional Productx images for WKR are found in Appendix D.

Appendix D, section ii: are the Productx output representations for the summer afternoon case study hour (2000 – 2050 Z). As seen in Figure 56, it is known that there are some lower reflectivity echoes between WKR and the Melancthon wind farm. The two green spikes due to ground clutter which were visible in the first case study hour still exist, along with the large blue

spike representing the WTC, however additional blue reflectivity values are also seen in these images. Those blue corrected reflectivities represent biological clutter with reflectivity values between 0 and 20 DBZ. The WTC at the afternoon hour is recorded from the Productx images to be less than the morning hour all being below 30 DBZ with the exception of 2010Z which is near 40 DBZ (Figure 59).

The CLOGZPPI C-TRIP output in Appendix E, section ii: displays maximum reflectivity values of about 30 DBZ with 2010 Z recording the expected 40 DBZ. It is interesting to note that there are more pixels impacted in the wind farm box which could be due to biological clutter seen in Figure 56 however the values of the maximum reflectivity are closer to what was recorded in the original IRIS file. This may suggest that any clutter suppression performed in CARDS may not be as effective if there is weather, or other echoes in the area. Taking a look at the radial velocity, again there are more pixels being impacted than the CLOGZPPI product with the majority of them recorded toward the radar in blue (most likely the biological clutter) with some discrete WTC as represented toward and away in the top right corner of the wind farm box. Velocity values here vary but do go over 70 knots or 130 km/h from the wind turbines. As seen before, more pixels are visible in similar magnitudes of reflectivity in the PRECIP product.

Given the previous RLOS analyses, one would expect that the WTC from the Melancthon wind farm would be more severe in the winter as the operational weather radar elevation angle is lower, at 0°. When viewing the Productx images for the winter morning case study, Appendix D, section iii:, it is evident that the ground clutter is much greater in the winter. This is expected as the beam is lower and would be coming into contact with the ground more frequently. Luckily, it seems that the Doppler filters within the signal processor do a good job correcting this as there it only shows up in the total reflectivity (DBT in green) and not the corrected reflectivity (DBZ in blue). WTC is still seen in the DOPVOL1A IRIS file as shown in the Productx outputs with reflectivity generally higher than seen in the summer case studies just under 38 DBZ for the first 30 minutes and over 40 DBZ for the final 30 minutes studied.

The C-TRIP images found in Appendix E, section iii: display minimal WTC with only turbines in the upper right (or northeast corner) causing reflectivity returns. Again, the values are less than or similar to those in the IRIS file displayed through Productx, however there are similar number of pixels impacted to the summer case study. This may suggest that there is some terrain blockage causing the turbines in the southern section to not be “seen” by the radar. Additionally, operational wind farm data were not collected so there could be a chance that those wind

turbines were not actually spinning and thus not contaminating the weather radar data. The VRPPI product contains approximately the same number of pixels shown in the CLOGZPPI product with velocities towards and away the radar varying in magnitude up to about 70 knots or 130 km/h. The PRECIP product output again shows a lower resolution but less observed WTC pixels than the summer PRECIP product in Appendix E, section i: which is interesting to note.

In the winter afternoon case study high ground clutter reflectivities are again filtered out in the corrected reflectivity as seen in the Productx outputs in Appendix D, section iv:. WTC values are shown around 40 DBZ with up to 50 DBZ being recorded at 2110Z. Although larger reflectivity values are seen in Productx the CLOGZPPI C-TRIP output in Appendix E, section iv: only shows reflectivity maximums around 40 DBZ suggesting again that the CARDS is suppressing some of the higher reflectivity values. Similar to the morning case study, there are not a lot of pixels being impacted. A similar number of impacted pixels from WTC are seen in the VRPPI product with relative velocity values with generally lower magnitudes towards and away from the radar with one pixel representing a relative velocity near 70 knots or 130 km/h. The PRECIP product output again shows an expected lower resolution however it seems that fewer pixels are being impacted when compared to the summer case study.

Overall, the comparison of RLOS to observed WTC for the Melancthon wind farm / King City weather radar was not as expected. RLOS predictions indicated that the wind turbines which could potentially cause WTC would be on the eastern side of the wind farm and this was verified. However, the observed wind turbines actually impacted more pixels in the summer case study than the observed WTC in the winter case study. There are many potential reasons for this. The reason why WTC is visible in the summer case study but is not predicted based on RLOS could be due to radar beam side lobes or the curving of the radar beam due to atmospheric propagation. Since in the winter the radar beam is much lower (0° rather than 0.5°) the radar beam may be blocked or partially blocked by the terrain before reaching the wind farm. Additionally, it is not known which turbines were operating and when for these case studies.

5.2 Greenwich Wind Farm / Lasseter Lake Weather Radar

As stated in Section 3.2, the Greenwich wind farm was selected as a case study due to the fact that the wind farm is located very close to the Lasseter Lake weather radar. The Greenwich wind turbines are located within 21 and 33 km from the Lasseter Lake weather radar with total heights of 126 meters.

All RLOS studies were completed using standard atmospheric conditions where $K = 4/3$. The output of the Wind Farm Summary, Figure 34, displays that the tips of the turbine should not be visible at elevation angles greater than 0.31° . Lasseter Lake weather radar scan elevation angles for DOPVOL1A, Table 11, are approximately 0.5° for the center of the main beam in the summer and 0.2° for the center of the main beam in the winter. Taking into account these operational radar scan angles, one would assume that the Greenwich wind turbines would only be visible in the winter. This is further shown in Figure 38 where the two closest wind turbines, turbines 3 and 7, are only seen in the bottom of the summer main beam but are seen in more than half of the winter main beam. Also shown in Figure 37, is that the wind farm is located on similar elevation to the weather radar with no terrain blockage expected for the wind turbines. The GIS Viewsheds in Figures 39 and 40, however show that only some turbines are expected to be seen at the bottom of the main beam in both the summer and winter as it appears that turbines in the northern and eastern sections may not be visible. According to the GIS viewsheds analyzed on the CDED data this means that only about half (20) of the turbines will be visible to the Lasseter Lake weather radar, which may explain why WTC is not as prevalent as predicted due to distance.

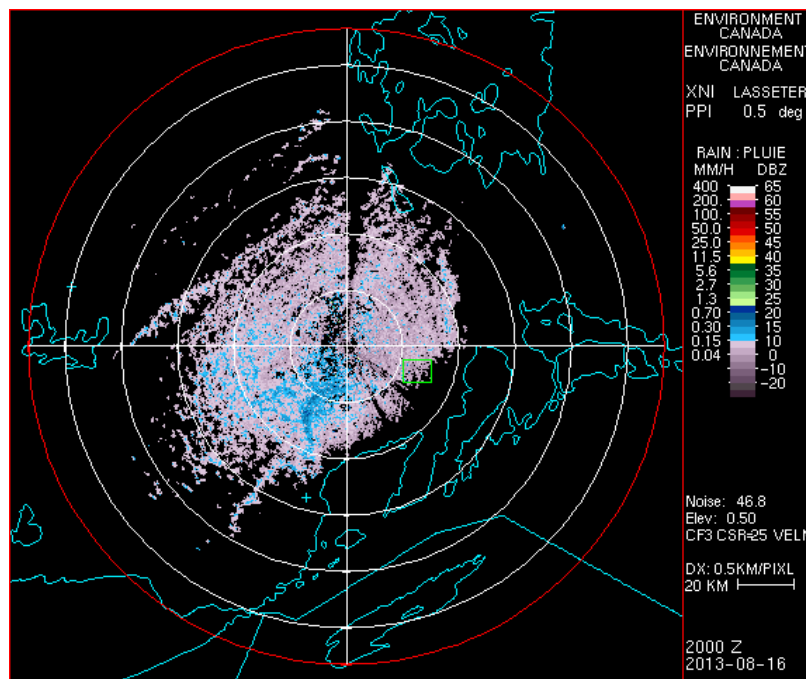


Figure 60: C-TRIP CLOGZPPI product of the XNI radar which depicts lower reflectivity radar echoes near the Greenwich wind farm (large green box) on 2013-08-16 at 2000Z

Two case studies days were selected to study, a summer one (2013-08-16) and a winter one (2013-11-15) for the hours of 04:00 and 16:00 local time. Table 13 displays that for both days and both hours the weather conditions at the nearest hourly weather station, Thunder Bay Airport, were mainly clear with light snow occurring during the winter morning case study. For the purposes of this thesis it was decided to only focus on clear-air radar images where weather would not be confused for WTC and vice-versa. However, when viewing radar images from the summer case study day (2013-08-16) it was discovered that although the weather reported was clear and mainly clear there did appear to be some lower reflectivity signatures recorded near the radar at the second study hour (2000 Z) and thus this case needs to take into account the possible data contamination (Figure 60).

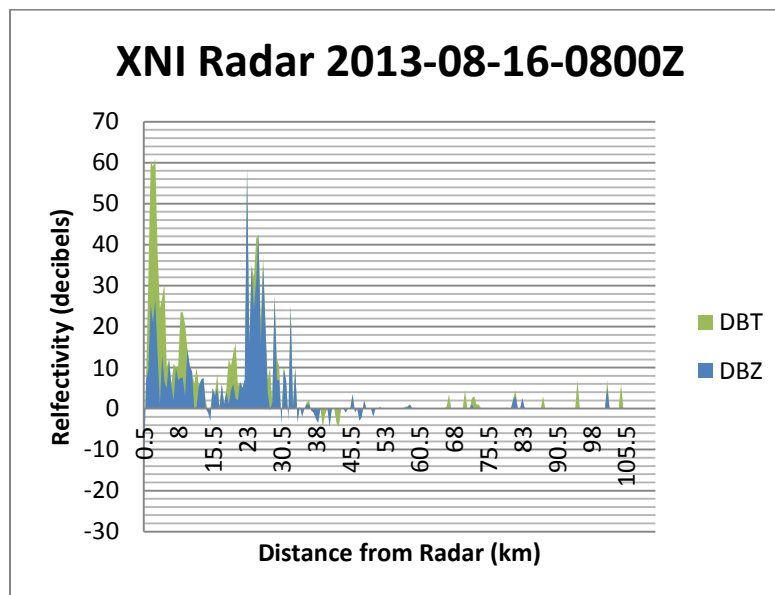


Figure 61: Sample Lasseter Lake Productx output for 2013-08-16-0800Z where the maximum dBZ and dBZ values for the azimuth range of 103° - 123° are displayed. Additional Productx images for WKR are found in Appendix G.

Appendix G, section i: displays Productx outputs of the DOPVOL1A IRIS files for 0800Z – 0850Z for the Lasseter Lake weather radar (XNI) created using Productx and then plotted in Excel. The maximum values in the impacted azimuth XNI radar rays of corrected reflectivity (labeled DBZ) and the total reflectivity (DBT) are shown as blue and green. In all images there are two major spikes of reflectivity seen. The sample image in Figure 61 shows the first is a green spike close to the weather radar and a second blue and green spike between 20 and 35 km. Since the first spike is only green this means that the radar processor has filtered the total reflectivity meaning that the reflectivity values do not have associated velocity values and are

thus due to ground clutter. The second spike in reflectivity which is evident in both DBT and DBZ is due to the wind farm and is the first indication of WTC. The maximum reflectivity seen from the WTC is on average around 40 DBZ with some minor spikes between 50 and 60 DBZ.

Appendix H displays the C-TRIP outputs for the Greenwich wind farm / Lasseter Lake weather radar pair. Appendix H, section i: displays the C-TRIP output for the summer winter case study. The CLOGZPPI product displays multiple pixels are impacted by the wind turbines causing WTC with maximum reflectivity values near about 50 DBZ. Again the values of reflectivity are less than those in the DOPVOL1A IRIS file as shown by Productx which suggests clutter suppression in CARDS post-processing. The pattern of the WTC is similar to what was predicted by the GIS Viewsheds being on the western and southwestern sides, however there is a lot of WTC at this time. The relative velocity displayed by the VRPPI product again shows similar pixels being impacted with velocities both away and towards the radar at magnitudes up to 70 knots or 130 km/h. The PRECIP product shows a more predominant echo shape of the WTC with a lower resolution as it was created using DOPVOL2 rather than DOPVOL1A.

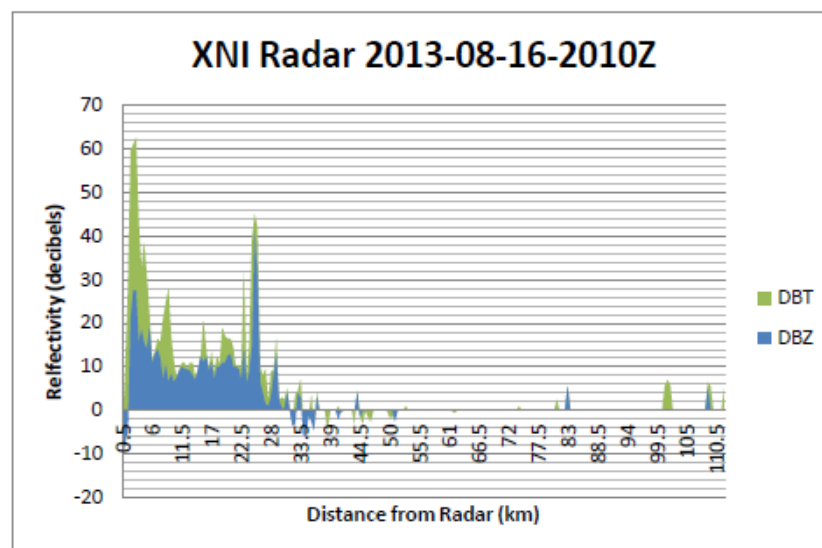


Figure 62: Sample Lasseter Lake Productx output for 2013-08-16-2010Z where the maximum dBZ and dBZ values for the azimuth range of 103° - 123° are displayed. Additional Productx images for WKR are found in Appendix G.

Appendix G, section ii: displays the Productx output representations for the summer afternoon case study hour (2010 – 2050 Z – with data missing from 2000 Z). As seen in Figure 60, it is known that there are some lower reflectivity echoes between XNI and the Greenwich wind farm. Figure 62 shows green spikes due to ground clutter which were visible in the first case study hour still exist, along with the large blue spike representing the WTC; however, additional blue

reflectivity values are also seen in these images. Those blue corrected reflectivities represent radar echoes with reflectivity values between 0 and 20 DBZ. The WTC at the afternoon hour is recorded from the Productx images to be less than the morning hour all being closer to 30 DBZ.

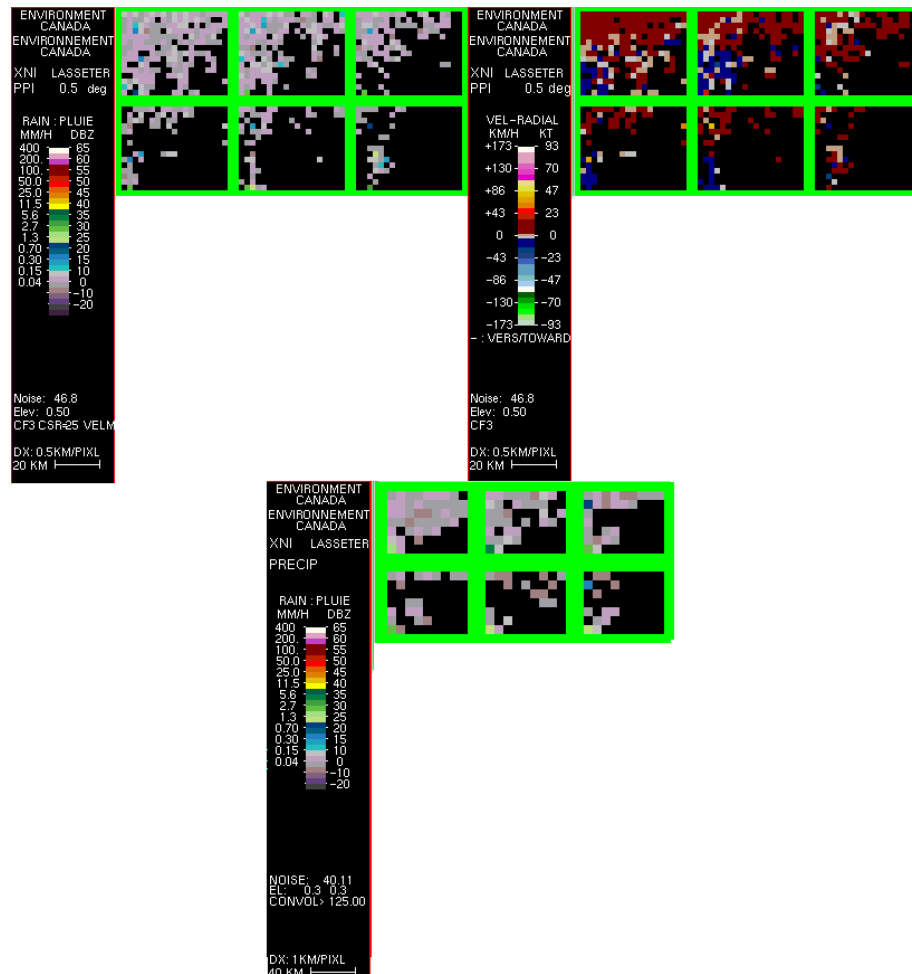


Figure 63: Sample C-TRIP CLOGZPPI, VRPPI and PRECIP products of the Greenwich wind farm box on 2013-08-16 from 2000 Z – 2050 Z created using the DOPVOL1A and DOPVOL2 XNI IRIS files. Additional C-TRIP images for WKR are found in Appendix H.

Figure 63 displays the C-TRIP output for the summer afternoon case study. The CLOGZPPI product is cluttered only displaying one or two pixels with maximum reflectivity values of about 30 DBZ. The abundance of lower reflectivity pixels seems to almost mask the expected WTC. Taking a look at the VRPPI product we again see more pixels being impacted with the majority of velocities recorded away from the radar in red (most likely the biological clutter) with some discrete WTC as represented toward and away in the bottom left corner of the wind farm box. Relative velocity values here vary but do only seem to reach 47 knots or 86 km/h from the wind turbines. Most of the WTC cannot be differentiated in the PRECIP product.

Given the previous RLOS analyses, one would expect that the WTC from the Greenwich wind farm would be more severe in the winter as the operational weather radar elevation angle is lower, at 0.21° . When viewing the Productx images for the winter morning case study, Appendix G, section iii:, WTC is still seen in the DOPVOL1A IRIS file with reflectivity generally lower than seen in the summer case studies all being under 40 DBZ. The C-TRIP images, Appendix H, section iii:, display very minimal WTC with only turbines in the lower left (or southwest corner) causing reflectivity returns. Again, the values are less than or similar to those in the IRIS file displayed through Productx, however there are fewer pixels impacted when compared to the summer case study. Operational wind farm data were not collected so there could be a chance that those wind turbines were not actually spinning and thus not contaminating the weather radar data. Relative velocities shown in the VRPPI product contain approximately the same number of pixels shown in the CLOGZPPI product with velocities towards and away the radar varying in magnitude only up to about 23 knots or 43 km/h. The PRECIP product output in shows a lower resolution but less observed WTC pixels than the summer PRECIP product in Appendix G, section i:.

In the winter afternoon case study WTC values are shown around 30 DBZ in the Productx outputs in Appendix G, section iv:. In the C-TRIP images in Appendix H, section iv:, the C-TRIP product is comparable to the winter morning case study, there are not a lot of pixels being impacted. A lesser number of impacted pixels from WTC are seen in the VRPPI product with relative velocity values barely visible. The PRECIP product output again shows an expected lower resolution however it seems fewer pixels are being impacted again.

Overall, the comparison of RLOS to observed WTC for the Greenwich wind farm / Lasseter Lake weather radar was similar to expected, however the WTC was more prevalent in the summer case study. RLOS predictions indicated that the WTC would be on the southwestern side of the wind farm and this was verified. However, the observed wind turbines actually impacted more pixels in the summer case study than the observed WTC in the winter case study. There are many potential reasons for this including propagation of the radar beam, impacts of side lobes or wind turbines not being in operation on the winter case study day.

5.3 Nuttby Mountain Wind Farm / Gore Weather Radar

As stated in Section 3.3, the Nuttby Mountain wind farm was selected as a case study due to the fact that the wind farm is located a far distance from the Gore weather radar, however

persistent WTC is seen, although not predicted by RLOS. The Nuttby Mountain wind turbines are located within 62 and 66 km from the Gore weather radar with total heights of 125 meters.

RLOS studies were completed using standard atmospheric conditions where $K = 4/3$. The output of the Wind Farm Summary, Figure 43, displays that the tips of the turbine should not be visible at elevation angles greater than 0.11° . Gore weather radar scan elevation angles for DOPVOL1A, Table 15, are approximately 0.5° for the center of the main beam in the summer and 0° for the center of the main beam in the winter. Taking into account these operational radar scan angles, one would assume that the Nuttby Mountain wind turbines would only be visible in the winter. This is further shown in Figure 47 where the two closest wind turbines, turbines 4 and 9, are not seen in the summer main beam but are seen in the lower half of the winter main beam. Also shown in Figure 46, is that the wind farm is located on higher elevation than the weather radar with no terrain blockage expected for the wind turbines. The GIS Viewsheds in Figures 48 and 49 show that the turbines are only expected to be seen at the bottom of the main beam in the winter.

Two case studies days were selected to study, a summer one (2013-08-16) and a winter one (2013-11-15) for the hours of 04:00 and 16:00 local time. Table 17 displays that for both days and both hours the weather conditions at the nearest hourly weather station, Halifax International Airport, were mainly clear with the winter morning case study reporting cloudy conditions. For the purposes of this thesis it was decided to only focus on clear-air radar images where weather would not be confused for WTC and vice-versa.

First, Appendix J display outputs of the DOPVOL1A IRIS files for the Gore weather radar (XGO) created using Productx and then plotted in Excel. The maximum values in the impacted azimuth XGO radar rays of corrected reflectivity (labeled DBZ) and the total reflectivity (DBT) are shown as blue and green. In Appendix J, section i: there are two major spikes of reflectivity seen. The first is a green spike close to the weather radar and a second blue and green spike between 62 and 66 km. Since the first spike is only green this means that the radar processor has filtered the total reflectivity meaning that the reflectivity values do not have associated velocity values and are thus due to ground clutter. The second spike in reflectivity which is evident in both DBT and DBZ is due to the wind farm and is the first indication of WTC.

Appendix J, section i: shows the maximum reflectivity seen from the summer case study for 0710Z – 0750Z Productx outputs is on average around 40 DBZ. Appendix K, section i: shows the CLOGZPPI C-TRIP product where multiple pixels are impacted by the wind turbines causing WTC with maximum reflectivity values near about 40 DBZ. The relative velocity displayed in the VRPPI product shows similar pixels being impacted with velocities both away and towards the radar at magnitudes up to 70 knots or 130 km/h. The PRECIP product shows WTC with a lower resolution as it was created using DOPVOL2 rather than DOPVOL1A and also has higher magnitudes of reflectivity up to 45 DBZ which may be due to the lower scanning angle of 0.3° rather than 0.48°.

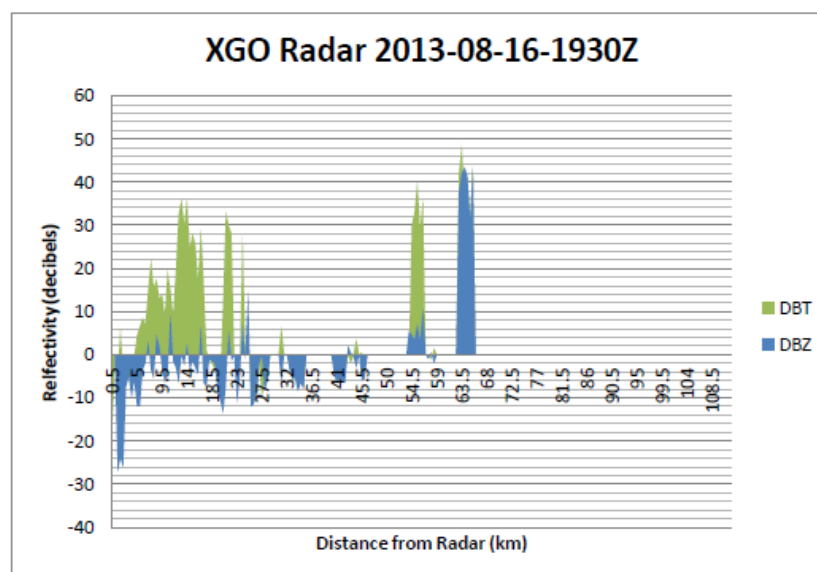


Figure 64: Sample Gore Productx output for 2013-08-16-1930Z where the maximum dBT and dBZ values for the azimuth range of 34° - 38° are displayed. Additional Productx images for XGO are found in Appendix J.

Appendix J, section ii: displays the Productx output representations for the summer afternoon case study hour (1900 – 1950 Z). The green spikes due to ground clutter which were visible in the first case study hour still exist and seem to be more prominent, along with the large blue spike representing the WTC. Additionally in Figure 64 there seems to be larger ground clutter spike at 55 km. The WTC at the afternoon hour is recorded from the Productx images to be greater than the morning hour all being closer to 45 DBZ with a spike of 50 DBZ at 1940Z.

The C-TRIP output for the afternoon in Appendix K, section ii: is similar to the morning summer case study however it seems more pixels are now being impacted. The maximum reflectivity seen is about 45 DBZ which is similar to those magnitudes recorded in the IRIS file. Taking a

look at the relative velocity from the VRPPI product we again see similar pixels being impacted with velocities of varying magnitude and direction towards or away from the radar up to 70 knots or 130 km/h. The PRECIP product shows pixels with magnitudes of reflectivity up to about 50 DBZ similar to the difference between CLOGZPPI and PRECIP in the morning hour.

Given the previous RLOS analyses, one would expect that the WTC from the Nuttby Mountain wind farm would be more severe in the winter as the operational weather radar elevation angle is lower, at 0.02°. When viewing the Productx images for the winter morning case study, Appendix J, section iii:, WTC is still seen in the DOPVOL1A IRIS file with reflectivity generally higher than seen in the summer case study up to 60 DBZ. The Productx images also display more ground clutter which is expected as the radar beam is lower and the bottom of the main beam would come into contact with more terrain. Table 18 displays the operational wind turbine data for the Nuttby Mountain wind farm for the winter morning hour. Based on the wind turbine orientation model in Table 16 and Figure 45 all turbines are operating and expected to produce moderate WTC as illustrated in Figure 65.

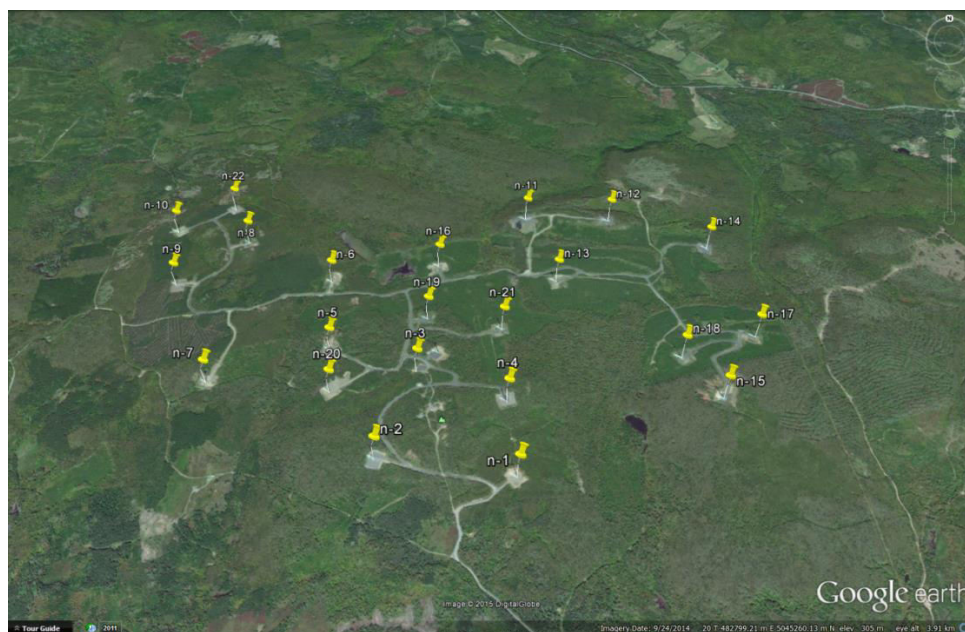


Figure 65: Representation of operational wind turbine data (Table 18) where all Nuttby wind turbines are operating and moderate impacts are expected on 2013-11-15 morning hour based on Table 16 and Figure 45 of the wind turbine orientation model

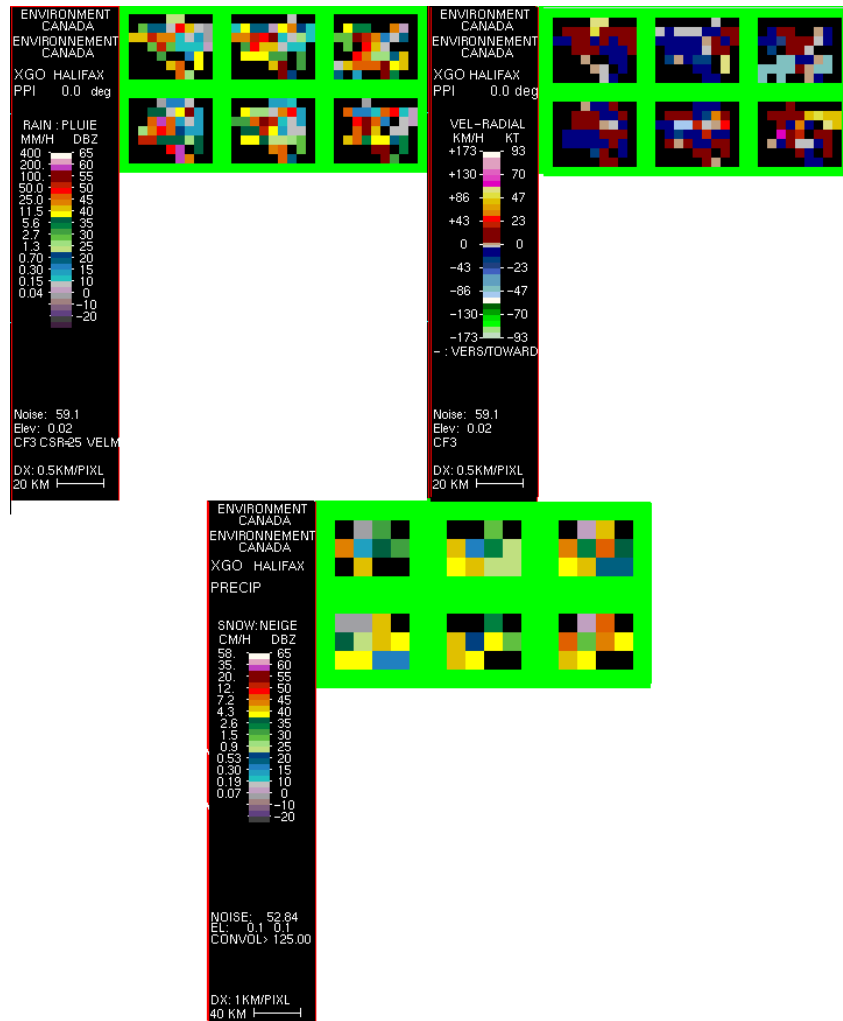


Figure 66: Sample C-TRIP CLOGZPPI, VRPPI and PRECIP products of the Nuttby Mountain wind farm box on 2013-11-15 from 2000 Z – 2050 Z created using the DOPVOL1A and DOPVOL2 XGO IRIS files. Additional C-TRIP images for XGO are found in Appendix K.

Figure 66 displays much more WTC than the summer case studies with reflectivity values up to 60 DBZ. Relative velocities shown in the VRPPI product contain approximately the same number of pixels shown in the CLOGZPPI product with velocities towards and away the radar varying in magnitude up to about 70 knots or 130 km/h. The PRECIP product again shows a lower resolution but less observed WTC pixels than the CLOGZPPI product possibly due to the higher elevation angle of 0.1° compared to 0.02°.

In the winter afternoon case study WTC values are shown around 55 DBZ in the Productx outputs in Appendix J, section iv: with 60 DBZ recorded at 2000 Z. Table 19 displays the operational wind turbine data for the Nuttby Mountain wind farm for the winter afternoon hour. Based on the wind turbine orientation model in Table 16 and Figure 45 all turbines are operating

and expected to produce moderate WTC with three turbines expected to produce marginal WTC as illustrated in Figure 67.

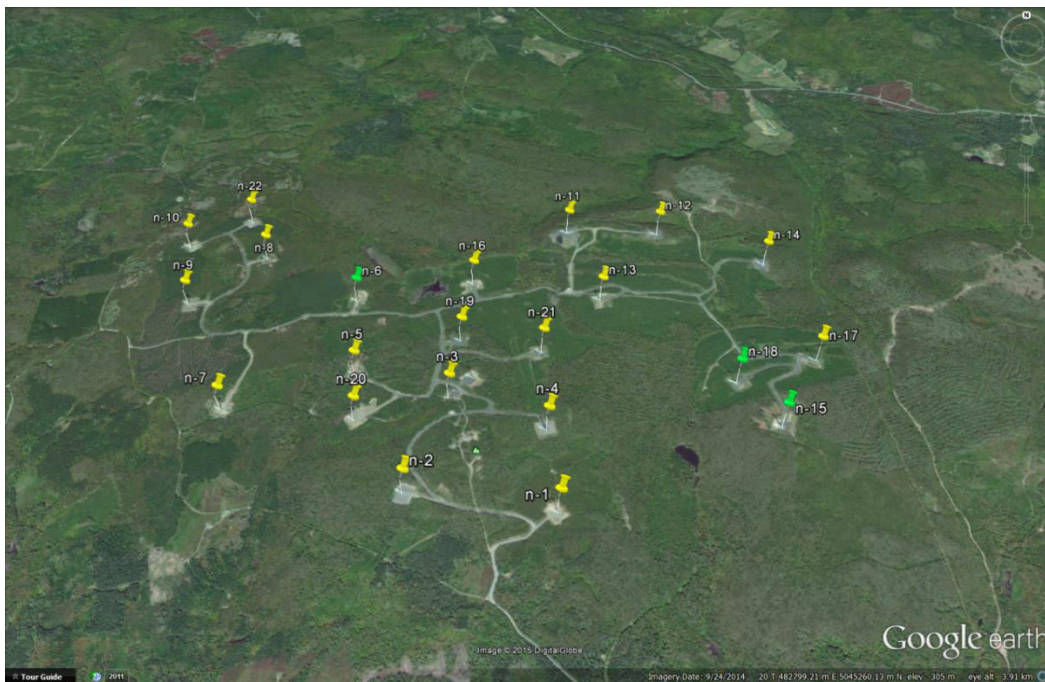


Figure 67: Representation of operational wind turbine data (Table 19) where all Nuttby wind turbines are operating and green represent marginal expected impact and yellow moderate impact expected on 2013-11-15 afternoon hour based on Table 16 and Figure 45 of the wind turbine orientation model

In Appendix K, section iv: the CLOGZPPI product is comparable to the winter morning case study, where there are a lot of pixels being impacted with reflectivity values up to 60 DBZ. The three turbines in Figure 64 were expected to produce marginal WTC (in green), however; the pixels do not seem to be much different than the winter morning study. A similar number of impacted pixels from WTC are seen in the VRPPI product with relative velocity lower near 47 knots or 86 km/h. The PRECIP product output again shows an expected lower resolution with reflectivity values near 55 DBZ.

Overall, the comparison of RLOS to observed WTC for the Nuttby Mountain wind farm / Gore weather radar was not as expected. RLOS predictions did indicate that the WTC would be more significant in the winter given the lower scanning angles and this was verified. However, there was significant observed WTC in the summer case study which was not predicted by RLOS. There are many of potential reasons for this including propagation of the radar beam or impacts of side lobes. To further explore radar beam propagation, Chapter 4 provided results of study of modeling radar beam propagation using MOLTS points on 2014-07-07.

In Section 4.2 the height of the radar beam was estimated with atmospheric conditions using MOLTS points. Using standard RLOS the center of the Gore weather radar beam in the summer would have been approximately 678 meters above the wind farm with the bottom of the main beam being approximately 316 meters above the wind farm. The results show that the height of the center of the radar beam calculated in Table 21 for the first hour (0700 – 0750 Z) would be about 500 meters above the wind farm with the bottom of the main beam about 140 meters above the wind farm. Knowing that the tips of the wind turbine blades are located approximately 125 meters above the ground this does not conclusively prove that the main beam is the only factor to determining if WTC exists. When taking a look at the C-TRIP outputs in Figure 53 it is shown that the WTC is consistent and reminiscent of the first summer case study day. For the next hour, it seems as if values of height of the center of the radar beam in Table 22 are a bit lower with the bottom of the main beam also being closer to the ground. Figure 54 again shows consistent WTC from the wind farm even though the turbines are not expected to intercept the main radar beam. The results from the third hour in Table 23 and Figure 56 also display this.

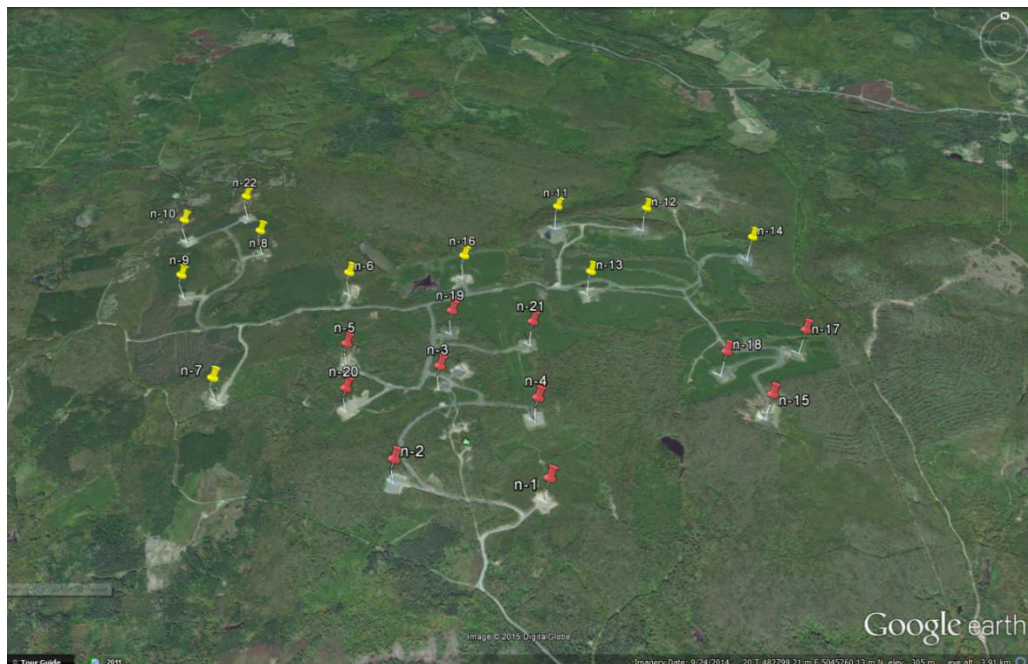


Figure 68: Representation of operational wind turbine data for 2014-07-07 from 0700 Z – 0950 Z where Nuttby wind turbines which are operating are in yellow representing moderate expected impacts on Table 16 and Figure 112 and turbines not in operation are shown in red

Another interesting thing was discovered in this case study. Operational wind turbine data were available for the Nuttby Mountain wind farm on the 2014-07-07 case study day during the three studied hours. The data indicated that many of the wind turbines were not in operation during

the case study hours. The turbines which were not operating were turbines 1-5, 15, and 17-21 as seen in Figure 68. Turbines which are not in operation are not expected to cause WTC, however, WTC was observed. This may suggest that WTC is prominent from the Nuttby Mountain wind farm even when the turbines are not operating, a fact that should be explored further.

5.4 Case Study Summary

This section summarizes the results and discussion from the various case studies:

- Melancthon wind farm / King City weather radar pair
 - Maximum corrected reflectivity values ranged from 23 – 50 DBZ
 - Maximum relative velocity values were 70 kts or 130 km/h
 - WTC occurred mainly on the eastern side of the wind farm (as expected)
- Greenwich wind farm / Lasseter Lake weather radar pair
 - Maximum corrected reflectivity values ranged from 27.5 – 63.5 DBZ
 - Maximum relative velocity values were 70 kts or 130 km/h
 - WTC was reduced in the summer afternoon hour, where lower reflectivity signal were in the area, was reduced
- Nuttby Mountain wind farm / Gore weather radar pair
 - Maximum corrected reflectivity values ranged from 36.5 – 59.5 DBZ
 - Maximum relative velocity values were 70 kts or 130 km/h
 - When using MOLTS data to calculate to model the radar beam and consider refractivity, turbines were still predicted to not be visible within the main beam.
 - WTC persisted even when turbines were not operating.

For each of the wind farm / radar pairs studied, WTC was observed on some occasions where the turbines were not predicted to be visible in the main radar beam according to standard RLOS. For two out of the three wind farm / radar pairs WTC was expected to be more prevalent in the winter. However, there were more pixels impacted with higher reflectivity values in the summer case studies. WTC impacted more pixels and recorded higher reflectivity values for all cases within the PRECIP product as compared to the CLOGZPPI product. Additionally, in most cases the reflectivity values were larger in the Level II Productx data than the Level III CLOGZPPI product.

6. Conclusions and Recommendations

6.1 Conclusions

There were three main objectives of this thesis including as illustrated in Section 1.1.2 which were completed and demonstrated through Chapters 2 – 4. The first objective was to use tools to identify, analyze and compare WTC which took into account RLOS, wind turbine orientation and atmospheric propagation of the radar beam. This was accomplished in several ways using RLOS tool such as Wind Farm Analysis (Section 2.2.1), the IDL Beamwidth program (Section 2.2.2) and GIS Viewsheds (Section 2.2.3). Additionally, wind turbine orientation models were developed for each wind farm case study (Section 2.5). Finally MOLTS data, radar beam height calculations and atmospheric refractivity equations were used to model the path of the radar beam due to atmospheric propagation.

The second objective of this thesis involved determining the expected WTC as predicated by the RLOS under standard atmospheric conditions and to make comparisons of the observed WTC for three wind farms. This was demonstrated throughout Chapter 3 where expected and observed WTC from the three wind farms were analyzed. Visualizations of the observed WTC were made possible through use of the Productx Utility which processed level II radar data and the created C-TRIP scripts which identified the wind turbines in level III radar data produced from CARDS. The predicted WTC impacts were then compared to the observed WTC for summer and winter case study days with interesting results.

1. Even when operational wind turbine data were available they did not seem to provide an accurate indication of WTC as over half of the turbines were not operating but the WTC was still consistent for the Nuttby Mountain wind farm. This was not expected and suggests further study is required.
2. Standard RLOS in the winter, where the radars scan at lower elevation angles, implies that the turbines would have more of an impact in the winter; however, for two out of the three case studies there were more pixels impacted with higher reflectivities in the summer case study. This indicates that there could be blockage from terrain which is actually lessening the impact of the turbines in the winter due to the lower scanning angles intercepting the terrain. This terrain blockage may occur in the summer due to higher scanning angles and thus WTC is more visible.

3. Observed maximum reflectivity values produced through C-TRIP images (Level III radar data) were lower than values of the Level II IRIS files which suggests that clutter suppression slightly reduces the impact of WTC through post-processing in CARDS.
4. WTC impacted more pixels and recorded higher reflectivity values in the PRECIP product which uses DOPVOL2 lower resolution radar data which was expected.
5. Although the aim was for clear-air case study days, there was an instance where it seemed weather in the area could reduce the impact of WTC as it was not easily differentiated in Level III radar data.

The final objective of this thesis was to determine the value of modeling the path of the radar beam with calculated atmospheric refractivity for the Nuttby Mountain wind farm / Gore weather radar pair. Initial standard RLOS indicated that WTC would not be observed and when MOLTS data were used to model the RLOS, the main beam was still not expected to intercept the wind turbines. Although the beam was not expected to intercept the turbines, it was lower meaning some superrefraction was indicated. Additionally, there is a high degree of error which may be introduced into the refractivity calculations using modeled MOLTS data which may not effectively model the boundary layer (first km or so of atmosphere).

6.2 Future Research and Recommendations

There are several research opportunities and investigations that can be made in the field of analyzing WTC within EC's weather radar network including the following:

- A more detailed study could be completed to compare observed WTC with operational wind turbine data.
- Given the consistent WTC being observed when standard RLOS indicates turbines should not be within the main beam, further studies using alternative methods of calculating atmospheric refractivity should be performed. Additionally, side lobes should be considered.
- It is recommended that C-TRIP wind farm boxes or similar identification be used internally for EC's meteorologists to quickly identify where WTC may exist.
- EC now displays PRECIP-ET (PRECIP Extension) radar products on their public website as opposed to PRECIP products. It is recommended that a comparison between WTC observed in the original PRECIP products versus the new PRECIP-ET products be completed or if possible CLOGZPPI products with finer resolutions be used where WTC is minimized slightly.

References

- ArcGIS. (2012): **Using Viewshed and Observer Points for visibility analysis**. ESRI:
<http://resources.arcgis.com/en/help/main/10.1/index.html#//00q90000008n000000>
- Bahnert, G. (1987): **Zur Bestimmung lokaler Refraktionskoeffizienten**.
Vermessungstechnik, 35(1), 14-17
- Barué, G. (2008): **Microwave Engineering: Land & Space Radiocommunications**. Wiley,
July 2008 pp. 47-67. ISBN: 978-0-470-08996-5
- Best, C. (2009): **Determining Likely Impacts of Wind Turbines on Meteorological Radar Data**. Environment Canada, WEM Administration. November 19, 2009.
- Brenner, M., Cazares S., Cornwall M., Dyson F., Eardley D., Horowitz P., Long D., Sullivan J., Vesecky J., Weinberger P.. (2008): **Wind Farms and Radar**. JASON report, MITRE Corporation, JSR-08-125.
- Butler, M. M., and Johnson, D. A. (2003): **Feasibility of Mitigating the Effects of Windfarms of Primary Radar**. 2003
http://users.ece.utexas.edu/~ling/EU1_Feasibility_Mitigating_Effects_Windfarms_on_Primary_Radar_Butler_Johnson_UK.pdf
- CanWEA. (2014): **Installed Capacity**. Canadian Wind Energy Association:
<http://canwea.ca/wind-energy/installed-capacity/>
- CanWEA. (2008): **WindVision 2025: Powering Canada's Future**. Canadian Wind Energy Association: http://canwea.ca/pdf/windvision/Windvision_summary_e.pdf
- Giardi, Ed. (2013): **Wind Farms and the WSR-99D, 2013 Update**. WSR-88D Radar Operations Center, NOAA:
https://www.roc.noaa.gov/WSR88D/Publicdocs/WIND_FARMS_AND_THE_WSR-88D_2013_UPDATE.pdf
- Donaldson, N., Best, C. & Paterson, B. (2008): **Development of Wind Turbine Assessments for Canadian Weather Radars**. Proceedings of the Fifth European Conference of Radar in Meteorology and Hydrology, ERAD 2008, pp. 1-4, Helsinki, Finland, July 2008. ISBN: 978-951-697-676-4
- Donaldson, N., Joe, P. & Scott, J. (2003): **Considerations for the Detection of Low Lying Winter Weather in the Canadian Weather Radar Network**. Preprints, 31st International Conference on Radar Meteorology. Seattle, AMS, 819-822.
- Douet, Marion. (2014): **France builds stealth wind turbines to avoid radar interference**. Reuters, September 5, 2014. Paris, France.
<http://www.reuters.com/article/2014/09/05/us-windfarm-renewables-radar-idUSKBN0H013C20140905>
- Environment Canada (EC). (2013): **Wind Turbine Interference with Weather Radar**. National Radar Program (weatherradars@ec.gc.ca): <http://www.ec.gc.ca/meteo-weather/default.asp?lang=En&n=1D1B608B-1>
- European Commission Energy. (2013):
http://ec.europa.eu/research/energy/nn/nn_rt/nn_rt_wind/images/wind_en_1370.gif

- Fogarty, Chris. (2013): **Radar Beam Height Nomogram**. NovaWeather: http://www.novaweather.net/radar_beam_heights.bmp
- Fortin, V., Roy, G., and Donaldson, N. (2014): **Assimilation of Radar QPE in the Canadian Precipitation Analysis (CaPA)**. 2014 ASCE International Symposium on Weather Radar and Hydrology
- Fournier, Jeffrey D. (1999): **Reflectivity-Rainfall Rate Relationships in Operational Meteorology**. National Weather Service Weather Forecast Office: <http://www.srh.noaa.gov/tae/?n=research-zrpaper>
- Gallardo-Hernando, B., Pérez-Martínez, F., and Aguado-Encabo, F. (2008): **Characterization Approach of Wind Turbine Clutter in the Spanish Weather Radar Network**. Proceedings of the Fifth European Conference on Radar in Meteorology and Hydrology, ERAD 2008, Helsinki, Finland, July 2008. ISBN: 978-9-51697-676-4
- GeoGratis. (2014): **Canadian Digital Elevation Data – 011E – Truro, Nova Scotia, Prince Edward Island**. Natural Resources Canada: <http://geogratis.gc.ca/api/en/nrcan-rncan/ess-sst/4eecb3ff-0806-4f8f-bb53-8bc9bc87849b.html>
- Hirt, C., Guillaume, S., Wisbar, A., Burki, B., and Sternberg, H. (2010): **Monitoring of the refraction coefficient of the lower atmosphere using a controlled set-up of simultaneous reciprocal vertical angle measurements**. Journal of Geophysical Research 115, D21102, doi: 10.1029/2010JD014067
- Hood, K., Torres, S., and Palmer, R. (2010): **Automatic Detection of Wind Turbine Clutter for Weather Radars**. Journal of Atmospheric and Oceanic Technology, AMS. Vol: 27. 1868-1880
- Isom, B.M. (2007): **Characterization and Mitigation of Wind Turbine Clutter on the WSR-88D Network**. M.S. thesis, School of Electrical and Computer Engineering, University of Oklahoma, 93 pp.
- Joe, P., and S. Lapczak. (2002): **Evolution of the Canadian Operational Radar Network**. Environment Canada. Proceedings of ERAD (2002): 370-382
- Kong, F., Zhang, Y., Palmer, R. (2014): **Characterization of micro-Doppler radar signature of commercial wind turbines**. Radar Sensor Technology. Vol XVIII, 907714 (May 29, 2014). DOI: 10.117/12.2050029
- Kong, F., Palmer, R., and Zhang, Y. (2013): **Mitigation Clutter Caused by Wind Turbines by Proper Siting**. 93rd Annual Meeting, American Meteorological Society, Austin, Texas, January 2013.
- Kong, F., Zhang, Y., Palmer, R., and Bai, Y. (2013): **Wind Turbine Radar Interference Studies by Polari- Metric Measurements of a Scaled Model**. IEEE Trans. Aerosp. Electron. Syst.
- Muller, Brad. (2015): **Radar Equation**. ERAU: http://wx.db.erau.edu/faculty/mullerb/Wx365/Radar_equation/radar_equation.pdf

- Nai, F., Palmer, R., and Torres, S. (2011): **Wind turbine clutter mitigation using range-Doppler domain signal processing method**. 27th Conference of Interactive Information and Processing Systems, American Meteorological Society, Seattle, Washington, 2011.
- National Weather Service (NWS). (2010): **Doppler Radar Beams**. National Weather Service – JetStream Max – Online School for Weather:
http://www.srh.weather.gov/jetstream/doppler/beam_max.htm
- Natural Resources Canada (NRC). (2014): **Canadian Digital Elevation Data (CDED)**. Natural Resources Canada. September 1, 2014:
<http://ftp2.cits.rncan.gc.ca/pub/geobase/official/cded/doc/CDED.pdf>
- ProQuest. (2008): **How Wind Turbines Work**. ProQuest LLC:
<http://www.csa.com/discoveryguides/wind/review2.php>
- Radio Advisory Board of Canada (RABC). (2013): **Technical Information and Coordination Process Between Wind Turbines and Radiocommunication and Radar Systems**. RABC & CANWEA: <http://www2.rabc-cccr.ca/Files/RABC%20CANWEA%20Guidelines.pdf>
- Rennie, C. J., Donaldson, N., & Young, J. M. C. (2012): **Improving the Analysis of Wind Turbine interactions with Weather Radar through the Addition of GIS Tools**. 2012 CMOS Congress, Montreal, Canada, June 2012.
- Rinhart, R.E. (1991): **Radar for Meteorologists**. Ronald E. Rinehart, Grand Forks, North Dakota, 1991.
- Vaisala. (2014): **IRIS Programmer's Manual**. Vaisala Oyj, Finland. Chapter 5.1 pp. 103-107
- Vogt, R.J., Crum, T.D., Sandifer, M.J.B. (2009): **A Way Forward Wind Farm – Weather Radar Coexistence**. NEXRAD Radar Operations Centre, NOAA
- Willis, M. (2007): **Propagation Tutorial: Refraction**. Mike Willis. May 5, 2007: <http://www.mike-willis.com/Tutorial/PF6.htm>

Appendix A: IDL Program: calc_beamheight.pro

```

;-----
FUNCTION ComputeHeight,elev,range_km
;COMMON MLConst
;slrange = range_km/cos(elev*!Dtor)
;return,(sin(elev*!Dtor)*slrange + (slrange*slrange)/$
;      (2.0*1.21*EarthRadiusKm))
aer=8500.0
return, (range_km^2.0 + aer^2.0 + 2.0*range_km*aer*sin(elev*!Dtor))^0.5 - aer
END

;-----
FUNCTION ComputeRangeFromHeight,height_km,elev
;COMMON MLConst
EarthRadiusKm=6371.0d
A = 4.0/3.0* EarthRadiusKm
sine_elev = sin(elev*!Dtor)
return,((-A*sine_elev) + sqrt( (A*A*sine_elev*sine_elev) + (height_km*height_km)$
+ (2.0*height_km*A) ))
END

;=====
function height_range,nbins,maxrange,elev_arr,range_arr,tle,h0,pngout
h_arr=fltarr(n_elements(elev_arr),nbins)
h_arr2=fltarr(n_elements(elev_arr),nbins)
h_arr3=fltarr(n_elements(elev_arr),nbins)
bw=1.1
for i=0,n_elements(elev_arr)-1 do begin
for j=0,nbins-1 do begin
h_arr(i,j)=ComputeHeight(elev_arr(i),range_arr(j))+ h0
;These next two equations compute the beamwidth height
h_arr2(i,j)=ComputeHeight((elev_arr(i) - (bw/2.0)),range_arr(j))+ h0
h_arr3(i,j)=ComputeHeight((elev_arr(i) + (bw/2.0)),range_arr(j))+ h0
endfor
endfor

window,0,xsize=800,ysize=400
!p.multi=[0,1,1,0,0]
device,decomposed=0
loadct,0
TVLCT,r,g,b,/GET
rr=reverse(r)
gg=reverse(g)
bb=reverse(b)
tvlct,rr,gg,bb
chsz=1.5
str=tle
;xrng will change depending on the distance of the turbine
xrng=[0,3.9]

```

```

pos=[0.15,0.15,0.9,0.9]
;yrange will change depending on elevation and height of turbine
plot,range_arr,h_arr(0,*),xstyle=1,ystyle=1,xrange=xrng,yrange=[0,0.7],xtitle='Range (km)',$
ytitle='Height (km)',charsize=chsz,thick=2.5,position=pos,title=str,/normal,/nodata

s=size(h_arr)
for i=0,s(1)-1 do begin
  oplot,range_arr,h_arr(i,*),thick=1.6
endfor
;these next two loops plot the beamwidth height
t=size(h_arr2)
for i=0,t(1)-1 do begin
  oplot,range_arr,h_arr2(i,*),thick=1.6,linestyle=3
endfor
q=size(h_arr3)
for i=0,q(1)-1 do begin
  oplot,range_arr,h_arr3(i,*),thick=1.6,linestyle=3
endfor

;add topo plot if desired
;open the topo file
;goto,skip_topo
;all topographical profiles are available - just replace radar site id
openr,lun,'WGJTopo_edit.met',/get_lun
ncols=700 ;binres=0.5km
nrows=720 ;azres=0.5 deg
topoarr=fltarr(ncols,nrows)
readf,lun,topoarr
close,lun
free_lun,lun
;azimuth changes based on turbine location
az=136.64 ;CARE at 34km
azres=0.5
binres=0.5
topo=reform(topoarr(*,round(az/azres)))/1000. ;in km
xtopo=binres*findgen(ncols)
oplot,xtopo,topo
;this plots the turbine hub height
oplot,[3.51,3.51],[0.520,0.621], linestyle=0
;this plots the turbine rotor radius
oplot,[3.51,3.51],[0.621,0.671], linestyle=3
;skip_topo:

im=TVRD(true=1)
;pngout='WKR_elevation_vs_range.png'
;pngout=tempstr+'_range_plots.png'
WRITE_PNG,pngout,im,rr,gg,bb
!p.multi=0

```



```

return,1
end

,*****
,
****
pro calc_beamheight

;enter scan angle(s)
elev_arr0=[0.0]
;elev_arr0=[0.3,0.5,0.7,0.9,1.1,1.4,1.7,2.0,2.4,2.9,3.4,4.1,4.8,5.6,6.6,7.7,9.0,10.4,12.1,14.1,16.3,18.7,21.
5,24.6]
;elev_arr1=[0.3,0.5,0.7,0.9,1.1,1.4,1.7,2.0,2.4,2.9,3.4,4.1,4.8,5.6,8.0,11.0,14.5,18.7]

nbins=250
maxrange=nbins
elev_arr=elev_arr0
range_arr=findgen(nbins)
;change tle
;can change pngout(not necessary but it will rewrite the images after each run)
tle='CONVOL (0.0 degrees) Bow Lake Turbine #1 at 3.11 km'
pngout='WGJ_CONVOL_beamheight.png'
h0=164.0 ; radar asl height + tower height
;this value is the elevation of the radar antenna
h0=0.5431
ok=height_range(nbins,maxrange,elev_arr,range_arr,tle,h0,pngout)

stop
end

```

Appendix B: C-TRIP Code

```
#!/usr/bin/perl
# Created by Carolyn Rennie (Junior Physical Scientist with the National Radar Program of Environment
Canada on August 2, 2012
# error checks added August 13, 2012
# additional edits to the code were performed on January 20, 2015 to update the code for inclusion in
Thesis
# Script will allow user to create a days worth of URP product GIF images
# USER INPUTS
*****
*****

# The user inputs the 3 letter code of the radar site they are wishing to create precipitation
accumulation products for ex: WSO, WKR, WHN
print "Input the 3 letter radar identifier in all capital letters\n";
$site = <>; # This reads the user input
chop $site;
# The following is an error check to ensure that the site input is correct
while (($site ne "WWW")&&($site ne "WKR")&&($site ne "XNC")&&($site ne "XGO")&&($site ne
"WTP")&&($site ne "XME")&&($site ne "XMB")&&($site ne "WHN")&&($site ne "WMB")&&($site ne
"WBI")&&($site ne "XDR")&&($site ne "WSO")&&($site ne "XFT")&&($site ne "XNI")&&($site ne
"WGJ")&&($site ne "XTI")&&($site ne "XBE")&&($site ne "WHK")&&($site ne "XFW")&&($site ne
"XRA")&&($site ne "XBU")&&($site ne "XSM")&&($site ne "XWL")&&($site ne "WUJ")&&($site ne
"XSI")&&($site ne "XPG")&&($site ne "XSS")&&($site ne "XLA")&&($site ne "XAM")&&($site ne "WVY"))
{
    print "This is not an identifier, please check it's in capital letters and is a Canadian radar site\n";
    $site = <>;
    chop $site;
}

# Now the user will decide which day to create the radar products for
# The user will input the 4 number year (yyyy) for example: 2012
print "Input the year in four digits\n";
$y = <>; # This reads the input
chop $y;
# The following is an error check to ensure that the year input is valid
while (($y != 2012)&&($y != 2011)&&($y != 2013)&&($y != 2014)&&($y != 2015)) {
    print "Sorry we only have radar data from 2011 up to January 20, 2015, please re-enter the year\n";
    $y = <>;
    chop $y;
}

# The user will input the 2 number month (mm) for example: 08
print "Input the month in two digits\n";
$m = <>; # This reads the input
chop $m;
# The following is an error check to ensure that the month input is valid
while (($m ne "01")&&($m ne "02")&&($m ne "03")&&($m ne "04")&&($m ne "05")&&($m ne
"06")&&($m ne "07")&&($m ne "08")&&($m ne "09")&&($m ne "10")&&($m ne "11")&&($m ne "12")) {
```

```

    print "This is not a valid two digit month, for January - September add a zero infront ex: 02, please
re-enter the month\n";
    $m = <>;
    chop $m;
}
# The user will input the 2 digit day (dd) for example: 31
print "Input the day in two digits\n";
$d = <>;
chop $d;
# The following is an error check to ensure that the day input is valid
while (($d ne "01")&&($d ne "02")&&($d ne "03")&&($d ne "04")&&($d ne "05")&&($d ne "06")&&($d
ne "07")&&($d ne "08")&&($d ne "09")&&($d ne "10")&&($d ne "11")&&($d ne "12")&&($d ne
"13")&&($d ne "14")&&($d ne "15")&&($d ne "16")&&($d ne "17")&&($d ne "18")&&($d ne
"19")&&($d ne "20")&&($d ne "22")&&($d ne "23")&&($d ne "24")&&($d ne "25")&&($d ne
"26")&&($d ne "27")&&($d ne "28")&&($d ne "29")&&($d ne "30")&&($d ne "31")) {
    print "This is not a valid two digit day for days less than 10 add a zero infront ex: 02, please re-enter
the day\n";
    $d = <>;
    chop $d;
}
# NOTE: There are no checks to ensure the inputs are correct given a month or day without data,
however there will be errors when trying to run the script if the inputs are not correct :)
# However, the inputs include a "newline" so.chomp is used to remove the terminal newline
chomp $site;
chomp $y;
chomp $m;
chomp $d;
# DIRECTORY AND PRODUCT VARIABLES
*****
*****
# The next statements join the year month and day inputs in a way that corresponds to where the iris
files are stored and how they are saved
$ym = $y."-".$m;
$date = $ym."-".$d;
$ymd = $y.$m.$d;

# $scan is the Radar scan that is required for the creation of the product either CONVOL, DOPVOL1_A,
DOPVOL1_B, DOPVOL1_C or DOPVOL2
$scan = "DOPVOL1_A";
# $scan 2 is only used for products that look at two scans ( for example PRECIP products )
#$scan2 = "CONVOL ";

# $product is the product you wish to create (CLOGZPPI, VRPPI, PRECIP)
$product = "CLOGZPPI";

# $geodef is the geographic definition file as found in the /apps/urp/config/geodef directory for
CLOGZPPI & VRPPI 240KM is used
$geodef = $site."_240KM";

```

```

# $geodef 480KM is only used for PRECIP
# $geodef = $site."_480KM";

# $imagedef is the image definition file as found in the /apps/urp/config/imagedef directory
# image def for which wind farms is under the form SITE_PRODUCT_WF for CLOGZPPI and PRECIP (from
April 1st – October 31st)
$imagedef = $site."_.$product."_WF";
# image def for which wind farms is under the form SITE_PRODUCT_SNOW_WF for PREIP (from
November 1st – March 30th)
# $imagedef = $site."_.$product."_SNOW_WF";
# image def for which wind farms is under the form SITE_PRODUCT_LOLAA_WF for VRPPI
# $imagedef = $site."_.$product."_LOLAA_WF";

# $provar is the additional product variable as a part of the product key for the module (default is for
CLOGZPPI)
$provar = "18,MPRATE";
# $provar = "18"; - for VRPPI
# $provar = "125,18,MPRATE"; - for PRECIP

# $type is the URP creation file found in /apps/urp/bin for ex: URPClogzPPI, URPPrecip, URPVrPPI
$type = "URPClogzPPI";

# CREATE DIRECTORIES IF NOT ALREADY CREATED
*****
*****

$dirpro = "/data/RADAR/crennie/$product";
$dirsite = "/data/RADAR/crennie/$product/$site";
$dirday = "/data/RADAR/crennie/$product/$site/$date" ;
$dirmet = "/data/RADAR/crennie/META";
$dirmeta = "/data/RADAR/crennie/META/$site";
if (! -d $dirpro) {
    system ("mkdir $dirpro");
}
if (! -d $dirsite) {
    system ("mkdir $dirsite");
}
if (! -d $dirday) {
    system ("mkdir $dirday");
}
if (! -d $dirmet) {
    system ("mkdir $dirmet");
}
if (! -d $dirmeta) {
    system ("mkdir $dirmeta");
}

# Script -----
# The first part of the script is used to create a list and array of the IRIS files in the directory
system("ls -l /data/RADAR/$site/$y/$ym/$date/$scan > listing.txt");

```

```

open(infile,"listing.txt");
@files=<infile>;
shift(@files);
close(infile);
# The datestring is a way to extract the day and product individual files based on the date starting at
# Column 50 and going for 12 columns
foreach $filename (@files) {
    chomp($filename);
    $datestring=substr($filename,$num,12);
# sometimes one will get errors because the listing filename picks up 01201030000_ instead of
201201030000 in this case adjust so substr($filename,49,12)

# PRODUCT GENERATION
*****
*****
# $in defines the input iris file
    $in = "/data/RADAR/$site/$y/$ym/$date/$scan/$site"."_"."$datestring."_$scan.iri";
# for PRECIP products $in2 is also used where:
# $in2 = "/data/RADAR/$site/$y/$ym/$date/$scan2/$site"."_"$datestring"."_"$scan2.iri";
# $meta defines the output & input meta file
    $meta = "$dirmeta/$product"."_"."$datestring.dat";
# this creates the meta files for VRPPI & CLOGZPPI
    system("/apps/urp/bin/$type -ms -i $in -o $meta -k
RADAR:*. $product,$scan,$provar:$geodef:$imagedef:META");
# this creates the meta files for PRECIP
# system("/apps/urp/bin/$type -ms -i $in1 $in2 -o $meta -k
RADAR:*. $product,$provar:$geodef:$imagedef:META");
# this is the ouput for gif files of the prodcut
    $gif = "$dirday/$datestring.gif";
# this creates the gif files for each product based on the meta file using URP Graphics
    system("/apps/urp/bin/URPGraphics -ms -i $meta -o $gif -k
RADAR:*. $product,$scan,$provar:$geodef:$imagedef:GIF");
# this check allows the user to be updated once the gif files have been created for each datestring
(YYYYMMDDHHH)
    if (-e $gif) {
        print "The imagefile has been created for $datestring\n";
# The final print statement varifies if the product has been created
# This code was produced with help from Jim Young, Sudesh Boodoo, Norman Donaldson and Janti Reid
of Environment Canada

```

Appendix C: Melancthon Turbine Coordinates (UTM Zone 17T)

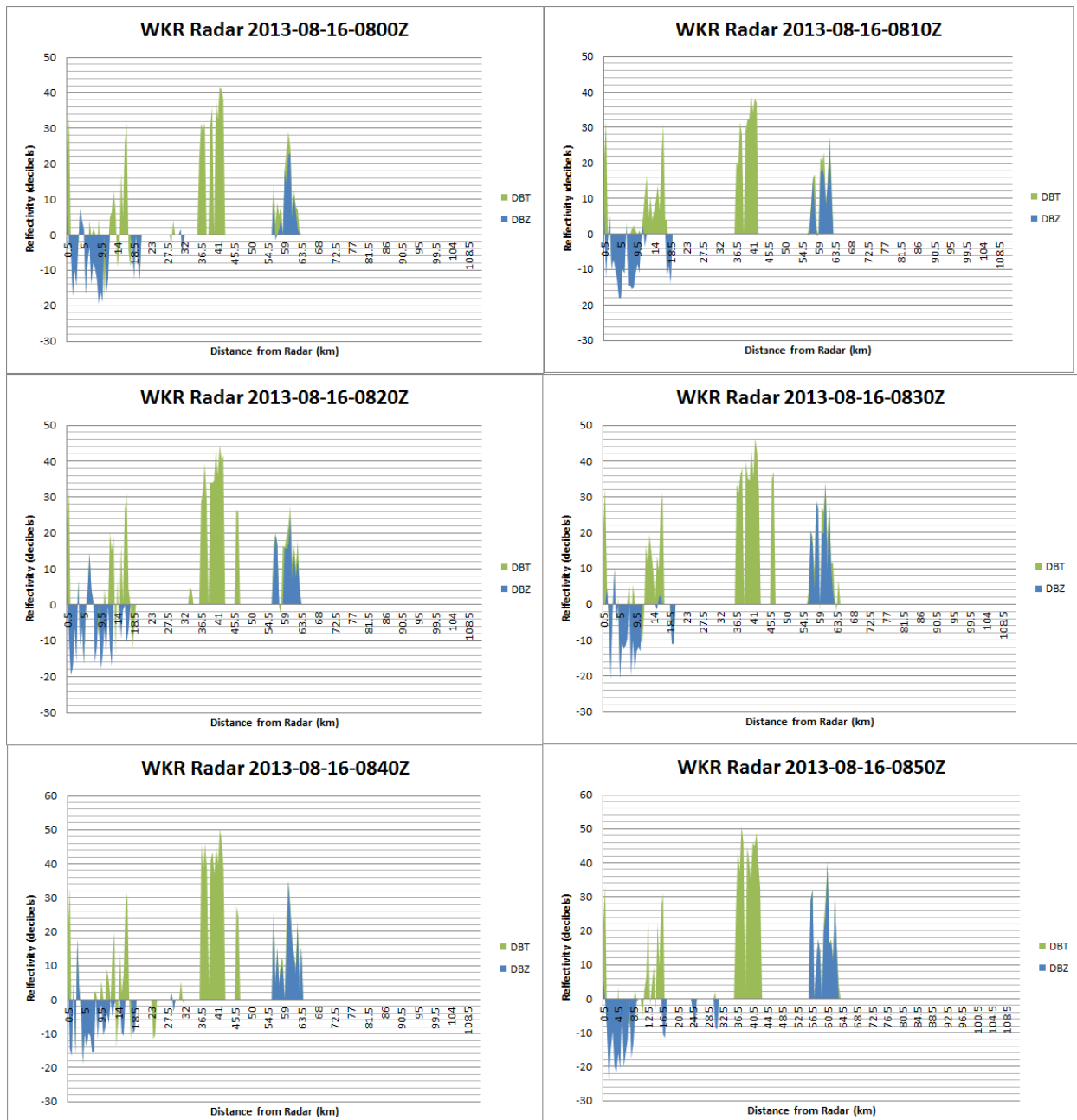
Turbine	Northing	Easting
101	4878521	550962
102	4878876	551099.3
104	4879856	552236.3
105	4880163	551945.8
106	4880557	551909.4
107	4880327	551035
108	4880646	551292.1
109	4881042	551601.9
110	4881642	550541.3
111	4882001	550459.3
112	4882989	551300.2
113	4882817	551641.2
114	4882388	551653
115	4881847	552215.4
116	4881109	553122.4
117	4881430	553683.5
118	4881665	553358.6
119	4882076	553505.6
122	4883353	552236.2
123	4883292	551520.1
124	4883981	552680
126	4883373	553958.8
127	4883022	554416.6
128	4882678	554437.3
129	4882502	554793.3
130	4882346	555202.2
131	4882018	555290.9
132	4883476	554618.1
134	4885181	553263.6
135	4884818	552858.3
136	4885009	552418
137	4885469	552881.4
138	4886196	551793.2
139	4885882	551637.9
141	4886368	550919.5
142	4886750	551158.8
143	4886030	553326.5
144	4886363	553594.9
145	4886892	554047.2
146	4887103	554425.1

147	4885201	554979.7
148	4884826	555096
149	4884560	555407.1
150	4885180	555793.9
151	4884706	556084.7
152	4884386	556239.7
153	4886320	557388.2
154	4885957	557145.9
155	4886461	557050.8
156	4886784	556803.4
157	4887136	556629.8
158	4887840	556133
159	4888020	555850
160	4887753	555339
161	4887863	554833.2
162	4888192	555181.6
163	4888522	555331
164	4889449	555806
165	4889921	556206
166	4886080	557679.6
204	4889713	556015
205	4886803	553004
206	4886063	554039.6
207	4885616	554224.7
208	4888105	557346.1
209	4888045	557784.6
510	4887645	558020.1
52	4875661	554589
54	4875073	554531.1
55	4876623	557126.9
56	4876444	554408.5
57	4876712	554201.6
60	4877008	555670.3
61	4876696	555264
62	4878239	556639.8
64	4877448	556821.3
65	4876880	556697.8
66	4876498	556748.5
67	4875828	556983.8
68	4875396	556913.7
69	4875728	558233.5

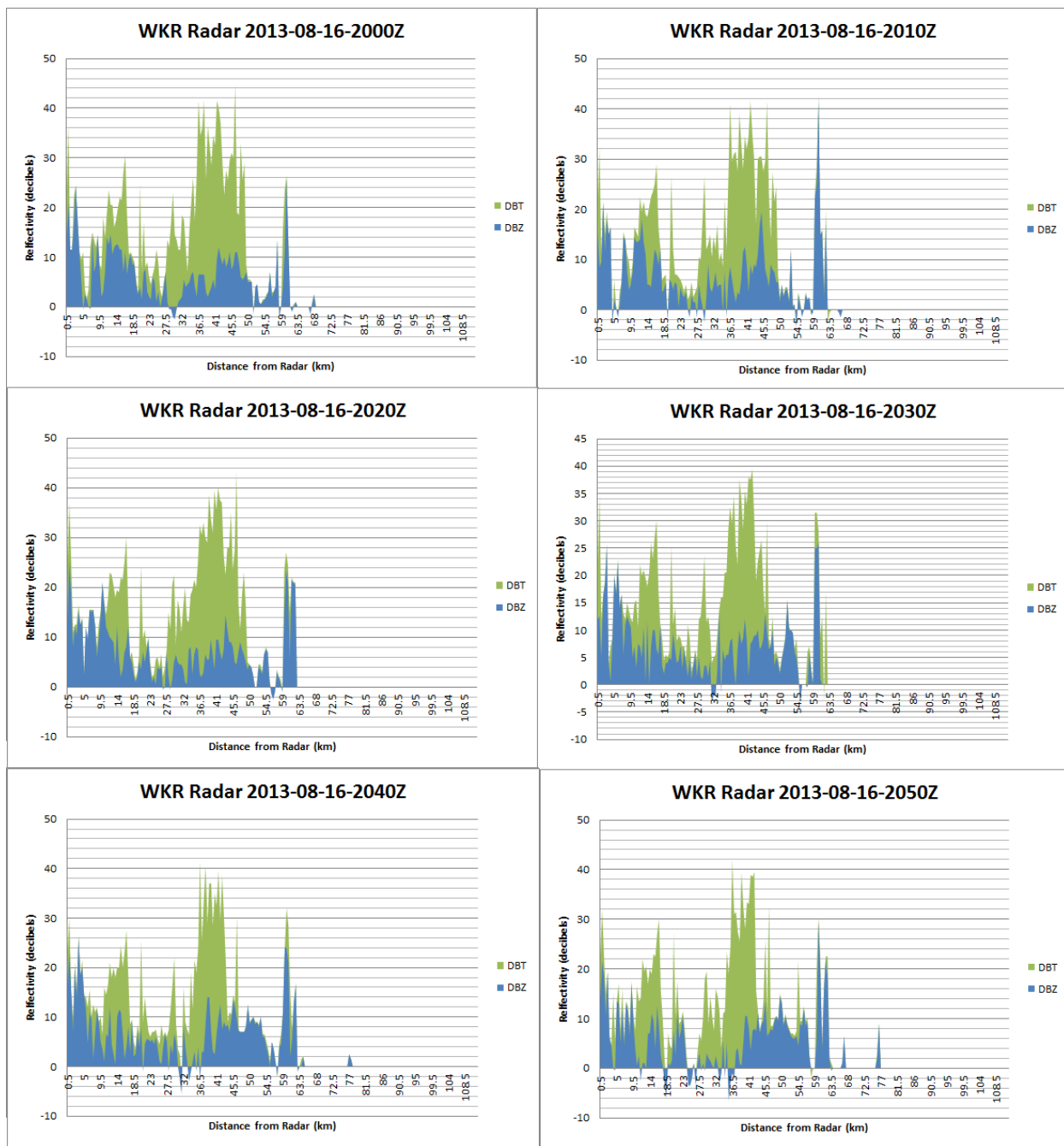
70	4876343	558382.1
71	4876952	558270.5
72	4877567	558222
73	4878239	559092.6
74	4877921	559554
75	4877547	559600
76	4877280	559391.8
77	4876115	554005.3
1	4878515	553932.4
2	4878711	553698.9
3	4878895	553469.7
4	4879035	553292.3
5	4879286	553517.1
6	4879494	553706
7	4879080	555776.4
8	4879302	555831.1
9	4880008	554778.5
10	4879946	558014.4
11	4879653	557937.5
12	4880530	558264.7
13	4880055	559179.4
14	4880272	558994.2
15	4880194	558138.9
16	4880744	558104
17	4881055	558109.8
18	4881856	556982
19	4880552	557026.4

20	4880928	557246.5
21	4881222	557088.6
22	4881547	556944.7
23	4881414	556087.1
24	4881793	556008.3
25	4882124	555970.2
26	4882472	556189.4
27	4881585	559336.1
28	4881832	559549.5
29	4882076	559416
30	4882025	556760
31	4879374	557716.7
32	4882506	558611.2
33	4882720	558511.3
34	4882975	558512
35	4883205	557376.1
37	4883475	557603.2
43	4880277	554801.8
44	4882372	559254
45	4880768	553759
46	4880485	553803.7
47	4884085	556363.1
48	4883889	556583.1
49	4883532	556645.4
50	4879729	554717.8
51	4882271	558424.1

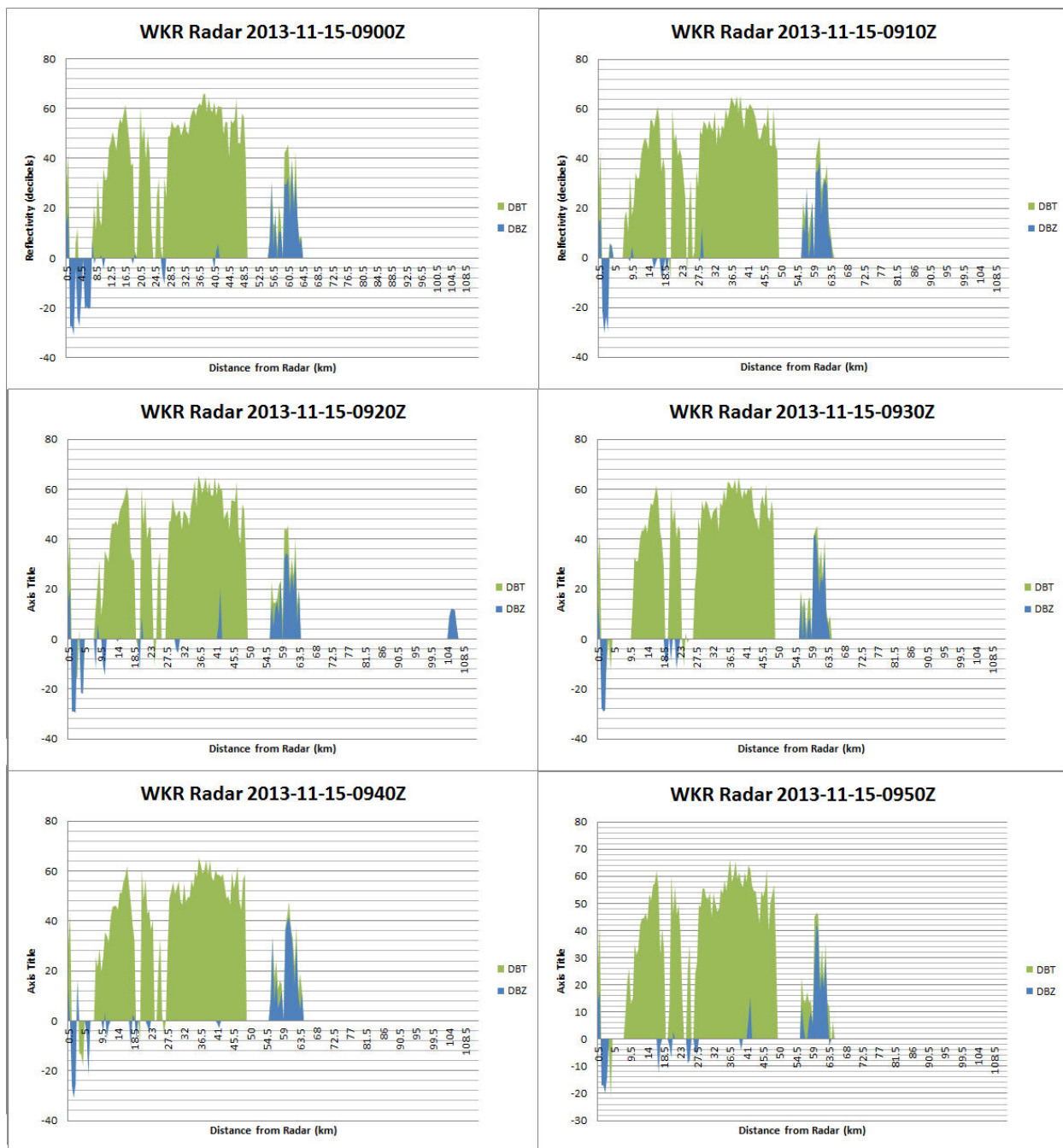
Appendix D: Productx Output WTC Examples of the Melancthon Wind Farm / King City Weather Radar Pair



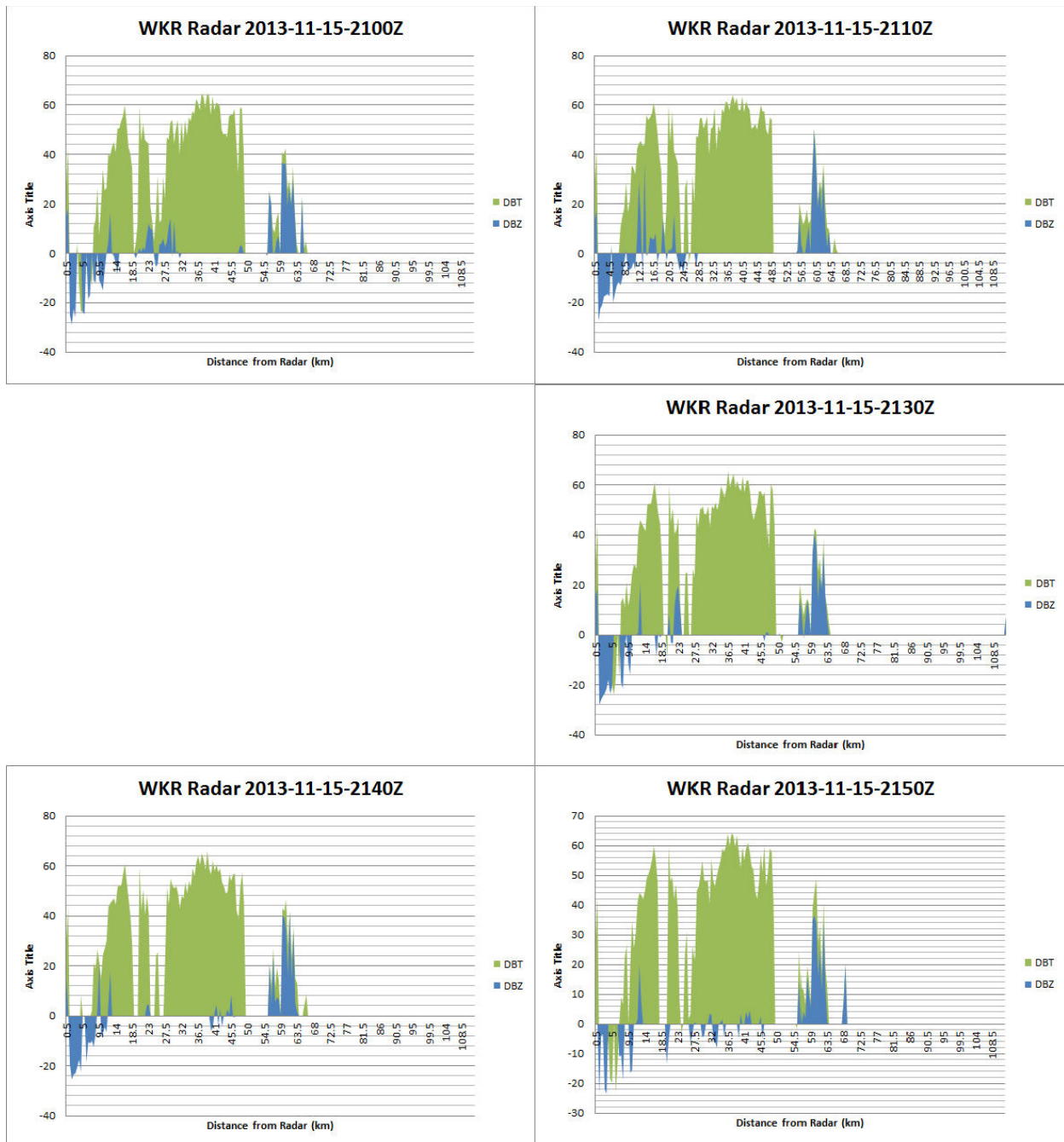
Appendix D: i. Productx images created from DOPVOL1A IRIS files for the King City weather radar on 2013-08-16 for 10 minute intervals during 04:00 EDT or 0800 Z – 0850 Z using the maximum DBT and DBZ values from the azimuth range 276° - 291°



Appendix D: ii. Productx images created from DOPVOL1A IRIS files for the King City weather radar on 2013-08-16 for 10 minute intervals during 16:00 EDT or 2000 Z – 2050 Z using the maximum DBT and DBZ values from the azimuth range 276° - 291°

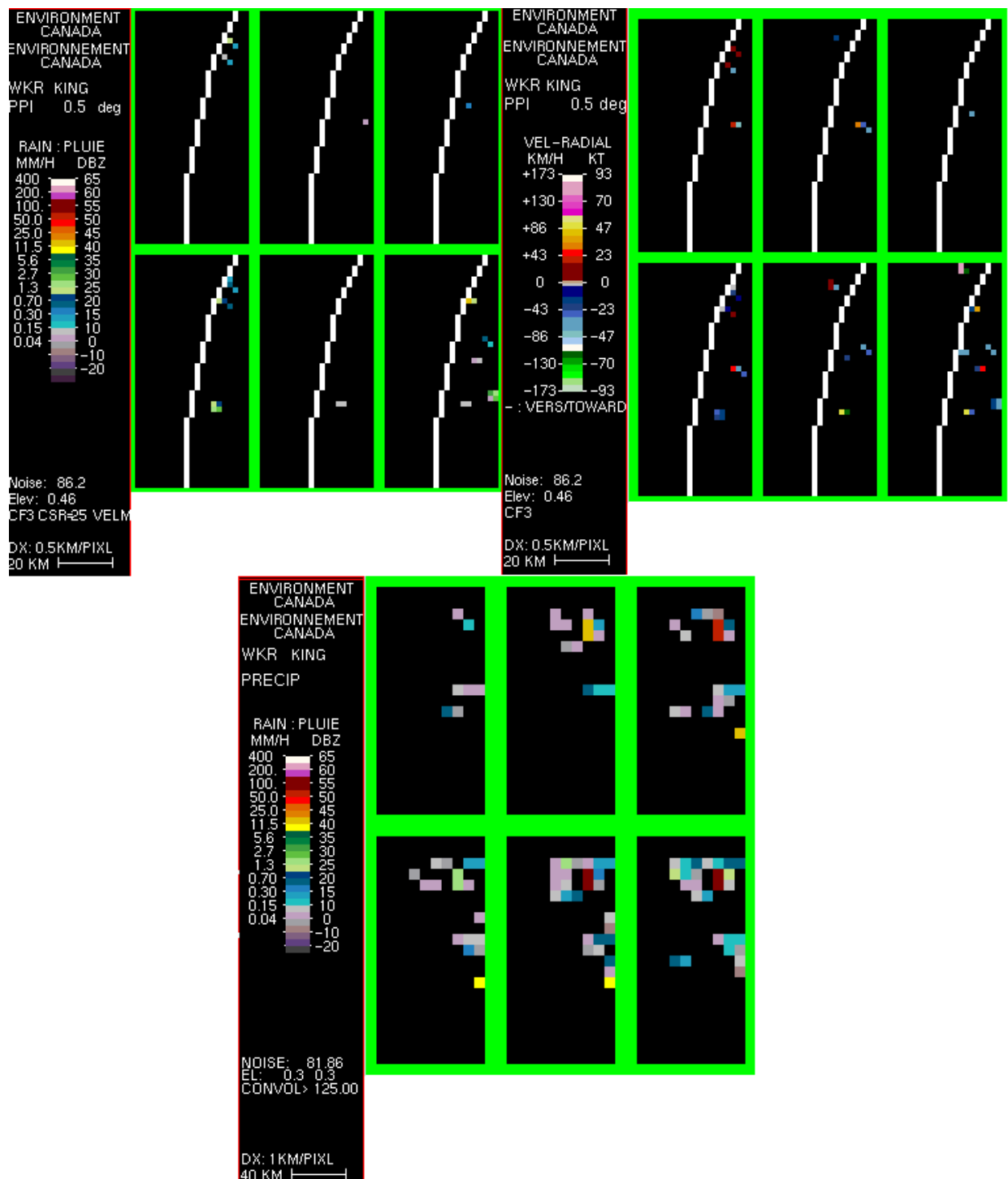


Appendix D: iii: Productx images created from DOPVOL1A IRIS files for the King City weather radar on 2013-11-15 for 10 minute intervals during 04:00 EST or 0900 Z – 0950 Z using the maximum DBT and DBZ values from the azimuth range 276° - 291°

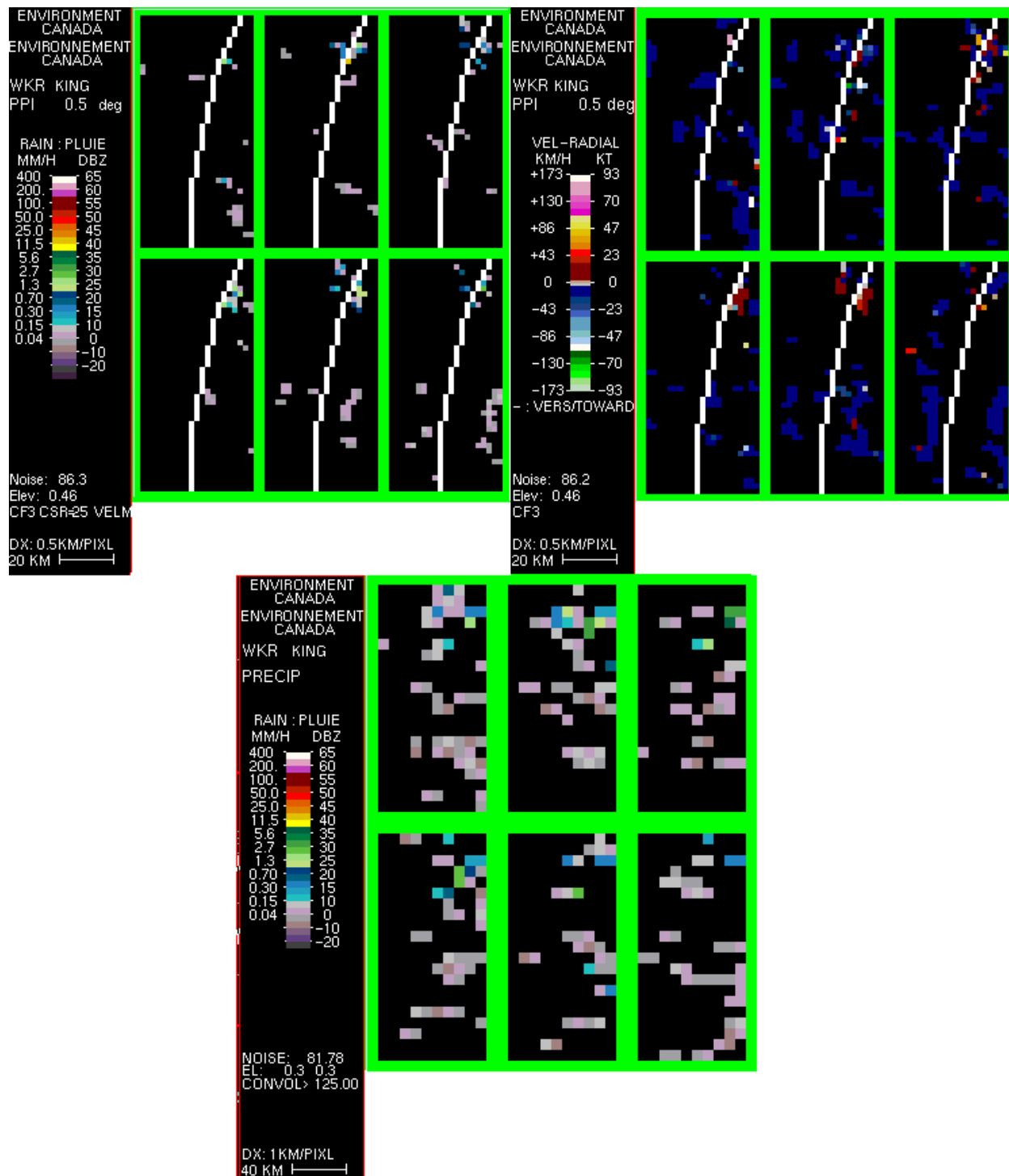


Appendix D: iv: Productx images created from DOPVOL1A IRIS files for the King City weather radar on 2013-11-15 for 10 minute intervals during 16:00 EST or 2100 Z – 2150 Z (with 2120 Z missing due to an data error) using the maximum DBT and DBZ values from the azimuth range 276° - 291°

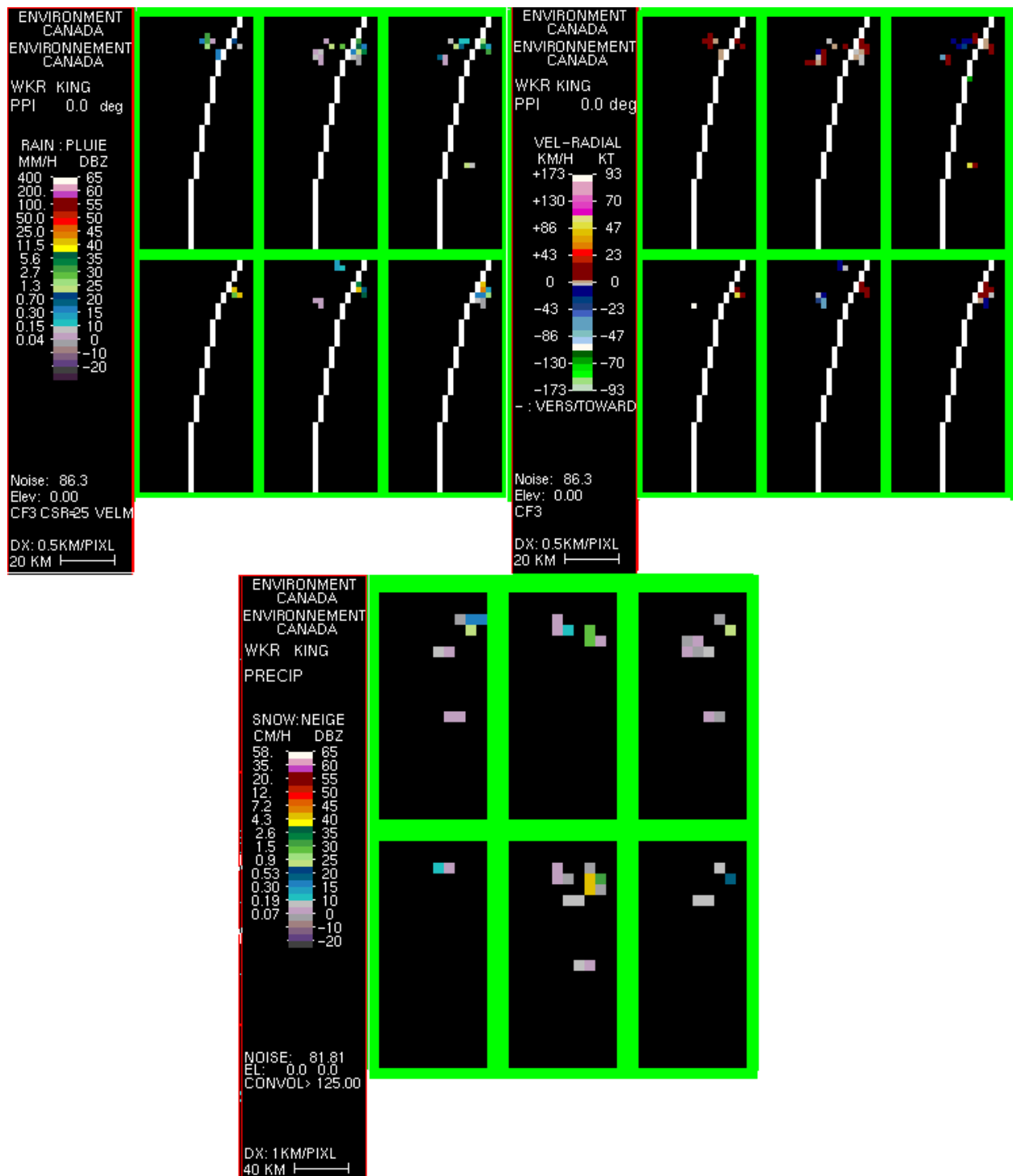
Appendix E: C-TRIP Output WTC Examples of the Melancthon Wind Farm / King City Weather Radar Pair



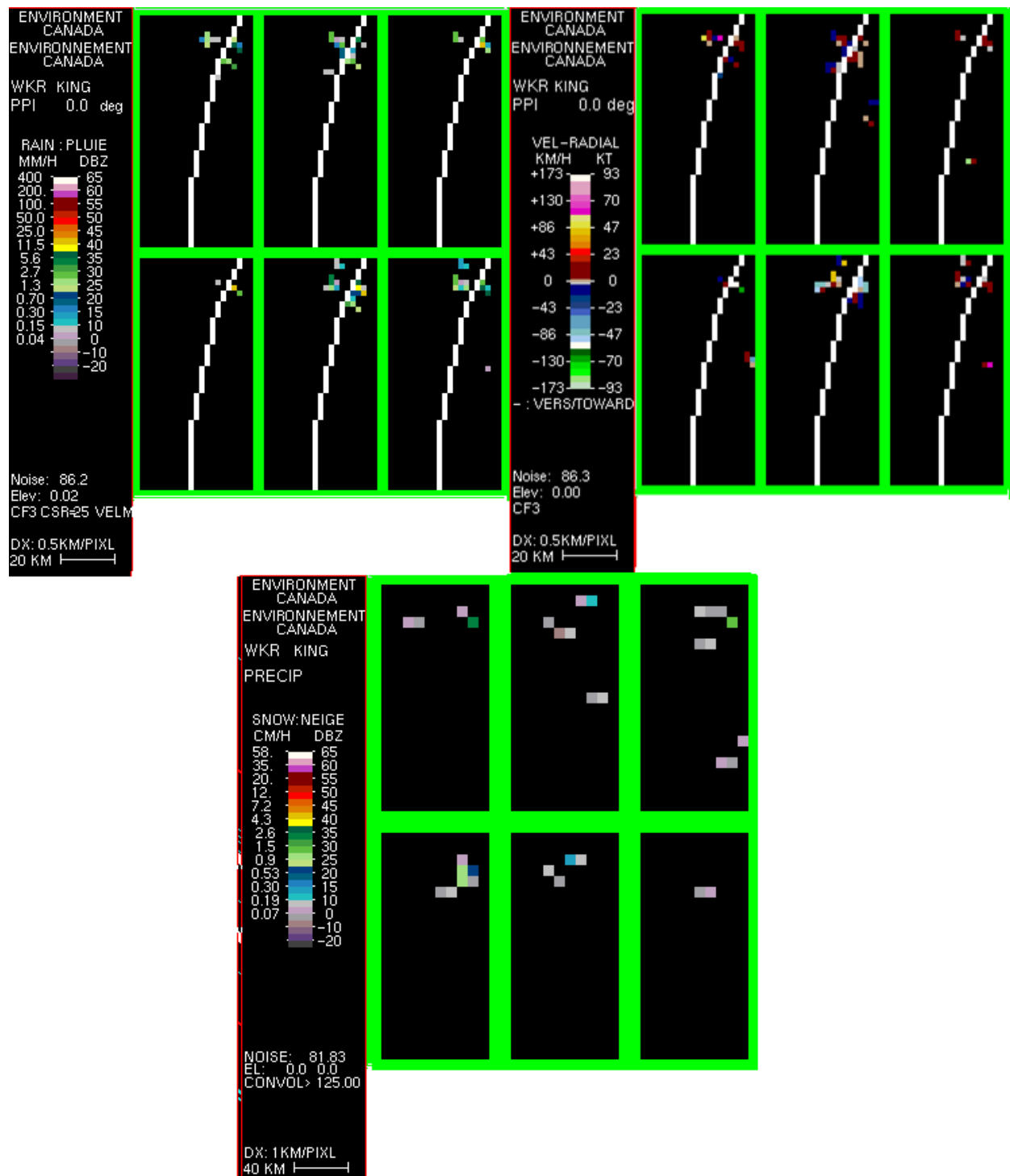
Appendix E: i. C-TRIP CLOGZPPI, VRPPI and PRECIP products of the Melancthon wind farm box on 2013-08-16 from 0800 Z – 0850 Z created using the DOPVOL1A and DOPVOL2 WKR IRIS files. The white quarter circle lines in the first two images are the 60 km range rings.



Appendix E: ii: C-TRIP CLOGZPPI, VRPPI and PRECIP products of the Melancthon wind farm box on 2013-08-16 from 2000 Z – 2050 Z created using the DOPVOL1A and DOPVOL2 WKR IRIS files. The white quarter circle lines in the first two images are the 60 km range rings.



Appendix E: iii: C-TRIP CLOGZPPI, VRPPI and PRECIP products of the Melancthon wind farm box on 2013-11-15 from 0900 Z – 0950 Z created using the DOPVOL1A and DOPVOL2 WKR IRIS files. The white quarter circle lines in the first two images are the 60 km range rings



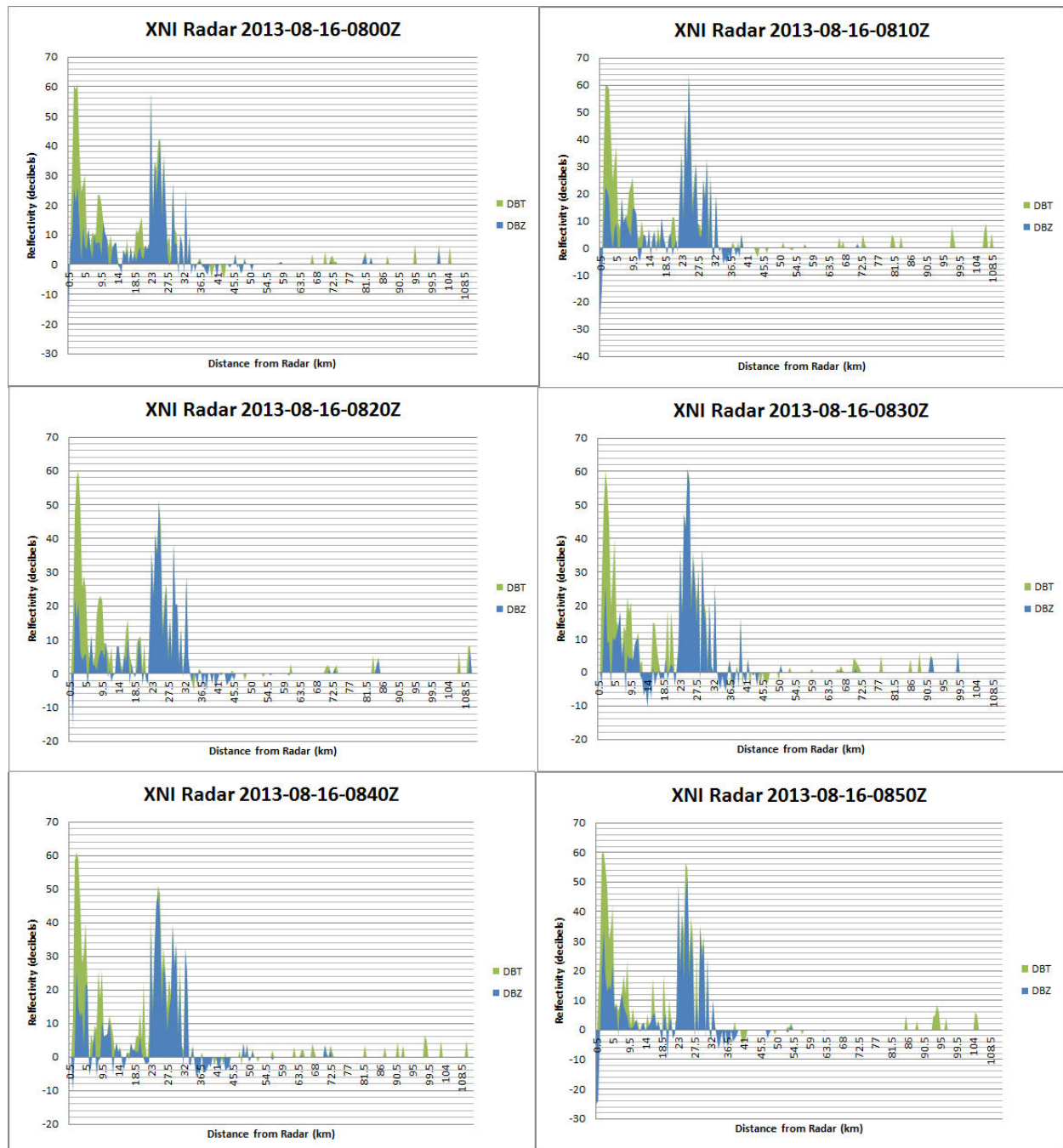
Appendix E: iv: C-TRIP CLOGZPPI, VRPPI and PRECIP products of the Melancthon wind farm box on 2013-11-15 from 2100 Z – 2150 Z created using the DOPVOL1A and DOPVOL2 WKR IRIS files. The white quarter circle lines in the first two images are the 60 km range rings

Appendix F: Greenwich Turbine Coordinates (UTM Zone 16 U)

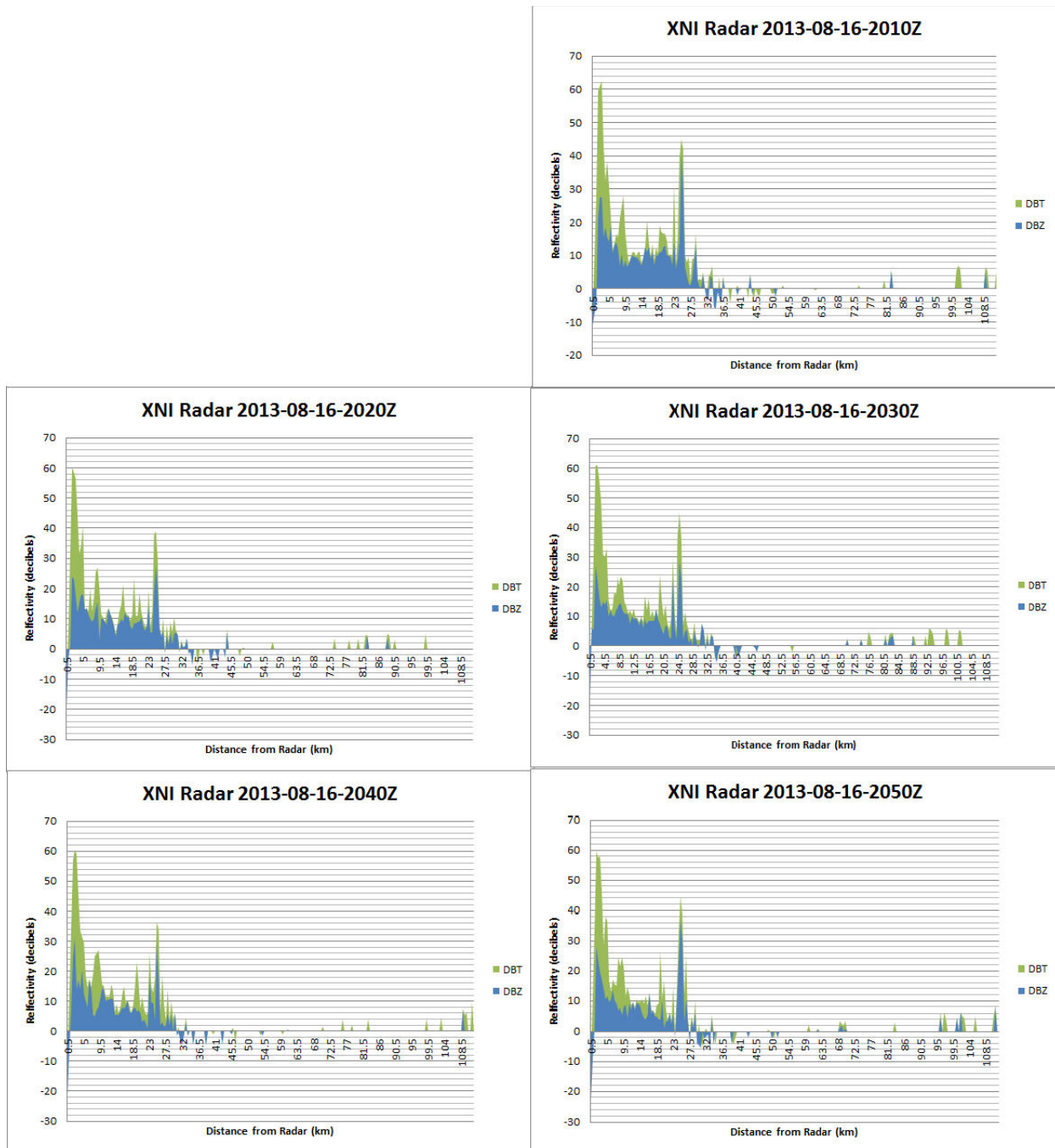
Turbine	Easting	Northing
1	364643	5399620
2	364861	5400000
3	365161	5400219
4	365676	5400114
5	365780	5401394
6	366108	5401531
7	366400	5401734
8	366718	5401893
9	365439	5402614
10	365756	5402788
11	366080	5402966
12	366984	5402622
13	367293	5402793
14	368094	5402707
15	368890	5402898
16	369195	5403163
17	369983	5403019
18	370234	5403323
19	371107	5403994
20	371417	5404164
21	371859	5403281

22	372169	5403451
23	372479	5403621
24	373094	5403624
25	372116	5400450
26	372390	5400672
27	373508	5400568
28	373835	5400747
29	374535	5400929
30	368468	5406572
31	368863	5406838
32	369339	5404162
33	369648	5404331
34	369534	5405458
35	369810	5405664
36	364938	5405781
37	365292	5405773
38	365629	5405902
39	365919	5406140
40	366485	5406150
41	366781	5406343
42	367557	5405986
43	368187	5406357

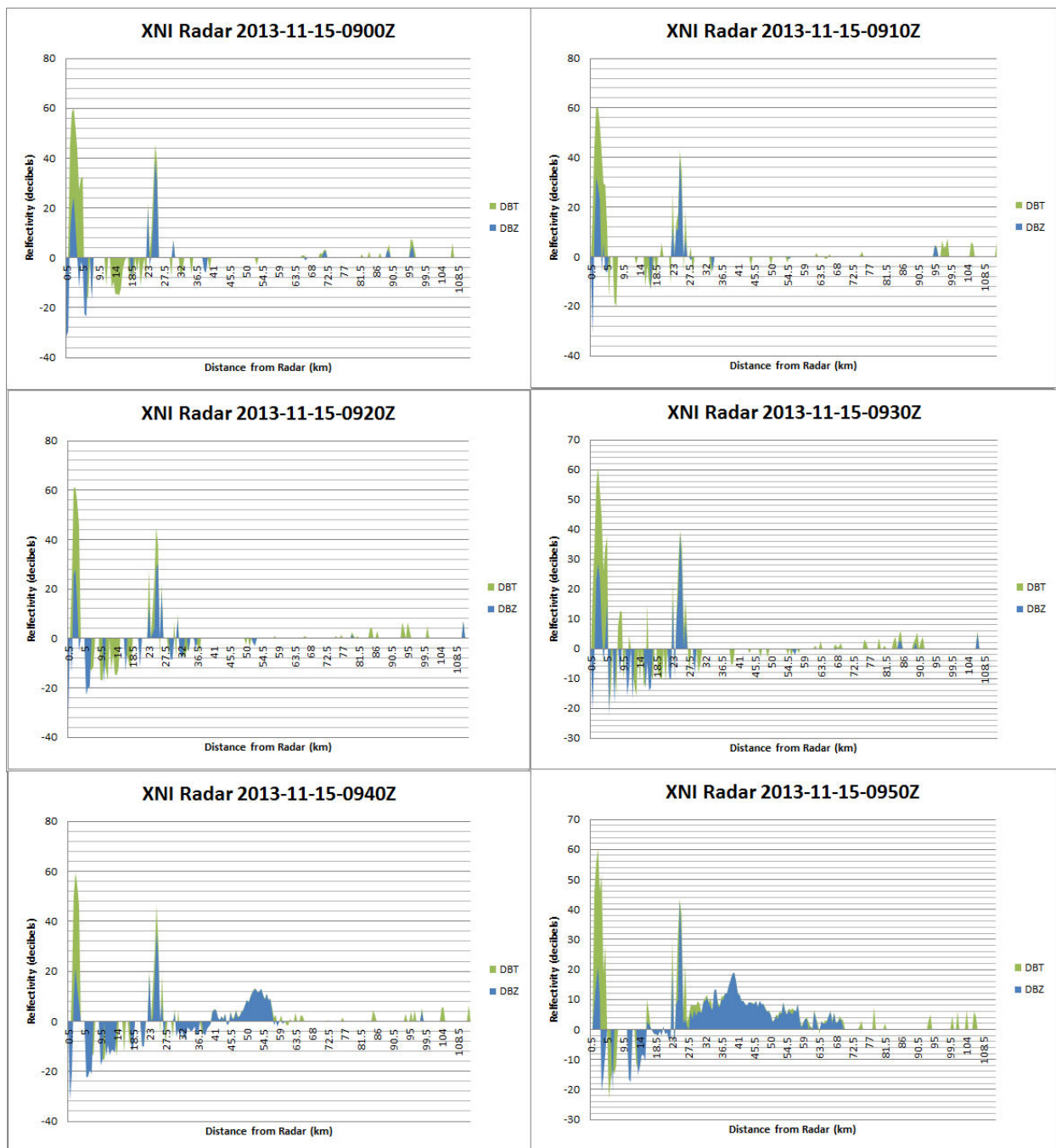
Appendix G: Productx Output WTC Examples of the Melancthon Wind Farm / King City Weather Radar Pair



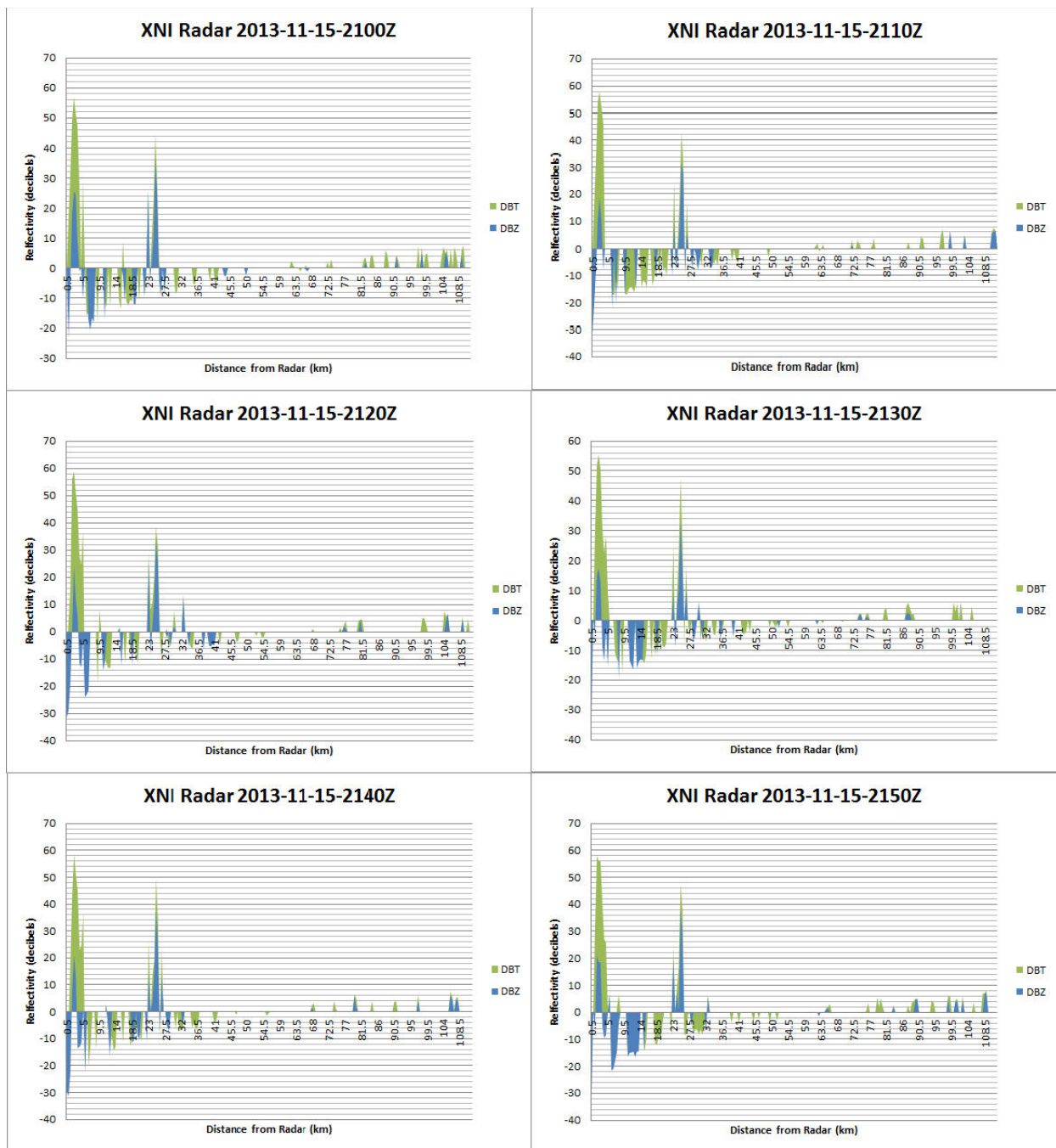
Appendix G: i: Productx images created from DOPVOL1A IRIS files for the Lasseter Lake weather radar on 2013-08-16 for 10 minute intervals during 04:00 EDT or 0800 Z – 0850 Z using the maximum DBT and DBZ values from the azimuth range 103° - 123°



Appendix G: ii: Productx images created from DOPVOL1A IRIS files for the Lasseter Lake weather radar on 2013-08-16 for 10 minute intervals during 16:00 EDT or 2000 Z – 2050 Z (with 2000 Z missing due to an data error) using the maximum DBT and DBZ values from the azimuth range 103° - 123°

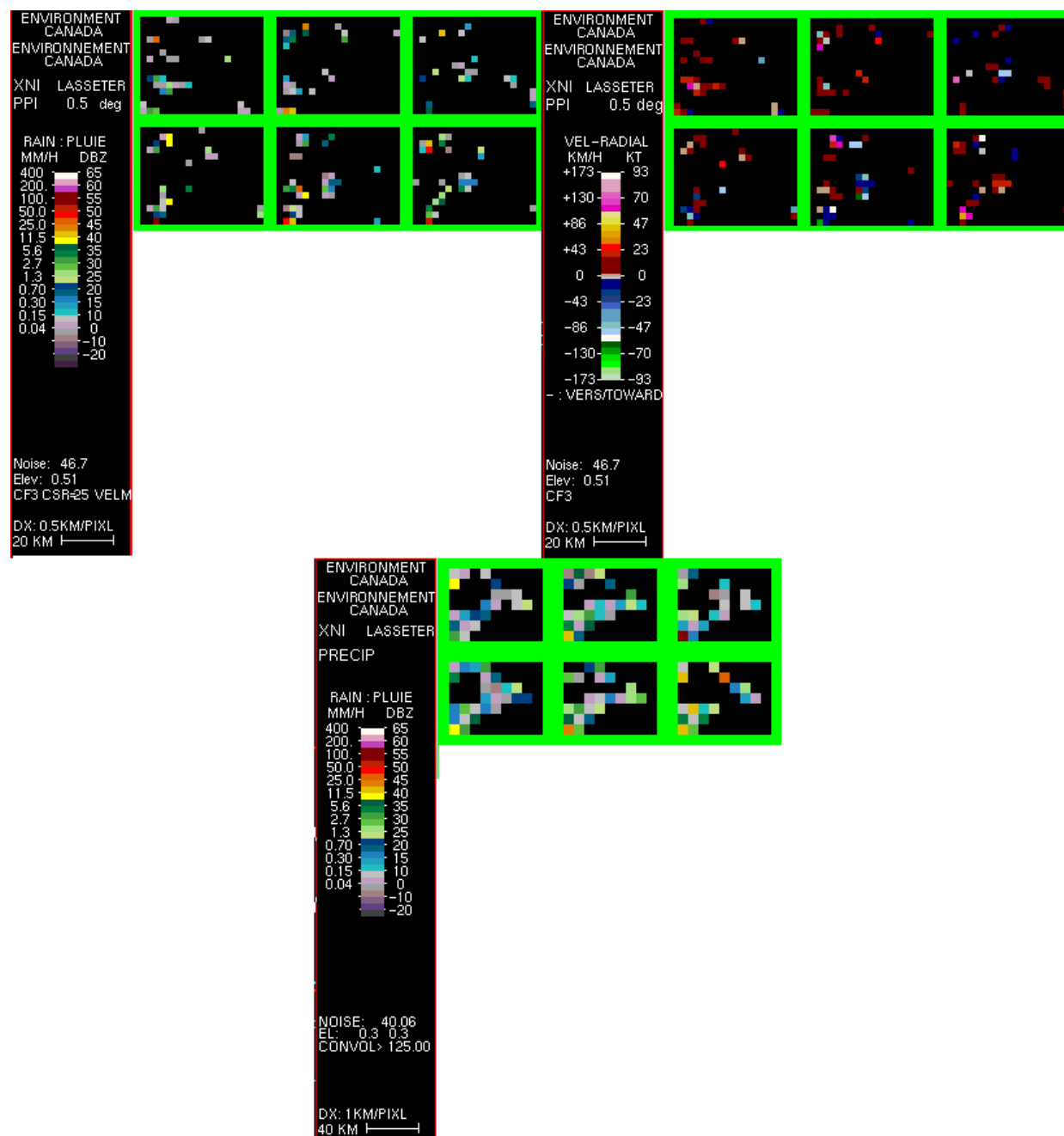


Appendix G: iii: Productx images created from DOPVOL1A IRIS files for the Lasseter Lake weather radar on 2013-11-15 for 10 minute intervals during 04:00 EST or 0900 Z – 0950 Z using the maximum DBT and DBZ values from the azimuth range 103° - 123°

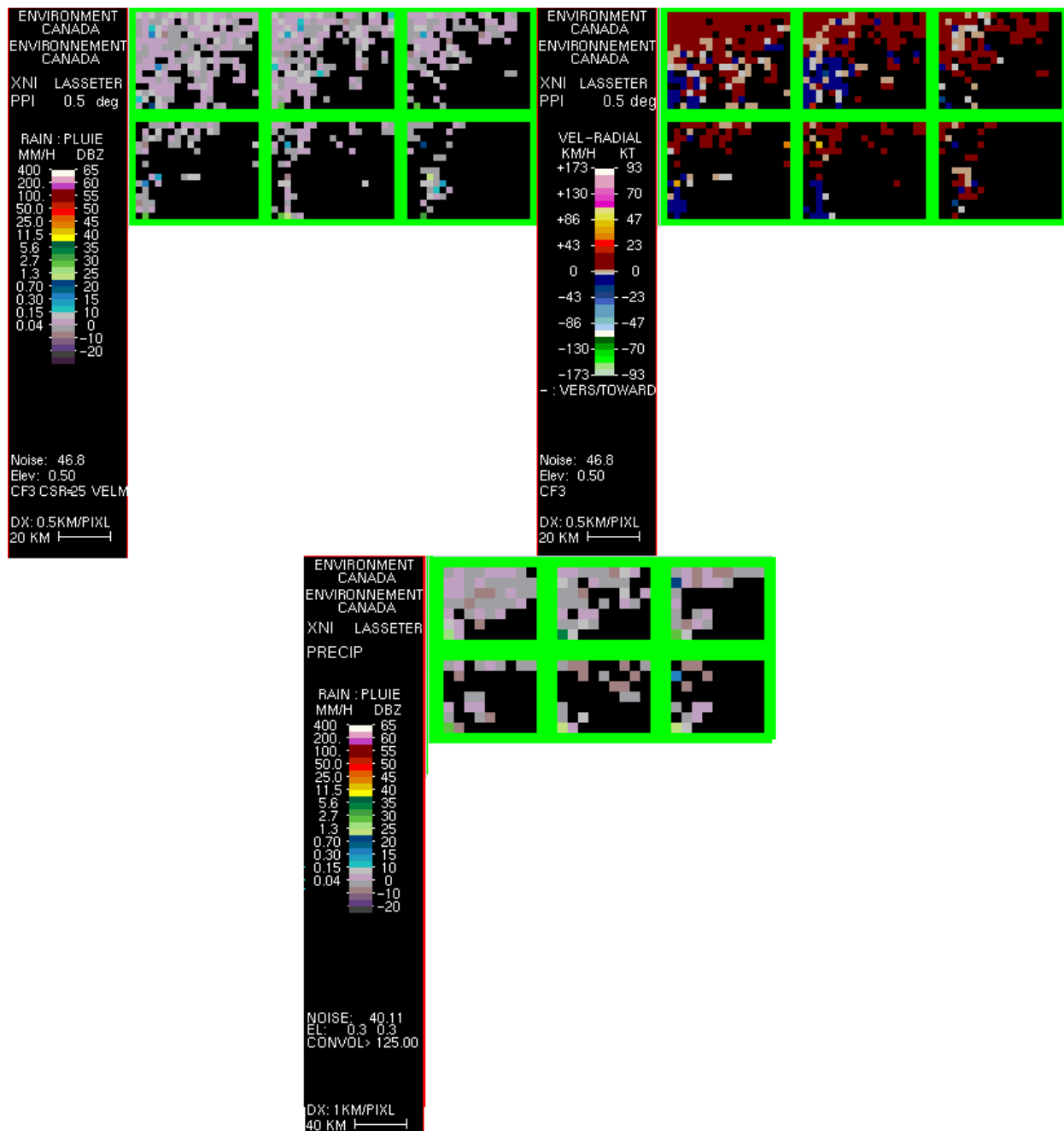


Appendix G: iv: Productx images created from DOPVOL1A IRIS files for the Lasseter Lake weather radar on 2013-11-15 for 10 minute intervals during 16:00 EST or 2100 Z – 2150 Z using the maximum DBT and DBZ values from the azimuth range 103° - 123°

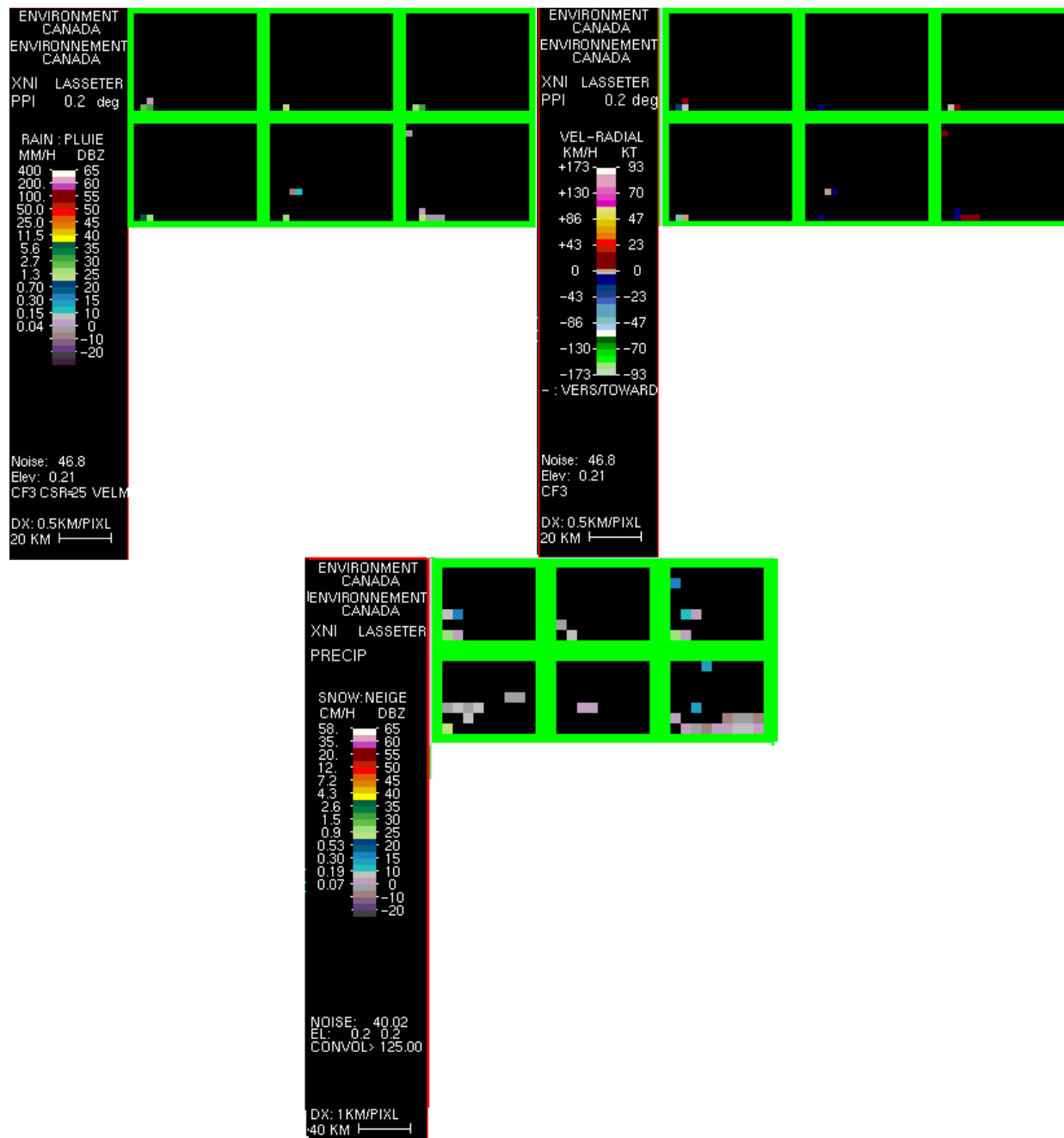
Appendix H: C-TRIP Output WTC Examples of the Greenwich Wind Farm / Lasster Lake Weather Radar Pair



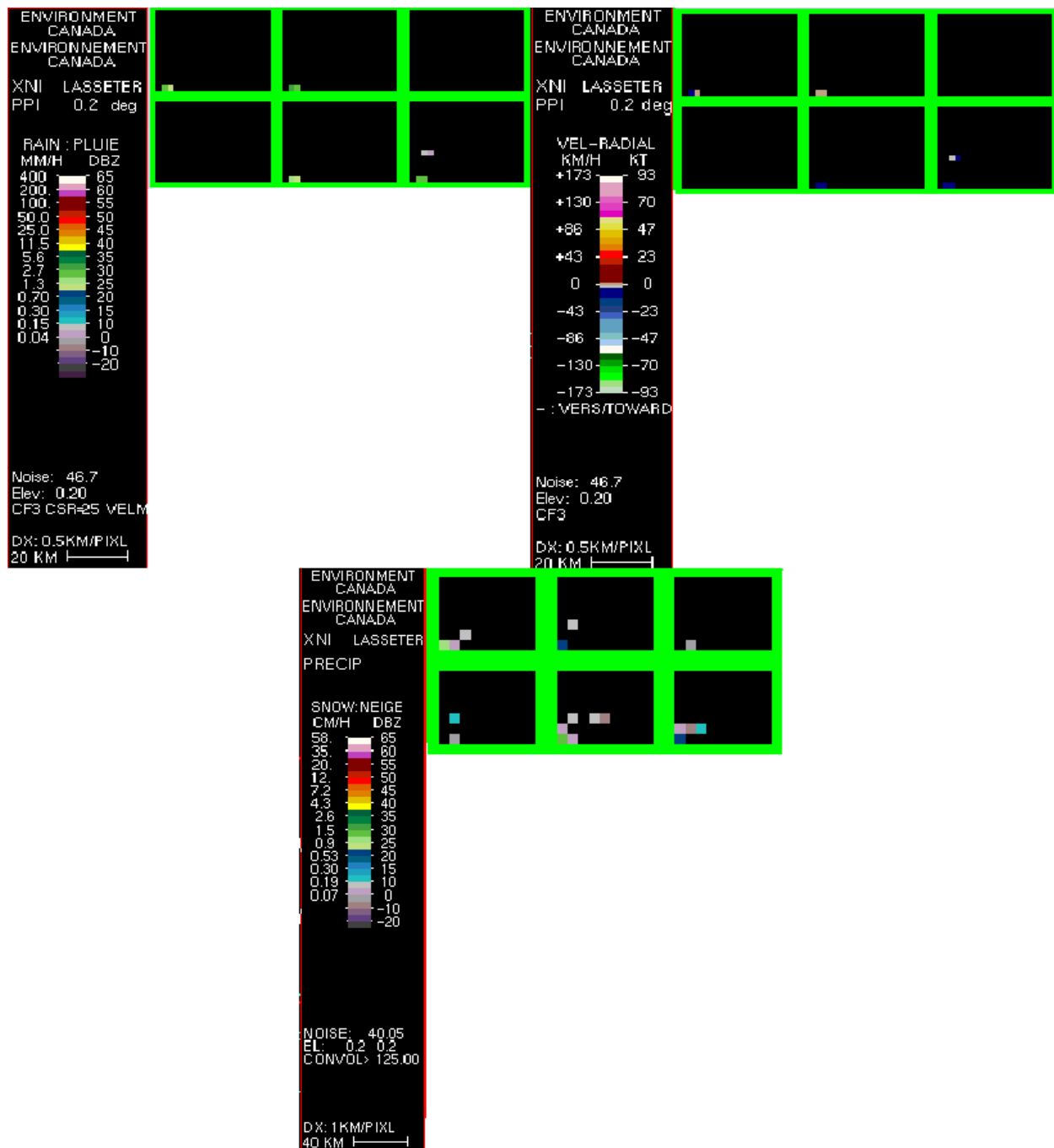
Appendix H: i: C-TRIP CLOGZPPI, VRPPI and PRECIP products of the Greenwich wind farm box on 2013-08-16 from 0800 Z – 0850 Z created using the DOPVOL1A and DOPVOL2 XNI IRIS files



Appendix H: ii: C-TRIP CLOGZPPI, VRPPI and PRECIP products of the Greenwich wind farm box on 2013-08-16 from 2000 Z – 2050 Z created using the DOPVOL1A and DOPVOL2 XNI IRIS files



Appendix H: iii: C-TRIP CLOGZPPI, VRPPI and PRECIP products of the Greenwich wind farm box on 2013-11-15 from 0900 Z – 0950 Z created using the DOPVOL1A and DOPVOL2 XNI IRIS files

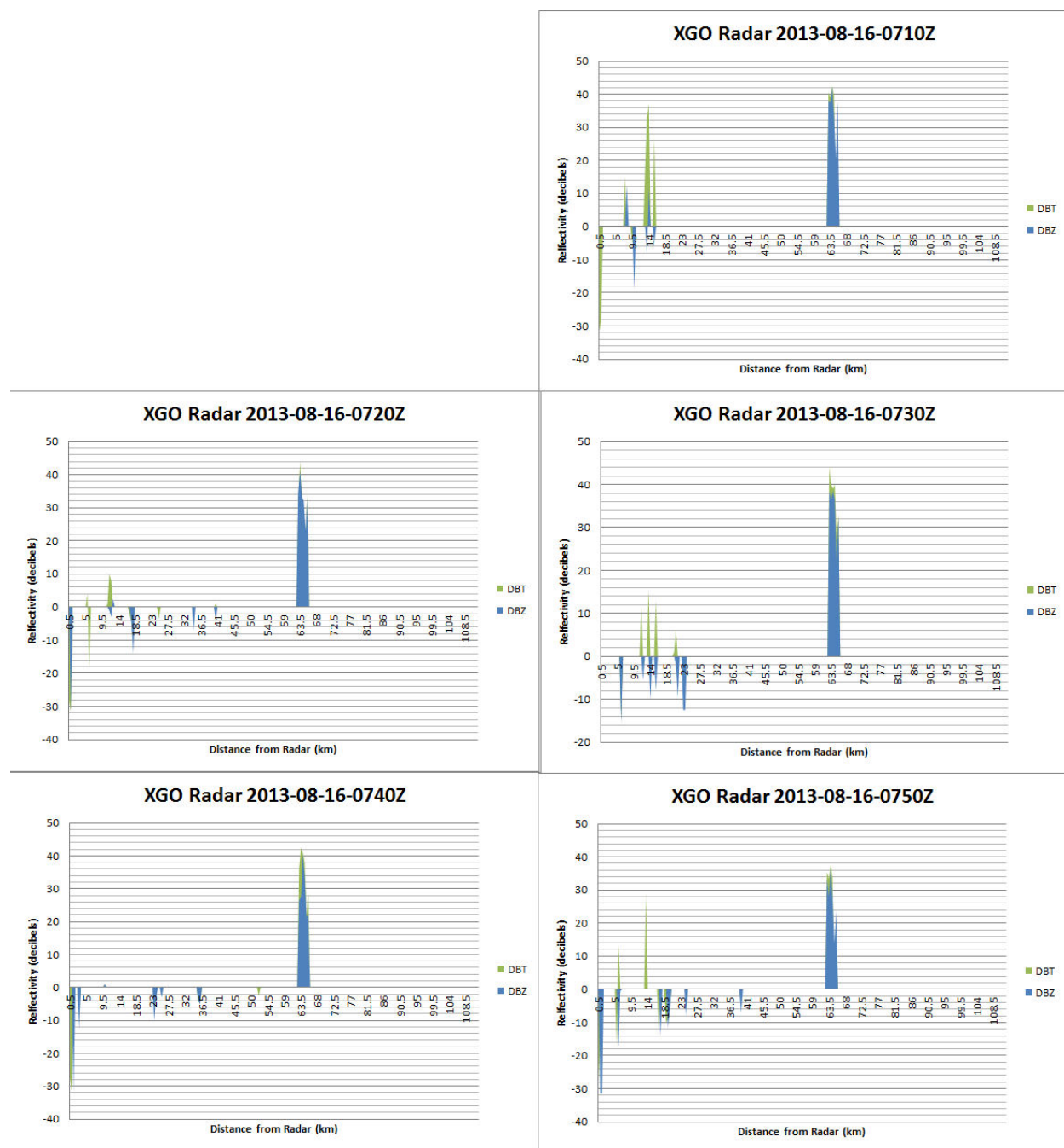


Appendix H: iv: C-TRIP CLOGZPPI, VRPPI and PRECIP products of the Greenwich wind farm box on 2013-11-15 from 2100 Z – 2150 Z created using the DOPVOL1A and DOPVOL2 XNI IRIS files

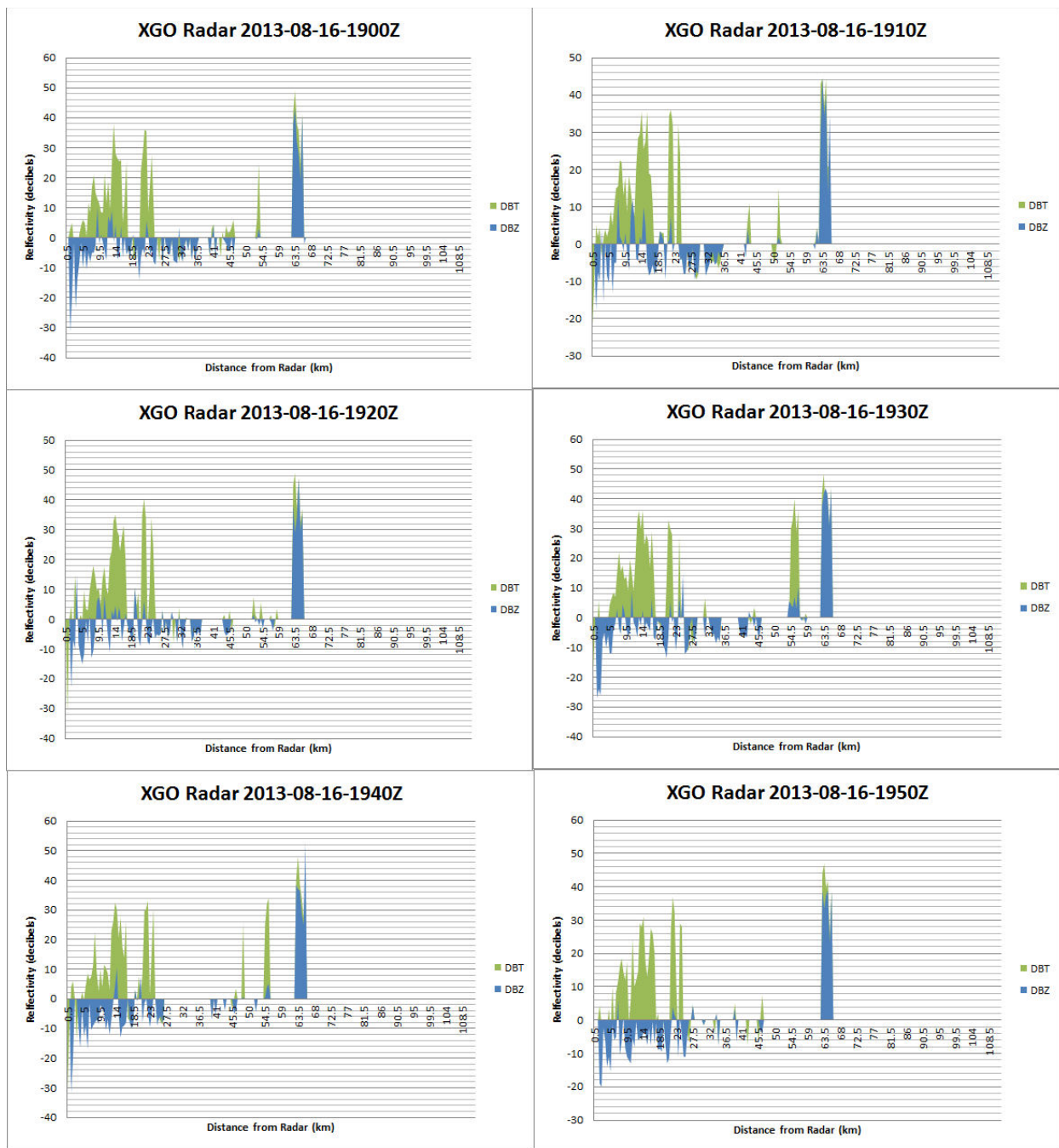
Appendix I: Nuttby Mountain Coordinates (Decimal Degrees Latitude and Longitude)

Turbine	Latitude	Longitude
1	45.551	-63.2188
2	45.5519	-63.2281
3	45.5571	-63.2258
4	45.5551	-63.2194
5	45.5587	-63.2323
6	45.5637	-63.2331
7	45.5565	-63.2406
8	45.5667	-63.2404
9	45.5632	-63.2452
10	45.5679	-63.2467
11	45.5693	-63.2175
12	45.5691	-63.2104
13	45.5639	-63.2153
14	45.5669	-63.2025
15	45.5555	-63.2042
16	45.5651	-63.2247
17	45.5599	-63.2006
18	45.5584	-63.2065
19	45.5609	-63.2253
20	45.556	-63.2319
21	45.5601	-63.2196
22	45.57	-63.2425

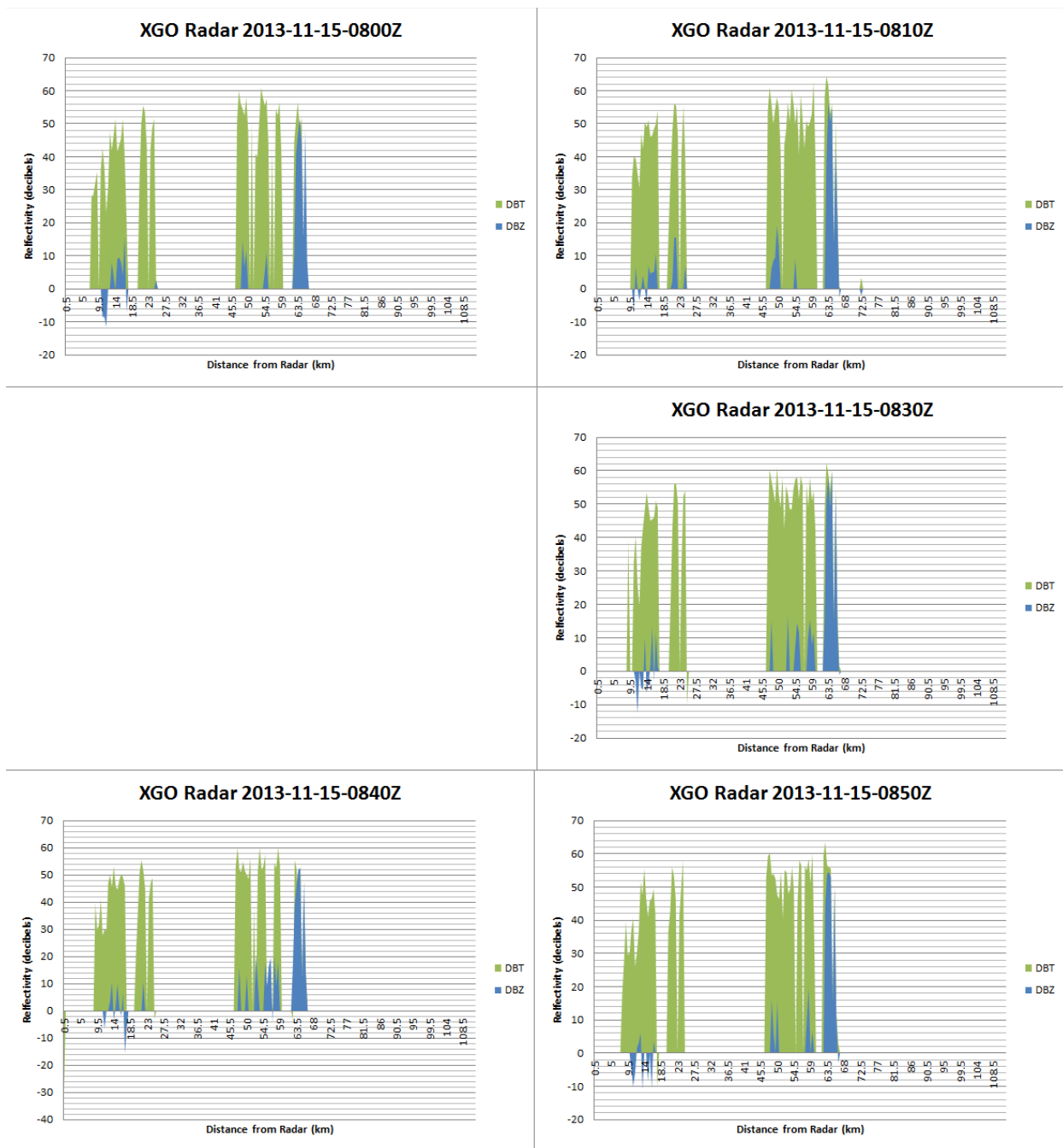
Appendix J: Productx Output WTC Examples of the Nuttby Mountain Wind Farm / Gore Weather Radar Pair



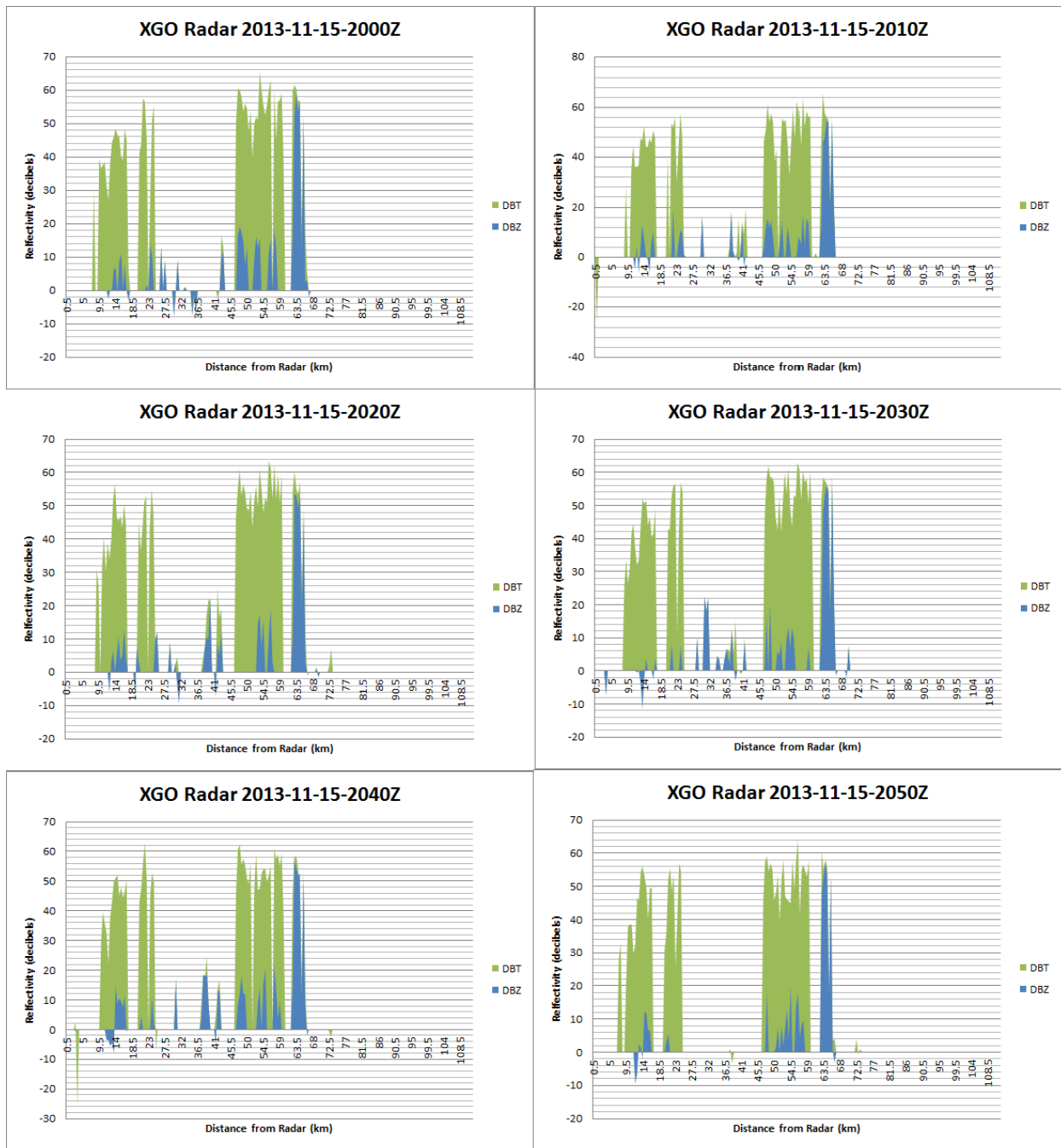
Appendix J: i: Productx images created from DOPVOL1A IRIS files for the Gore weather radar on 2013-08-16 for 10 minute intervals during 04:00 ADT or 0700 Z – 0750 Z (with 0700 Z missing due to an data error) using the maximum DBT and DBZ values from the azimuth range 34° - 38°



Appendix J: ii: Productx images created from DOPVOL1A IRIS files for the Gore weather radar on 2013-08-16 for 10 minute intervals during 16:00 ADT or 1900 Z – 1950 Z using the maximum DBT and DBZ values from the azimuth range 34° - 38°

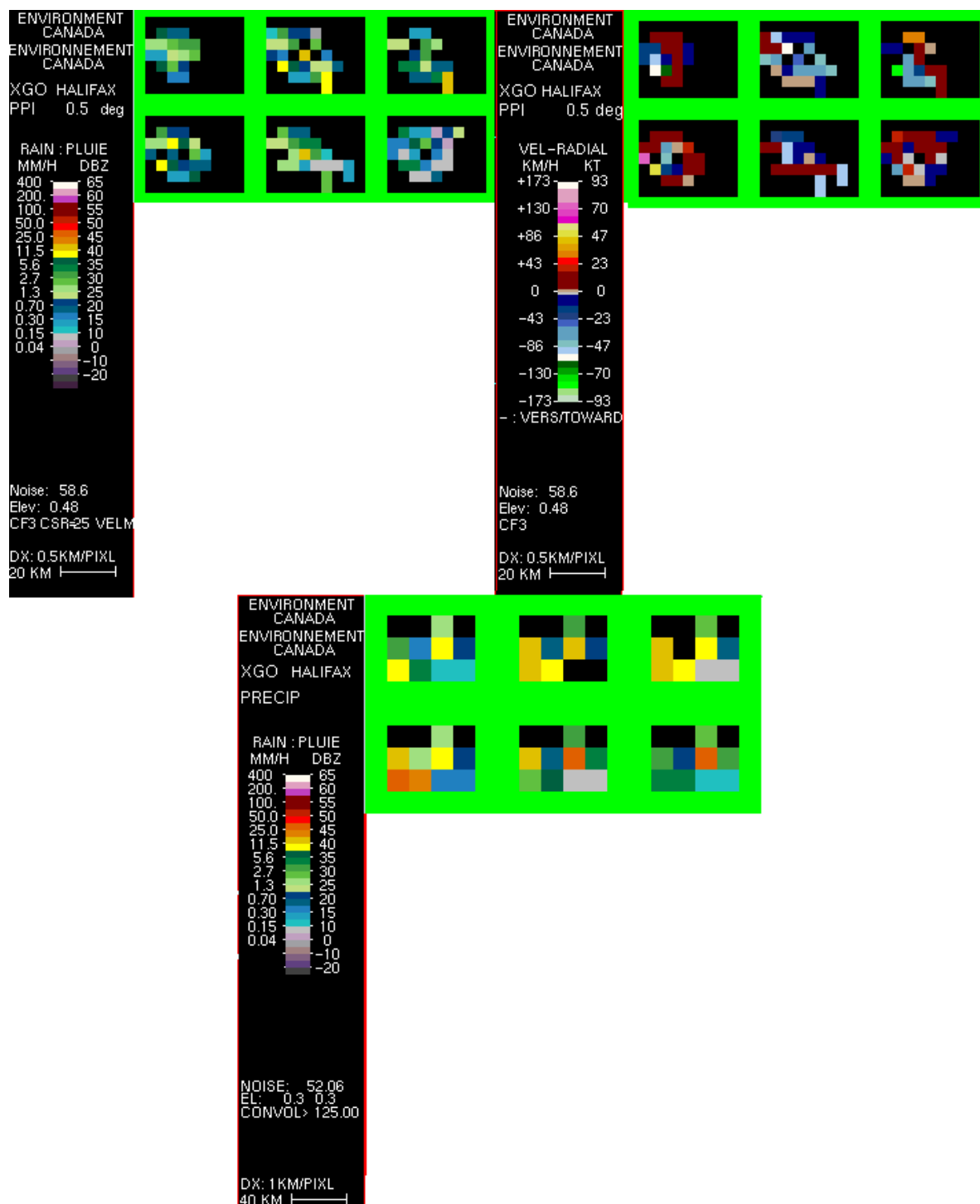


Appendix J: iii: Productx images created from DOPVOL1A IRIS files for the Gore weather radar on 2013-11-15 for 10 minute intervals during 04:00 AST or 0800 Z – 0850 Z (with 0820 Z missing due to an data error) using the maximum DBT and DBZ values from the azimuth range 34° - 38°

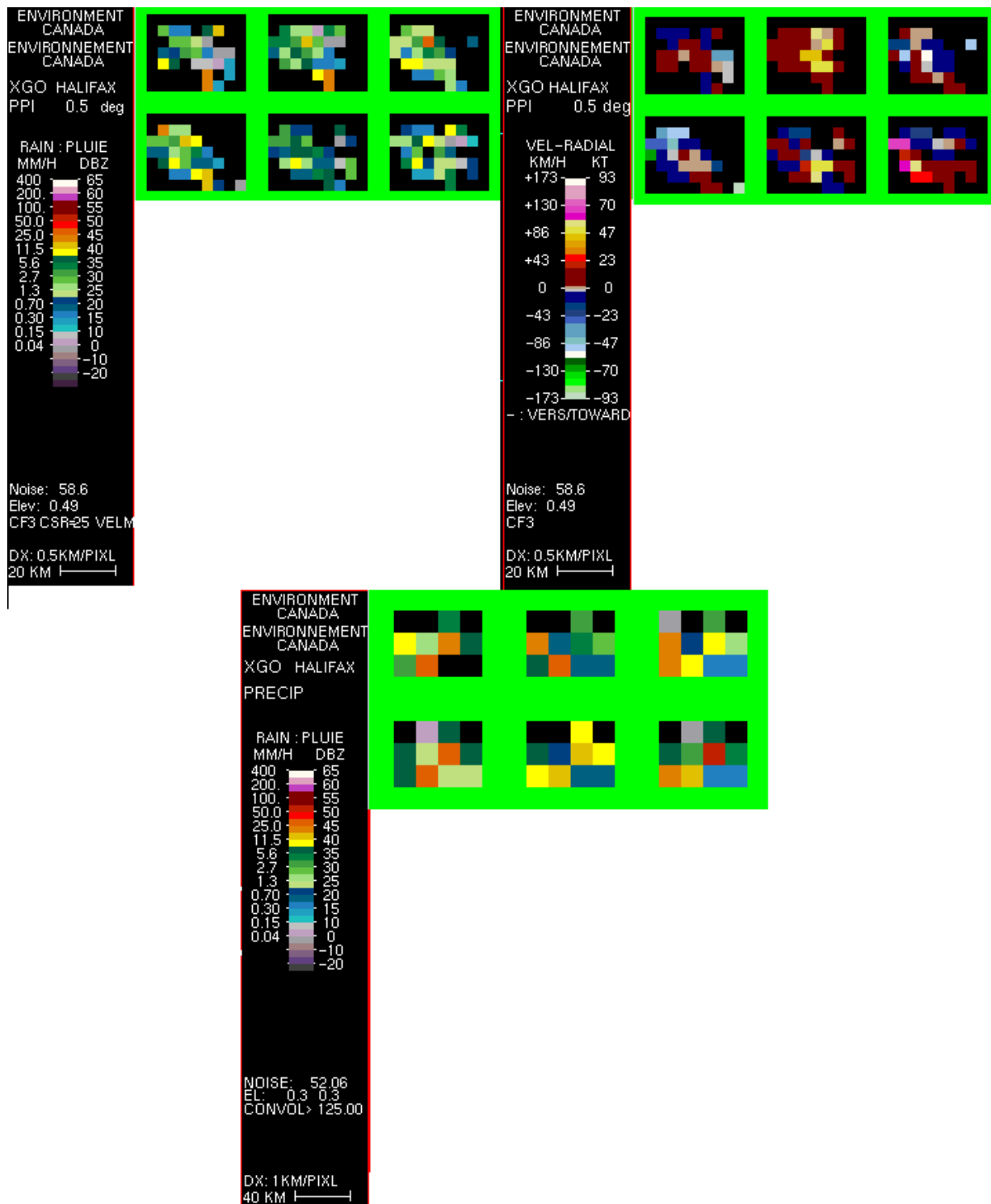


Appendix J: iv: Productx images created from DOPVOL1A IRIS files for the Gore weather radar on 2013-11-15 for 10 minute intervals during 16:00 AST or 2000 Z – 2050 Z using the maximum DBT and DBZ values from the azimuth range 34° - 38°

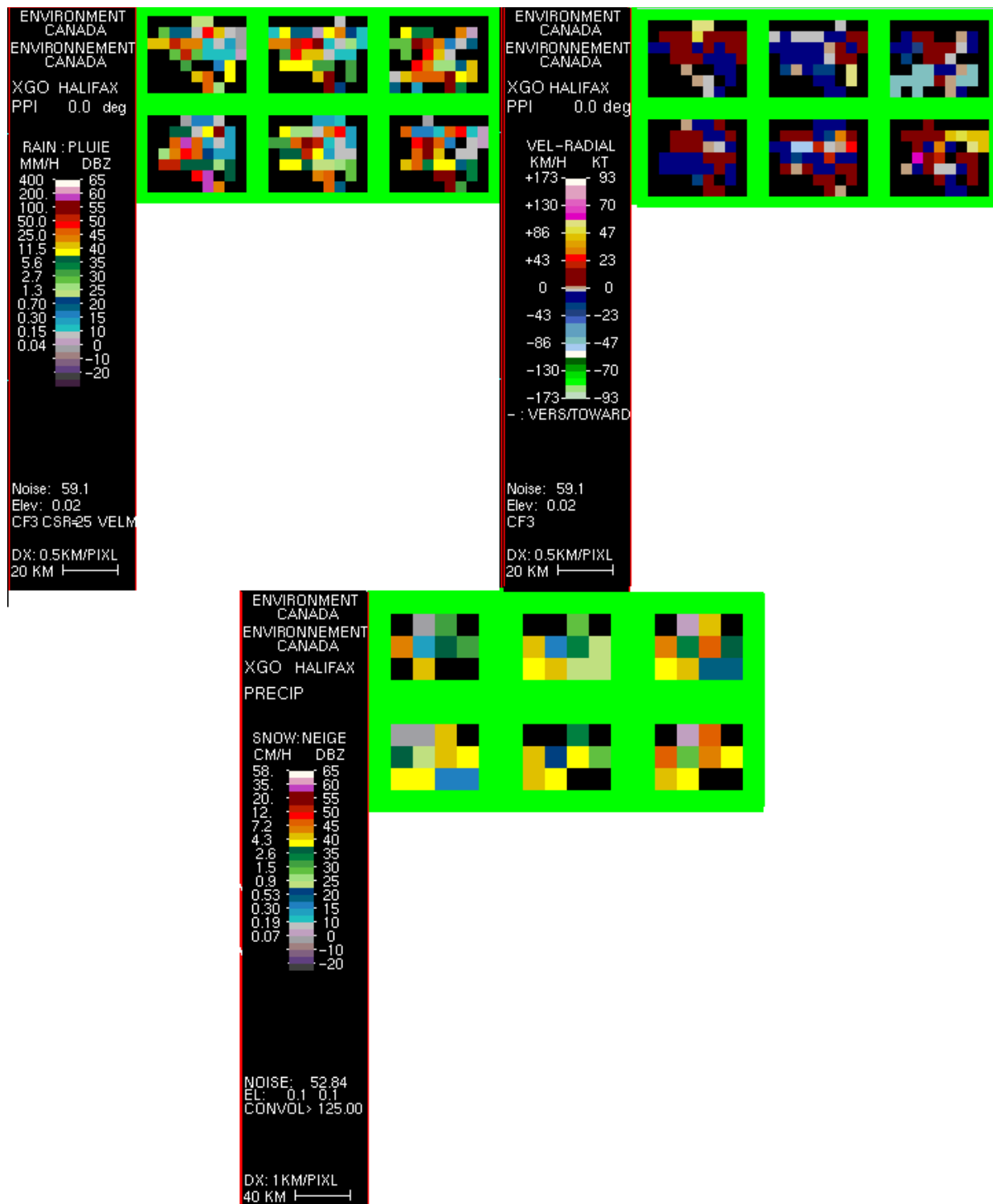
Appendix K: C-TRIP Output WTC Examples of the Nuttby Mountain Wind Farm / Gore Weather Radar Pair



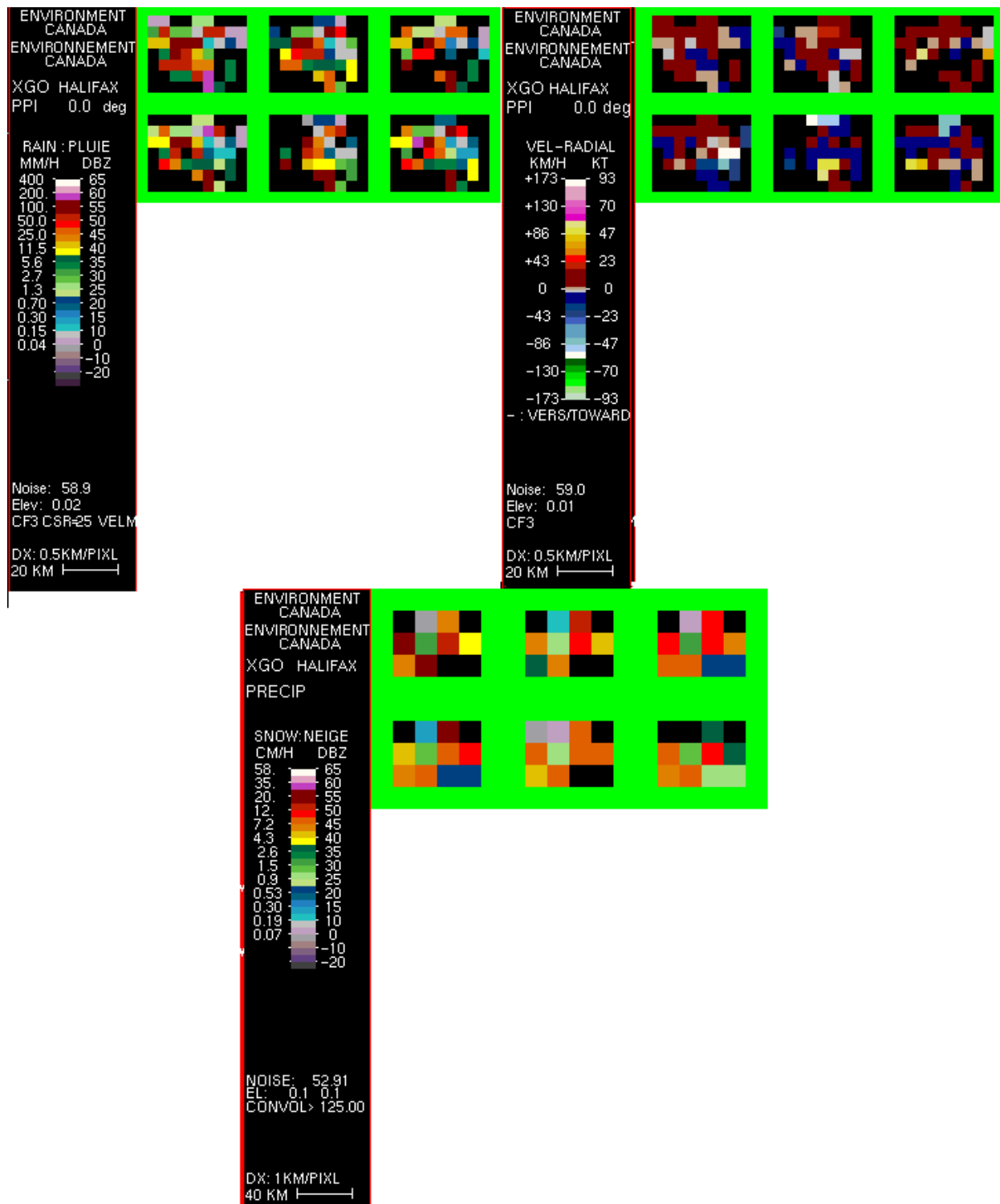
Appendix K: i: C-TRIP CLOGZPPI, VRPPI and PRECIP products of the Nuttby Mountain wind farm box on 2013-08-16 from 0700 Z – 0750 Z created using the DOPVOL1A and DOPVOL2 XGO IRIS files



Appendix K: ii: C-TRIP CLOGZPPI, VRPPI and PRECIP products of the Nuttby Mountain wind farm box on 2013-08-16 from 1900 Z – 1950 Z created using the DOPVOL1A and DOPVOL2 XGO IRIS files



Appendix K: iii: C-TRIP CLOGZPPI, VRPPI and PRECIP products of the Nuttby Mountain wind farm box on 2013-11-15 from 0800 Z – 0850 Z created using the DOPVOL1A and DOPVOL2 XGO IRIS files



Appendix K: iv: C-TRIP CLOGZPPI, VRPPI and PRECIP products of the Nuttby Mountain wind farm box on 2013-11-15 from 2000 Z – 2050 Z created using the DOPVOL1A and DOPVOL2 XGO IRIS files